

**Illuminating the structure of the pancreatic ATP-sensitive  
potassium channel by single particle cryo-electron microscopy**

**By**

**Gregory M Martin**

**A DISSERTATION**

Presented to the Biochemistry and Molecular Biology Graduate Program  
and the Oregon Health & Science University School of Medicine  
in partial fulfillment of  
the requirements for the degree of  
Doctor of Philosophy

## **Dedication**

To Steve and Linda Martin, the kindest people on Earth.

# Table of Contents

<b>Chapter 1: Introduction .....</b>	<b>1</b>
History of the KATP channel .....	3
Overview of KATP channel structure .....	5
Why solve a structure? .....	7
Kir6.2 structure .....	9
The ATP-binding site and impact on KATP channel gating .....	13
The PIP2 binding site and impact on channel structure and gating .....	15
SUR1 structure and function .....	18
TMD0/L0 .....	19
The ABC core structure of SUR1 .....	20
The effect of MgADP/MgATP on KATP channel activity .....	21
Allosteric regulation of KATP channel activity .....	23
KATP channels and disease .....	25
Pharmacological correction of CHI trafficking mutations .....	27
Towards a mechanism of PC rescue .....	28
References Cited .....	31

<b>Chapter 2 .....</b>	<b>41</b>
------------------------	-----------

## **Pharmacological Correction of Trafficking Defects in ATP-Sensitive Potassium Channels Caused by Sulfonylurea Receptor 1 Mutations**

Abstract .....	42
Introduction .....	43
Results .....	45
Discussion .....	56
Materials and methods .....	60
Acknowledgements .....	65
Figure legends .....	67
References Cited .....	80

<b>Chapter 3 .....</b>	<b>84</b>
------------------------	-----------

## **Cryo-EM structure of the ATP-sensitive potassium channel illuminates mechanisms of assembly and gating**

Abstract .....	85
Introduction .....	85
Results .....	88
Discussion .....	97
Materials and methods .....	100
Acknowledgements .....	107
Figure legends .....	110
References Cited .....	130

**Chapter 4 .....135**

**Anti-diabetic drug binding site in a mammalian KATP channel revealed by Cryo-EM**

Abstract .....	136
Introduction .....	136
Results .....	138
Discussion .....	151
Materials and methods .....	157
Acknowledgements .....	165
Figure legends .....	167
References Cited .....	190

**Chapter 5 .....196**

**A structural mechanism for pharmacological chaperone rescue of trafficking-impaired KATP channels**

Abstract .....	196
Introduction .....	198
Results .....	200
Discussion .....	209
Figure legends .....	212
References Cited .....	223

**Chapter 6: Conclusions and Perspectives .....226**

What can these structures tell us about KATP channel gating? .....	227
ATP sensitivity .....	227
The role of the Kir6.2 N-terminus .....	229
What can the structure tell us about KATP channel trafficking mutations? .....	231
What have we learned from other KATP channel structures? .....	233
Concluding Remarks .....	240
References Cited .....	243

## List of Figures and Tables

### Chapter 2

<b>Table 1.</b> Genetic and clinical data of HI patients bearing the TMD0 mutations .....	66
<b>Figure 1.</b> Pharmacological correction of SUR1 processing defects caused by SUR1-TMD0 mutations identified in congenital hyperinsulinism .....	72
<b>Figure 2.</b> KATP channel openers do not correct trafficking defects caused by SUR1 TMD0 mutations .....	73
<b>Figure 3.</b> Diazoxide does not promote intersubunit interactions between SUR1 and the N terminus of Kir6.2 as assessed by p-azidophenylalanine-mediated photocross-linking .....	74
<b>Figure 4.</b> Carbamazepine restores surface expression of trafficking-impaired SUR1 mutants .....	75
<b>Figure 5.</b> Gating properties of mutant channels rescued to the cell surface assessed by inside-out patch-clamp recording .....	76
<b>Figure 6.</b> Assessing metabolic response of mutant KATP channels rescued by CBZ using $^{86}\text{Rb}^+$ efflux assays .....	77
<b>Figure 7.</b> Diazoxide does not further increase $^{86}\text{Rb}^+$ efflux by increasing activity of channels already activated by metabolic inhibition .....	78
<b>Figure 8.</b> Metabolic response of mutant KATP channels rescued by tolbutamide assessed by $^{86}\text{Rb}^+$ efflux assays .....	79

### Chapter 3

<b>Table 1:</b> Statistics of cryo-EM data collection, 3D reconstruction and model building .....	109
<b>Figure 1.</b> Purification and single-particle EM imaging of the SUR1/Kir6.2 KATP channel .....	115
<b>Figure 1 - supplement 1.</b> Cryo-EM data processing flow-chart .....	116
<b>Figure 1-supplement 2.</b> Cryo-EM density map analysis .....	117
<b>Figure 2.</b> Three-dimensional reconstruction of the KATP channel .....	118
<b>Figure 2-supplement 1.</b> Sequence and structure comparison between Kir6.2 and Kir3.2 .....	119
<b>Figure 2-supplement 2.</b> Sequence alignment and structure comparison between SUR1 TMD1 and a bacterial peptidase-containing ABC transporter PCAT-1 (PDB ID: 4RY2) .....	120
<b>Figure 2-supplement 3.</b> Sequence alignment and structure comparison between SUR1 NBD1 and the mouse P-glycoprotein NBD1 (PDB ID: 4MLM) .....	121
<b>Figure 2-supplement 4.</b> Sequence alignment and structure comparison between SUR1 TMD2-NBD2 and a bacterial ABC exporter TM287/288 (PDB ID: 4Q4H) .....	122
<b>Figure 3.</b> Kir6.2 in a closed conformation .....	123
<b>Figure 4.</b> The ATP binding pocket .....	124
<b>Figure 5.</b> The interface between TMD0 and the N-terminal segment of L0 with Kir6.2 .....	125
<b>Figure 5-supplement 1.</b> Interactions between TMD0 and Kir6.2 .....	126
<b>Figure 6.</b> The SUR1-L0 connecting TMD0/Kir6.2 with the SUR1-ABC core .....	127
<b>Figure 7.</b> SUR1 with a twisted ABC core conformation in saturating concentrations of GBC .....	128
<b>Figure 8.</b> KATP channel gating model .....	129

## Chapter 4

<b>Key Resources Table</b> .....	157
<b>Table 1:</b> Statistics of cryo-EM data collection, 3D reconstruction and model building .....	166
<b>Figure 1.</b> Overall structure of the KATP channel bound to ATP and GBC .....	173
<b>Figure 1-figure supplement 1.</b> Data collection and image processing workflow .....	174
<b>Figure 1-figure supplement 2.</b> Cryo-EM density map analysis .....	175
<b>Figure 2.</b> Structural highlights of Kir6.2 and SUR1 .....	176
<b>Figure 2-figure supplement 1.</b> Cryo-EM density map of key structural features in Kir6.2 .....	177
<b>Figure 2-figure supplement 2.</b> Cryo-EM density map of transmembrane helices and the lasso (L0) motif of SUR1 .....	178
<b>Figure 3.</b> The interface between SUR1 and Kir6.2 .....	179
<b>Figure 4.</b> The ATP binding pocket .....	180
<b>Figure 4.-figure supplement 1</b> .....	181
<b>Figure 5.</b> Important molecular interactions surrounding the ATP binding site .....	182
<b>Figure 6.</b> The GBC binding site in SUR1 .....	183
<b>Figure 6-figure supplement 1.</b> GBC binding site .....	184
<b>Figure 7.</b> Functional testing of GBC binding residues .....	185
<b>Figure 7-figure supplement 1.</b> Functional testing of GBC binding residues by electrophysiology .....	186
<b>Figure 8.</b> Comparison of the current structure with the GBC-bound, ATP-free structure from Li et al. (PDB ID: 5WUA) .....	187
<b>Figure 8-figure supplement 1.</b> Reinterpretation of the GBC cryo-EM density proposed in Li et al. .....	188
<b>Figure 8-figure supplement 2.</b> .....	189
<b>Figure 9.</b> ATP and GBC gating models .....	190

## Chapter 5

<b>Figure 1.</b> The KATP channel in the presence of the diverse allosteric inhibitors .....	215
<b>Figure 2.</b> The allosteric inhibitor binding site on SUR1 .....	216
<b>Figure 3.</b> Details of GBC and RPG interaction in the sulfonylurea binding pocket .....	217
<b>Figure 4.</b> The effect of inhibitory ligand binding to SUR1 on the structure of SUR1 and Kir6.2 .....	218
<b>Figure 5.</b> Inhibitor binding to SUR1 strengthens a cytoplasmic interface between SUR1 and Kir6.2 .....	219
<b>Figure 6.</b> Location of the putative Kir6.2 N-terminus .....	220
<b>Figure 7.</b> Functional validation of SUR1 binding site model by $^{86}\text{Rb}^+$ efflux .....	221
<b>Figure 8.</b> Binding site mutations impair the ability of GBC and CBZ to rescue trafficking mutations within TMD0 .....	222

## Chapter 6

<b>Figure 1.</b> A model for gating regulation by the Kir6.2 N-terminus .....	242
---	-----

## List of Abbreviations

<b>ABC</b>	ATP-binding cassette
<b>ADP</b>	adenosine diphosphate
<b>AMP</b>	adenosine monophosphate
<b>ANOVA</b>	analysis of variance
<b>ATP</b>	adenosine triphosphate
<b>AzF</b>	azido-phenylalanine
<b>BIR</b>	$\beta$ -cell inward rectifier
<b>BSA</b>	bovine serum albumin
<b>C<math>\alpha</math></b>	alpha carbon
<b>CBZ</b>	carbamazepine
<b>CCW</b>	counterclockwise
<b>cDNA</b>	complementary DNA
<b>CFTR</b>	cystic fibrosis transmembrane conductance receptor
<b>CHI</b>	congenital hyperinsulinism
<b>CTD</b>	cytoplasmic domain
<b>CTF</b>	contrast transfer function
<b>CW</b>	clockwise
<b>DMSO</b>	dimethyl sulfoxide
<b>DTT</b>	dithiothreitol
<b>EC<sub>50</sub></b>	half-maximal effective concentration
<b>ECL</b>	extracellular loop
<b>EDTA</b>	Ethylenediaminetetraacetic acid
<b>EGTA</b>	ethylene glycol-bis( $\beta$ -aminoethyl ether)-N,N,N',N'-tetraacetic acid
<b>EM</b>	electron microscopy
<b>ER</b>	endoplasmic reticulum
<b>ERAD</b>	endoplasmic reticulum-associated degradation
<b>FSC</b>	Fourier shell correlation
<b>fSUR1</b>	FLAG-SUR1
<b>GBC</b>	glibenclamide
<b>GFP</b>	green fluorescent protein
<b>GSIS</b>	glucose stimulated insulin secretion
<b>GTP</b>	guanosine triphosphate
<b>HBC</b>	helix bundle crossing
<b>HEPES</b>	4-(2-hydroxyethyl)-1-piperazineethanesulfonic acid
<b>HI</b>	hyperinsulinism
<b>HRP</b>	horseradish peroxidase
<b>IC<sub>50</sub></b>	half-maximal inhibitory concentration
<b>ICL</b>	intracellular loop
<b>IF</b>	interfacial helix
<b>K-INT</b>	intracellular potassium solution
<b>K<sub>ATP</sub></b>	ATP-sensitive potassium channel
<b>KCO</b>	potassium channel opener
<b>kDa</b>	kilodalton
<b>Kir</b>	inward-rectifier potassium channel
<b>KirBac</b>	bacterial inward-rectifier potassium channel
<b>L0</b>	intracellular loop 0

<b>M1</b>	first (outer) transmembrane helix
<b>M2</b>	second (inner) transmembrane helix
<b>mDa</b>	megadalton
<b>MDR</b>	multidrug resistance
<b>MOI</b>	multiplicity of infection
<b>MRP1</b>	multidrug resistance-associated protein 1
<b>MW</b>	molecular weight
<b>NBD</b>	nucleotide binding domain
<b>NCS</b>	noncrystallographic symmetry
<b>NDM</b>	neonatal diabetes mellitus
<b>Ntp</b>	(Kir6.2) N-terminal peptide
<b>PAGE</b>	polyacrylamide gel electrophoresis
<b>PBS</b>	phosphate buffered saline
<b>PC</b>	pharmacological chaperone
<b>PCR</b>	polymerase chain reaction
<b>PDB</b>	protein data bank
<b>PgP</b>	P-glycoprotein
<b>PIP2</b>	phosphatidylinositol-4,5-bisphosphate
<b>PNDM</b>	permanent neonatal diabetes mellitus
<b>P<sub>o</sub></b>	open probability
<b>RPG</b>	repaglinide
<b>SDS</b>	sodium dodecyl sulfate
<b>SEC</b>	size exclusion chromatography
<b>SEM</b>	standard error of the mean
<b>SUR</b>	sulfonylurea receptor
<b>TAP</b>	transporter associated with antigen processing
<b>TM</b>	transmembrane
<b>TMD</b>	transmembrane domain
<b>tRNA</b>	transfer ribonucleic acid
<b>tTA</b>	tetracycline transactivator
<b>WT</b>	wild type

## Acknowledgements

Science is rarely done in isolation, and the work in this dissertation is no exception. None of this would have been possible without the constant support and direct assistance from talented people from all across the OHSU campus. For this, I am forever grateful.

First and foremost, I must thank my mentor Dr. Show-Ling Shyng. She has been as good and as supportive a mentor as a student could possibly ask for. Throughout these last five years, she has managed to strike a near ideal balance of motivation and patience, and I have grown much and achieved much as a scientist and as a person as a direct result. She is a great scientist, but also a wise and caring individual; Show-Ling is a role model for us all.

Thank you members of the Shyng lab, past and present, for all of your help and also for your friendship and camaraderie. The shared experience makes it all worth it.

I would also like to thank the entire BMB department, past and present. Jon Fay, Omar Davulcu, Nancy Meyers, Qing Xie, Danielle Williamson, Johannes Elferich, Larry David, Nick Caputo, James Chen, and many others. You have all provided crucial assistance at some point or another which has made this work possible.

Also a huge thanks to the Multi-Scale Microscopy core, in particular Dr. Craig Yoshioka and Dr. Claudia Lopez. Craig has taught me a lot of what I know about microscopy and has been a crucial collaborator on this project. Claudia keeps the whole EM operation running at OHSU and has been very helpful and supportive throughout the whole process.

Thank you to all the members of my dissertation committee. You are all brilliant scientists. I have learned so much from your numerous and insightful questions and ideas. You have also provided key support and encouragement along the way; an advisory committee in the truest sense.

As most scientists know, work-life balance is crucial for long-term sustainability. In this regard, my friends have also been integral to this work. Afternoon frisbee sessions, alpine starts on Mt. Baker, and late-night bike rides have all been key contributors.

Finally, I'd like to thank my family, whose love and support truly know no bounds. I am extremely fortunate, to say the least.

## Dissertation Abstract

The pancreatic  $\beta$ -cell is responsible for producing and secreting insulin, a critical hormone which keeps blood glucose within a narrow physiological range throughout the day. The  $\beta$ -cell senses blood glucose indirectly by sensing its metabolic products ATP and ADP, which fluctuate in the  $\beta$ -cell to parallel blood glucose levels. The sensor of glucose metabolism is a potassium ion channel called the ATP-sensitive  $K^+$  channel ( $K_{ATP}$ ), which can initiate or cease insulin secretion by coupling changes in ATP/ADP levels to electrical excitability.

Owing to its unrivaled role in insulin secretion, the  $K_{ATP}$  channel has been intensely studied over the last 35 years, and numerous gain- and loss-of-function mutations have been identified in patients throughout the  $K_{ATP}$  channel genes which cause insulin secretion disorders. The  $K_{ATP}$  channel is also the target for sulfonylurea drugs, a large class of insulin secretagogues which have been widely prescribed to treat type II diabetes since the 1950s and are still in use today.

However, in the absence of a 3D structure of the channel complex, fundamental aspects of  $K_{ATP}$  channel biology have remained a mystery. Specifically, where do sulfonylureas bind and how do they inhibit  $K_{ATP}$  channel activity to stimulate insulin secretion? Our group has also shown that these inhibitors can overcome the folding and/or trafficking defects of a specific class of loss-of-function mutations in the  $K_{ATP}$  channel which cause potentially life-threatening hypoglycemia. Because they offer a potential therapy for these patients, we wish to understand the molecular and structural basis for this rescue effect.

In this dissertation I describe my efforts to answer these questions by solving moderate to high resolution structures of the channel complex by cryo-electron microscopy, which illuminate how physiological and pharmacological ligands impact channel behavior and inform an overall

gating mechanism. These studies provide much-needed context to decades of experiments and provide fertile ground for new hypotheses aimed at understanding the unique role of the  $K_{ATP}$  channels in glucose-stimulated insulin secretion.

## Chapter 1: Introduction

As the body's primary energy source, blood glucose levels must be kept in a narrow range during periods of both feeding and fasting, i.e. entry into the blood via production and absorption from the diet must be balanced with uptake and removal. This is achieved primarily by the action of the hormone insulin, which inhibits production and stimulates uptake of glucose. Thus to avoid hyper- and hypoglycemia, high and low blood sugar respectively, the pancreatic  $\beta$ -cells, which produce and secrete insulin, must sense blood glucose levels and tailor insulin secretion such that the two are closely matched throughout the day. If this mechanism fails the result is diabetes mellitus (hyperglycemia) or its converse hyperinsulinism (hypoglycemia), both of which are deadly if left unchecked.

Pancreatic  $\beta$ -cells sense glucose indirectly by sensing its metabolic products ATP and ADP, which fluctuate in the  $\beta$ -cell to parallel blood glucose. The sensor is an ion channel called the ATP-sensitive  $K^+$  channel ( $K_{ATP}$ ), which can initiate or cease insulin secretion by coupling changes in ATP/ADP levels to the membrane potential (Rorsman & Trube, 1985). Thus increasing blood glucose closes  $K_{ATP}$  channels via increasing intracellular ATP, depolarizing the membrane and activating voltage-gated  $Ca^{2+}$  channels; the resulting  $Ca^{2+}$  influx triggers fusion of insulin secretory granules with the plasma membrane. As insulin reduces blood glucose, increased intracellular ADP opens  $K_{ATP}$  channels, silencing electrical activity and inhibiting further insulin release.

$K_{ATP}$  channels are therefore a central hub in the canonical glucose-induced insulin secretion (GSIS) pathway, which is underscored by the fact that numerous mutations throughout the  $K_{ATP}$  channel subunits can uncouple insulin secretion from changes in blood glucose (Ashcroft, 2005). Gain-of-function mutations often yield a severe form of diabetes called

neonatal diabetes mellitus (NDM), i.e. absent insulin secretion despite very high blood glucose, while loss-of-function gives rise to hyperinsulinism (HI), i.e. unregulated insulin secretion in the face of severe hypoglycemia.  $K_{ATP}$  channels are also the target of multiple and diverse classes of inhibitory allosteric ligands which stimulate insulin secretion by closing  $K_{ATP}$  channels, thereby lowering blood glucose. Most notable are the widely-prescribed sulfonylurea drugs, which have been used to treat type II diabetes since the 1950s and are still in use today (Sola et al., 2015).

Due to their unrivaled role in insulin secretion and pharmacological importance,  $K_{ATP}$  channels have been intensely investigated for more than 3 decades, being first discovered in cardiac myocytes in 1983 (Noma, 1983).  $K_{ATP}$  channels were later discovered in the pancreas (Ashcroft et al., 1984; Cook & Hales, 1984; Rorsman & Trube, 1985), showing nearly identical electrical properties and regulation by ATP as the heart channels, and were subsequently identified in the brain and vascular and nonvascular smooth muscle (Ashford et al., 1988; Inagaki et al., 1996; Nicholas et al., 1989). In each of these tissues,  $K_{ATP}$  channels couple changes in cellular energetics to the membrane potential to mediate, for instance, protection during ischemia or hypoxia, vasodilation, and GSIS.

Molecular cloning techniques of the 1990s enabled discovery of the basic properties of the channel and some understanding of the functional role particular mutations had in causing either NDM or HI. However, until recently, obtaining true structural information on the channel complex was nearly impossible and relied on homology modelling of related proteins. Thus, the field's detailed knowledge of  $K_{ATP}$  channel behavior lacked context and major questions remained, particularly concerning how and where ATP and sulfonylureas bind to the channel to stimulate insulin secretion.

Recent advances in cryo-electron microscopy (cryo-EM) (Cheng, 2015), which arose during the initial phases of this dissertation, suddenly enabled structure determination on a wide range of samples to near-atomic resolution. This was particularly significant for large and dynamic membrane proteins like the  $K_{ATP}$  channel, which are resistant to crystallization. In light of this, the work outlined in this dissertation set out to achieve the following goals: 1) elucidate the domain organization and key subunit interactions by determining a structure of an intact  $K_{ATP}$  channel complex by cryo-EM; 2) elucidate the location of the inhibitory sulfonylurea and ATP binding sites; 3) define the structural basis for how these two compounds both separately inhibit  $K_{ATP}$  channel activity; 4) determine if the sulfonylurea binding pocket is the general inhibitory allosteric site and if so how it can accommodate such a diverse array of compounds.

What follows is an overview of the history of  $K_{ATP}$  channel research, which goes back many decades, its role in human health and disease, and the key experiments which led to our current understanding of its fundamental properties. This will be presented with respect to what could be accessed experimentally, and how the development of cryo-EM enabled the field to address long-standing questions concerning  $K_{ATP}$  channel assembly and gating.

### **History of the $K_{ATP}$ channel**

The history of the  $\beta$ -cell  $K_{ATP}$  channel begins during WWII in Montpellier, France, where chemist Marcel Janbon was experimenting with a newly developed class of sulfonamides as antibiotics for the treatment of typhoid fever. In patients given a compound called 2254 RP, Janbon noted a high incidence of often severe hypoglycemia (Janbon et al., 1942). His colleague physician Auguste Loubatieres later showed that this compound stimulated insulin secretion, thus giving rise to the hypoglycemia (Loubatieres, 1957). The clinical relevance of this finding was immediately apparent, leading to clinical trials for the use of this class of sulfonamides in

the treatment of type II diabetes, which was the first non-insulin treatment for diabetes.

Tolbutamide was the first derivative of 2254 RP which retained hypoglycemic and antidiabetic properties without any bacteriostatic action (Bander et al., 1956), and went into general use as a diabetes therapy.

More than a decade would pass before the basic mechanism of action of this new class of compounds, termed sulfonylureas, was known. At this time, the ionic mechanism of insulin secretion was just being discovered. By studying the membrane potential of pancreatic  $\beta$ -cells, it was shown that both glucose and tolbutamide independently initiate action potential firing necessary for insulin release (Dean & Matthews, 1968), thus there was likely a sulfonylurea receptor mediating the response. Shortly after the discovery of the  $K_{ATP}$  current in  $\beta$ -cells, it was shown that multiple sulfonylureas inhibit  $K_{ATP}$  channels (Ashcroft et al., 1987; Schmid-Antomarchi et al., 1987; Sturgess et al., 1985; Trube et al., 1986) over the same concentration range required to reduce  $^{86}\text{Rb}^+$  (a radioactive tracer for  $\text{K}^+$ ) efflux from  $\beta$ -cells (Schmid-Antomarchi et al., 1987) and to stimulate insulin secretion (Gaines et al., 1988), thus it was postulated that the  $K_{ATP}$  channel was the sulfonylurea receptor. However, a second messenger could not be ruled out.

Medicinal chemistry led to the development of over 1000 sulfonylureas in the 1960s and 70s, some showing greater than 1000-fold higher potency than tolbutamide (Bander, 1969). Glibenclamide was representative of this second generation of compounds and an [ $^{125}\text{I}$ ] derivative azido-iodo-glibenclamide was synthesized to enable more direct studies on the sulfonylurea receptor (Aguilar-Bryan et al., 1990), as it could be covalently cross-linked following exposure to UV. Two membrane proteins were specifically photolabeled by this compound, a ~140 kDa protein with high affinity and a 43 kDa protein with lower affinity. This

enabled partial purification of the high affinity receptor, which allowed sequencing by mass spec and cloning of the gene encoding the receptor, termed SUR (Aguilar-Bryan et al., 1995). The low affinity receptor, cloned from pancreatic islets shortly thereafter, turned out to be a  $K^+$  channel which was initially called BIR, for  $\beta$ -cell inward-rectifier (Inagaki et al., 1995).

Until this point,  $K_{ATP}$  channels were identified as a current,  $I_{KATP}$ , which was inhibited by application of ATP to the intracellular side of an excised membrane patch (Cook & Hales, 1984; Noma, 1983; Trube & Hescheler, 1984), hence their initial description as the ATP-sensitive  $K^+$  channel.  $K_{ATP}$  channels were further defined by their stimulation by ADP in the presence of  $Mg^{2+}$  (Dunne & Peterson, 1986; Mislner et al., 1986), inhibition by sulfonylureas and activation by a diverse class of compounds called  $K^+$  channel openers (KCOs) (Inagaki et al., 1995).

Heterologous co-expression of the sulfonylurea receptor SUR with the BIR  $K^+$  channel (i.e. the low affinity sulfonylurea receptor) reconstituted all of these basic properties, strongly suggesting  $K_{ATP}$  channels were obligate complexes of these two proteins. This complex was shown to be stable in mild detergents and to be an octamer with 4:4 stoichiometry and apparent molecular weight of 950 kDa (Clement et al., 1997). Thus more than 50 years after the discovery of sulfonylureas, the molecular identity of the sulfonylurea receptor and apparent metabolic sensor governing  $\beta$ -cell excitability had been revealed. This has led to two more decades of study into the mechanisms governing  $K_{ATP}$  channel expression and gating regulation, all in hopes to more fully understand the process of GSIS.

### **Overview of $K_{ATP}$ channel structure**

The cloning experiments detailed above allowed for discovery of the molecular composition of the  $K_{ATP}$  channel, which is a hetero-octamer of 4 SUR subunits surrounding a tetrameric  $K^+$  channel Kir6 (Clement et al., 1997; Inagaki et al., 1997; Shyng & Nichols, 1997).

In rodents and in humans, three SUR subunits SUR1, SUR2A, and SUR2B, can combine with either of the two Kir6 subunits, Kir6.1 or Kir6.2, and the various combinations of subunits give rise to functionally distinct  $K_{ATP}$  channels which are expressed in distinct tissues. Notable examples include the cardiac channel, SUR2A/Kir6.2, the first  $K_{ATP}$  channel to be discovered in 1983 (Noma, 1983) which plays a critical cardio-protective role during ischemia, or low blood flow to the heart (Nichols & Lederer, 1991; Noma, 1983; Terzic et al., 1995), and the smooth muscle  $K_{ATP}$  channel comprising SUR2B/Kir6.1, which mediates vasodilation, a phenomenon that is commonly targeted with specific KCO drugs like cromakalin (Brayden, 2002; Nicholas et al., 1989). The pancreatic  $\beta$ -cell channel, which comprises SUR1/Kir6.2, is the most well-studied isoform due to its pivotal role in insulin secretion and glucose homeostasis, and is the focus of this dissertation.

The overall assembly of the  $K_{ATP}$  channel complex was confirmed by a low-resolution EM study yielding a  $\sim 20\text{\AA}$  resolution molecular envelope which could accommodate a tetrameric Kir channel in the center surrounded by 4 SUR1 homology models (Mikhailov et al., 2005). However, no conclusions could be made regarding the SUR1-Kir6.2 interface nor binding sites of drugs or ligands. This paper did, however, highlight the challenges that structural biologists meet when working with the  $K_{ATP}$  channel, most notably involving the lability of the association of SUR1 and Kir6.2, which has frustrated many attempts to purify an intact channel complex.

A defining feature of  $K_{ATP}$  channels is the co-dependence of SUR1 and Kir6.2 for cell surface expression, such that either subunit expressed alone cannot exit the ER (Zerangue et al., 1999). However, it was serendipitously discovered that deletion of the C-terminal 35 amino acids of Kir6.2 allowed for independent expression and trafficking of Kir6.2 in the absence of SUR1 (Tucker et al., 1997) and permitted assignment of specific functions to either subunit. In

fact, both SUR1 and Kir6.2 possess ER retention and retrieval motifs, comprising a tripeptide RKR, which interact directly with chaperone proteins in the ER to ensure only fully-assembled, octameric complexes traffic out of the ER, and that this signal was removed in the C-terminal truncation of Kir6.2 (Zerangue et al., 1999). This signal could also be mutated in SUR1 (RKR → AAA) to allow Kir6.2-independent expression of SUR1 (Cartier et al., 2001; Zerangue et al., 1999).

With these tools in hand, it was shown that Kir6.2 was independently sensitive to ATP inhibition (Tucker et al., 1997) and that contributions came from both the cytoplasmic N- and C-termini (Tucker et al., 1998). MgADP stimulation occurs through direct interaction with SUR1 (Gribble, Tucker, et al., 1997; Nichols et al., 1996), and while MgATP can also stimulate channel activity via SUR1 (Gribble, Tucker, Haug, et al., 1998) it must likely be hydrolyzed to MgADP first (Zingman et al., 2001). Importantly, while Kir6.2 is intrinsically ATP-sensitive, SUR1 increases this sensitivity roughly 10-fold (Tucker et al., 1997), and MgADP stimulation via interaction with SUR1 works through a reduction in the ATP sensitivity of Kir6.2 (Nichols, 2006), leading to an increase in open probability ( $P_O$ ).

Thus in the context of the full assembly, the  $K_{ATP}$  channel acts as an elegant sensor of the *ratio* of intracellular adenine nucleotides, which can be tuned through differential nucleotide sensitivities of the various  $K_{ATP}$  channel isoforms expressed in different tissues, i.e. SUR1-containing channels (pancreas) show greater MgADP stimulation than SUR2A-containing channels (cardiac myocytes) (Masia et al., 2005). Moreover, this sensor can be re-calibrated by SUR interaction with sulfonylureas or KCOs. Yet a perpetual question is how all of these inputs converge on the  $K^+$  pore of Kir6.2, i.e. what is the structural basis for Kir6.2 gating regulation?

*Why solve a structure?*

A mechanistic understanding of  $K_{ATP}$  channel gating and assembly would be greatly aided by a 3D structure of the complex. In particular, a question remaining to be answered has been the location of the binding sites for ATP on Kir6.2 and sulfonylureas on SUR1, and how binding of these compounds affect the structure to impact Kir6.2 gating. Homologous structures within the ABC transporter and Kir channel families have provided a rough framework for interpretation of experimental data (Antcliff et al., 2005; Haider et al., 2007; Vedovato et al., 2015), but confident conclusions can be made generally for mutations only within highly conserved regions of the sequence. For example, C166F is a neonatal diabetes mutation in Kir6.2 which causes very high  $P_O$  (Gloyn et al., 2006; Trapp et al., 1998), and a cysteine is conserved at this position in all Kir3 family members. From crystal structures of KirBac1.1 (Kuo et al., 2003), Kir2.2 (Tao et al., 2009), and Kir3.2 (Whorton & MacKinnon, 2011), C166 is clearly placed two residues upstream of the helix bundle crossing (HBC) gate, which appears to be the primary gate in all Kir channels (Bichet et al., 2003). Thus a molecular interpretation of this mutation is fairly readily fashioned by presuming that perturbation of TM2 just above the gate would lead to an increase in  $P_O$ .

However, SUR1 and Kir6.2 are unique members of both of the ABC transporter and Kir channel families, which leaves big gaps in understanding in the absence of structures of these proteins for the following reasons: (1) Kir6.1 and Kir6.2 are the only Kir channels that are ATP sensitive; (2) the Kir6 ATP binding site itself is non-canonical and  $Mg^{2+}$ -independent, thus it could not be modeled based on known structures of other ATP-binding proteins; (3) SUR1 is the only ABC transporter known to couple to an ion channel, thus there was no structural precedent for this type of interaction; (4) the two domains of SUR1 thought to directly couple to Kir6.2,

called TMD0 and L0 (see *SUR1 structure* below) had no structural homologs in the PDB, thus a structural interpretation for how these two proteins interact amounts to educated guesswork.

It is for these reasons, among others, that the  $K_{ATP}$  channel field is greatly motivated to solve a structure of the intact channel complex. The work outlined in this dissertation set out to do just that, and in the process solved the first structure of the complex at moderate and then high resolution, notably identifying the inhibitory ATP binding site on Kir6.2, the allosteric sulfonylurea binding site on SUR1, and elucidating the structure of the SUR1-Kir6.2 interface. This has greatly aided the interpretation of decades' worth of functional data, much of which corresponds nicely with what we observe in the structure, and has provided unprecedented details into the regulation of the channel complex by inhibitory ligands and plausible mechanisms for channel activation. In the following sections will be a more detailed introduction into what was already known regarding structural details of Kir6.2 and SUR1, and how those were interpreted in terms of gating mechanisms, as these data were crucial in interpretation of our own structural data.

### **Kir6.2 structure**

The Kir channel family contains a total of 7 subfamilies (Kir1-Kir7) and at least 15 members identified in humans (Hibino et al., 2010). All Kir channels are characterized by their greater tendency to allow inward rather than outward currents, due to intracellular block by  $Mg^{2+}$  and polyamines at positive membrane potentials (Lopatin et al., 1994) and are critical regulators of membrane excitability. Kir channels show a high degree of evolutionary and structural conservation, with presumably a common fold shared among all members from bacteria to humans. This consists of a tetrameric architecture with two transmembrane helices (TMs) interspersed by the canonical  $K^+$  channel pore loop and selectivity filter, and cytoplasmic N- and

C-termini. The C-terminal domain (CTD) is a relatively large soluble domain which extends the ion permeation pathway and mediates extensive interactions among subunits, many of which play important roles in channel gating (Wang et al., 2012; Whorton & MacKinnon, 2013). The relatively short N-terminus contains a highly variable distal portion and a conserved transverse amphipathic helix termed the “slide helix,” which is speculated to aid in coupling transitions between the CTD and TMD (Kuo et al., 2003; Mannikko et al., 2010; Proks et al., 2004; Winkler et al., 2009).

A hallmark of eukaryotic Kir channel gating is a reliance on phosphatidylinositol-4,5-bisphosphate (PIP<sub>2</sub>) for channel opening (Xie et al., 2007). Crystal structures of Kir2.2 and Kir3.2 in apo and PIP<sub>2</sub>-bound forms provide a structural basis for PIP<sub>2</sub> activation and Kir channel gating transitions (Hansen et al., 2011; Tao et al., 2009; Whorton & MacKinnon, 2011, 2013). These studies have generally recapitulated what has been observed in crystal structures of prokaryotic Kir channels (Bavro et al., 2012; Clarke et al., 2010; Kuo et al., 2003; Zubcevic et al., 2014), with the important caveat that all prokaryotic channels are *inhibited* by PIP<sub>2</sub> rather than activated (Enkvetchakul et al., 2005).

Despite differences in the specifics of how the activity of each Kir channel is regulated, the basic structural principles governing Kir channel opening appear to be conserved. These consist of transitions between the CTD and the TMD that are communicated by the TMD-CTD linker, or C-linker, and the slide helix. These motions converge upon the two primary Kir channel gates: the helix bundle crossing (HBC), a conserved K<sup>+</sup> channel feature which is at the base of TM2 and consists of a bulky hydrophobic residue (usually Phe), and the G-loop gate, which is just below the HBC at the apex of the cytoplasmic domain and is unique to Kir channels.

Crystal structures of all Kir channels studied thus far support the existence of separable “activation” and “opening” steps. Activation in KirBac (prokaryotic) Kir channels likely occurs spontaneously, whereas activation in eukaryotic Kir channels entails PIP2 binding, and in the case of Kir3.2, for example, concomitant interaction with G-proteins. Regardless of the stimulus, in this step the CTD undergoes a mostly rigid-body rotation about the C4 axis which widens the G-loop gate and introduces strain to the inner helices (Bavro et al., 2012; Clarke et al., 2010; Whorton & MacKinnon, 2011, 2013). This rotation is coupled to motions in the slide helix which bring residues from the N-terminus and CTD into register to stabilize a widened G-loop configuration. This activated state, with open G-loop and closed helix bundle crossing gates, has been observed directly in KirBac3.1 and Kir3.2 (GIRK) and is inferred for Kir2.2 on the basis of molecular dynamic simulations (Li et al., 2015). Opening has been harder to observe, and the only structures available for this are of activating mutations of KirBac3.1 and Kir3.2. In these structures, it appears that strain introduced by the CTD rotation promotes a rotation in the TM2 (inner) helices and a bending at a highly conserved glycine within TM2 (Jiang et al., 2002; Jin et al., 2002; Magidovich & Yifrach, 2004), which ultimately dilates the helix bundle crossing wide enough to allow passage of a hydrated  $K^+$  ion.

Kir6.2 is expected to adhere to this general gating model as it possesses all of the conserved structural elements of the Kir channel family and also behaves as a typical inward-rectifier, showing weak inward-rectification and strong PIP2 activation. In particular, key residues involved in activation of Kir3.2 and Kir2.2 are conserved in Kir6.2 and nearly every eukaryotic Kir channel member. These include residues which surround the PIP2 binding site in the slide helix (R54 and D65 in 6.2) in the C-linker (R177, and R206 in 6.2), and are all involved in stabilizing interactions between the N-terminus and the CTD in the PIP2-bound activated state

of Kir2.2. However, Kir6.2 PIP2 sensitivity is profoundly influenced by SUR1, which suggests a unique mechanism by which Kir6.2 engages or responds to PIP2.

Thus overall, Kir channel activation appears to proceed through a conserved sequence of CTD and TMD transitions mediated by the C-linker and possibly the slide helix. However, the specific mechanisms governing eukaryotic and prokaryotic channel opening appear distinct. Aside from the important difference that PIP2 activates and inhibits eukaryotic and prokaryotic Kir channels, respectively, the coupling between the CTD and TMD is also different: 1) Prokaryotic and eukaryotic channel activation (i.e. pre-open states showing HBC dilation) likely occur through CTD rotation in opposite directions (counterclockwise when viewed down the pore from extracellular side for Kir3.2; clockwise for KirBac 3.1). This is significant, as the CCW rotation in eukaryotic Kir channels would promote unwinding of a short helix within the C-linker which is absent in prokaryotic channels, likely allowing for a rearrangement of TMD-CTD interactions in this region. 2) The KirBac CTD may possess far greater rotational freedom than eukaryotic counterparts, as the CTD rotation is much more pronounced in KirBac 3.1 ( $23^\circ$ ) than in Kir3.2 ( $8^\circ$ ) and presumably other eukaryotic Kir channels (Bavro et al., 2012; Whorton & MacKinnon, 2011). This suggests a divergent mechanism by which the TMD engages the CTD in eukaryotic versus prokaryotic channels. 3) CTD rotation in KirBac 3.1 is argued (with some controversy) to be coupled to ion occupancy within the selectivity filter without changes in the HBC gate (Clarke et al., 2010), suggesting that the selectivity filter acts as an independent gate which can be biased towards open or closed states based on the conformation of the CTD. This has not yet been observed in eukaryotic channels and thus it remains to be seen whether this is an anomaly of this particular KirBac channel or a true gating mechanism. Therefore, despite their structural conservation, data gleaned from the study of prokaryotic Kir channels may not directly

apply to eukaryotic channels and vice versa. Further, because so few Kir channels structures are available, any new structure (i.e. a structure of Kir6.2) will go a long way toward a more comprehensive understanding of Kir channel gating.

#### *The ATP-binding site and impact on $K_{ATP}$ channel gating*

Kir6.1/2 are the only members of the eukaryotic Kir channel family to be allosterically inhibited by a physiological ligand. Thus perennial questions in the  $K_{ATP}$  channel field have been: 1) how does ATP inhibit the channel and 2) where is the ATP binding site on Kir6.2? Much could be learned about the mechanism of ATP inhibition solely through a combination of electrophysiological and mutagenesis studies, but identifying the binding site was challenging in the absence of a structure, in large part because the Kir6.1/2 sequences do not contain any known ATP binding motifs.

Single channel kinetic studies have gleaned much of the “how”. In the absence of ATP, the  $K_{ATP}$  channel exhibits spontaneous “intrinsic gating” characterized by short opening and closings referred to as bursts, with predominantly one short open and one short closed time, and long non-conducting interburst intervals, containing multiple closed times (Alekseev et al., 1998; Drain et al., 1998; Enkvetchakul et al., 2000; Fan & Makielski, 1999; Proks et al., 2001). Thus, there is expected to be one open state and at least two closed states (short “intraburst” and long “interburst” states). ATP causes a pronounced decrease in burst duration and extends the interburst closed state, and therefore likely interacts with all of these states (Craig et al., 2008). In more structural terms, the ATP binding site is available in both open and closed states, and ATP binding to either state reduces  $P_O$  by stabilizing the long interburst closed conformation.

Kir6.2 possesses four identical ATP-binding sites comprising residues from both the cytoplasmic N- and C-terminal domains (Cukras et al., 2002; Drain et al., 1998; Proks et al.,

1999; Tucker et al., 1998). The site is thought to reside exclusively on Kir6.2, although SUR1 increases Kir6.2 ATP sensitivity roughly 10-fold (Pratt et al., 2009; Tucker et al., 1997). It is presumed that SUR1 achieves this through stabilization of the ATP-bound conformation of Kir6.2, but functional and mutagenesis data alone cannot entirely rule out a direct role of SUR1 in ATP inhibition of Kir6.2.

The primary readout for identifying key residues involved in ATP inhibition has been to measure either macroscopic or single channel currents of mutant channels. However, this measures ATP sensitivity, not affinity, therefore one must differentiate between direct and indirect effects on ATP binding to Kir6.2. Specifically, mutations which cause an increase in intrinsic  $P_O$  will indirectly reduce ATP inhibition of the  $K_{ATP}$  channel, and vice versa (Cukras et al., 2002; Shyng et al., 1997; Trapp et al., 1998). With this in mind, a number of residues were identified which greatly impact ATP sensitivity without affecting intrinsic gating properties, including R50, I182, K185, R201, Y330, F333, and G334 (Drain et al., 1998; Koster, Sha, Shyng, et al., 1999; Li et al., 2000; Masia, Koster, et al., 2007; Proks et al., 2004; Tammaro et al., 2005). Of these, R50 and K185 were thought to interact directly with the  $\gamma$  and  $\beta$  phosphates of ATP, respectively, based on differential sensitivities to ATP, ADP, and AMP when mutated (Trapp et al., 2003).

A crystal structure of the Kir3.1 cytoplasmic domain enabled homology modelling of this region of Kir6.2 (Nishida & MacKinnon, 2002), which was used as a complementary approach to map the ATP binding site (Antcliff et al., 2005; Trapp et al., 2003). Automated docking into the model placed the ATP binding pocket at the interface of adjacent cytoplasmic N- and C-terminal domains, with one end of the pocket formed by R50 and the opposing by K185, which

appeared to interact with the  $\gamma$  and  $\beta$  phosphates, as had been predicted. Further, other residues predicted to form direct interactions with ATP lined the pocket, including I182, F333, and G334.

The docking of ATP at an interface formed by the N-terminus and the CTD corroborates a wealth of experimental data, however, the details of this binding site model are undoubtedly flawed owing to errors inherent in both ligand docking and homology modeling. The PIP2 binding pocket, as described for Kir2.2 (Hansen et al., 2011) and Kir3.2 (Whorton & MacKinnon, 2011), also lies at an interface of the cytoplasmic N-terminus and the C-linker, adjacent to the putative ATP site, which is interesting given that binding of PIP2 to Kir6.2 displaces ATP analogues and vice versa (MacGregor et al., 2002; Wang et al., 2002). In light of this observation and of the Kir channel gating model described above, in which channel opening relies on a rotation of the CTD to open the G-loop gate and place tension at the base of the M2 helices, which instigates opening of the helix bundle crossing, this tentative placement of ATP allows for an intriguing hypothesis regarding the structural basis for ATP inhibition of Kir6 channels: ATP binding, by coordinating residues from adjacent N- and C-terminal domains, reduces channel  $P_O$  by (1) remodeling the PIP2 binding site thus reducing PIP2 sensitivity, and (2) strengthening interactions between the N-terminus, C-linker, and the CTD in order to prevent CTD rotation and an unwinding of the C-linker which would open the gates.

#### *The PIP2 binding site and impact on channel structure and gating*

Kir6.2, as with all other Kir6s, requires PIP2 for channel opening; thus PIP2 has a profound impact on nearly all aspects of  $K_{ATP}$  channel gating. At the single channel level, PIP2 increases  $P_O$  by lengthening the open time and shortening the inter-burst closed times (Fan & Makielski, 1999). Macroscopically, it reduces ATP sensitivity (Baukrowitz et al., 1998; Fan & Makielski, 1997, 1999; Shyng & Nichols, 1998), by both displacing ATP directly (MacGregor et

al., 2002; Wang et al., 2002) and by increasing  $P_O$ , which indirectly reduces sensitivity to ATP inhibition (Enkvetchakul et al., 2000; Trapp et al., 1998). Further, PIP2 will reduce stimulation by MgADP and KCOs (Baukrowitz et al., 1998; Koster, Sha, & Nichols, 1999) and reduce inhibition by sulfonylureas (Krauter et al., 2001). All of these effects, however, beside the direct effect on ATP sensitivity, are likely a result of the increase in  $P_O$  conferred by PIP2 interaction.

The residues thought to be involved in PIP2 interaction in Kir channels are highly conserved, thus all Kir channels likely possess a common PIP2 binding pocket comprising residues from the base of the M1 (outer) transmembrane helix and the TMD-CTD linker (C-linker) of the same channel subunit. These residues coordinate the phosphatidyl inositol head group, while the acyl chains reside within the inner leaflet of the bilayer and may interact with the M1 and M2 helices, but this region of the PIP2 molecule is mostly disordered in PIP2-bound crystal structures of Kir2.2 and Kir3.2 (Hansen et al., 2011; Whorton & MacKinnon, 2011, 2013).

In terms of the response to PIP2, there is some diversity between the different Kir channel families. Kir2 channels, for example, only require PIP2 for opening (Rohacs et al., 1999; Zhang et al., 1999). PIP2 activation of GIRK channels (Kir3) requires concomitant interaction of the CTD with the G-protein subunits  $G\beta\gamma$  (Huang et al., 1998; Zhang et al., 1999). Kir6 channels also have low intrinsic PIP2 sensitivity which is substantially increased by interaction with sulfonylurea receptors, i.e. Kir6.2 $\Delta$ C channels expressed in the absence of SUR1 show about 10-fold reduced PIP2 sensitivity relative to  $K_{ATP}$  channels (Enkvetchakul et al., 2000).

This mechanistic variability suggests diversity in the impact of PIP2 on Kir channel structure and the structural basis for channel activation. This is in fact what has been observed

for Kir2.2 and Kir3.2. Specifically, Kir2.2, in the absence of PIP2, shows disordered portions of the N-terminus and C-linker near the inner leaflet of the bilayer, and the CTD is “disengaged” from the TMD (Tao et al., 2009). In the PIP2-bound structure, these previously disordered linkers rigidify to form the PIP2 binding pocket and the CTD translates vertically towards the bilayer to engage the TMD, in the process splaying the M2 helices to cause the helix bundle crossing gate to open slightly (yet is still closed overall), whereas the diameter of the G-loop is mostly unaffected (Hansen et al., 2011). In contrast, the Kir3.2 apo and PIP2-bound conformations are nearly identical with the exception of the helix bundle crossing gate, which opens slightly in the PIP2-bound structure owing to a rotation of the M2 (inner) helix (Whorton & MacKinnon, 2011).

Thus it seems likely that the structural mechanism by which Kir6.2 responds to PIP2 is unique. Further, there is reason to believe the way in which PIP2 binds to Kir6.2 is also unique, given the facts that 1) SUR1 increases PIP2 sensitivity of Kir6.2 by roughly 10-fold and 2) Kir6.2 has two mutations at highly conserved positions within the PIP2 binding pocket, Pro69 (Arg in every other Kir) and His175 (consensus residue Lys). Because  $K_{ATP}$  channel PIP2 sensitivity is roughly the same as most other Kir6.2s, an intriguing hypothesis is that SUR1 restores this high sensitivity to Kir6.2 by contributing directly to the binding pocket. Alternatively, there may be specific protein contacts which indirectly stabilize PIP2 interaction with Kir6.2, as is the case with Kir3.2 (Whorton & MacKinnon, 2013).

By expressing Kir6.2 $\Delta$ C channels alone and with various domains of SUR1, it was found that the first transmembrane domain of SUR1, TMD0, is sufficient to restore high  $P_O$  and thus high PIP2 sensitivity to Kir6.2 (Babenko & Bryan, 2003; Chan et al., 2003). TMD0 does not, however, restore the high ATP sensitivity seen in WT  $K_{ATP}$  channels, which suggests that the

regions on SUR1 which both increase channel  $P_O$  and increase ATP inhibition are distinct structures. However, in the absence of a structure of the entire  $K_{ATP}$  channel complex, it is hard to envision a mechanism for these observations and is in fact a major motivation of the work in this dissertation, i.e. to understand the structural basis for how SUR1 conveys information to Kir6.2 in order to regulate sensitivity to ligands and ultimately open probability.

### **SUR1 structure and function**

SUR1 and SUR2 are members of the ABC transporter superfamily, a diverse and ancient class of membrane transporters that are expressed in all domains of life. They are characterized by their ability to mediate ATP-dependent import or export of a wide variety of substrates. SUR is in the ABC exporter subfamily, which contains two transmembrane domains (TMDs) of six helices each and two soluble (usually cytosolic) nucleotide binding domains (NBDs), which can bind and hydrolyze MgATP. Each NBD contains one ATP binding site, and ATP binding is thought to induce dimerization of the two NBDs which stimulates their ATPase activity, as the full ATP binding site at each NBD comprises residues from both NBD1 and NBD2. These transporters typically display the famous “alternating access” mechanism of membrane transport (Jardetzky, 1966), in which NBD dimerization drives conformational change in the TMD to allow transport of substrate across the bilayer. This typically occurs through a transition from an “inward-facing” state, in which the NBDs are separated and the TMD is competent to bind substrate, to an “outward-facing” state, in which NBDs are dimerized and the helices of the TMDs shift to allow access to the external compartment.

SUR1 and SUR2 possess all these basic ABC transporter structural elements, but are unique because 1) they have no known transport substrate, despite still functioning as ATPases, and 2) they are the only members known to form an obligate complex with another protein,

namely Kir6. They do, however, possess the ability to bind to a high diversity of hydrophobic and amphipathic small molecules, most notably the sulfonylureas, but also glinides and potassium channel openers (KCOs), which may reflect their evolutionary history as member of a family of multidrug resistance proteins.

### *TMD0/L0*

In addition to what will be referred to as the “ABC core structure” comprising TMD1, NBD1, TMD2, and NBD2, SUR1 and SUR2 possess an N-terminal transmembrane domain predicted to contain 5 TM helices (Conti et al., 2001) termed TMD0, which is evolutionarily unrelated to TMD1/2, and a cytoplasmic and amphipathic linker domain termed L0 which couples TMD0 to the ABC core structure. A few other members of the ABCC subfamily, to which SUR1/2 belong, also possess these N-terminal structures, e.g. the multidrug resistance associated protein 1 (MRP1), but their functional role in these proteins remains unclear. In SUR, TMD0 has been shown to be the domain primarily responsible for direct interactions with Kir6.2 (Schwappach et al., 2000), and numerous loss-of-function mutations have been identified in this domain which act by disrupting assembly of the channel complex in the ER (reviewed in (Martin et al., 2013)).

TMD0 also has a profound effect on Kir6.2 gating. TMD0 alone can increase surface expression of and co-assemble with Kir6.2 to form so-called “mini-K<sub>ATP</sub>” channels, which display similar single channel kinetics and open probability as WT channels without response to Mg<sup>2+</sup> nucleotides or allosteric modulators (Babenko & Bryan, 2003; Chan et al., 2003). It is thought that TMD0 achieves this primarily through stabilization of PIP2 interaction with Kir6.2 (Pratt et al., 2011), but this is likely an oversimplification. For example, the nominally loss-of-function mutations in TMD0 E128K and R74W reduce surface expression by disrupting K<sub>ATP</sub>

channel assembly, but paradoxically cause gain-of-function once at the plasma membrane by reducing ATP sensitivity while at the same time reducing channel  $P_O$  (Pratt et al., 2009). Thus these mutations are said to “functionally uncouple” SUR1 from Kir6.2, and suggest that structures within TMD0 are necessary to confer both high  $P_O$  and hypersensitivity to ATP.

At the cytosolic end of TM5 of TMD0 (resi 195) begins the roughly 100 amino acid linker termed L0. There are two predicted amphipathic helices in L0 which are both critically involved in  $K_{ATP}$  structure and function. One is termed the “sliding helix” (Babenko, 2005) based on analogy to the Kir6.2 “slide helix,” and is predicted to lie between K205–F217. Co-expression of this region along with TMD0 (resi 1-232 of SUR1) affords Kir6.2 maximal  $P_O$  (near 0.9) (Babenko & Bryan, 2003), yet interestingly mutations within the sliding helix, e.g. K205, dramatically reduce ATP sensitivity (Pratt et al., 2012). A second amphipathic helix is predicted to lie between Y230 and K242 and is in fact the most highly conserved region of TMD0/L0 within the ABCC subfamily. Removal of this helix from SUR1 (Zhou and Shyng, unpublished) or MRP1 (Bakos et al., 2000) completely prevents trafficking out of the ER, suggesting a critical role in folding or stability of an SUR1 monomer. Functionally, this helix reverses the stimulatory effect on  $P_O$  conferred by the “sliding helix”, thus L0 is said to exert “bidirectional” control on  $K_{ATP}$  channel gating (Bryan et al., 2004), likely by modulating both ATP and PIP2 sensitivity via distinct structures. Therefore, because of the multiple critical roles that TMD0 and L0 play, any understanding of  $K_{ATP}$  channel structure and function relies on understanding the structure of this domain; but of course this has been difficult to address in the absence of any known homologous structures.

*The ABC core structure of SUR1*

SUR1 is a so-called “full transporter,” which has TMD1, NBD1, TMD2, and NBD2 on a single polypeptide, as opposed to “half-transporters” where two separate polypeptides each contribute one TMD and one NBD which assemble as either homo- or hetero-dimers. The topology of the TMDs was shown through a combination of biochemical experiments and sequence analysis (Aguilar-Bryan et al., 1995; Conti et al., 2001; Tusnady et al., 1997), which generally agreed with homology models of the few crystal structures of eukaryotic full transporters available, e.g. P-glycoprotein (PgP) (Aller et al., 2009). In general, however, the TMDs are less well-conserved than the NBDs, which limits the accuracy of these models (~10-15% identity of SUR1 to PgP in TMD1/2).

Each TMD is followed by an NBD through highly variable linkers of around 20-25 amino acids. The NBDs are much more well conserved across the whole ABC transporter family (35% identity between NBDs of SUR1 and PgP), which reflects their role as enzymes in ATP binding and hydrolysis. Each NBD contains one nucleotide binding site, and in most ABC transporters these are both functionally active. SUR1, along with most other members of the ABCC subfamily (MRP1, CFTR) has one active (NBD2) and one inactive (NBD1) site, referred to as the consensus and degenerate sites, respectively. In either case, MgATP binding to each NBD stimulates dimerization of the NBDs through a rearrangement of the TMD helices. Upon forming the so-called “sandwich” dimer, the ATP binding site of each NBD becomes catalytically complete, thus enabling ATP hydrolysis. Bound ADP will stabilize the NBD dimer, and upon dissociation will favor NBD dimer dissociation and a resetting of the nucleotide cycle. In most ABC exporters this is coupled to export of substrate out of the cell, whereas in SUR1 or SUR2 NBD dimerization increases Kir6 channel  $P_O$ .

*The effect of MgADP/MgATP on  $K_{ATP}$  channel activity*

The  $K_{ATP}$  channel is a metabolic sensor as it is inhibited by ATP, via direct interaction with the Kir6.2 CTD, and stimulated by MgADP via interaction with the NBDs of SUR1. ADP stimulation is thought to occur by antagonizing ATP inhibition of Kir6.2 (Nichols et al., 1996; Terzic et al., 1995), and because ATP concentrations in the  $\beta$ -cell are almost always high enough to fully inhibit Kir6.2 ( $IC_{50} \sim 10 \mu M$ ), the  $K_{ATP}$  channel is functionally an ADP sensor, as MgADP levels experience much greater relative fluctuations in concentrations than does ATP. Thus SUR1, by sensing MgADP levels in the cell, endows the  $K_{ATP}$  channel with a greater dynamic range of physiological response.

A huge question in the field is how Mg-nucleotide interaction with the NBDs of SUR1 actually modulates the Kir6.2 pore. Biochemically, it has been shown that NBD1 lacks ATPase activity and binds ATP in a  $Mg^{2+}$ -independent manner (Matsuo et al., 1999; Matsuo et al., 2000), whereas NBD2 is a functional ATPase requiring  $Mg^{2+}$  for interaction with nucleotide (Bienengraeber et al., 2000; de Wet et al., 2007; Masia et al., 2005; Zingman et al., 2001). Thus NBD1 and NBD2 appear to have distinct roles in nucleotide activation. Mutation of a conserved lysine within the ATP-binding pocket of NBD1 (K719) reduces high-affinity 8-azido-[ $\alpha$ - $^{32}P$ ]ATP labeling (Ueda et al., 1997) and markedly shifts the  $EC_{50}$  for MgADP activation (Proks et al., 2014), which suggests that ATP binding at NBD1 is necessary for dimerization with NBD2 and thus stimulation of channel activity. At NBD2, the post-hydrolytic state favors channel opening but ATP hydrolysis at NBD2 is not necessary *per se*, as MgADP is sufficient to activate the channel. This is supported by the fact that orthovanadate, which mimics the  $\gamma$ -phosphate and greatly stabilizes the post-hydrolytic MgADP·Pi state, stimulates channel opening in the absence of any hydrolyzable ATP (Zingman et al., 2001). In contrast, BeF<sub>3</sub>, which inhibits ATP hydrolysis of SUR1 and SUR2 (de Wet et al., 2010; de Wet et al., 2007) by stabilizing a

prehydrolytic MgATP bound state (MgADP·BeF), instigates  $K_{ATP}$  channel closure and blocks MgADP activation (Zingman et al., 2001).

Because MgATP/ADP both simultaneously inhibit and stimulate channel activity through direct interactions with Kir6.2 and SUR1, respectively, it is hard to isolate the role of Mg-nucleotide interaction at the NBDs on  $K_{ATP}$  channel gating. This was achieved by utilization of a disease mutation G334D in Kir6.2, which all but eliminates ATP inhibition at Kir6.2 without impacting intrinsic gating properties (Masia, Koster, et al., 2007; Proks et al., 2010). Thus in G334D-Kir6.2/WT-SUR1 channels, the same maximal  $P_O$  (0.83) was achieved for both MgADP and MgATP, with MgADP being about 10X more potent, without any inhibitory component seen in WT channels. This suggests that MgADP/ATP stimulate channel activity not just by antagonizing ATP inhibition but by directly increasing open probability, which is likely a result of strengthening PIP2 interactions with Kir6.2.

#### *Allosteric regulation of $K_{ATP}$ channel activity*

$K_{ATP}$  channels have a rich pharmacology mediated through SUR1/SUR2. Sulfonylureas and glinides are the two primary classes of inhibitors and generally have higher affinity for SUR1 than SUR2 (Gribble & Ashcroft, 1999; Gribble, Tucker, Seino, et al., 1998; Reimann et al., 2001; Song & Ashcroft, 2001). These compounds have been in use for decades as oral therapeutics for type 2 diabetes, as inhibiting  $K_{ATP}$  channel activity in the  $\beta$ -cell mimics high glucose to stimulate insulin secretion. There is also a structurally very diverse class of activators (KCOs) (Coghlan et al., 2001; Mannhohld, 2004) which also display subunit specificity, i.e. SUR1 is primarily only responsive to diazoxide (Aguilar-Bryan et al., 2001; Shyng et al., 1997) and a novel activator VU0071063 (Raphemot et al., 2014), whereas SUR2 responds to a wide array of KCOs with sometimes very high affinity (Ashcroft & Gribble, 2000; Bryan et al., 2004;

Uhde et al., 1999; Yamada & Kurachi, 2004). Because SUR2 is prominently expressed in vascular smooth muscle, KCOs are sometimes used clinically as vasodilators, as activation of  $K_{ATP}$  channels here will attenuate action potential firing to reduce contractility.

The search to understand the mechanism of action of sulfonylureas, in a sense, began with their discovery in the 1940s and continues today. This work was greatly aided by the cloning of SUR1 and Kir6.2 (Aguilar-Bryan et al., 1995; Inagaki et al., 1995), which allowed definitive assignment of SUR as the receptor and sulfonylureas' classification as allosteric inhibitors. More specifically, sulfonylureas are partial antagonists of  $K_{ATP}$  channel activity as they only induce ~80% inhibition in macroscopic patches (Gribble, Tucker, et al., 1997), and single-channel experiments revealed the reason: that sulfonylurea-bound channels can still open, but with reduced  $P_O$  (Barrett-Jolley & Davies, 1997). One primary mechanism by which sulfonylureas act is by reducing MgADP stimulation (Gribble, Tucker, et al., 1997); conversely, MgATP interaction with SUR1 reduces binding of the high affinity sulfonyurea glibenclamide (Hambrock et al., 2002; Schwanstecher et al., 1991). Thus it has been speculated that sulfonylureas interact primarily with the “inward-facing” conformation, in which the NBDs are separated, and that binding to this state prevents Mg-nucleotide induced NBD dimerization and transition to an “outward-facing” conformation, if one exists for SUR1, and that they do this by binding within the TMDs to act as a wedge to actively block TM movement (Bryan et al., 2004; Ortiz et al., 2012).

However, a true understanding of the mechanism of allosteric regulation by a small molecule relies on knowledge of the binding pocket, something that has been difficult to determine for SUR1. Utilizing chimeras between SUR1 and SUR2, a single residue in TMD2, S1238 in SUR1, was identified as necessary for high affinity sulfonylurea inhibition (Ashfield et

al., 1999; Babenko, Gonzalez, & J., 1999). L0, but not TMD0, was also shown to be involved (Mikhailov et al., 2001), and this was later localized to two residues in the conserved L0 amphipathic helix, Y230 and W232 (Vila-Carriles et al., 2007). Interestingly, early studies with the photo-crosslinkable sulfonylurea [<sup>125</sup>I]-azido-glibenclamide (Chudziak et al., 1994) showed specific labelling of both SUR1 and Kir6.2 (Clement et al., 1997; Schwanstecher et al., 1994), and the region necessary for labelling of Kir6.2 was the Kir6.2 distal N-terminus (Vila-Carriles et al., 2007).

Yet it was difficult to envision a physical binding pocket comprising these disparate regions of the complex, as L0 lacked any homologues of known structure and the distal N-terminus of Kir channels is disordered and typically removed for crystallography. Thus a structure of the channel complex bound to sulfonylureas is crucial to gain insight into: 1) the mechanism of sulfonylurea inhibition, which is so commonly taken advantage of to treat type 2 diabetes; and 2) the ability of SUR1 to accommodate such a wide array of small molecules, as the binding pocket seems to tolerate numerous modifications to both the sulfonylurea and glinide backbones.

### **K<sub>ATP</sub> channels and disease**

Cloning of the K<sub>ATP</sub> channel subunits was followed almost immediately by identification of mutations within SUR1 and Kir6.2 associated with insulin secretion disorders (Ashcroft, 2007). These mutations fall into two categories: *gain-of-function*, which generally increase P<sub>O</sub> and reduce ATP inhibition, and *loss-of-function*, which either result from a gating defect (i.e. reduced P<sub>O</sub>) or an expression or trafficking defect, resulting in *de facto* loss-of-function by reducing or eliminating plasma membrane expression of the channel complex.

Gain of function mutations in Kir6.2 or SUR1 are the most common cause of neonatal diabetes (NDM), a rare disease (1 in 200,000 live births) characterized by sometimes severe diabetes which manifests in the first six months of life (Edghill et al., 2004). Many mutations in both SUR1 and Kir6.2 have been characterized in recombinant systems (Aguilar-Bryan & Bryan, 2008; McTaggart et al., 2010; Zhou et al., 2010), and it was shown that all reduce inhibition by ATP at physiologically relevant concentrations. This results in hyperpolarization of the  $\beta$ -cell membrane even at high glucose, effectively impairing or eliminating glucose stimulated insulin secretion. Until the mid-2000s, most patients were treated exclusively with insulin, as it was assumed NDM was an early onset form of Type I diabetes. The discovery that most cases are the result of activating  $K_{ATP}$  channel mutations allowed for ~90% of these patients to be transferred to sulfonylureas, which are able to inhibit mutant channels and thus offer a much more convenient and also very effective way to manage blood sugar (Gloyn et al., 2004; Pearson et al., 2006).

In contrast, loss-of-function mutations in  $K_{ATP}$  channel subunits are the most common cause of congenital hyperinsulinism (CHI), also a rare disease (1 in 50,000 live births) which is characterized by persistent insulin secretion irrespective of blood glucose (Dunne et al., 2004; Snider et al., 2013). Mutations impairing both trafficking and gating are found throughout the sequences of both proteins, though NBD2 contains an unusually high density of gating mutations which impair MgADP stimulation, indicative of the special role of NBD2 in Mg-nucleotide regulation of  $K_{ATP}$  channel activity. Treatment options for CHI are limited, though a number of patients with gating mutations (low  $P_O$ ) are successfully treated with the KCO diazoxide, which opens channels in order to attenuate action potential firing in the  $\beta$ -cell and thus reduce insulin secretion. All loss-of-function mutations due to defective trafficking are obviously diazoxide-

unresponsive, and the only treatment for these patients is partial or near complete removal of the pancreas, resulting in lifelong insulin dependence.

#### *Pharmacological correction of CHI trafficking mutations*

The discovery that a subset of CHI mutations causes defective trafficking of the channel complex (Cartier et al., 2001) placed this form of CHI in a broad class of diseases referred to as proteostasis disorders (Powers et al., 2009). These are mutations that do not necessarily affect function but rather the folding and/or assembly of the protein, and in the case of membrane proteins, an inability to traffic out of the ER leading to ER-associated degradation (ERAD). Close to 90% of cystic fibrosis cases are the result of such a trafficking mutation,  $\Delta F508$  in the cystic fibrosis transmembrane conductance regulator (CFTR), which is another member of the ABCC subfamily containing SUR1 and SUR2.

CHI trafficking mutations have been identified throughout the SUR1 and Kir6.2 sequences. Interestingly, for a subset of these mutations found almost exclusively within TMD0 of SUR1, the trafficking defect could be overcome by expressing channel subunits in the presence of sulfonylureas (Martin et al., 2013; Yan et al., 2004; Yan et al., 2006; Yan et al., 2007), and they achieve this by directly binding to the channel complex to enhance maturation and slow degradation. Furthermore, most TMD0 trafficking mutants rescued by the low-affinity sulfonylurea tolbutamide (which unbinds rapidly upon buffer exchange) showed normal ATP inhibition as well as MgADP and diazoxide stimulation (Yan et al., 2004; Yan et al., 2007). Because these are in essence specific, small-molecule versions of molecular chaperones in the ER, sulfonylureas (and also glinides) are termed pharmacological chaperones (PCs), and because most of the mutations they correct produce functional channels, they are a potential therapy for this form of CHI.

The most effective PCs for TMD0 trafficking mutations are very high affinity inhibitors with very slow off rates, notably glibenclamide (GBC) and repaglinide (RPG), and experimentally it is nearly impossible to record currents from channels rescued with these drugs, even hours after drug removal. Thus in terms of therapy, there is a need to identify PCs which are both safe and effective, but also unbind or can be displaced by channel activators in order to attenuate insulin secretion.

Based on a screen for CFTR correctors, carbamazepine (CBZ) was identified as a novel PC which could rescue the same TMD0 trafficking mutations as GBC and RPG but lacking the near irreversible inhibition of channel activity to allow for functional expression and activation with diazoxide (Chen, Olson, et al., 2013). CBZ is also in use clinically as an anti-convulsant (trade name tegretol) and has an established pharmacological profile. Thus while the ideal PC for CHI would be a  $K_{ATP}$  channel activator (none of which rescue CHI trafficking mutations), CBZ nonetheless represents significant progress toward the goal of identifying small-molecule therapies for diazoxide-unresponsive CHI.

Because CBZ is structurally unrelated to sulfonylureas or glinides, much stands to be learned by studying the mechanism of GBC- and CBZ-mediated rescue of mutant  $K_{ATP}$  channels regarding 1) the nature of the sulfonylurea binding pocket and how it can accommodate such a diversity of small molecules and 2) the mechanism of allosteric inhibition of  $K_{ATP}$  channel gating.

### **Towards a mechanism of PC rescue**

We had shown that CBZ binds with high affinity to the channel complex and that, like GBC, strengthens interactions between SUR1 and the distal N-terminus of Kir6.2 (Devaraneni et al., 2015), a region known to be important for channel biogenesis. The chaperone effect of both

CBZ and GBC appears to be dependent on the N-terminal 30 amino acids of Kir6.2; because the N-terminus was also necessary for photoaffinity labelling of Kir6.2 by [<sup>125</sup>I]-azido-GBC (Vila-Carriles et al., 2007), this suggested that both CBZ and GBC, despite being structurally unrelated, bound to the same pocket in SUR1 that also included at least some portion of the N-terminal 30 amino acids of Kir6.2. Therefore I hypothesize that this tripartite interaction stabilizes an otherwise transient association of the Kir6.2 N-terminus and SUR1, and in the context of CHI-causing trafficking mutations in TMD0, compensates for a weakened association between TMD0 and Kir6.2 to allow for proper assembly and expression at the plasma membrane.

In this dissertation, I have utilized a combination of biochemistry and structural biology in order to test this hypothesis. The first chapter builds on the initial finding that CBZ is a K<sub>ATP</sub> channel PC by characterizing a novel set of CHI mutations in TMD0 identified immediately prior to my joining the lab. In this study we tested the function and expression of 14 new patient mutations and showed that each mutation impacted K<sub>ATP</sub> channel surface expression, with some being more severe than others, and showed that the trafficking defect could be overcome by both CBZ and GBC in a majority of cases. Further, most mutations displayed normal gating responses and diazoxide stimulation following removal of CBZ. As observed previously, we showed that GBC and CBZ stabilize an interaction between the N-terminus of Kir6.2 and SUR1, and that channel activators, none of which enhance channel trafficking, do not promote or even destabilize this interaction.

These data suggest that CBZ and GBC act by binding directly to the same pocket in SUR1 that included the Kir6.2 N-terminus, and that this underlies their inhibition mechanism. Perhaps the most direct way of testing this hypothesis is to solve structures of the channel

complex bound to CBZ and GBC. Advances in camera technology and image processing methods which took place as I was beginning work on Chapter 2 made solving a structure by cryo-electron microscopy a distinct possibility, as the method requires far less purified protein and does not require growth of large, highly ordered crystals. Until now, these requirements had inhibited structure solution of any domain of the  $K_{ATP}$  channel, let alone the intact channel complex.

Thus chapters 3-5 utilize these advances to (1) solve the first structure of the WT intact channel complex (chapter 3) in the presence of ATP and GBC, elucidating the overall architecture of the complex, the structure of TMD0/L0, and the ATP-binding site; (2) improve the ATP+GBC-bound reconstruction to near-atomic resolution, to allow for construction of an atomic model for most of the protein and elucidation of the sulfonylurea binding site and details of the mode of GBC binding to SUR1 (chapter 4); and (3) solve structures in the presence of CBZ and repaglinide, either with or without ATP, in order to elucidate the nature of the sulfonylurea binding pocket in SUR1 and to clarify the mechanism of inhibition of Kir6.2 activity by allosteric SUR1 ligands and by direct interaction of ATP with Kir6.2 (chapter 5).

These studies have contributed greatly to our understanding of  $K_{ATP}$  channel biology, and the methods established in this dissertation can be immediately applied to address the mechanism of PIP2 and Mg-nucleotide activation of the channel, which were not directly studied here. This work also lays the foundation for many years of structure-function experiments by providing much-needed context to interpret these data and formulate new hypotheses in order to gain a comprehensive understanding of the role of  $K_{ATP}$  channels in GSIS.

## References Cited

- Aguilar-Bryan, L., & Bryan, J. (2008). Neonatal diabetes mellitus. *Endocr Rev*, 29(3), 265-291. doi:10.1210/er.2007-0029
- Aguilar-Bryan, L., Bryan, J., & Nakazaki, M. (2001). Of mice and men: K(ATP) channels and insulin secretion. *Recent Prog Horm Res*, 56, 47-68.
- Aguilar-Bryan, L., Nelson, D. A., Vu, Q. A., Humphrey, M. B., & Boyd, A. E., 3rd. (1990). Photoaffinity labeling and partial purification of the beta cell sulfonylurea receptor using a novel, biologically active glyburide analog. *J Biol Chem*, 265(14), 8218-8224.
- Aguilar-Bryan, L., Nichols, C. G., Wechsler, S. W., Clement, J. P. t., Boyd, A. E., 3rd, Gonzalez, G., . . . Nelson, D. A. (1995). Cloning of the beta cell high-affinity sulfonylurea receptor: a regulator of insulin secretion. *Science*, 268(5209), 423-426.
- Alekseev, A. E., Brady, P. A., & Terzic, A. (1998). Ligand-insensitive state of cardiac ATP-sensitive K<sup>+</sup> channels. Basis for channel opening. *J Gen Physiol*, 111(2), 381-394.
- Aller, S. G., Yu, J., Ward, A., Weng, Y., Chittaboina, S., Zhuo, R., . . . Chang, G. (2009). Structure of P-glycoprotein reveals a molecular basis for poly-specific drug binding. *Science*, 323(5922), 1718-1722. doi:10.1126/science.1168750
- Antcliff, J. F., Haider, S., Proks, P., Sansom, M. S., & Ashcroft, F. M. (2005). Functional analysis of a structural model of the ATP-binding site of the KATP channel Kir6.2 subunit. *EMBO J*, 24(2), 229-239. doi:10.1038/sj.emboj.7600487
- Ashcroft, F. M. (2005). ATP-sensitive potassium channelopathies: focus on insulin secretion. *J Clin Invest*, 115(8), 2047-2058. doi:10.1172/JCI25495
- Ashcroft, F. M. (2007). The Walter B. Cannon Physiology in Perspective Lecture, 2007. ATP-sensitive K<sup>+</sup> channels and disease: from molecule to malady. *Am J Physiol Endocrinol Metab*, 293(4), E880-889. doi:10.1152/ajpendo.00348.2007
- Ashcroft, F. M., & Gribble, F. M. (2000). New windows on the mechanism of action of K(ATP) channel openers. *Trends Pharmacol Sci*, 21(11), 439-445.
- Ashcroft, F. M., Harrison, D. E., & Ashcroft, S. J. (1984). Glucose induces closure of single potassium channels in isolated rat pancreatic beta-cells. *Nature*, 312(5993), 446-448.
- Ashcroft, F. M., Kakei, M., Kelly, R. P., & Sutton, R. (1987). ATP-sensitive K<sup>+</sup> channels in human isolated pancreatic B-cells. *FEBS Lett*, 215(1), 9-12.
- Ashfield, R., Gribble, F. M., Ashcroft, S. J., & Ashcroft, F. M. (1999). Identification of the high-affinity tolbutamide site on the SUR1 subunit of the K(ATP) channel. *Diabetes*, 48(6), 1341-1347.
- Ashford, M. L. J., Sturgess, N. C., Trout, N. J., Gardner, N. J., & Hales, C. N. (1988). Adenosine-5' -triphosphate-sensitive ion channels in neonatal rat cultured central neurones. *Pflügers Archiv*, 412(3), 297-304.
- Babenko, A. P. (2005). K(ATP) channels "vingt ans apres": ATG to PDB to Mechanism. *J Mol Cell Cardiol*, 39(1), 79-98. doi:10.1016/j.yjmcc.2004.12.004
- Babenko, A. P., & Bryan, J. (2003). Sur domains that associate with and gate KATP pores define a novel gatekeeper. *J Biol Chem*, 278(43), 41577-41580. doi:10.1074/jbc.C300363200
- Babenko, A. P., Gonzalez, G., & J., B. (1999). The tolbutamide site of SUR1 and a mechanism for its functional coupling to KATP channel closure. *FEBS Lett*, 459(3), 367-376.
- Bakos, E., Evers, R., Calenda, G., Tusnady, G. E., Szakacs, G., Varadi, A., & Sarkadi, B. (2000). Characterization of the amino-terminal regions in the human multidrug resistance protein (MRP1). *J Cell Sci*, 113 Pt 24, 4451-4461.

- Bander, A. (1969). Chemical structure and blood glucose lowering effect. *Acta Diabetol Lat*, 6(Suppl 1), 429-440.
- Bander, A., Creutzfeldt, W., Dorfmueller, T., Ehrhart, H., Marx, R., Maske, H., . . . Ulrich, H. (1956). Oral therapy of diabetes mellitus by N-tolyl-sulfonyl-N'-butyl urea (D 860); clinical and experimental studies. *Deutsche Medizinische Wochenschrift*, 81(21), 823-846.
- Barrett-Jolley, R., & Davies, N. W. (1997). Kinetic analysis of the inhibitory effect of glibenclamide on KATP channels of mammalian skeletal muscle. *J Membrane Biol*, 155(3), 257-262.
- Baukowitz, T., Schulte, U., Oliver, D., Herlitze, S., Krauter, T., Tucker, S. J., . . . Fakler, B. (1998). PIP2 and PIP as determinants for ATP inhibition of KATP channels. *Science*, 282(5391), 1141-1144.
- Bavro, V. N., De Zorzi, R., Schmidt, M. R., Muniz, J. R., Zubcevic, L., Sansom, M. S., . . . Tucker, S. J. (2012). Structure of a KirBac potassium channel with an open bundle crossing indicates a mechanism of channel gating. *Nat Struct Mol Biol*, 19(2), 158-163. doi:10.1038/nsmb.2208
- Bichet, D., Haass, F. A., & Jan, L. Y. (2003). Merging functional studies with structures of inward-rectifier K(+) channels. *Nat Rev Neurosci*, 4(12), 957-967.
- Bienengraeber, M., Alekseev, A. E., Abraham, M. R., Carrasco, A. J., Moreau, C., Vivaudou, M., . . . Terzic, A. (2000). ATPase activity of the sulfonylurea receptor: a catalytic function for the KATP channel complex. *FASEB J*, 14(13), 1943-1952. doi:10.1096/fj.00-0027com
- Brayden, J. E. (2002). Functional roles of KATP channels in vascular smooth muscle. *Clin Exp Pharmacol Physiol*, 29(4), 312-316.
- Bryan, J., Vila-Carriles, W. H., Zhao, G., Babenko, A. P., & Aguilar-Bryan, L. (2004). Toward linking structure with function in ATP-sensitive K+ channels. *Diabetes*, 53 Suppl 3, S104-112.
- Cartier, E. A., Conti, L. R., Vandenberg, C. A., & Shyng, S. L. (2001). Defective trafficking and function of KATP channels caused by a sulfonylurea receptor 1 mutation associated with persistent hyperinsulinemic hypoglycemia of infancy. *Proc Natl Acad Sci U S A*, 98(5), 2882-2887. doi:10.1073/pnas.051499698
- Chan, K. W., Zhang, H., & Logothetis, D. E. (2003). N-terminal transmembrane domain of the SUR controls trafficking and gating of Kir6 channel subunits. *EMBO J*, 22(15), 3833-3843. doi:10.1093/emboj/cdg376
- Chen, P. C., Olson, E. M., Zhou, Q., Kryukova, Y., Sampson, H. M., Thomas, D. Y., & Shyng, S. L. (2013). Carbamazepine as a novel small molecule corrector of trafficking-impaired ATP-sensitive potassium channels identified in congenital hyperinsulinism. *J Biol Chem*, 288(29), 20942-20954. doi:10.1074/jbc.M113.470948
- Cheng, Y. (2015). Single-Particle Cryo-EM at Crystallographic Resolution. *Cell*, 161(3), 450-457.
- Chudziak, F., Schwanstecher, M., Laatsch, H., & Panten, U. (1994). Synthesis of a I-125 labelled azido-substituted glibenclamide analogue for photoaffinity labelling of the sulfonylurea receptor. *J Labelled Compd Radiopharm*, 34, 675-680.
- Clarke, O. B., Caputo, A. T., Hill, A. P., Vandenberg, J. I., Smith, B. J., & Gulbis, J. M. (2010). Domain reorientation and rotation of an intracellular assembly regulate conduction in Kir potassium channels. *Cell*, 141(6), 1018-1029.

- Clement, J. P. t., Kunjilwar, K., Gonzalez, G., Schwanstecher, M., Panten, U., Aguilar-Bryan, L., & Bryan, J. (1997). Association and stoichiometry of K(ATP) channel subunits. *Neuron*, *18*(5), 827-838.
- Coghlan, M. J., Carroll, W. A., & Gopalakrishnan, P. (2001). Recent developments in the biology and medicinal chemistry of potassium channel modulators: update from a decade of progress. *J Med Chem*, *44*(11), 1627-1653.
- Conti, L. R., Radeke, C. M., Shyng, S. L., & Vandenberg, C. A. (2001). Transmembrane topology of the sulfonylurea receptor SUR1. *J Biol Chem*, *276*(44), 41270-41278. doi:10.1074/jbc.M106555200
- Cook, D. L., & Hales, C. N. (1984). Intracellular ATP directly blocks K<sup>+</sup> channels in pancreatic B-cells. *Nature*, *311*(5983), 271-273.
- Craig, T. J., Ashcroft, F. M., & Proks, P. (2008). How ATP inhibits the open K(ATP) channel. *J Gen Physiol*, *132*(1), 131-144. doi:10.1085/jgp.200709874
- Cukras, C. A., Jeliaskova, I., & Nichols, C. G. (2002). The role of NH<sub>2</sub>-terminal positive charges in the activity of inward rectifier KATP channels. *J Gen Physiol*, *120*(3), 437-446.
- de Wet, H., Fotinou, C., Amad, N., Dreger, M., & Ashcroft, F. M. (2010). The ATPase activities of sulfonylurea receptor 2A and sulfonylurea receptor 2B are influenced by the C-terminal 42 amino acids. *FEBS J*, *277*(12), 2654-2662.
- de Wet, H., Mikhailov, M. V., Fotinou, C., Dreger, M., Craig, T. J., Venien-Bryan, C., & Ashcroft, F. M. (2007). Studies of the ATPase activity of the ABC protein SUR1. *FEBS J*, *274*(14), 3532-3544.
- Dean, P. M., & Matthews, E. K. (1968). Electrical activity in pancreatic islet cells. *Nature*, *219*(5152), 389-390.
- Devaraneni, P. K., Martin, G. M., Olson, E. M., Zhou, Q., & Shyng, S. L. (2015). Structurally distinct ligands rescue biogenesis defects of the KATP channel complex via a converging mechanism. *J Biol Chem*, *290*(12), 7980-7991. doi:10.1074/jbc.M114.634576
- Drain, P., Li, L., & Wang, J. (1998). KATP channel inhibition by ATP requires distinct functional domains of the cytoplasmic C terminus of the pore-forming subunit. *Proc Natl Acad Sci U S A*, *95*(23), 13953-13958.
- Dunne, M. J., Cosgrove, K. E., Shepherd, R. M., Aynsley-Green, A., & Lindley, K. J. (2004). Hyperinsulinism in infancy: from basic science to clinical disease. *Physiol Rev*, *84*(1), 239-275.
- Dunne, M. J., & Peterson, O. H. (1986). Intracellular ADP activates K<sup>+</sup> channels that are inhibited by ATP in an insulin-secreting cell line. *FEBS Lett*, *208*(59-62).
- Edghill, E. L., Gloyn, A. L., Gillespie, K. M., Lambert, A. P., Raymond, N. T., Swift, P. G., . . . Hattersley, A. T. (2004). Activating mutations in the KCNJ11 gene encoding the ATP-sensitive K channel subunit Kir6.2 are rare in clinically defined type 1 diabetes diagnosed before 2 years. *Diabetes*, *53*(11), 2998-3001.
- Enkvetchakul, D., Jeliaskova, I., & Nichols, C. G. (2005). Direct modulation of Kir channel gating by membrane phosphatidylinositol 4,5-bisphosphate. *J Biol Chem*, *280*(43), 35785-35788.
- Enkvetchakul, D., Loussouarn, G., Makhina, E., Shyng, S. L., & Nichols, C. G. (2000). The kinetic and physical basis of K(ATP) channel gating: toward a unified molecular understanding. *Biophys J*, *78*(5), 2334-2348. doi:10.1016/S0006-3495(00)76779-8
- Fan, Z., & Makielski, J. C. (1997). Anionic phospholipids activate ATP-sensitive potassium channels. *J Biol Chem*, *272*(9), 5388-5395.

- Fan, Z., & Makielski, J. C. (1999). Phosphoinositides decrease ATP sensitivity of the cardiac ATP-sensitive K(+) channel. A molecular probe for the mechanism of ATP-sensitive inhibition. *J Gen Physiol*, *114*(2), 251-269.
- Gaines, K. L., Hamilton, S., & Boyd, A. E. (1988). Characterization of the sulfonylurea receptor on beta cell membranes. *J Biol Chem*, *263*(6), 2589-2592.
- Gloyn, A. L., C., D.-Z., Edghill, E. L., Bellane-Chantelot, C., Nivot, S., Coutant, R., . . . Robert, J. J. (2006). KCNJ11 activating mutations are associated with developmental delay, epilepsy and neonatal diabetes syndrome and other neurological features. *Eur J Hum Genet*, *14*(7), 824-830.
- Gloyn, A. L., Pearson, E. R., Antcliff, J. F., Proks, P., Bruining, G. J., Slingerland, A. S., . . . Hattersley, A. T. (2004). Activating mutations in the gene encoding the ATP-sensitive potassium-channel subunit Kir6.2 and permanent neonatal diabetes. *N Engl J Med*, *350*(18), 1838-1849. doi:10.1056/NEJMoa032922
- Gribble, F. M., & Ashcroft, F. M. (1999). Differential sensitivity of  $\beta$ -cell and extrapancreatic KATP channels to gliclazide. *Diabetologia*, *42*(7), 845-848.
- Gribble, F. M., Tucker, S. J., & Ashcroft, F. M. (1997). The essential role of the Walker A motifs of SUR1 in K-ATP channel activation by Mg-ADP and diazoxide. *EMBO J*, *16*, 1145-1152.
- Gribble, F. M., Tucker, S. J., & Ashcroft, F. M. (1997). The interaction of nucleotides with the tolbutamide block of cloned ATPsensitive K<sup>+</sup> channel currents expressed in *Xenopus*. *J Physiol*, *504*(Pt 1), 35-45.
- Gribble, F. M., Tucker, S. J., Haug, T., & Ashcroft, F. M. (1998). MgATP activates the beta cell KATP channel by interaction with its SUR1 subunit. *Proc Natl Acad Sci U S A*, *95*(12), 7185-7190.
- Gribble, F. M., Tucker, S. J., Seino, S., & Ashcroft, F. M. (1998). Tissue specificity of sulfonylureas: studies on cloned cardiac and beta-cell K(ATP) channels. *Diabetes*, *47*(9), 1412-1418.
- Haider, S., Tarasov, A. I., Craig, T. J., Sansom, M. S. P., & Ashcroft, F. M. (2007). Identification of the PIP2-binding site on Kir6.2 by molecular modelling and functional analysis. *EMBO J*, *26*(16), 3749-3759.
- Hambrock, A., Loffler-Walz, C., & Quast, U. (2002). Glibenclamide binding to sulphonylurea receptor subtypes: dependence on adenine nucleotides. *Br J Pharmacol*, *136*(7), 995-1004.
- Hansen, S. B., Tao, X., & MacKinnon, R. (2011). Structural basis of PIP2 activation of the classical inward rectifier K<sup>+</sup> channel Kir2.2. *Nature*, *477*(7365), 495-498. doi:10.1038/nature10370
- Hibino, H., Inanobe, A., Furutani, K., Murakami, S., Findlay, I., & Kurachi, Y. (2010). Inwardly rectifying potassium channels: their structure, function, and physiological roles. *Physiol Rev*, *90*(1), 291-366. doi:10.1152/physrev.00021.2009
- Huang, C. L., Feng, S., & Hilgemann, D. W. (1998). Direct activation of inward rectifier potassium channels by PIP2 and its stabilization by Gbetagamma. *Nature*, *391*(6669), 803-806.
- Inagaki, N., Gono, T., Clement, J. P., Wang, C. Z., Aguilar-Bryan, L., Bryan, J., & Seino, S. (1996). A family of sulfonylurea receptors determines the pharmacological properties of ATP-sensitive K<sup>+</sup> channels. *Neuron*, *16*(5), 1011-1017.

- Inagaki, N., Gonoï, T., Clement, J. P. t., Namba, N., Inazawa, J., Gonzalez, G., . . . Bryan, J. (1995). Reconstitution of IKATP: an inward rectifier subunit plus the sulfonylurea receptor. *Science*, 270(5239), 1166-1170.
- Inagaki, N., Gonoï, T., & Seino, S. (1997). Subunit stoichiometry of the pancreatic beta-cell ATP-sensitive K<sup>+</sup> channel. *FEBS Lett*, 409(2), 232-236.
- Janbon, M., Chaptal, J., Vedel, A., & Schaap, J. (1942). Accidents hypoglycemiques graves par un sulfamidothiazol (le VK ou 2254 RP). *Montpellier Med*, 21-22, 441-444.
- Jardetzky, O. (1966). Simple allosteric model for membrane pumps. *Nature*, 211(5052), 969-970.
- Jiang, Y., Lee, A., Chen, J., Cadene, M., Chait, B. T., & MacKinnon, R. (2002). The open pore conformation of potassium channels. *Nature*, 417(6888), 523-526.
- Jin, T., Peng, L., Mirshahi, T., Rohacs, T., K.W., C., Sanchez, R., & Logothetis, D. E. (2002). The  $\beta$  Subunits of G Proteins Gate a K<sup>+</sup> Channel by Pivoted Bending of a Transmembrane Segment. *Mol Cell*, 10(3), 469-481.
- Koster, J. C., Sha, Q., & Nichols, C. G. (1999). Sulfonylurea and K(+)-channel opener sensitivity of K(ATP) channels. Functional coupling of Kir6.2 and SUR1 subunits. *J Gen Physiol*, 114(2), 203-213.
- Koster, J. C., Sha, Q., Shyng, S., & Nichols, C. G. (1999). ATP inhibition of KATP channels: control of nucleotide sensitivity by the N-terminal domain of the Kir6.2 subunit. *J Physiol*, 515 ( Pt 1), 19-30.
- Krauter, T., Ruppertsberg, J. T., & Baukowitz, T. (2001). Phospholipids as Modulators of KATP Channels: Distinct Mechanisms for Control of Sensitivity to Sulphonylureas, K<sup>+</sup> Channel Openers, and ATP. *Mol Pharmacol*, 59(5), 1086-1093.
- Kuo, A., Gulbis, J. M., Antcliff, J. F., Rahman, T., Lowe, E. D., Zimmer, J., . . . Doyle, D. A. (2003). Crystal structure of the potassium channel KirBac1.1 in the closed state. *Science*, 300(5627), 1922-1926. doi:10.1126/science.1085028
- Li, J., Lu, S., Liu, Y., Pang, C., Chen, Y., Zhang, S., . . . An, H. (2015). Identification of the Conformational transition pathway in PIP<sub>2</sub> Opening Kir Channels. *Sci Rep*, 5, 11289. doi:10.1038/srep11289
- Li, L., Wang, J., & Drain, P. (2000). The I182 region of k(ir)6.2 is closely associated with ligand binding in K(ATP) channel inhibition by ATP. *Biophys J*, 79(2), 841-852. doi:10.1016/S0006-3495(00)76340-5
- Lopatin, A. N., Makhina, E. N., & Nichols, C. G. (1994). Potassium channel block by cytoplasmic polyamines as the mechanism of intrinsic rectification. *Nature*, 372(6504), 366-369.
- Loubatieres, A. (1957). The mechanism of action of the hypoglycemic sulfonamides; a concept based on investigations in animals and in man. *Diabetes*, 6(5), 408-417.
- MacGregor, G. G., Dong, K., Vanoye, C. G., Tang, L., Geibisch, G., & Herbert, S. C. (2002). Nucleotides and phospholipids compete for binding to the C terminus of KATP channels. *Proc Natl Acad Sci USA*, 99(5), 2726-2731.
- Magidovich, E., & Yifrach, O. (2004). Conserved gating hinge in ligand-and voltage-dependent K<sup>+</sup> channels. *Biochemistry*, 43(42), 13242-13247.
- Mannhold, R. (2004). KATP channel openers: structure-activity relationships and therapeutic potential. *Med Res Rev*, 24(2), 213-266.
- Mannikko, R., Jefferies, C., Flanagan, S. E., Hattersley, A., Ellard, S., & Ashcroft, F. M. (2010). Interaction between mutations in the slide helix of Kir6.2 associated with neonatal

- diabetes and neurological symptoms. *Hum Mol Genet*, 19(6), 963-972.  
doi:10.1093/hmg/ddp554
- Martin, G. M., Chen, P. C., Devaraneni, P., & Shyng, S. L. (2013). Pharmacological rescue of trafficking-impaired ATP-sensitive potassium channels. *Front Physiol*, 4, 386.  
doi:10.3389/fphys.2013.00386
- Masia, R., Enkvetchakul, D., & Nichols, C. G. (2005). Differential nucleotide regulation of KATP channels by SUR1 and SUR2A. *J Mol Cell Cardiol*, 39(3), 491-501.  
doi:10.1016/j.yjmcc.2005.03.009
- Masia, R., Koster, J. C., Tumini, S., Chiarelli, F., Colombo, C., Nichols, C. G., & Barbetti, F. (2007). An ATP-binding mutation (G334D) in KCNJ11 is associated with a sulfonylurea-insensitive form of developmental delay, epilepsy, and neonatal diabetes. *Diabetes*, 56(2), 328-336. doi:10.2337/db06-1275
- Matsuo, M., Kioka, N., Amachi, T., & Ueda, K. (1999). ATP binding properties of the nucleotide-binding folds of SUR1. *J Biol Chem*, 274(52), 37479-37482.
- Matsuo, M., Tanabe, K., Kioka, N., Amachi, T., & Ueda, K. (2000). Different Binding Properties and Affinities for ATP and ADP among Sulfonylurea Receptor Subtypes, SUR1, SUR2A, and SUR2B\*. *J Biol Chem*, 275(37), 28757-28763.
- McTaggart, J. S., Clark, R. H., & Ashcroft, F. M. (2010). The role of the KATP channel in glucose homeostasis in health and disease: more than meets the islet. *J Physiol*, 588(Pt 17), 3201-3209.
- Mikhailov, M. V., Campbell, J. D., de Wet, H., Shimomura, K., Zadek, B., Collins, R. F., . . . Ashcroft, F. M. (2005). 3-D structural and functional characterization of the purified KATP channel complex Kir6.2-SUR1. *EMBO J*, 24(23), 4166-4175.  
doi:10.1038/sj.emboj.7600877
- Mikhailov, M. V., Mikhailova, E. E., & Ashcroft, S. J. (2001). Molecular structure of the glibenclamide binding site of the beta-cell K(ATP) channel. *FEBS Lett*, 499(1-2), 154-160.
- Misler, S., Falke, L. C., Gillis, K., & McDaniel, M. L. (1986). A metabolite-regulated potassium channel in rat pancreatic B cells. *Proc Natl Acad Sci USA*, 83, 7119-7123.
- Nicholas, B., Quayle, J. M., Davis, N. W., Brayden, J. E., Huang, Y., & Nelson, M. T. (1989). Hyperpolarizing vasodilators activate ATP-sensitive K<sup>+</sup> channels in arterial smooth muscle. *Science*, 245(4914), 177-180.
- Nichols, C. G. (2006). KATP channels as molecular sensors of cellular metabolism. *Nature*, 440(7083), 470-476. doi:10.1038/nature04711
- Nichols, C. G., & Lederer, W. J. (1991). Adenosine triphosphate-sensitive potassium channels in the cardiovascular system. *Am J Physiol*, 261, H1675-1686.
- Nichols, C. G., Shyng, S. L., Nestorowicz, A., Glaser, B., Clement, J. P. t., Gonzalez, G., . . . Bryan, J. (1996). Adenosine diphosphate as an intracellular regulator of insulin secretion. *Science*, 272(5269), 1785-1787.
- Nishida, M., & MacKinnon, R. (2002). Structural basis of inward rectification: cytoplasmic pore of the G protein-gated inward rectifier GIRK1 at 1.8 Å resolution. *Cell*, 111(7), 957-965.
- Noma, A. (1983). ATP-regulated K<sup>+</sup> channels in cardiac muscle. *Nature*, 305(5930), 147-148.
- Ortiz, D., Voyvodic, P., Gossack, L., Quast, U., & Bryan, J. (2012). Two neonatal diabetes mutations on transmembrane helix 15 of SUR1 increase affinity for ATP and ADP at nucleotide binding domain 2. *J Biol Chem*, 287(22), 17985-17995.  
doi:10.1074/jbc.M112.349019

- Pearson, E. R., Flechtner, I., Njolstad, P. R., Malecki, M. T., Flanagan, S. E., Larkin, B., . . . Neonatal Diabetes International Collaborative, G. (2006). Switching from insulin to oral sulfonylureas in patients with diabetes due to Kir6.2 mutations. *N Engl J Med*, *355*(5), 467-477. doi:10.1056/NEJMoa061759
- Powers, E. T., Morimoto, R. I., Dillin, A., Kelly, J. W., & Balch, W. E. (2009). Biological and chemical approaches to diseases of proteostasis deficiency. *Annu Rev Biochem*, *78*, 959-991. doi:10.1146/annurev.biochem.052308.114844
- Pratt, E. B., Tewson, P., Bruederle, C. E., Skach, W. R., & Shyng, S. L. (2011). N-terminal transmembrane domain of SUR1 controls gating of Kir6.2 by modulating channel sensitivity to PIP2. *J Gen Physiol*, *137*(3), 299-314. doi:10.1085/jgp.201010557
- Pratt, E. B., Yan, F. F., Gay, J. W., Stanley, C. A., & Shyng, S. L. (2009). Sulfonylurea receptor 1 mutations that cause opposite insulin secretion defects with chemical chaperone exposure. *J Biol Chem*, *284*(12), 7951-7959. doi:10.1074/jbc.M807012200
- Pratt, E. B., Zhou, Q., Gay, J. W., & Shyng, S. L. (2012). Engineered interaction between SUR1 and Kir6.2 that enhances ATP sensitivity in KATP channels. *J Gen Physiol*, *140*(2), 175-187. doi:10.1085/jgp.201210803
- Proks, P., Antcliff, J. F., Lippiat, J., Gloyn, A. L., Hattersley, A. T., & Ashcroft, F. M. (2004). Molecular basis of Kir6.2 mutations associated with neonatal diabetes or neonatal diabetes plus neurological features. *Proc Natl Acad Sci U S A*, *101*(50), 17539-17544. doi:10.1073/pnas.0404756101
- Proks, P., Capener, C. E., Jones, P., & Ashcroft, F. M. (2001). Mutations within the P-loop of Kir6.2 modulate the intraburst kinetics of the ATP-sensitive potassium channel. *J Gen Physiol*, *118*(4), 341-353.
- Proks, P., de Wet, H., & Ashcroft, F. M. (2010). Activation of the K(ATP) channel by Mg-nucleotide interaction with SUR1. *J Gen Physiol*, *136*(4), 389-405. doi:10.1085/jgp.201010475
- Proks, P., de Wet, H., & Ashcroft, F. M. (2014). Sulfonylureas suppress the stimulatory action of Mg-nucleotides on Kir6.2/SUR1 but not Kir6.2/SUR2A KATP channels: a mechanistic study. *J Gen Physiol*, *144*(5), 469-486. doi:10.1085/jgp.201411222
- Proks, P., Gribble, F. M., Adhikari, R., Tucker, S. J., & Ashcroft, F. M. (1999). Involvement of the N-terminus of Kir6.2 in the inhibition of the KATP channel by ATP. *J Physiol*, *514* (Pt 1), 19-25.
- Raphemot, R., Swale, D. R., Dadi, P. K., Jacobson, D. A., Cooper, P., Wojtovich, A. P., . . . Denton, J. S. (2014). Direct activation of beta-cell KATP channels with a novel xanthine derivative. *Mol Pharmacol*, *85*(6), 858-865. doi:10.1124/mol.114.091884
- Reimann, F., Proks, P., & Ashcroft, F. M. (2001). Effects of mitiglinide (S 21403) on Kir6.2/SUR1, Kir6.2/SUR2A and Kir6.2/SUR2B types of ATP-sensitive potassium channel. *Br J Pharmacol*, *132*(7), 1542-1548.
- Rohacs, T., Chen, J., Prestwich, G. D., & Logothetis, D. E. (1999). Distinct specificities of inwardly rectifying K(+) channels for phosphoinositides. *J Biol Chem*, *274*(51), 36065-36072.
- Rorsman, P., & Trube, G. (1985). Glucose dependent K<sup>+</sup>-channels in pancreatic beta-cells are regulated by intracellular ATP. *Pflugers Arch*, *405*(4), 305-309.
- Schmid-Antomarchi, H., De Weille, J., Fosset, M., & Lazdunski, M. (1987). The receptor for antidiabetic sulfonylureas controls the activity of the ATP-modulated K<sup>+</sup> channel in insulin-secreting cells. *J Biol Chem*, *262*(33), 15840-15844.

- Schwanstecher, M., Loser, S., Chudziak, F., & Panten, U. (1994). Identification of a 38-kDa high affinity sulfonylurea-binding peptide in insulin-secreting cells and cerebral cortex. *J Biol Chem*, 269(27), 17768-17771.
- Schwanstecher, M., Loser, S., Rietze, I., & Panten, U. (1991). Phosphate and thiophosphate group donating adenine and guanine nucleotides inhibit glibenclamide binding to membranes from pancreatic islets. *Naunyn Schmiedebergs Arch Pharmacol*, 343(1), 83-89.
- Schwappach, B., Zerangue, N., Jan, Y. N., & Jan, L. Y. (2000). Molecular basis for K(ATP) assembly: transmembrane interactions mediate association of a K<sup>+</sup> channel with an ABC transporter. *Neuron*, 26(1), 155-167.
- Shyng, S., Ferrigni, T., & Nichols, C. G. (1997). Control of rectification and gating of cloned KATP channels by the Kir6.2 subunit. *J Gen Physiol*, 110(2), 141-153.
- Shyng, S., Ferrigni, T., & Nichols, C. G. (1997). Regulation of KATP channel activity by diazoxide and MgADP. Distinct functions of the two nucleotide binding folds of the sulfonylurea receptor. *J Gen Physiol*, 110(6), 643-654.
- Shyng, S., & Nichols, C. G. (1997). Octameric stoichiometry of the KATP channel complex. *J Gen Physiol*, 110(6), 655-664.
- Shyng, S. L., & Nichols, C. G. (1998). Membrane phospholipid control of nucleotide sensitivity of KATP channels. *Science*, 282(5391), 1138-1141.
- Snider, K. E., Becker, S., Boyajian, L., Shyng, S. L., MacMullen, C., Hughes, N., . . . Ganguly, A. (2013). Genotype and phenotype correlations in 417 children with congenital hyperinsulinism. *J Clin Endocrinol Metab*, 98(2), E355-363. doi:10.1210/jc.2012-2169
- Sola, D., Rossi, L., Schianca, G. P., Maffioli, P., Bigliocca, M., Mella, R., . . . Derosa, G. (2015). Sulfonylureas and their use in clinical practice. *Arch Med Sci*, 11(4), 840-848. doi:10.5114/aoms.2015.53304
- Song, D. K., & Ashcroft, F. M. (2001). Glimpiride block of cloned  $\beta$ -cell, cardiac and smooth muscle K-ATP channels. *Br J Pharmacol*, 133(1), 193-199.
- Sturgess, N. C., Ashford, M. L. J., Cook, D. L., & Hales, C. N. (1985). The sulphonylurea receptor may be an ATP-sensitive potassium channel. *Lancet*, 2(8453), 474-475.
- Tamaro, P., Girard, C., Molnes, J., Njolstad, P. R., & Ashcroft, F. M. (2005). Kir6.2 mutations causing neonatal diabetes provide new insights into Kir6.2-SUR1 interactions. *EMBO J*, 24(13), 2318-2330. doi:10.1038/sj.emboj.7600715
- Tao, X., Avalos, J. L., Chen, J., & MacKinnon, R. (2009). Crystal structure of the eukaryotic strong inward-rectifier K<sup>+</sup> channel Kir2.2 at 3.1 Å resolution. *Science*, 326(5960), 1668-1674. doi:10.1126/science.1180310
- Terzic, A., Jahangir, A., & Kurachi, Y. (1995). Cardiac ATP-sensitive K channels: regulation by intracellular nucleotides and K channel-opening drugs. *Am J Physiol Cell Physiol*, 269, C525-C545.
- Trapp, S., Haider, S., Jones, P., Sansom, M. S. P., & Ashcroft, F. M. (2003). Identification of residues contributing to the ATP binding site of Kir6.2. *EMBO J*, 22(12), 2903-2912.
- Trapp, S., Proks, P., Tucker, S. J., & Ashcroft, F. M. (1998). Molecular analysis of ATP-sensitive K channel gating and implications for channel inhibition by ATP. *J Gen Physiol*, 112(3), 333-349.
- Trube, G., & Hescheler, J. (1984). Inward-rectifying channels in isolated patches of the heart cell membrane: ATP dependence and comparison with cell-attached patches. *Pflügers Archiv*, 401, 178-184.

- Trube, G., Rorsman, P., & Ohno-Shosaku, T. (1986). Opposite effects of tolbutamide and diazoxide on the ATP-dependent K<sup>+</sup> channel in mouse pancreatic beta-cells. *Pflügers Archiv*, *407*(5), 493-499.
- Tucker, S. J., Gribble, F. M., Proks, P., Trapp, S., Ryder, T. J., Haug, T., . . . Ashcroft, F. M. (1998). Molecular determinants of KATP channel inhibition by ATP. *EMBO J*, *17*(12), 3290-3296. doi:10.1093/emboj/17.12.3290
- Tucker, S. J., Gribble, F. M., Zhao, C., Trapp, S., & Ashcroft, F. M. (1997). Truncation of Kir6.2 produces ATP-sensitive K<sup>+</sup> channels in the absence of the sulphonylurea receptor. *Nature*, *387*(6629), 179-183. doi:10.1038/387179a0
- Tusnady, G. E., Bakos, E., Varadi, A., & Sakadi, B. (1997). Membrane topology distinguishes a subfamily of the ATP-binding cassette (ABC) transporters. *FEBS Lett*, *402*(1), 1-3.
- Ueda, K., Inagaki, N., & Seino, S. (1997). MgADP Antagonism to Mg<sup>2+</sup>-independent ATP Binding of the Sulfonylurea Receptor SUR1. *J Biol Chem*, *272*, 22983-22986.
- Uhde, I., Toman, A., Gross, I., Schwanstecher, C., & Schwanstecher, M. (1999). Identification of the Potassium Channel Opener Site on Sulfonylurea Receptors. *J Biol Chem*, *274*(40), 28079-28082.
- Vedovato, N., Ashcroft, F. M., & Puljung, M. C. (2015). The Nucleotide-Binding Sites of SUR1: A Mechanistic Model. *Biophys J*, *109*, 2452-2460.
- Vila-Carriles, W. H., Zhao, G., & Bryan, J. (2007). Defining a binding pocket for sulfonylureas in ATP-sensitive potassium channels. *FASEB J*, *21*(1), 18-25. doi:10.1096/fj.06-6730hyp
- Wang, C., Wang, K., Wang, W., Cui, Y., & Fan, Z. (2002). Compromised ATP binding as a mechanism of phosphoinositide modulation of ATP-sensitive K<sup>+</sup> channels. *FEBS Lett*, *532*(1-2), 177-182.
- Wang, S., Lee, S., Heyman, S., Enkvetchakul, D., & Nichols, C. G. (2012). Structural rearrangements underlying ligand-gating in Kir channels. *Nat Commun*, *3*, 617.
- Whorton, M. R., & MacKinnon, R. (2011). Crystal structure of the mammalian GIRK2 K<sup>+</sup> channel and gating regulation by G proteins, PIP<sub>2</sub>, and sodium. *Cell*, *147*(1), 199-208. doi:10.1016/j.cell.2011.07.046
- Whorton, M. R., & MacKinnon, R. (2013). X-ray structure of the mammalian GIRK2-beta gamma G-protein complex. *Nature*, *498*(7453), 190-197. doi:10.1038/nature12241
- Winkler, M., Lutz, R., Russ, U., Quast, U., & Bryan, J. (2009). Analysis of two KCNJ11 neonatal diabetes mutations, V59G and V59A, and the analogous KCNJ8 I60G substitution: differences between the channel subtypes formed with SUR1. *J Biol Chem*, *284*(11), 6752-6762. doi:10.1074/jbc.M805435200
- Xie, L. H., S.A., J., Ribalet, B., & Weiss, J. N. (2007). Activation of inwardly rectifying potassium (Kir) channels by phosphatidylinositol-4,5-bisphosphate (PIP<sub>2</sub>): interaction with other regulatory ligands. *Prog Biophys Mol Biol*, *94*(3), 320-335.
- Yamada, K., & Kurachi, Y. (2004). The nucleotide-binding domains of sulfonylurea receptor 2A and 2B play different functional roles in nicorandil-induced activation of ATP-sensitive K<sup>+</sup> channels. *Mol Pharmacol*, *65*(5), 1198-1207.
- Yan, F., Lin, C. W., Weisiger, E., Cartier, E. A., Taschenberger, G., & Shyng, S. L. (2004). Sulfonylureas correct trafficking defects of ATP-sensitive potassium channels caused by mutations in the sulfonylurea receptor. *J Biol Chem*, *279*(12), 11096-11105. doi:10.1074/jbc.M312810200

- Yan, F. F., Casey, J., & Shyng, S. L. (2006). Sulfonylureas correct trafficking defects of disease-causing ATP-sensitive potassium channels by binding to the channel complex. *J Biol Chem*, *281*(44), 33403-33413. doi:10.1074/jbc.M605195200
- Yan, F. F., Lin, Y. W., MacMullen, C., Ganguly, A., Stanley, C. A., & Shyng, S. L. (2007). Congenital hyperinsulinism associated ABCC8 mutations that cause defective trafficking of ATP-sensitive K<sup>+</sup> channels: identification and rescue. *Diabetes*, *56*(9), 2339-2348. doi:10.2337/db07-0150
- Zerangue, N., Schwappach, B., Jan, Y. N., & Jan, L. Y. (1999). A new ER trafficking signal regulates the subunit stoichiometry of plasma membrane K(ATP) channels. *Neuron*, *22*(3), 537-548.
- Zhang, H., He, C., Yan, X., Mirshahi, T., & Logothetis, D. E. (1999). Activation of inwardly rectifying K<sup>+</sup> channels by distinct PtdIns(4,5)P<sub>2</sub> interactions. *Nat Cell Biol*, *1*(3), 183-188.
- Zhou, Q., Garin, I., Castano, L., Argente, J., Munoz-Calvo, M. T., Perez de Nanclares, G., & Shyng, S. L. (2010). Neonatal diabetes caused by mutations in sulfonylurea receptor 1: interplay between expression and Mg-nucleotide gating defects of ATP-sensitive potassium channels. *J Clin Endocrinol Metab*, *95*(12), E473-478. doi:10.1210/jc.2010-1231
- Zingman, L. V., Alekseev, A. E., Bienengraeber, M., Hodgson, D., Karger, A. B., Dzeja, P. P., & Terzic, A. (2001). Signaling in channel/enzyme multimers: ATPase transitions in SUR module gate ATP-sensitive K<sup>+</sup> conductance. *Neuron*, *31*(2), 233-245.
- Zubcevic, L., Bavro, V. N., Muniz, J. R., Schmidt, M. R., Wang, S., De Zorzi, R., . . . Tucker, S. J. (2014). Control of KirBac3.1 potassium channel gating at the interface between cytoplasmic domains. *J Biol Chem*, *289*(1), 143-151. doi:10.1074/jbc.M113.501833

## Chapter 2

### Pharmacological Correction of Trafficking Defects in ATP-Sensitive Potassium Channels Caused by Sulfonylurea Receptor 1 Mutations

Gregory M. Martin,<sup>1†</sup> Emily A. Rex,<sup>1†</sup> Prasanna Devaraneni,<sup>1</sup> Jerod S. Denton,<sup>2</sup> Kara E. Boodhansingh,<sup>3</sup> Diva D. DeLeon,<sup>3</sup> Charles A. Stanley,<sup>3</sup> and Show-Ling Shyng<sup>1\*</sup>

<sup>1</sup>Department of Biochemistry and Molecular Biology, Oregon Health & Science University, Portland, OR 97239, USA; Department of Anesthesiology, Vanderbilt University, Nashville, TN 37232; <sup>3</sup>Division of Endocrinology/Diabetes, The Children's Hospital of Philadelphia, Philadelphia, PA 19104, USA.

**Published in:** Martin GM, Rex EA, Devaraneni PK, Denton JS, Boodhansingh KE, DeLeon DD, Stanley CA, Shyng SL. (2016). Pharmacological correction of trafficking defects in ATP-sensitive potassium channels caused by sulfonylurea receptor 1 mutations. *J Biol Chem.* 291:21971-21983.

<sup>†</sup>These authors contributed equally to this work. \*To whom correspondence should be addressed.

#### AUTHOR CONTRIBUTIONS

**GMM:** conducted experiments for Figures 1, 3, 4, and 5. Experimental design; writing: original draft and revision; figure making. **ER:** conducted experiments for Figures 2, 3, 4, 6-8. Experimental design; writing: editing draft and revision; figure making. **PD:** conducted experiments for Figure 3A; construct design; Experimental design. **SLS:** conducted experiments for Figures 5-8. Experimental design; writing: original draft and revision; figure making. **JD:** provided expert help on using the potassium channel potentiators. **KB, CAS, and DDDL** collected genetic and clinical data from patients.

## Abstract

ATP-sensitive potassium ( $K_{ATP}$ ) channels play a key role in mediating glucose-stimulated insulin secretion by coupling metabolic signals to  $\beta$ -cell membrane potential. Loss of  $K_{ATP}$  channel function due to mutations in *ABCC8* or *KCNJ11*, genes encoding the sulfonylurea receptor 1 (SUR1) or the inwardly rectifying potassium channel Kir6.2, respectively, results in congenital hyperinsulinism. Many SUR1 mutations prevent trafficking of channel proteins from the endoplasmic reticulum to the cell surface. Channel inhibitors including sulfonylureas and carbamazepine have been shown to correct channel trafficking defects. In the present study, we identified 13 novel SUR1 mutations that cause channel trafficking defects, the majority of which are amenable to pharmacological rescue by glibenclamide and carbamazepine. By contrast, none of the mutant channels were rescued by  $K_{ATP}$  channel openers. Crosslinking experiments showed that  $K_{ATP}$  channel inhibitors promoted interactions between the N-terminus of Kir6.2 and SUR1, whereas channel openers did not, suggesting the inhibitors enhance inter-subunit interactions to overcome channel biogenesis and trafficking defects. Functional studies of rescued mutant channels indicate that most mutants rescued to the cell surface exhibited wild-type like sensitivity to ATP, MgADP, and diazoxide. In intact cells, recovery of channel function upon trafficking rescue by reversible sulfonylureas or carbamazepine was facilitated by the  $K_{ATP}$  channel opener diazoxide. Our study expands the  $K_{ATP}$  channel trafficking mutations whose function can be recovered by pharmacological ligands and provides further insight into the structural mechanism by which channel inhibitors correct channel biogenesis and trafficking defects.

## Introduction

Protein function relies on the proper folding, assembly, and trafficking to specific cellular compartments. In the case of plasma membrane proteins such as ion channels and receptors, they must pass quality surveillance in the endoplasmic reticulum (ER) in order to enter the secretory pathway and ultimately reach the cell surface. Numerous diseases arise due to mutations which disrupt protein folding, assembly, and subsequent trafficking to the cell surface (Welch, 2004), hereinafter referred to as trafficking mutations. Small molecules termed pharmacological chaperones hold promise as a means of therapy for such diseases by interacting with mutant proteins and correcting their folding and trafficking defects (Convertino et al., 2016; Leidenheimer & Ryder, 2014; Powers et al., 2009).

Congenital hyperinsulinism (HI) is a rare, life-threatening disease characterized by persistent insulin secretion despite extreme hypoglycemia (Stanley, 2016). The most common cause of HI is loss-of-function mutations in the *ABCC8* or *KCNJ11* genes encoding the sulfonylurea receptor 1 (SUR1) and inwardly rectifying potassium channel Kir6.2 proteins, respectively (Aguilar-Bryan et al., 2001; Ashcroft, 2005; Stanley, 2016). SUR1 and Kir6.2 form the pancreatic subtype of the ATP-sensitive  $K^+$  ( $K_{ATP}$ ) channel, which plays a key role in glucose-stimulated insulin secretion by coupling glucose metabolism to  $\beta$ -cell membrane excitability (Aguilar-Bryan & Bryan, 1999; Ashcroft, 2005; Nichols, 2006). SUR1 or Kir6.2 mutations identified in patients with HI have been shown to disrupt channel gating and/or biogenesis and trafficking (Martin et al., 2013; Snider et al., 2013). While a small number (<10%) of affected individuals are successfully treated with the  $K_{ATP}$  channel opener diazoxide, those with the more severe form due to loss of channel surface expression are diazoxide-unresponsive and often require partial or total pancreatectomy in order to avoid severe

consequences of hypoglycemia (Stanley, 2016). Restoring channel expression with pharmacological chaperones is therefore an attractive alternative therapy.

HI-causing  $K_{ATP}$  channel trafficking mutations are found throughout both SUR1 and Kir6.2, but most of them are in the larger SUR1 subunit. SUR1 is a member of the ATP-binding cassette (ABC) transporter superfamily (Martin et al., 2013; Snider et al., 2013). In addition to the ABC core domain found in each member (TMD1/NBD1/TMD2/NBD2, see Figure 1A), SUR1 contains an N-terminal transmembrane domain TMD0 and a long cytoplasmic loop L0 which connects TMD0 to TMD1 (Aguilar-Bryan et al., 1995). We have previously found that sulfonylureas (SUs),  $K_{ATP}$  channel inhibitors, such as glibenclamide (GBC) and tolbutamide could act as pharmacological chaperones to correct  $K_{ATP}$  channel trafficking defects (Pratt et al., 2009; Yan et al., 2004; Yan et al., 2006; Yan et al., 2007). More recently, we identified a novel  $K_{ATP}$  channel inhibitor carbamazepine (CBZ) which also rescues trafficking-impaired  $K_{ATP}$  channels to the cell surface (Chen, Olson, et al., 2013; Zhou et al., 2014). Remarkably, the SUR1 trafficking mutations tested so far that are amenable to rescue by SUs or CBZ are all in TMD0 (Chen, Olson, et al., 2013; Sampson et al., 2013; Yan et al., 2004; Yan et al., 2007), a region known to mediate functional and physical interactions between SUR1 and Kir6.2 (Babenko & Bryan, 2003; Chan et al., 2003; Schwappach et al., 2000). Accordingly, we have found that the rescue effect of GBC and CBZ on TMD0 mutants is dependent on Kir6.2 and that both drugs promote the interaction between Kir6.2 and SUR1 (Devaraneni et al., 2015; Yan et al., 2004), suggesting the pharmacological chaperones work in concert with Kir6.2 during translation and/or folding to overcome the structural defects imposed by the TMD0-SUR1 mutations. Importantly, mutants rescued to the cell surface by the reversible inhibitor CBZ or the reversible sulfonylurea tolbutamide often retain normal responses to ATP and MgADP upon

CBZ washout (Chen, Olson, et al., 2013; Yan et al., 2004; Yan et al., 2007), suggesting these mutant channels may reestablish normal insulin secretion if surface expression were restored.

In the present study we have identified and characterized 14 new, diazoxide-unresponsive HI mutations, each found within TMD0 of SUR1. We show that each of these mutations disrupts trafficking to the cell surface to varying degrees, and that most are rescued by both GBC and CBZ. Within the group amenable to pharmacological chaperone rescue, most mutants exhibit normal responses to ATP and MgADP and their functional recovery can be further facilitated by exposure to the  $K_{ATP}$  channel opener diazoxide. Interestingly, in contrast to  $K_{ATP}$  channel inhibitors, none of the several  $K_{ATP}$  channel openers we tested showed chaperoning effects on the trafficking mutants. Further analysis using unnatural amino acid mediated crosslinking showed that the opener diazoxide does not promote physical interactions between Kir6.2 and SUR1, in contrast to GBC or CBZ. The therapeutic and mechanistic implications of our findings broaden the applicability of pharmacological chaperones in treating HI.

## **Results**

*Identification and pharmacological rescue of novel HI-causing  $K_{ATP}$  trafficking mutants*--In a previous study we identified a new  $K_{ATP}$  channel pharmacological chaperone (PC) carbamazepine (CBZ) which, like the sulfonylurea drugs glibenclamide and tolbutamide, can restore surface expression of several  $K_{ATP}$  trafficking mutants caused by mutations in the TMD0 region of SUR1 (Devaraneni et al., 2015; Sampson et al., 2013). We sought to expand this finding by searching for additional HI-associated TMD0 mutations that disrupt channel trafficking and that are amenable to rescue by CBZ. Fourteen single nucleotide mutations in TMD0 identified by us or reported in the literature (Flanagan et al., 2009; Snider et al., 2013) are

included in this study, two of which resulted in the same amino acid change at position 111 from glycine to arginine, yielding a total of thirteen missense mutations (Table 1; note this number will be used hereinafter). The positions of these thirteen mutations are shown in a topology map of SUR1 (Fig.1A). Based on published as well as our own genetic and clinical data, all thirteen mutations are associated with diazoxide-unresponsive HI (Table 1). Of these mutations, only G70E and G111R have been subjected to biochemical and functional analysis (Tornovsky et al., 2004), while channel defects caused by the other mutations are yet to be determined.

We first asked whether the mutations disrupt  $K_{ATP}$  channel biogenesis and whether CBZ can correct the adverse effects of the mutations, using western blot of SUR1 as a readout. SUR1 has two N-linked glycosylation sites which undergo core, high mannose glycosylation in the ER (Aguilar-Bryan et al., 1995; Raab-Graham et al., 1999). Upon assembly with Kir6.2 into octameric  $K_{ATP}$  channels and exit of the ER, SUR1 undergoes further glycosylation modifications in the Golgi before reaching the cell surface (Schwappach et al., 2000; Zerangue et al., 1999). The core and complex glycosylated species can be separated by SDS-PAGE, producing a lower immature and a higher mature band, respectively. As only fully assembled channels can pass ER quality control (Schwappach et al., 2000; Zerangue et al., 1999), we can use the relative abundance of the upper and lower bands of SUR1 as an approximation for processing efficiency. COSm6 cells co-transfected with mutant SUR1 and WT Kir6.2 cDNAs (both human forms of the gene) were treated overnight (~16 hr) with vehicle control (0.1% DMSO), 5  $\mu$ M GBC, or 10  $\mu$ M CBZ followed by western blotting of the whole-cell lysate. GBC was included as a comparison, as this sulfonylurea has been shown to be the most effective pharmacological chaperone for multiple TMD0 trafficking mutations (Yan et al., 2004; Yan et al., 2007) and acts similarly to CBZ (Devaraneni et al., 2015). WT SUR1/Kir6.2 was also

included in each blot to serve as a positive control. Results from these experiments are shown in Fig.1B. All thirteen mutations reduced or diminished the upper SUR1 band. G70E, and G111R have previously been reported to compromise channel biogenesis and trafficking (Tornovsky et al., 2004), which are in agreement with our results. C6 in SUR1 has been shown previously to form a disulfide bond with C26 and mutation of C6 to an alanine prevents maturation of the SUR1 band in cells co-expressing Kir6.2 (Fukuda et al., 2011). Our observation that C6G also disrupts SUR1 processing is consistent with the importance of this cysteine residue in channel biogenesis. Of the thirteen trafficking mutations, L31P and L40R showed little or no response to either GBC or CBZ, and C6G responded only slightly to GBC but not at all to CBZ. The processing defects of the other mutations were rescued by both GBC and CBZ, although the response was variable especially for CBZ rescue. Of note, we have previously shown that both GBC and CBZ also enhance the processing efficiency of WT channels, leading to ~5-10% increase in surface expression (Chen, Olson, et al., 2013; Yan et al., 2004; Yan et al., 2007).

*K<sub>ATP</sub> channel openers do not correct the processing defects of K<sub>ATP</sub> trafficking mutants*--Our published studies have shown that while CBZ and sulfonylureas such as GBC and tolbutamide, all inhibitors of the K<sub>ATP</sub> channel, can act as pharmacological chaperones for a subset of K<sub>ATP</sub> trafficking mutants, the K<sub>ATP</sub> channel opener diazoxide (7-Chloro-3-methyl-2H-1,2,4-benzothiadiazine 1,1-dioxide) cannot (Yan et al., 2004; Yan et al., 2007). We wondered whether the difference between channel inhibitors and openers with regard to rescuing trafficking-impaired K<sub>ATP</sub> channels is generalizable. This is of interest because identification of a potassium channel opener that could act as a pharmacological chaperone for trafficking-impaired K<sub>ATP</sub> channels would circumvent the problem of having to remove the inhibitory chaperones subsequently to recover channel function. To address this question, we tested several other

compounds that have been reported to stimulate  $K_{ATP}$  channel activity, including VU0071063 (7-[[4-(1,1-Dimethylethyl)phenyl]methyl]-3,7-dihydro-1,3-dimethyl-1H-purine-2,6-dione) (Raphemot et al., 2014), Y26763 [(-)-(3S,4R)-4-(N-acetyl-N-hydroxyamino)-6-cyano-3,4-dihydro-2,2-dimethyl-2H-1-benzopyran-3-ol] (Cosgrove et al., 2004), and NN414 [6-Chloro-3-(1-methylcyclopropyl)amino-4*H*-thieno[3,2-*e*]-1,2,4-thiadiazine 1,1-Dioxide] (Nielsen et al., 2006). Although  $EC_{50}$  values of these compounds for  $K_{ATP}$  channels have been reported or estimated previously (Cosgrove et al., 2004; Nielsen et al., 2006; Raphemot et al., 2014), they were obtained using different experimental systems. We therefore wanted to determine each compound's  $EC_{50}$  under our experimental conditions. Channel activation was assessed by  $^{86}Rb^+$  efflux assays performed on cells transiently expressing the SUR1/Kir6.2 channels (see Experimental Procedures). In our system we found that Y26763 is a poor activator of SUR1/Kir6.2 channels. At 25  $\mu M$  (the  $EC_{50}$  provided by the vendor is 27  $\mu M$ ), Y26763 only gave a partial channel activation of  $\sim 10\%$  with an  $EC_{50}$  of  $\sim 1.8$  mM (data not shown). Therefore, we focused our efforts on VU0071063 and NN414. The chemical structures of VU0071063 and NN414 are shown in Fig. 2A, along with that of diazoxide. Based on dose response curves of efflux activity normalized to that observed in cells treated with metabolic inhibitors, we calculated the  $EC_{50}$  of diazoxide, VU0071063 and NN414 to be 36.23  $\mu M$ , 0.34  $\mu M$ , and 3.52  $\mu M$ , respectively (Fig. 2B). These results indicate that VU0071063 is the most potent  $K_{ATP}$  channel opener, followed by NN414, then diazoxide. Interestingly, we also noted that the maximal efficacy of NN414 in this assay appeared lower than that of either diazoxide or VU0071063.

Having estimated the  $EC_{50}$  for the three  $K_{ATP}$  channel openers, we next tested each compound for its ability to rescue TMD0-SUR1 trafficking mutants, using the D29G as an

example since it has the greatest response to GBC and CBZ. For each compound, we tested two different concentrations that were near (2-3 fold) or well above the  $EC_{50}$  but within solubility of the compound (5-12 fold). For comparison, cells transfected with the D29G mutant channel cDNAs were also treated overnight with GBC, CBZ, or tolbutamide at concentrations near or well above the reported  $IC_{50}$  values of each inhibitor (Aguilar-Bryan & Bryan, 1999; Devaraneni et al., 2015). In contrast to all three channel inhibitors: GBC, CBZ, and tolbutamide, which increased the upper band of the D29G SUR1 mutant at both concentrations (Fig.2C), none of the potassium channel openers showed any effects at either concentrations (Fig.2D). The lack of a chaperoning effect of diazoxide has been reported for several other TMD0-SUR1 mutations (Martin et al., 2013; Yan et al., 2004; Yan et al., 2007), and our results here show that two other more potent channel openers also fail to correct trafficking defects of such mutants. These results indicate that in contrast to  $K_{ATP}$  channel inhibitors,  $K_{ATP}$  channel openers are unable to correct trafficking defects caused by SUR1-TMD0 mutations.

*The  $K_{ATP}$  channel opener diazoxide does not enhance SUR1-Kir6.2 subunit interactions as assessed by p-azidophenylalanine mediated photocrosslinking--*Using a genetically encoded photocrosslinkable amino acid, p-azidophenylalanine, engineered into the distal N-terminus of Kir6.2, we have recently shown that both GBC and CBZ promote crosslinking of Kir6.2 N-terminus to SUR1 (Devaraneni et al., 2015). Based on this observation and findings that deleting the N-terminus of Kir6.2 severely compromised the biogenesis efficiency of WT channels and prevented rescue of trafficking-impaired mutants by GBC or CBZ (Devaraneni et al., 2015), we proposed that GBC and CBZ rescue TMD0-SUR1 trafficking mutants by promoting physical interactions between the N-terminus of Kir6.2 and SUR1 to overcome channel protein folding

and assembly defects caused by SUR1 TMD0 mutations. According to this model,  $K_{ATP}$  channel openers which do not correct channel trafficking defects should have no effect on the extent of photocrosslinking between Kir6.2 N-terminus and SUR1. To test this, we expressed FLAG-tagged SUR1 and a Kir6.2 variant carrying a TAG stop codon at amino acid position 12, as well as an orthogonal pair of tRNA and tRNA synthetase that incorporated *p*-azidophenylalanine (AzF) at the TAG stop codon position when cells were grown in culture medium containing the photocrosslinkable unnatural amino acid, as described in Experimental Procedures. As shown in Fig.3A and 3B, while overnight treatment with GBC and CBZ increased the intensity of crosslinked Kir6.2-SUR1 band compared to control cells treated overnight with 0.1% DMSO as previously reported (Devaraneni et al., 2015), overnight treatment with 200  $\mu$ M diazoxide did not. Quantification of the ratio of crosslinked band signal to total SUR1 signal from four independent experiments showed that GBC significantly increased the extent of crosslinking ( $13.54 \pm 2.43\%$  for GBC versus  $4.88 \pm 0.91\%$  for DMSO control;  $p < 0.05$ ), but diazoxide did not ( $5.49 \pm 2.78\%$  for diazoxide versus  $4.88 \pm 0.91\%$  for DMSO control) (Fig.3C). VU0071063 at 25  $\mu$ M also failed to increase crosslinking between Kir6.2 and SUR1, although the results were less quantifiable since the drug also compromised the maturation of WT SUR1 (data not shown), possibly because it interferes with association of Kir6.2 N-terminus with SUR1 necessary for channel biogenesis and maturation as we reported previously (Devaraneni et al., 2015). Taken together, these results support the notion that compounds that do not rescue TMD0-SUR1 trafficking mutants also fail to promote the physical interaction between Kir6.2 N-terminus and SUR1.

*Trafficking-impaired  $K_{ATP}$  channels rescued by CBZ reach the cell surface*--Having found that

CBZ corrected the processing defects caused by the majority of the SUR1 TMD0 mutations, we directed our efforts towards further characterizing mutant channels rescued by the drug. As a first step, we performed immunostaining and quantitative immuno-chemiluminescence assays to confirm that the increased SUR1 upper band upon CBZ treatment corresponds to an increased expression of mutant channels at the cell surface. For these experiments, higher signal to noise ratio is important for good quality results, we therefore used hamster SUR1/rat Kir6.2 recombinant channels because these channels express at a higher level compared to human channels (Chen, Olson, et al., 2013; Macmullen et al., 2011; Yan et al., 2007). Western blot experiments as those done for human mutant channels were repeated in cells co-expressing hamster SUR1 with corresponding mutations and WT rat Kir6.2. By and large, the hamster SUR1/rat Kir6.2 mutant channels responded to GBC and CBZ similarly to their human counterparts (Fig.4A). However, some differences are noted. For example, most mutants showed better processing efficiency even without any drug treatment; this is particularly true for G92D. Also, C6G, L31P, and L40R had better response to GBC compared to their human counterparts.

To track  $K_{ATP}$  channel surface expression, we used a SUR1 construct containing an N-terminal FLAG-tag located at the extracellular N-terminus (FLAG-SUR1). When staining cells that have not been fixed and permeabilized, only surface FLAG-SUR1 is accessible to labeling by anti-FLAG antibody present in the medium. Fig. 4B shows representative examples (D29G and A30T). Comparing surface staining of WT and D29G- or A30T-SUR1 with or without overnight CBZ treatment, CBZ had a clear effect on the mutant channels, with generally more cells showing more intense surface staining following treatment.. Quantitative surface chemiluminescence experiments (see Experimental Procedures) were further performed on the mutants, (excluding hamster G70E and G92D which showed WT-like processing efficiency even

without GBC or CBZ treatment; see Fig. 4A). Results from these experiments (Fig. 4C) correlate well with immunoblotting and staining results, and further confirm the efficacy of CBZ in rescuing this class of trafficking mutations to the cell surface.

*Gating properties of mutant channels rescued to the cell surface*--K<sub>ATP</sub> channels are gated by intracellular adenine nucleotides: ATP binds to Kir6.2 in a Mg<sup>2+</sup>-independent manner to block channel activity, whereas MgATP binds to SUR1 to stimulate channel activity (Ashcroft & Gribble, 1998; Nichols, 2006). At low glucose concentrations, MgADP stimulation of K<sub>ATP</sub> channels dominates, producing K<sup>+</sup> efflux that keeps the β-cell hyperpolarized and prevents insulin secretion. When blood glucose concentrations rise, the β-cell intracellular ATP concentration also rises, leading to K<sub>ATP</sub> channel inhibition, membrane depolarization, and insulin secretion. The ability of the channel to respond to ATP inhibition and MgADP stimulation is critical for its physiological function to ensure correct insulin secretion response (Ashcroft, 2005; Gloyn et al., 2004; Nichols et al., 1996). In addition, diazoxide is a potassium channel opener that can be used to enhance K<sub>ATP</sub> channel activity to suppress insulin secretion, and is clinically effective in treating HI patients with residual channel function (Stanley, 2016). Because some trafficking mutations have been shown to cause both trafficking and gating defects (Cartier et al., 2001; Pratt et al., 2009; Taschenberger et al., 2002), it is important to ascertain that trafficking-impaired channels rescued to the cell surface are gated properly by ATP, MgADP, and diazoxide. To this end, we performed inside-out patch clamp recording using COSm6 cells transfected with mutant channels and treated overnight with CBZ. We have previously shown that CBZ inhibits channel activity (Chen, Olson, et al., 2013), specifically abolishing channel response to MgADP (Zhou et al., 2014), and this effect is reversible (Chen,

Olson, et al., 2013; Zhou et al., 2014). Therefore, recordings were made after CBZ was thoroughly washed out, by incubating cells in CBZ-free medium for 2 hours, to unmask the gating properties of rescued channels. Also, because C6G, L31P, and L40R showed little rescue by CBZ, these mutations were excluded from our analysis.

All mutants tested had detectable currents after CBZ rescue and washout. Current traces from two mutants, V21D and D29G, in response to ATP and MgADP or ATP and diazoxide are shown in Fig.5A and 5B as examples. Quantification of MgADP and diazoxide sensitivity for all mutants, expressed as the percent current relative to nucleotide-free bath solution, is shown in Fig. 5C. The results show that sensitivities of these mutants to MgADP or diazoxide stimulation were not significantly different from those of WT channels, with the exception of R168C which showed a small increase in sensitivity to MgADP ( $p = 0.03$ ). The results suggest that upon rescue to the cell surface, these mutant channels will open in response to metabolic inhibition or diazoxide stimulation to suppress insulin secretion.

*Assessing functional recovery of mutant channels rescued to the cell surface in intact cells--*To directly test whether CBZ rescued channels can respond to metabolic signals, we performed  $^{86}\text{Rb}^+$  efflux assays which assess channel activity in intact cells. COSm6 cells were transiently transfected with each of the ten different trafficking mutants which showed response to CBZ rescue in Fig.1B. Cells were then treated overnight with 10  $\mu\text{M}$  CBZ and subjected to  $^{86}\text{Rb}^+$  efflux assays as described in Experimental Procedures. To mimic hypoglycemic conditions that activate the channels, cells were pre-incubated with metabolic inhibitors in Ringer's solution for 30 min and efflux was monitored during a 40 min period in Ringer's solution with metabolic inhibitors. CBZ was not present in the metabolic inhibitors pre-incubation solution or the efflux

solution to allow CBZ to unbind thus removing channel inhibition. In parallel, we also included experimental groups in which the  $K_{ATP}$  channel opener diazoxide or VU0071063 was included (see schematic shown in Fig.6A). We chose diazoxide and VU0071063 because the former has previously been shown to facilitate functional recovery of CBZ rescued channels in another TMD0-SUR1 trafficking mutation F27S (Chen, Olson, et al., 2013), and VU0071063 is the most potent and effective WT  $K_{ATP}$  channel opener amongst the channel openers we tested in this study. These experiments revealed differential functional recovery for the various mutants and differential effects of the two  $K_{ATP}$  channel openers on functional recovery of CBZ-rescued mutant channels (Fig.6B).

Upon CBZ overnight treatment followed by CBZ washout (total washout of 70 minutes including the 30 min metabolic inhibition and the 40 min efflux period), several mutations showed significantly more efflux activity in response to metabolic inhibition compared to cells treated overnight with the vehicle (DMSO) control; these include D29G, A30T, and G92D (Fig.6B). Two mutations, V21D and G70E actually showed decreased efflux activity compared to vehicle treated controls, which was also observed in WT channels, indicating that CBZ had not been completely washed out. It is interesting to point out that both V21D and G70E only had mild trafficking defects such that CBZ overnight treatment likely only had a small effect on channel numbers at the cell surface and this effect was masked by the inhibitory effect of CBZ on channel gating. Other mutations including M80R, G111R, A113V, R168C, and G173R showed only very small (not statistically significant) increase in efflux activity. When 200  $\mu$ M diazoxide was included in the metabolic inhibitor preincubation and efflux solutions, an additional amount of significant functional recovery was observed in D29G, A30T, G92D, and R168C mutants (Fig.6B). Note that this increase in efflux activity was not due to additional

stimulation of channel activity by diazoxide beyond that stimulated by metabolic inhibition, but actually reflects recovery of function of CBZ-rescued mutant channels. This conclusion is based on experiments comparing the efflux activity of cells expressing trafficking mutants, treated with the vehicle DMSO (vehicle), and then subjected to metabolic inhibition in the absence or presence of diazoxide, which showed no difference whether diazoxide was present or not (Fig.7). In V21D, the addition of diazoxide enhanced efflux activity, while in G70E, diazoxide recovered efflux that was inhibited by residually bound CBZ. For M80R, G111R, A113V, and G173R, diazoxide did not improve efflux activity significantly. To our surprise, inclusion of 25  $\mu$ M VU0071063, a concentration that maximally stimulated WT channels similar to metabolic inhibition did not facilitate functional recovery of CBZ-rescued mutant channels (Fig.6B), in contrast to what was observed for diazoxide.

Results shown in Fig.6 suggest CBZ was not completely removed during the efflux experiment. Therefore, we repeated the efflux experiments for mutants that showed little functional rescue effects, specifically M80R, G111R, A113V, and G173R, using a different pharmacological chaperone, tolbutamide (Fig.8A). Tolbutamide is a low-affinity sulfonylurea drug that has been shown in our previous studies to rescue TMD0 trafficking mutations (Yan et al., 2004; Yan et al., 2007). Although it is less effective than the irreversible sulfonylurea GBC in rescuing trafficking defects caused by TMD0 mutations, it is easily washed out to recover the function of rescued channels. Indeed, as shown in Fig.8B, the four mutants did show small but significant increases in efflux activity upon tolbutamide washout, demonstrating the surface expression rescue effect of tolbutamide and removal of tolbutamide during washout. The small improvement in functional recovery observed in these mutants are consistent with the extent of CBZ rescue observed in western blot experiments (Fig.1B). Of note, diazoxide had very small or

negligible effects in further increasing the efflux activity. The results suggest that tolbutamide was washed out efficiently such that diazoxide did little to facilitate unbinding of the channel inhibitor. In conclusion, using tolbutamide or CBZ in combination with diazoxide, most trafficking mutants showed functional recovery in response to metabolic signals.

## **Discussion**

HI is a rare disease, with loss of function mutations in the  $K_{ATP}$  channel genes, *ABCC8* and *KCNJ11*, accounting for more than ~50% of the cases (Stanley, 2016). Patients with mutations which impair trafficking of  $K_{ATP}$  channels to the cell surface often present with severe disease phenotypes that are not responsive to diazoxide treatment, requiring pancreatectomy to prevent life-threatening hypoglycemia (Snider et al., 2013; Stanley, 2016). Pharmacological chaperone therapy represents a promising noninvasive treatment approach to this group of patients. However, unlike cystic fibrosis in which ~90% patients carry one or two copies of a highly prevalent misfolding mutation,  $\Delta F508$ , in the cystic fibrosis transmembrane conductance regulator (CFTR) protein (Cutting, 2015), there is no single highly prevalent mutation in the  $K_{ATP}$  channel genes that underlies channel trafficking defects. Instead, HI-associated channel trafficking mutations are rare mutations scattered throughout the two channel proteins (Martin et al., 2013; Snider et al., 2013), making it challenging to identify small molecules that can be applied to most patients.

Our previous studies have shown that several compounds that bind to the channel and inhibit channel activity were able to correct trafficking defects of  $K_{ATP}$  channels (Chen, Olson, et al., 2013; Sampson et al., 2013; Yan et al., 2004; Yan et al., 2006; Yan et al., 2007). These include two classes of oral hypoglycemic agents: sulfonylureas and glinides, with tolbutamide

and glibenclamide in the former class (Yan et al., 2004; Yan et al., 2007) and rapaglinide the latter (Yan et al., 2006), as well as the anticonvulsant carbamazepine we recently reported (Chen, Olson, et al., 2013; Sampson et al., 2013). Interestingly, these earlier studies found that of more than twenty trafficking mutations scattered throughout the SUR1 protein tested, only those located in TMD0 domain were rescued. The emerging pattern led us to focus in the current study on searching for more TMD0 trafficking mutations that are amenable to pharmacological rescue by  $K_{ATP}$  channel inhibitors. Such a targeted search led to identification of 10 SUR1-TMD0 missense trafficking mutations that responded to CBZ rescue as determined by western blots. All of these mutations had detectable currents and exhibited WT like gating properties upon washout of CBZ in patch-clamp recordings. These results expand the list of mutant candidates amenable to pharmacological chaperone therapy from the previously identified seven mutations to now seventeen mutations. Expansion of this list is highly significant for a rare disease like HI as it provides the impetus for future efforts towards developing pharmacological chaperones for clinical application.

Among the thirteen SUR1 mutations tested, L31P and L40R showed no trafficking rescue by either GBC or CBZ in any assay tested, while C6G showed only a barely detectable increase in the upper band in response to GBC but not with CBZ in western blots. The other mutations which responded to both GBC and CBZ also exhibited variable rescue. The lack of or weak response of some mutants could be due to inability or reduced affinity of the mutant proteins to bind GBC or CBZ because of mutation-induced misfolding. Alternatively, the drug binding pockets may remain unaffected in the mutant proteins but drug-binding fails to overcome channel biogenesis/trafficking defects induced by these mutations due to mutation-dependent

structural constraints. Detailed analysis of binding affinities to GBC and CBZ of the various mutants will be needed in the future to answer these question.

One of the major barriers to using  $K_{ATP}$  channel inhibitors for pharmacological chaperone therapy is the need to remove the inhibitors once mutant channels are rescued to the cell surface in order to recover the function of rescued channels (Chen, Olson, et al., 2013; Yan et al., 2004; Yan et al., 2007). For this reason, we tested several  $K_{ATP}$  channel openers reported in the literature in hopes of identifying ligands that will both correct channel trafficking defects and boost channel function despite our previous studies showing that the most widely used  $K_{ATP}$  channel opener diazoxide failed to rescue TMD0 trafficking mutations examined (Chen, Olson, et al., 2013; Yan et al., 2004; Yan et al., 2007). Our experimental results showed that none of the four other  $K_{ATP}$  channel openers tested corrected the processing defects of TMD0 mutants, over a wide range of concentrations, regardless of the potency or efficacy of the opener estimated from  $^{86}\text{Rb}^+$  efflux assays. Thus, the contrast between channel inhibitors and openers with regard to their ability to correct biogenesis/trafficking defects of TMD0-SUR1 mutations appears generalizable. Interestingly, using an unnatural amino acid mediated photocrosslinking experimental paradigm we developed previously to probe GBC- or CBZ-induced conformational change in  $K_{ATP}$  channels (Devaraneni et al., 2015), we found that in contrast to GBC and CBZ, both of which significantly increased crosslinking between an AzF placed at the 12<sup>th</sup> amino acid position in the distal N-terminal region of Kir6.2 and SUR1 [Fig.3A;(Devaraneni et al., 2015)], diazoxide did not. These findings support a mechanistic model in which channel inhibitors correct TMD0 mutation-induced channel biogenesis/trafficking defects by promoting interactions between the N-terminus of Kir6.2 and SUR1, whereas openers do not correct defects in these mutations because they do not enhance the physical interactions/assembly between

Kir6.2 N-terminus and SUR1. This model is consistent with a channel gating model proposed previously in which the N-terminus of Kir6.2 interacts with the cytoplasmic loop following TMD0 of SUR1 known as L0 (see Fig.1A) to modulate channel open probability (Babenko & Bryan, 2003). A possible scenario is that channel inhibitors such as GBC and CBZ reduce channel open probability, at least in part, by increasing the probability of interaction between Kir6.2 N-terminus and SUR1-L0 to decrease channel open probability, whereas channel agonists such as diazoxide stabilizes channel in a conformation that prevents the N-terminus of Kir6.2 from interacting with L0 of SUR1 to increase channel open probability. Identification of residues in SUR1 to which the AzF in Kir6.2 is crosslinked will provide a rigorous test of this hypothesis.

Of the  $K_{ATP}$  inhibitors that exhibit chaperoning effects on TMD0 trafficking mutants, GBC is the most potent and effective; however, its high binding affinity for the channel makes it nearly impossible to wash out (Yan et al., 2004). The glinide drug, rapaglinide also resulted in nearly irreversible inhibition even after removal of the drug from the culture medium (Yan et al., 2006). By contrast, CBZ and tolbutamide could be washed out to allow channel function recovery. Our previous and present studies indicate, however, that complete removal of CBZ inhibition requires extensive washout longer than the efflux experimental duration (Fig.6A). This is based on the lower efflux activity observed in the CBZ washout group compared to the vehicle treated control group for WT channels and several mutant channels that exhibit higher levels of basal surface expression such as V21D and G70E (Fig.6B). Removal of CBZ inhibition was facilitated by the addition of diazoxide, which was especially evident in trafficking mutants that showed a significant increase in surface expression upon CBZ treatment such as D29G, A30T, and G92D. To our surprise, VU0071063, which is a more potent  $K_{ATP}$  channel opener than diazoxide [Fig.2B; (Raphemot et al., 2014)], did not facilitate functional recovery of CBZ-

rescued channels. These findings suggest that diazoxide and VU0071063 may interact with the  $K_{ATP}$  channel via different sites and/or with different kinetics such that only diazoxide can efficiently remove residually bound CBZ. Finally, for several mutations which only showed a weak response to CBZ rescue in western blots and little improvement in efflux activity, we were able to observe greater functional rescue when tolbutamide was used as the pharmacological chaperone; in this case, diazoxide did not further improve efflux activity in these mutants. These results can be explained by the much lower binding affinity of tolbutamide and hence the higher efficiency of drug washout.

In summary, our present study further strengthens the rationale of repurposing CBZ and tolbutamide to treat HI caused by TMD0 trafficking mutations. The choice of which reversible channel inhibitor to use and whether diazoxide can further improve functional recovery may depend on the mutation. Biochemical and functional characterizations of mutation response like those presented here will help with this decision. It is important to point out that although functional recovery in some mutants are small, such small improvement may be sufficient to avoid severe HI (32). In addition, our study provides further insight into a structural mechanism by which  $K_{ATP}$  channel inhibitors do, whereas openers do not, rescue SUR1-TMD0 trafficking mutants. The improved mechanistic understanding of pharmacological chaperoning will be helpful in designing more efficient ligands to manipulate  $K_{ATP}$  surface expression and function for disease treatment.

## **Experimental Procedures**

*Genetic and Clinical studies*—The subjects included in this study were patients referred to The Children’s Hospital of Philadelphia Congenital Hyperinsulinism Center or reported by others in the literature (see Table 1). Patients were defined as being unresponsive to diazoxide if

hypoglycemia could not be controlled by treatment with 15 mg/kg/day diazoxide for a minimum of 5 days (i.e., able to keep blood glucose >70 mg/dL for more than 8-10 hrs fasting). Most of these diazoxide-unresponsive patients required surgical pancreatectomy. Clinical information was abstracted from the medical records. Written informed consent was obtained from parents of the probands included in this study. The study was reviewed and approved by the Institutional Review Board of the Children's Hospital of Philadelphia.

For genetic analysis, peripheral blood was obtained from patients for isolation of genomic DNA (5 PRIME, Gaithersburg, Maryland). Coding sequences and intron/exon splice junctions were amplified and directly sequenced on an ABI 3730 capillary DNA analyzer (Applied Biosystems, Carlsbad, California). The nucleotides of *ABCC8* and corresponding SUR1 amino acids were numbered according to the sequence reported by Nestorowicz et al. (Nestorowicz et al., 1996) that includes the alternatively spliced exon 17 sequence (NCBI accession no. L78224).

*Molecular biology*--For the majority of the experiments, human SUR1 cDNA in pCMV6b (kindly provided by Dr. Joseph Bryan) and human Kir6.2 in pcDNA3.1 were used. Point mutations were introduced using the QuikChange site-directed mutagenesis kit (Stratagene). For immunostaining and chemiluminescence experiments, rat Kir6.2 in pcDNA1 and hamster FLAG epitope tagged SUR1 (referred to as f-SUR1) in pECE were used. The FLAG-epitope (DYKDDDDK) was inserted at the N-terminus of the hamster SUR1 cDNA as previously described (Cartier et al., 2001). We have demonstrated in previous studies that the FLAG epitope placed at the extracellular N-terminus of SUR1 does not affect channel assembly or function (Cartier et al., 2001; Yan et al., 2004; Yan et al., 2007). All mutations were confirmed by DNA

sequencing and mutant clones from two independent PCR reactions were analyzed in all experiments to avoid false results caused by undesired mutations introduced by PCR.

*Immunoblotting*--COSm6 cells were transfected with SUR1 and Kir6.2 using FuGENE®6 and lysed in 20 mM HEPES, pH 7.0/5 mM EDTA/150 mM NaCl/1% Nonidet P-40 with CompleteTR protease inhibitors (Roche) 48-72 hours post-transfection. Proteins in cell lysates were separated by SDS/PAGE (8%), transferred to nitrocellulose membrane, analyzed by M2 anti-FLAG antibody followed by HRP-conjugated anti-mouse secondary antibodies (Amersham Pharmacia), and visualized by chemiluminescence (Super Signal West Femto; Pierce) with FluorChem E (ProteinSimple).

*Immunofluorescence staining*--COSm6 were grown on coverslips and transfected with hamster f-SUR1 and rat Kir6.2. Cells were treated with 0.1% DMSO or 10  $\mu$ M carbamazepine 32-40 hours post-transfection for overnight (~16 hours) and then processed for immunofluorescence staining. To stain for surface  $K_{ATP}$  channels, cells were incubated with anti-FLAG M2 mouse monoclonal antibody [Sigma, diluted to 10  $\mu$ g/ml in OptiMEM containing 0.1% bovine serum albumin (BSA)] for one hour at 4°C to detect f-SUR1, washed with ice-cold PBS, then fixed with -20°C methanol for 10 min. Fixed cells were incubated with Cy-3 conjugated donkey anti-mouse secondary antibodies (Jackson) for 30 min at room temperature followed by 3x5 min washes in phosphate buffered saline (PBS). Coverslips were mounted on glass slides using Vectashield Mounting Medium for Fluorescence with DAPI to counter stain the nuclei. Cells were viewed using an Olympus FV1000 laser-scanning confocal microscope.

*Chemiluminescence assays*--COSm6 cells were plated on 35 mm dishes and transfected with cDNAs for the  $K_{ATP}$  channel subunits using FuGENE®6. Drug treatment was carried out 32-40 hours post-transfection and lasted for ~16 hours. Cells were then processed for

chemiluminescence assay as described previously (15). In brief, cells were fixed with 2% paraformaldehyde for 30 min at 4°C, preblocked in PBS + 0.1% BSA for 30 min, incubated in M2 anti-FLAG antibody (10 µg/ml) for an hour, washed 4x30 min in PBS + 0.1% BSA, incubated in HRP-conjugated anti-mouse antibody (Jackson, 1:1000 dilution) for 20 min, and washed again 4x30 min in PBS + 0.1% BSA. Peak chemiluminescence signal of each dish was quantified in a TD-20/20 luminometer (Turner Designs) following 5 sec incubation in Power Signal Elisa Femto luminol solution (Pierce). All steps after fixation were carried out at room temperature. For data quantification, chemiluminescence signal in untransfected cells was subtracted as background, which was typically < 10% of total signal observed in cells transfected with WT channels. The signal from each mutant with or without CBZ treatment was then normalized to that of WT channels.

*<sup>86</sup>Rb<sup>+</sup> efflux assays*--Transfected COSm6 cells in 12-well plates were incubated overnight in medium containing <sup>86</sup>RbCl (0.1 µCi/ml) with or without 10 µM carbamazepine or 300 µM tolbutamide as specified. Cells were washed in Krebs-Ringer solution twice and incubated with metabolic inhibitors (2.5µg/ml oligomycin and 1mM 2-deoxy-D-glucose) in Krebs-Ringer solution for 30 min in the presence of <sup>86</sup>Rb<sup>+</sup> without carbamazepine but with or without 200 µM diazoxide or 10 µM VU0071063. Following two quick washes in efflux solution (as specified in Fig.6), 0.5 ml efflux solution was added to each well and incubated for 40 min. At the end of the 40 min incubation, solution was collected and cells were lysed in Krebs-Ringer containing 1% SDS. <sup>86</sup>Rb<sup>+</sup> in the solution and the cell lysate was counted. The percentage efflux was calculated as the radioactivity in the efflux solution divided by the total activity from the solution and cell lysate, as described previously (Chen, Olson, et al., 2013; Yan et al., 2007).

*Patch-clamp recordings*--COSm6 cells were transfected using FuGENE®6 and plated onto

coverslips. The cDNA for the green fluorescent protein (GFP) was co-transfected with SUR1 and Kir6.2 to facilitate identification of transfected cells. Patch-clamp recordings were made 36-72 hours post-transfection. All experiments were performed at room temperature as previously described (15). Micropipettes were pulled from non-heparinized Kimble glass (Fisher Scientific) on a horizontal puller (Sutter Instrument, Co., Novato, CA, USA). Electrode resistance was typically 1-2 M $\Omega$  when filled with K-INT solution (below). Inside-out patches were voltage-clamped with an Axopatch 1D amplifier (Axon Inc., Foster City, CA). The standard bath (intracellular) and pipette (extracellular) solution (K-INT) had the following composition: 140 mM KCl, 10 mM K-HEPES, 1 mM K-EGTA, pH 7.3. ATP was added as the potassium salt. All currents were measured at a membrane potential of -50 mV (pipette voltage = +50 mV). Data were analyzed using pCLAMP10 software (Axon Instrument). Off-line analysis was performed using Microsoft Excel programs. Data were presented as mean  $\pm$  standard error of the mean (SEM).

*Construction, expression, and UV-induced photocrosslinking of Kir6.2 with genetically encoded p-Azido-L-phenylalanine*--COSm6 cells were co-transfected with plasmids coding for azidophenylalanine tRNA, azidophenylalanine tRNA synthetase, wild-type (WT) SUR1 and Kir6.2 containing stop codons at position 12 using FuGENE®6 as described previously (Devaraneni et al., 2015). Growth media is supplemented with 0.5-1 mM azidophenylalanine 12 hours after transfection and cells were grown for 36-48 hours with or without K<sub>ATP</sub> channel inhibitors or openers as specified. Cells were harvested in cold PBS and incubated with drugs for 10 min at 37°C and exposed to UV for 15 min. Cells were pelleted and lysed in lysis buffer (20 mM HEPES, pH 7.2, 125 mM NaCl, 4 mM EDTA, 1 mM EGTA, 1% Triton X-100) with complete protease inhibitors for 30 mins, centrifuged for 15 min in a table top centrifuge, and

supernatant was collected and incubated with anti-FLAG antibody conjugated agarose beads overnight, washed 3X with 1 ml of a buffer containing 20 mM HEPES, pH 7.2, 150 mM NaCl, 4 mM EDTA, 1 mM EGTA, 1% Nonidet P-40, 0.1% SDS, and 0.04% deoxycholic acid, and finally bound proteins were eluted with 1% SDS, run on 3-8% SDS Tris-Acetate gels and subjected to western blot analysis.

*Statistics*--Data are presented as mean  $\pm$  SEM. Differences were tested using analysis of variance (ANOVA) when comparing three or more groups, and Dunnett's post-hoc test was used to compare treated versus control group. When only two groups were compared, unpaired Student's t-tests were used. Differences were considered significant if  $p \leq 0.05$ .

## **ACKNOWLEDGEMENTS**

We thank Erik Olson for technical help, Dr. Yelena Kryukova for sharing data, and Dr. Pei-Chun Chen for helpful discussion. We also thank Dr. Dale Fortin, Dr. Yi Wu, and Veronica Cochrane for critical reading of the manuscript. This work was supported by National Institutes of Health [grant R01DK066485] (to S.-L. S.), [grant F31DK105800] (to G.M.M.), [grant R01DK098517] (to D.D.D.L.), [grant R37DK056268] (to C.A.S.), and [grant from the Goldsmith Foundation] (to D.D.D.L. and C.A.S.)

**Table 1. Genetic and clinical data of HI patients bearing the TMD0 mutations**

<u>Exon</u>	<u>nucleotide</u>	<u>change</u>	<u>codon</u>	<u>a.a. change</u>	<u>diaz responsive</u>	<u>References</u>
1	16	T>G	<b>6</b>	<b>Cys-Gly</b>	NO	(Snider et al., 2013)
1	62	T>A	<b>21</b>	<b>Val-Asp</b>	NO	(Suchi et al., 2006)
1	86	A>G	<b>29</b>	<b>Asp-Gly</b>	NO	(Snider et al., 2013)
1	88	G>A	<b>30</b>	<b>Ala-Thr</b>	NO	(Snider et al., 2013)
1	92	T>C	<b>31</b>	<b>Leu-Pro</b>	NO	(Snider et al., 2013)
1	119	T>G	<b>40</b>	<b>Leu-Arg</b>	NO	(Snider et al., 2013)
2	209	G>A	<b>70</b>	<b>Gly-Glu</b>	NO	(Tornovsky et al., 2004)
2	239	T>G	<b>80</b>	<b>Met-Arg</b>	NO	(Greer et al., 2007)
2	275	G>A	<b>92</b>	<b>Gly-Asp</b>	NO	(Otonkoski et al., 2006)
3	331	G>C	<b>111</b>	<b>Gly-Arg</b>	NO	(Fernandez-Marmiesse et al., 2006)
3	331	G>A	<b>111</b>	<b>Gly-Arg</b>	NO	(De Vroede et al., 2004; Tornovsky et al., 2004; Verheul et al., 2011)
3	338	C>T	<b>113</b>	<b>Ala-Val</b>	NO	(Otonkoski et al., 2006)
4	502	C>T	<b>168</b>	<b>Arg-Cys</b>	NO	(Greer et al., 2007)
4	517	G>A	<b>173</b>	<b>Gly-Arg</b>	NO	(Hardy et al., 2007)

## Figure Legends

**Figure 1. Pharmacological correction of SUR1 processing defects caused by SUR1-TMD0 mutations identified in congenital hyperinsulinism.** (A) Positions of SUR1 mutations included in this study are marked on a SUR1 topology model (Conti et al., 2001). (B) Western blots of SUR1 from COSm6 cells co-transfected with human WT Kir6.2 and mutant SUR1 cDNA, and treated with 0.1% DMSO (Veh), 5 $\mu$ M GBC or 10 $\mu$ M CBZ for 16 hours. Untransfected cells (Unt) and cells expressing WT channels were included for comparison. The thin lines separate different parts of the same blot and thick vertical lines separate different blots. The empty circle points to the core-glycosylated immature SUR1 and the solid circle points to the complex-glycosylated mature SUR1. Molecular mass markers shown on the right side of the blots are in kDa in this and all subsequent figures.

**Figure 2. K<sub>ATP</sub> channel openers do not correct trafficking defects caused by SUR1 TMD0 mutations.** (A) Chemical structures of diazoxide, VU0071063, and NN414 (from PubChem). (B) Dose-response curves of K<sub>ATP</sub> channel stimulation by diazoxide, VU0071063, and NN414 in <sup>86</sup>Rb<sup>+</sup> efflux assays as described in Experimental Procedures. % Efflux during a 40-minute incubation period was derived by subtracting background efflux in untransfected cells and normalized to that observed in cells incubated with metabolic inhibitors. EC<sub>50</sub> values were calculated by fitting the dose-response curve with an exponential equation using Excel. Each data point represents the mean $\pm$ SEM of three independent measurements. Note the error bars for some data points are smaller than the size of the symbols and therefore not visible. (C) Western blots of SUR1 from COSm6 cells co-transfected with WT Kir6.2 and WT or D29G SUR1 cDNA (both human clones), and treated with 0.1% DMSO (-), 0.01 or 5 $\mu$ M GBC, 0.025 or 10 $\mu$ M CBZ, or 100 or 300  $\mu$ M tolbutamide (Tolb) for 16 hours. In DMSO treated sample, only the core-

glycosylated lower immature SUR1 band was observed (empty circle). All three channel inhibitors corrected the processing defect of the D29G mutant at both concentrations as evident by the appearance of the upper mature SUR1 band (solid circle). Cells expressing WT channels were included for comparison. **(D)** Same as (C) except cells were treated with two different concentrations of diazoxide (Diaz), VU0071063 (VU063), or NN414 as indicated. None of the  $K_{ATP}$  channel openers tested corrected the processing defect of the D29G mutant SUR1.

**Figure 3. Diazoxide does not promote intersubunit interactions between SUR1 and the N terminus of Kir6.2 as assessed by *p*-azidophenylalanine-mediated photocross-linking.** **(A)** COSm6 cells co-transfected with plasmids coding for azidophenylalanine tRNA, azidophenylalanine tRNA synthetase, WT hamster f-SUR1, and a rat Kir6.2 variant containing a stop codon at position 12 were grown in medium containing 1 mM azidophenylalanine and 0.1% DMSO (*Veh*), 5  $\mu$ M GBC, or 10  $\mu$ M CBZ for 36–48 h. Cells were harvested in cold PBS and subjected to photocross-linking as described under “Experimental Procedures.” Western blots of FLAG antibody affinity-purified SUR1 showed a cross-linked SUR1-Kir6.2 species (*gray circle*; confirmed by probing with anti-Kir6.2 antibody as we have reported previously (23), not shown) in addition to the lower (*open circle*) and upper (*solid circle*) SUR1 bands in cells expressing the Kir6.2Y12AzF variant and exposed to UV. The intensity of the cross-linked band was significantly higher in GBC- and CBZ-treated cells compared with DMSO-treated cells, as reported previously (23). Cells expressing WT Kir6.2 and WT f-SUR1 did not show the cross-linked species even with UV exposure, as expected. **(B)** same as in *A*, except cells treated with DMSO, 5  $\mu$ M GBC, or 200  $\mu$ M diazoxide (*Diaz*) were compared. Two representative blots probed with anti-SUR1 (*top*) are shown. In both blots, GBC-treated cells showed an increased cross-linked band (*gray circle*) signal upon UV exposure compared with DMSO-treated controls.

By contrast, diazoxide-treated cells did not show increased cross-linking compared with DMSO-treated controls. (C) quantification of the intensity of the cross-linked band (as a percentage of total SUR1 signal) in the DMSO, GBC, and diazoxide groups. \*,  $p < 0.05$  by Student's  $t$  test,  $n = 4$ . Error bars, S.E.; IB, immunoblotting; IP, immunoprecipitation.

**Figure 4. Carbamazepine restores surface expression of trafficking-impaired SUR1 mutants.** (A) Western blots of f-SUR1 from COSm6 cells co-transfected with rat WT Kir6.2 and mutant hamster f-SUR1 cDNA, and treated with 0.1% DMSO (Veh), 5 $\mu$ M GBC or 10 $\mu$ M CBZ for 16 hours. Note in hamster SUR1, amino acid position 80 is an isoleucine rather than a methionine found in human SUR1. Untransfected cells (Unt) and cells expressing WT channels were included for comparison. The thin lines separate different parts of the same blot and thick vertical lines separate different blots. The empty circle points to the core-glycosylated immature SUR1 and the solid circle points to the complex-glycosylated mature SUR1. (B) Surface expression of the D29G or A30T SUR1 mutants in cells transfected with WT rat Kir6.2 and hamster D29G or A30T f-SUR1 was monitored by immunostaining of the extracellular FLAG-epitope tag of f-SUR1 (red) in non-permeabilized cells. The nuclei were stained with DAPI (blue). Scale bar: 5 $\mu$ m. WT channels were included for comparison. The staining was repeated twice with qualitatively similar results. (C) Quantification of surface expression rescue of trafficking-impaired  $K_{ATP}$  channels by chemiluminescence assays. Each bar represents mean $\pm$ SEM of 3-4 experiments. \* $p < 0.05$  comparing DMSO (0.1%) treated versus CBZ treated (10 $\mu$ M) by Student's  $t$ -test. Note while the average surface expression level for all mutants was higher in CBZ treated cells compared to DMSO treated cells, the increase did not reach statistical significance for some of the mutants.

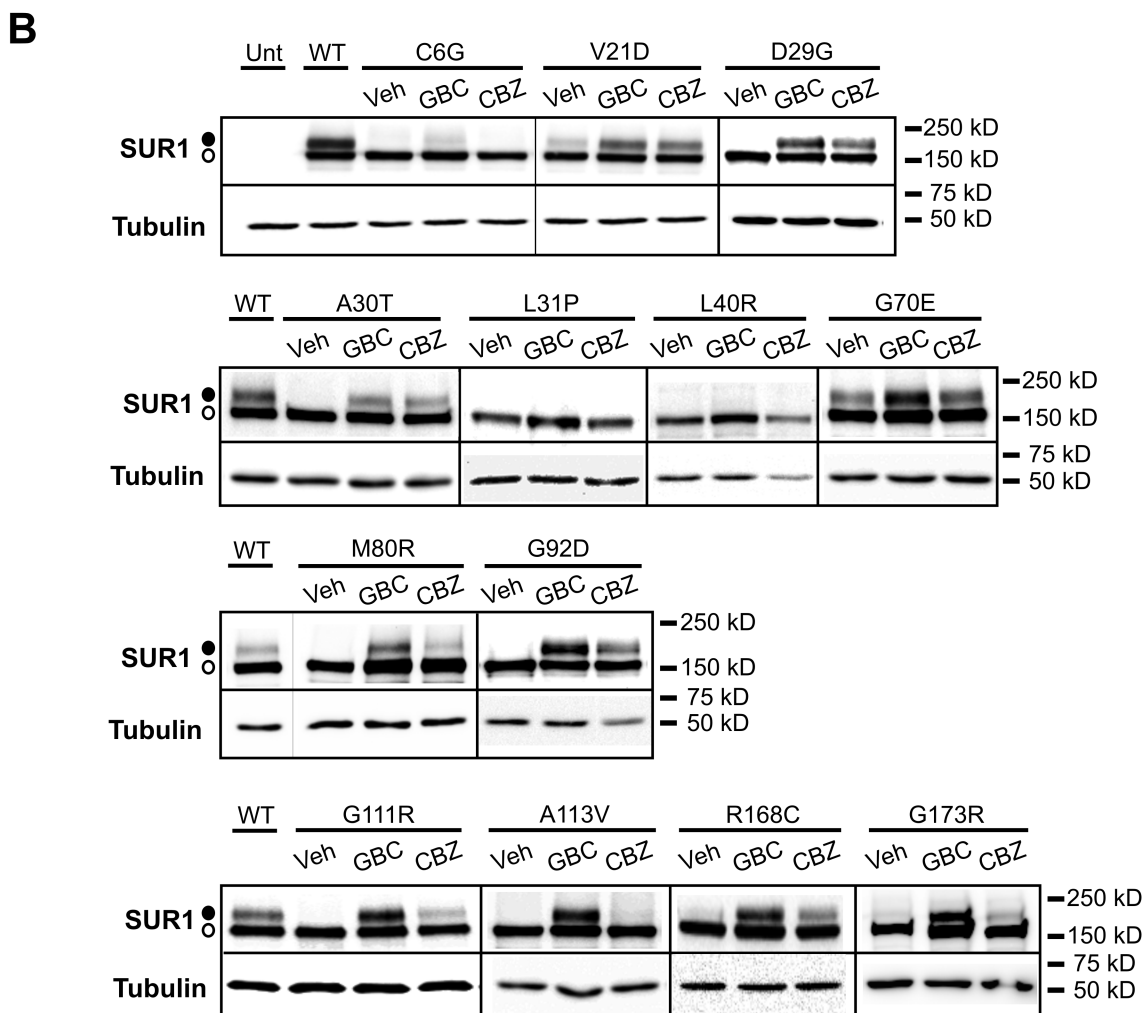
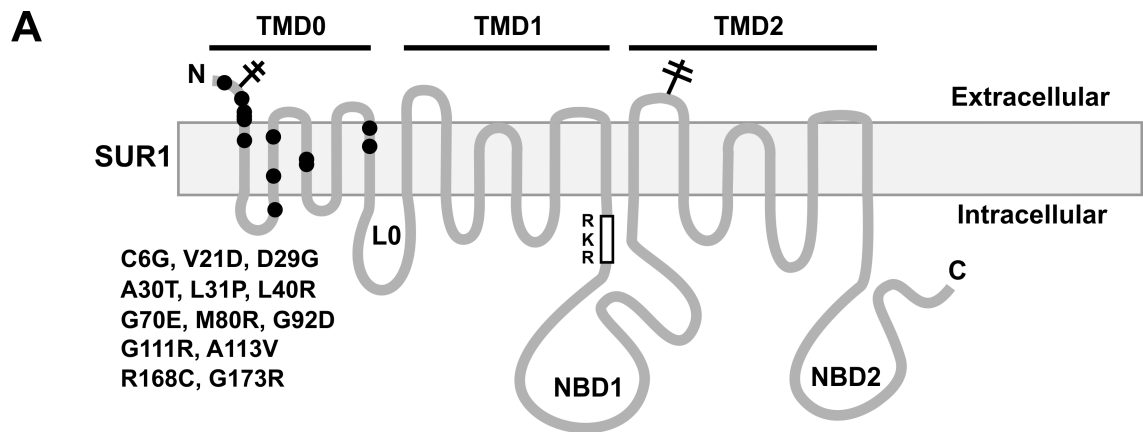
**Figure 5. Gating properties of mutant channels rescued to the cell surface assessed by inside-out patch-clamp recording.** COSm6 cells expressing the various trafficking mutants (human SUR1 + human Kir6.2) were treated overnight with 10 $\mu$ M CBZ to rescue channels to the cell surface. CBZ was removed from the culture medium for at least two hours prior to subjecting cells to inside-out patch-clamp recording as described in Experimental Procedures. **(A)** Representative current traces from WT, V21D, and D29G channels exposed to K-INT solution with or without ATP and MgADP as indicated. **(B)** Current traces from WT, V21D, and D29G exposed to K-INT solution with or without ATP and diazoxide as indicated. For both (A) and (B), currents were recorded at -50mV and inward currents shown as upward deflections. **(C)** Quantification of channel response to 0.1 mM ATP + 0.5 mM MgADP, or 0.1 mM ATP + 0.2 mM diazoxide. Currents were normalized to those observed in K-INT only. Each bar represents mean  $\pm$  SEM (n=17-18 for WT MgADP, n=6 for WT diazoxide, n=3-8 for mutants). \* $p$  < 0.05 (R168C vs WT MgADP response by Student's  $t$ -test).

**Figure 6. Assessing metabolic response of mutant  $K_{ATP}$  channels rescued by CBZ using  $^{86}\text{Rb}^+$  efflux assays.** **(A)** Schematic of experimental design. COSm6 cells transfected with WT or various mutant channels (human clones) were treated with 0.1% DMSO (vehicle control) or 10  $\mu$ M CBZ overnight in the presence of  $^{86}\text{Rb}^+$ . Before efflux measurements, cells were incubated with metabolic inhibitors (1mM deoxyglucose and 2.5 $\mu$ g/ml oligomycin) to activate channels at the cell surface;  $^{86}\text{Rb}^+$  was included during this time to maintain  $^{86}\text{Rb}^+$  loading. During the 30 min metabolic inhibition (MI) period, CBZ was not included to wash it out from rescued channels, while 200  $\mu$ M diazoxide or 25  $\mu$ M VU063 was included to test their effects on facilitating CBZ removal. Efflux was then measured for 40 min in the same solutions as during metabolic inhibition but in the absence of  $^{86}\text{Rb}^+$ . **(B)** Efflux over a 40-minute period is expressed

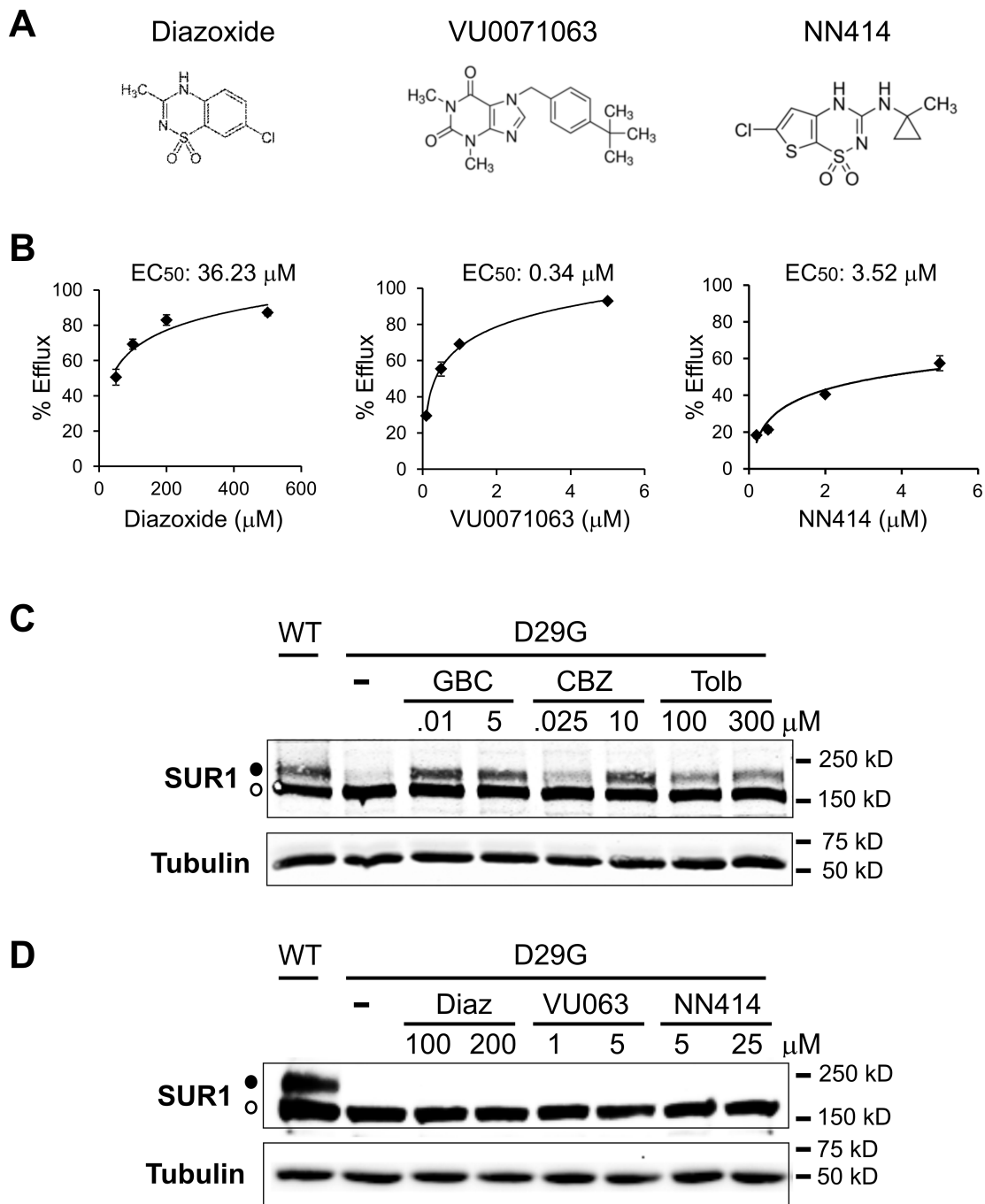
as % of total  $^{86}\text{Rb}^+$  counts. Untreated untransfected cells and cells transfected with WT channels were included as controls. Each bar represents mean $\pm$ SEM of three independent experiments. \*Significant increase comparing CBZ+MI, CBZ+MI+Diaz, or CBZ+MI+VU with Vehicle+MI ( $p < 0.05$  by one-way ANOVA and Dunnett's post hoc test).

**Figure 7. Diazoxide does not further increase  $^{86}\text{Rb}^+$  efflux by increasing activity of channels already activated by metabolic inhibition.** (A) Schematic of Rb efflux experiment. COSm6 cells expressing WT or various mutant channels and loaded with  $^{86}\text{Rb}^+$  overnight without CBZ resuce (only 0.1% DMSO vehicle was added to the medium). Metabolic inhibition and efflux was carried out in the presence of 200  $\mu\text{M}$  diazoxide. (B) Efflux over a 40-minute period is expressed as % of total  $^{86}\text{Rb}^+$  counts. Note that diazoxide did not significantly enhance efflux activity of WT or mutant channels present in the membrane, suggesting that existing channels were already maximally activated by metabolic inhibition. Each bar represents mean $\pm$ SEM of three independent experiments. No statistically significant difference was found between the two treatment groups in all mutants by Student's  $t$ -test.

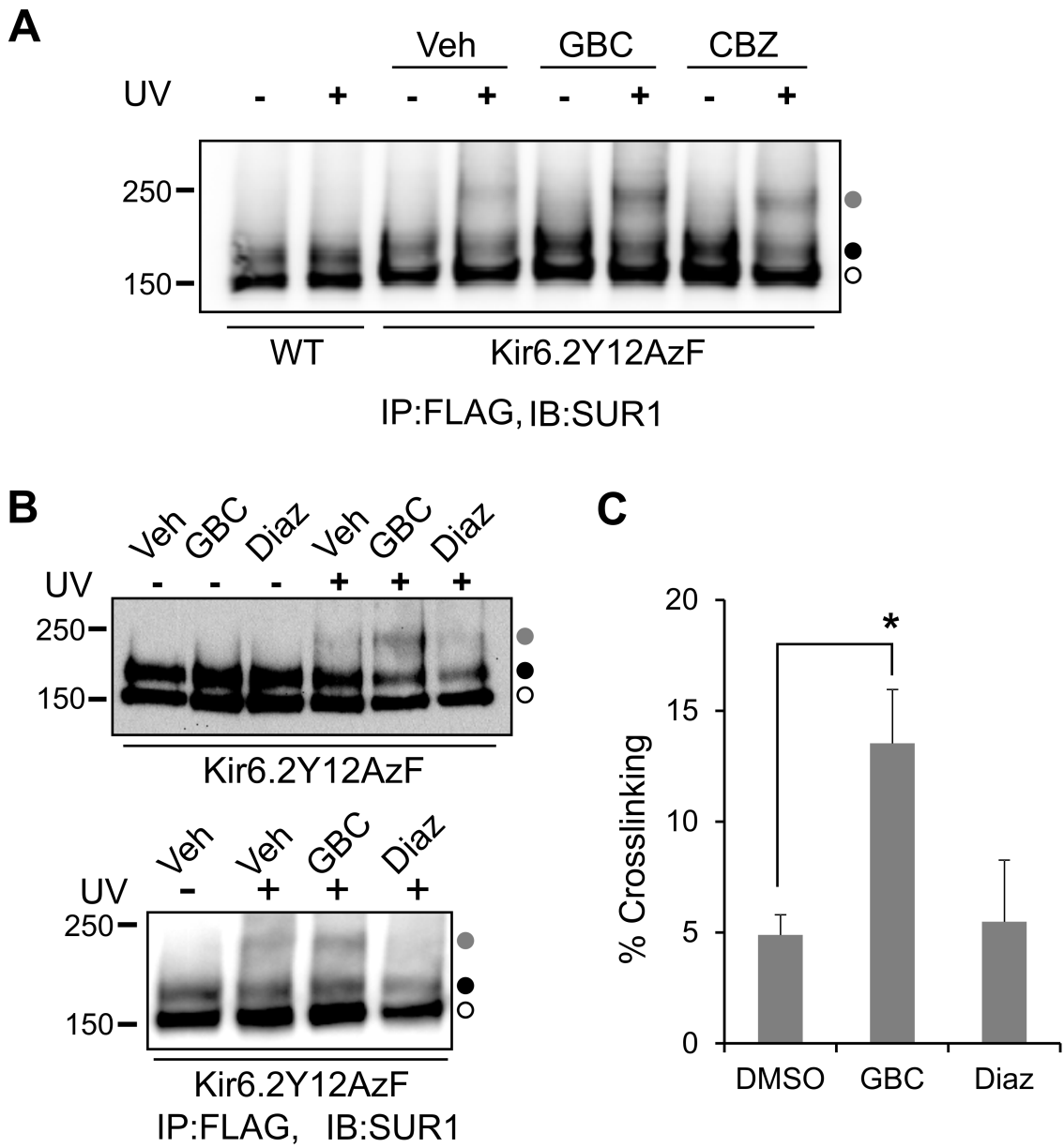
**Figure 8. Metabolic response of mutant  $\text{K}_{\text{ATP}}$  channels rescued by tolbutamide assessed by  $^{86}\text{Rb}^+$  efflux assays.** (A) Schematic of experimental design as in Fig.6A except that 300  $\mu\text{M}$  tolbutamide overnight treatment was used to rescue mutant channels. (B) Efflux of tested mutants over a 40-minute period is expressed as % of total  $^{86}\text{Rb}^+$  counts. Each bar represents mean $\pm$ SEM of three independent experiments. \*Significant increase comparing Tolb+MI, Tolb+MI+Diaz, or Tolb+MI+VU with Vehicle+MI ( $p < 0.05$  by one-way ANOVA and Dunnett's post hoc test).



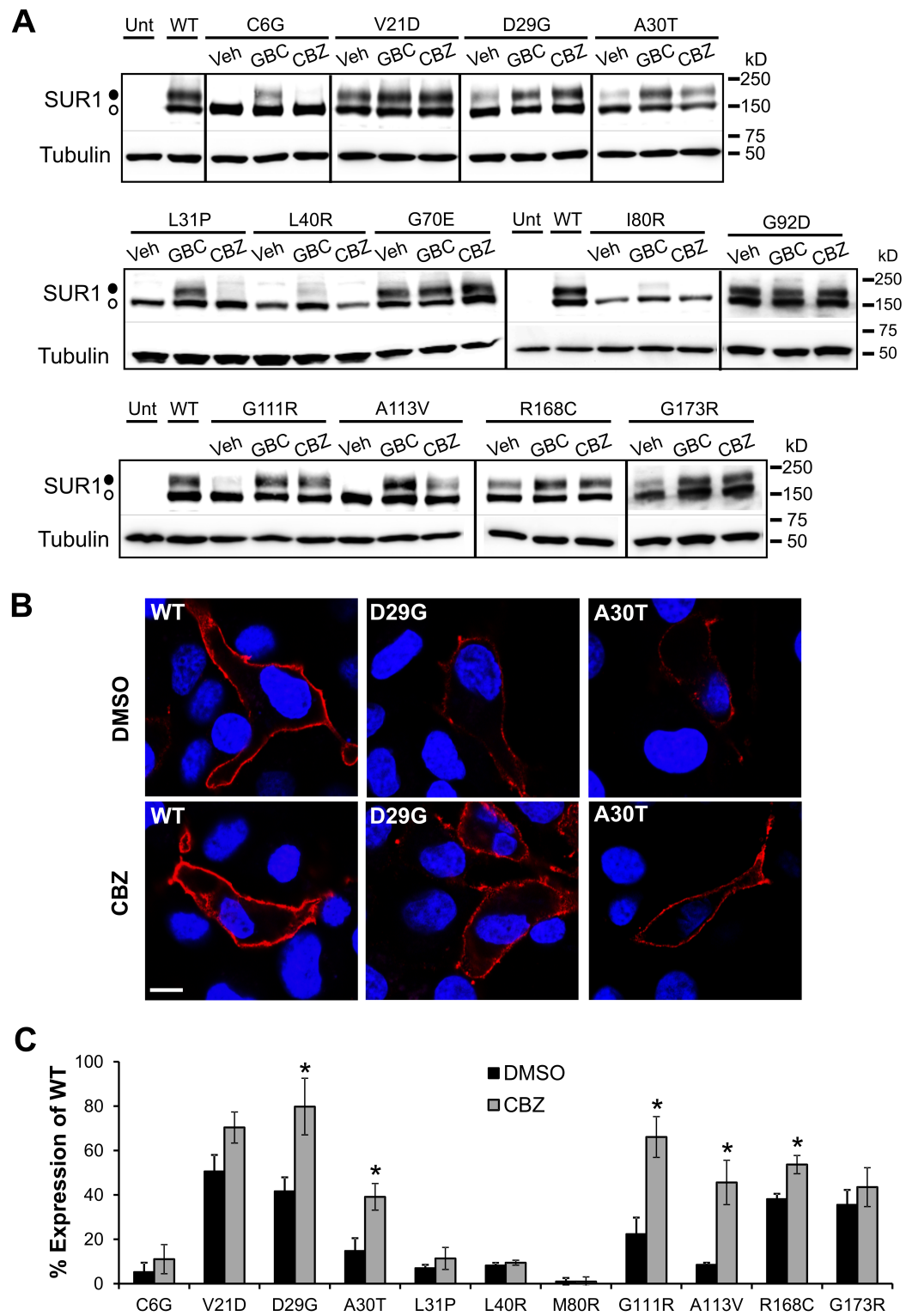
**Figure 1**



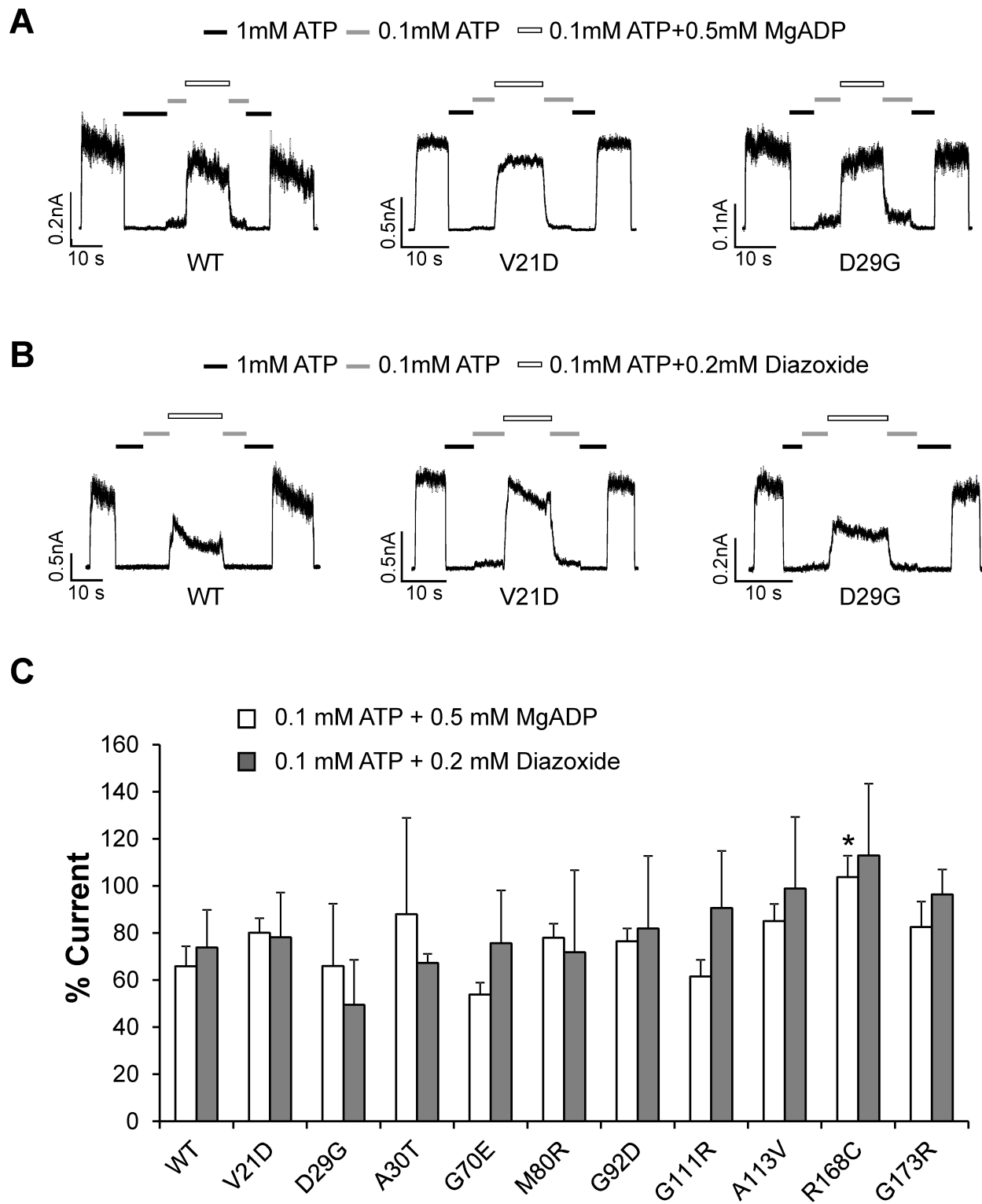
**Figure 2**



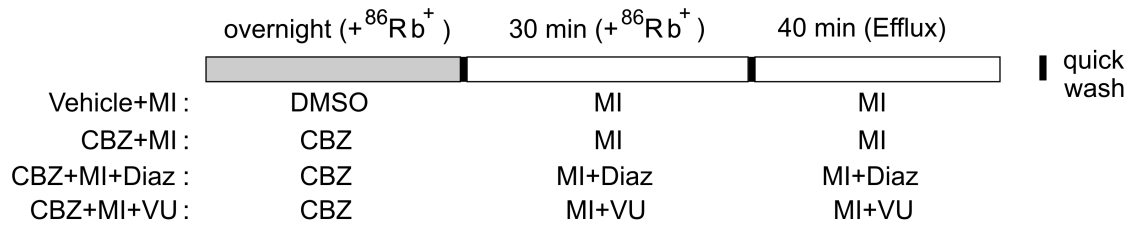
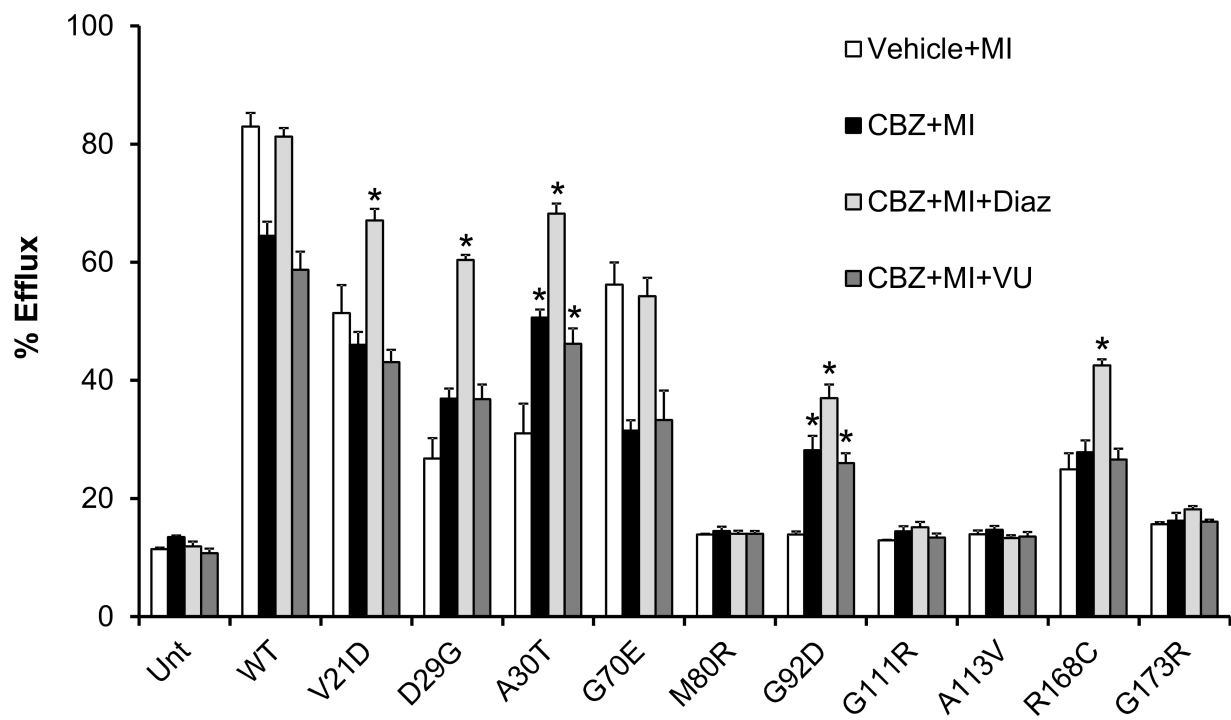
**Figure 3**

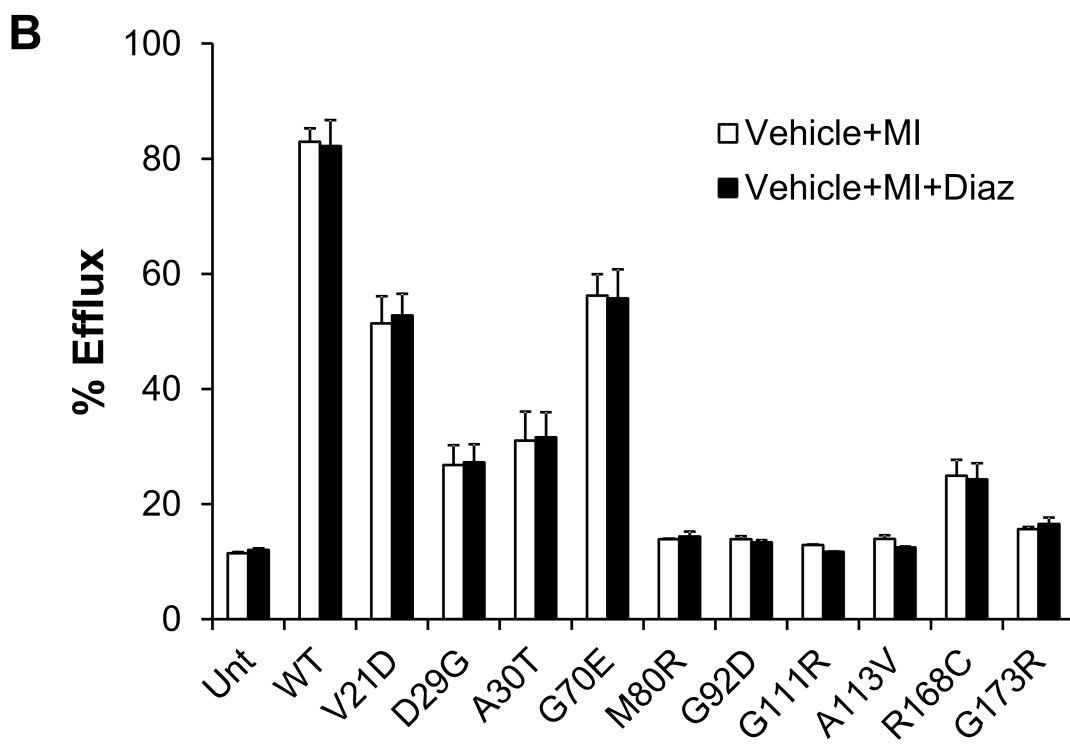
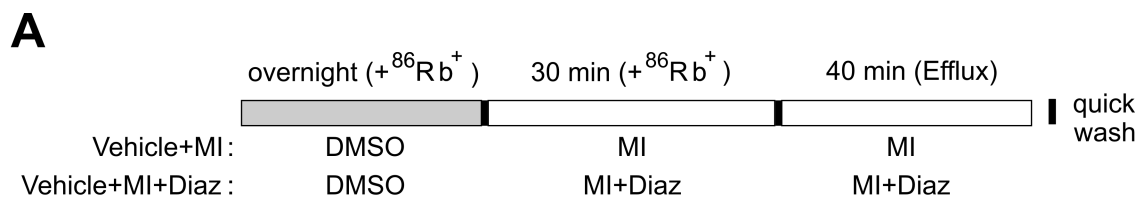


**Figure 4**

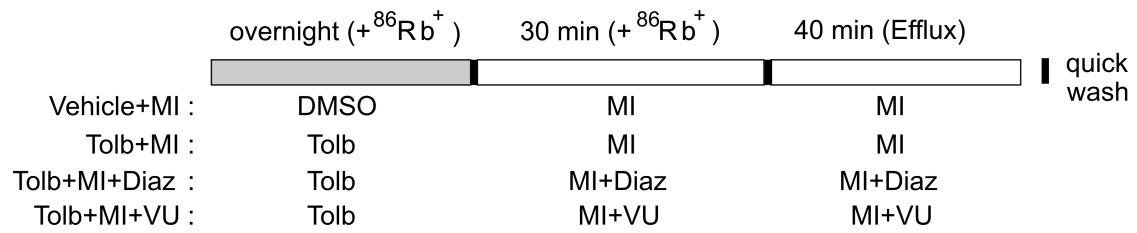
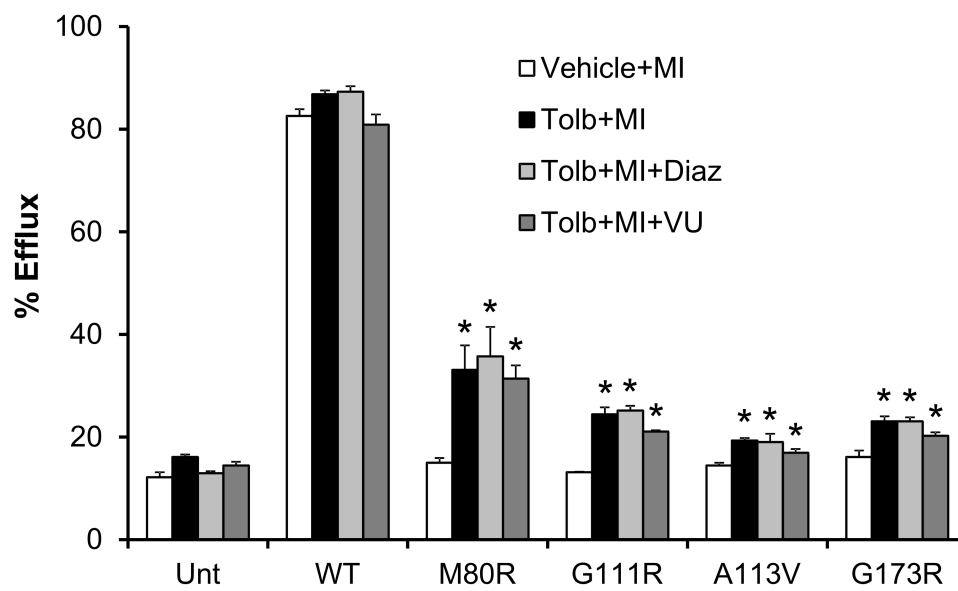


**Figure 5**

**A****B****Figure 6**



**Figure 7**

**A****B****Figure 8**

## References Cited

- Welch, W. J. (2004) Role of quality control pathways in human diseases involving protein misfolding. *Semin Cell Dev Biol* **15**, 31-38
- Convertino, M., Das, J., and Dokholyan, N. V. (2016) Pharmacological Chaperones: Design and Development of New Therapeutic Strategies for the Treatment of Conformational Diseases. *ACS Chem Biol* **11**, 1471-1489
- Leidenheimer, N. J., and Ryder, K. G. (2014) Pharmacological chaperoning: a primer on mechanism and pharmacology. *Pharmacol Res* **83**, 10-19
- Powers, E. T., Morimoto, R. I., Dillin, A., Kelly, J. W., and Balch, W. E. (2009) Biological and chemical approaches to diseases of proteostasis deficiency. *Annu. Rev. Biochem.* **78**, 959-991
- Stanley, C. A. (2016) Perspective on the Genetics and Diagnosis of Congenital Hyperinsulinism Disorders. *J Clin Endocrinol Metab* **101**, 815-826
- Aguilar-Bryan, L., Bryan, J., and Nakazaki, M. (2001) Of mice and men: K(ATP) channels and insulin secretion. *Recent Prog Horm Res* **56**, 47-68
- Ashcroft, F. M. (2005) ATP-sensitive potassium channelopathies: focus on insulin secretion. *J. Clin. Invest.* **115**, 2047-2058
- Aguilar-Bryan, L., and Bryan, J. (1999) Molecular biology of adenosine triphosphate-sensitive potassium channels. *Endocr. Rev.* **20**, 101-135
- Nichols, C. G. (2006) K<sub>ATP</sub> channels as molecular sensors of cellular metabolism. *Nature* **440**, 470-476
- Martin, G. M., Chen, P. C., Devaraneni, P., and Shyng, S. L. (2013) Pharmacological rescue of trafficking-impaired ATP-sensitive potassium channels. *Front. Physiol.* **4**, 386
- Snider, K. E., Becker, S., Boyajian, L., Shyng, S. L., MacMullen, C., Hughes, N., Ganapathy, K., Bhatti, T., Stanley, C. A., and Ganguly, A. (2013) Genotype and phenotype correlations in 417 children with congenital hyperinsulinism. *J. Clin. Endocrinol. Metab.* **98**, E355-363
- Aguilar-Bryan, L., Nichols, C. G., Wechsler, S. W., Clement, J. P. t., Boyd, A. E., 3rd, Gonzalez, G., Herrera-Sosa, H., Nguy, K., Bryan, J., and Nelson, D. A. (1995) Cloning of the beta cell high-affinity sulfonylurea receptor: a regulator of insulin secretion. *Science* **268**, 423-426
- Yan, F., Lin, C. W., Weisiger, E., Cartier, E. A., Taschenberger, G., and Shyng, S. L. (2004) Sulfonylureas correct trafficking defects of ATP-sensitive potassium channels caused by mutations in the sulfonylurea receptor. *J. Biol. Chem.* **279**, 11096-11105
- Yan, F. F., Casey, J., and Shyng, S. L. (2006) Sulfonylureas correct trafficking defects of disease-causing ATP-sensitive potassium channels by binding to the channel complex. *J. Biol. Chem.* **281**, 33403-33413
- Yan, F. F., Lin, Y. W., MacMullen, C., Ganguly, A., Stanley, C. A., and Shyng, S. L. (2007) Congenital hyperinsulinism associated ABCC8 mutations that cause defective trafficking of ATP-sensitive K<sup>+</sup> channels: identification and rescue. *Diabetes* **56**, 2339-2348
- Pratt, E. B., Yan, F. F., Gay, J. W., Stanley, C. A., and Shyng, S. L. (2009) Sulfonylurea receptor 1 mutations that cause opposite insulin secretion defects with chemical chaperone exposure. *J Biol Chem* **284**, 7951-7959
- Chen, P. C., Olson, E. M., Zhou, Q., Kryukova, Y., Sampson, H. M., Thomas, D. Y., and Shyng, S. L. (2013) Carbamazepine as a novel small molecule corrector of trafficking-impaired

- ATP-sensitive potassium channels identified in congenital hyperinsulinism. *J. Biol. Chem.* **288**, 20942-20954
- Zhou, Q., Chen, P. C., Devaraneni, P. K., Martin, G. M., Olson, E. M., and Shyng, S. L. (2014) Carbamazepine inhibits ATP-sensitive potassium channel activity by disrupting channel response to MgADP. *Channels (Austin)* **8**
- Sampson, H. M., Lam, H., Chen, P. C., Zhang, D., Mottillo, C., Mirza, M., Qasim, K., Shrier, A., Shyng, S. L., Hanrahan, J. W., and Thomas, D. Y. (2013) Compounds that correct F508del-CFTR trafficking can also correct other protein trafficking diseases: an in vitro study using cell lines. *Orphanet J. Rare Dis.* **8**, 11
- Babenko, A. P., and Bryan, J. (2003) SUR domains that associate with and gate  $K_{ATP}$  pores define a novel gatekeeper. *J. Biol. Chem.* **278**, 41577-41580
- Chan, K. W., Zhang, H., and Logothetis, D. E. (2003) N-terminal transmembrane domain of the SUR controls trafficking and gating of Kir6 channel subunits. *EMBO J.* **22**, 3833-3843
- Schwappach, B., Zerangue, N., Jan, Y. N., and Jan, L. Y. (2000) Molecular basis for  $K_{ATP}$  assembly: transmembrane interactions mediate association of a  $K^+$  channel with an ABC transporter. *Neuron* **26**, 155-167
- Devaraneni, P. K., Martin, G. M., Olson, E. M., Zhou, Q., and Shyng, S. L. (2015) Structurally distinct ligands rescue biogenesis defects of the  $K_{ATP}$  channel complex via a converging mechanism. *J Biol Chem* **290**, 7980-7991
- Flanagan, S. E., Clauin, S., Bellanne-Chantelot, C., de Lonlay, P., Harries, L. W., Gloyn, A. L., and Ellard, S. (2009) Update of mutations in the genes encoding the pancreatic beta-cell K(ATP) channel subunits Kir6.2 (KCNJ11) and sulfonylurea receptor 1 (ABCC8) in diabetes mellitus and hyperinsulinism. *Hum Mutat* **30**, 170-180
- Tornovsky, S., Crane, A., Cosgrove, K. E., Hussain, K., Lavie, J., Heyman, M., Nesher, Y., Kuchinski, N., Ben-Shushan, E., Shatz, O., Nahari, E., Potikha, T., Zangen, D., Tenenbaum-Rakover, Y., de Vries, L., Argente, J., Gracia, R., Landau, H., Eliakim, A., Lindley, K., Dunne, M. J., Aguilar-Bryan, L., and Glaser, B. (2004) Hyperinsulinism of infancy: novel ABCC8 and KCNJ11 mutations and evidence for additional locus heterogeneity. *J Clin Endocrinol Metab* **89**, 6224-6234
- Raab-Graham, K. F., Cirilo, L. J., Boettcher, A. A., Radeke, C. M., and Vandenberg, C. A. (1999) Membrane topology of the amino-terminal region of the sulfonylurea receptor. *J Biol Chem* **274**, 29122-29129
- Zerangue, N., Schwappach, B., Jan, Y. N., and Jan, L. Y. (1999) A new ER trafficking signal regulates the subunit stoichiometry of plasma membrane  $K_{ATP}$  channels. *Neuron* **22**, 537-548
- Fukuda, Y., Aguilar-Bryan, L., Vaxillaire, M., Dechaume, A., Wang, Y., Dean, M., Moitra, K., Bryan, J., and Schuetz, J. D. (2011) Conserved intramolecular disulfide bond is critical to trafficking and fate of ATP-binding cassette (ABC) transporters ABCB6 and sulfonylurea receptor 1 (SUR1)/ABCC8. *J Biol Chem* **286**, 8481-8492
- Chen, P. C., Olson, E. M., Zhou, Q., Kryukova, Y., Sampson, H. M., Thomas, D. Y., and Shyng, S. L. (2013) Carbamazepine as a novel small molecule corrector of trafficking-impaired ATP-sensitive potassium channels identified in congenital hyperinsulinism. *The Journal of biological chemistry* **288**, 20942-20954
- Yan, F., Lin, C. W., Weisiger, E., Cartier, E. A., Taschenberger, G., and Shyng, S. L. (2004) Sulfonylureas correct trafficking defects of ATP-sensitive potassium channels caused by

- mutations in the sulfonylurea receptor. *The Journal of biological chemistry* **279**, 11096-11105
- Raphemot, R., Swale, D. R., Dadi, P. K., Jacobson, D. A., Cooper, P., Wojtovich, A. P., Banerjee, S., Nichols, C. G., and Denton, J. S. (2014) Direct activation of beta-cell KATP channels with a novel xanthine derivative. *Mol Pharmacol* **85**, 858-865
- Cosgrove, K. E., Straub, S. G., Barnes, P. D., Chapman, J., Sharp, G. W., and Dunne, M. J. (2004) Y-26763: ATP-sensitive K<sup>+</sup> channel activation and the inhibition of insulin release from human pancreatic beta-cells. *Eur J Pharmacol* **486**, 133-139
- Nielsen, F. E., Ebdrup, S., Jensen, A. F., Ynddal, L., Bodvarsdottir, T. B., Stidsen, C., Worsaae, A., Boonen, H. C., Arkhammar, P. O., Fremming, T., Wahl, P., Korno, H. T., and Hansen, J. B. (2006) New 3-alkylamino-4H-thieno-1,2,4-thiadiazine 1,1-dioxide derivatives activate ATP-sensitive potassium channels of pancreatic beta cells. *J Med Chem* **49**, 4127-4139
- Macmullen, C. M., Zhou, Q., Snider, K. E., Tewson, P. H., Becker, S. A., Aziz, A. R., Ganguly, A., Shyng, S. L., and Stanley, C. A. (2011) Diazoxide-unresponsive congenital hyperinsulinism in children with dominant mutations of the beta-cell sulfonylurea receptor SUR1. *Diabetes* **60**, 1797-1804
- Ashcroft, F. M., and Gribble, F. M. (1998) Correlating structure and function in ATP-sensitive K<sup>+</sup> channels. *Trends Neurosci* **21**, 288-294
- Gloyn, A. L., Pearson, E. R., Antcliff, J. F., Proks, P., Bruining, G. J., Slingerland, A. S., Howard, N., Srinivasan, S., Silva, J. M., Molnes, J., Edghill, E. L., Frayling, T. M., Temple, I. K., Mackay, D., Shield, J. P., Sumnik, Z., van Rhijn, A., Wales, J. K., Clark, P., Gorman, S., Aisenberg, J., Ellard, S., Njolstad, P. R., Ashcroft, F. M., and Hattersley, A. T. (2004) Activating mutations in the gene encoding the ATP-sensitive potassium-channel subunit Kir6.2 and permanent neonatal diabetes. *New Engl. J. Med.* **350**, 1838-1849
- Nichols, C. G., Shyng, S. L., Nestorowicz, A., Glaser, B., Clement, J. P. t., Gonzalez, G., Aguilar-Bryan, L., Permutt, M. A., and Bryan, J. (1996) Adenosine diphosphate as an intracellular regulator of insulin secretion. *Science* **272**, 1785-1787
- Cartier, E. A., Conti, L. R., Vandenberg, C. A., and Shyng, S. L. (2001) Defective trafficking and function of KATP channels caused by a sulfonylurea receptor 1 mutation associated with persistent hyperinsulinemic hypoglycemia of infancy. *Proc Natl Acad Sci U S A* **98**, 2882-2887
- Taschenberger, G., Mougey, A., Shen, S., Lester, L. B., LaFranchi, S., and Shyng, S. L. (2002) Identification of a familial hyperinsulinism-causing mutation in the sulfonylurea receptor 1 that prevents normal trafficking and function of KATP channels. *J Biol Chem* **277**, 17139-17146
- Cutting, G. R. (2015) Cystic fibrosis genetics: from molecular understanding to clinical application. *Nature reviews. Genetics* **16**, 45-56
- Nestorowicz, A., Wilson, B. A., Schoor, K. P., Inoue, H., Glaser, B., Landau, H., Stanley, C. A., Thornton, P. S., Clement, J. P. t., Bryan, J., Aguilar-Bryan, L., and Permutt, M. A. (1996) Mutations in the sulfonylurea receptor gene are associated with familial hyperinsulinism in Ashkenazi Jews. *Hum Mol Genet* **5**, 1813-1822
- Snider, K. E., Becker, S., Boyajian, L., Shyng, S. L., MacMullen, C., Hughes, N., Ganapathy, K., Bhatti, T., Stanley, C. A., and Ganguly, A. (2013) Genotype and phenotype correlations in 417 children with congenital hyperinsulinism. *J Clin Endocrinol Metab* **98**, E355-363

- Suchi, M., MacMullen, C. M., Thornton, P. S., Adzick, N. S., Ganguly, A., Ruchelli, E. D., and Stanley, C. A. (2006) Molecular and immunohistochemical analyses of the focal form of congenital hyperinsulinism. *Modern pathology : an official journal of the United States and Canadian Academy of Pathology, Inc* **19**, 122-129
- Greer, R. M., Shah, J., Jeske, Y. W., Brown, D., Walker, R. M., Cowley, D., Bowling, F. G., Liaskou, D., Harris, M., Thomsett, M. J., Choong, C., Bell, J. R., Jack, M. M., and Cotterill, A. M. (2007) Genotype-phenotype associations in patients with severe hyperinsulinism of infancy. *Pediatric and developmental pathology : the official journal of the Society for Pediatric Pathology and the Paediatric Pathology Society* **10**, 25-34
- Otonkoski, T., Nanto-Salonen, K., Seppanen, M., Veijola, R., Huopio, H., Hussain, K., Tapanainen, P., Eskola, O., Parkkola, R., Ekstrom, K., Guiot, Y., Rahier, J., Laakso, M., Rintala, R., Nuutila, P., and Minn, H. (2006) Noninvasive diagnosis of focal hyperinsulinism of infancy with [18F]-DOPA positron emission tomography. *Diabetes* **55**, 13-18
- Fernandez-Marmiesse, A., Salas, A., Vega, A., Fernandez-Lorenzo, J. R., Barreiro, J., and Carracedo, A. (2006) Mutation spectra of ABCC8 gene in Spanish patients with Hyperinsulinism of Infancy (HI). *Hum Mutat* **27**, 214
- De Vroede, M., Bax, N. M., Brusgaard, K., Dunne, M. J., and Groenendaal, F. (2004) Laparoscopic diagnosis and cure of hyperinsulinism in two cases of focal adenomatous hyperplasia in infancy. *Pediatrics* **114**, e520-522
- Verheul, J. C., Ris-Stalpers, C., Bikker, H., Bakker-van Waarde, W. M., and Noordam, C. (2011) [Congenital hyperinsulinism in the north-east Netherlands. Clinical features and DNA diagnostics in 22 children]. *Nederlands tijdschrift voor geneeskunde* **155**, A3343
- Hardy, O. T., Hernandez-Pampaloni, M., Saffer, J. R., Suchi, M., Ruchelli, E., Zhuang, H., Ganguly, A., Freifelder, R., Adzick, N. S., Alavi, A., and Stanley, C. A. (2007) Diagnosis and localization of focal congenital hyperinsulinism by 18F-fluorodopa PET scan. *J Pediatr* **150**, 140-145
- Conti, L. R., Radeke, C. M., Shyng, S. L., and Vandenberg, C. A. (2001) Transmembrane topology of the sulfonylurea receptor SUR1. *The Journal of biological chemistry* **276**, 41270-41278

## Chapter 3

### Cryo-EM structure of the ATP-sensitive potassium channel illuminates mechanisms of assembly and gating

Gregory M. Martin<sup>1</sup>, Craig Yoshioka<sup>2</sup>, Emily A. Rex<sup>1</sup>, Jonathan F. Fay<sup>1</sup>, Qing Xie<sup>1</sup>, Matt R. Whorton<sup>3</sup>, James Z. Chen<sup>1\*</sup> & Show-Ling Shyng<sup>1\*</sup>

<sup>1</sup>Department of Biochemistry and Molecular Biology, Oregon Health & Science University, Portland, OR 97239, USA; <sup>2</sup>Department of Biomedical Engineering, Oregon Health & Science University, 2730 SW Moody Ave, Portland, OR 97239, USA. <sup>3</sup>Vollum Institute, Oregon Health & Science University, Portland, OR 97239, USA.

\*Correspondence to: Show-Ling Shyng ([shyngs@ohsu.edu](mailto:shyngs@ohsu.edu)) or James Chen ([chezh@ohsu.edu](mailto:chezh@ohsu.edu)), Department of Biochemistry and Molecular Biology, School of Medicine, Oregon Health & Science University, 3181 S.W. Sam Jackson Park Road, Portland, OR 97239.

**Published in:** Martin GM, Yoshioka C, Rex EA, Fay JF, Xie Q, Whorton MR, Chen JZ, Shyng SL. (2017). Cryo-EM structure of the ATP-sensitive potassium channel illuminates mechanisms of assembly and gating. *eLife*. Jan 16; 6.

#### Author Contributions

**GMM:** Experimental design, conceived of project. Writing: original draft and revision; Figure making. Sample preparation: cell culture and protein expression, protein purification, negative stain and cryo-EM sample prep. Electron microscopy: data collection (cryo-EM and negative stain EM). Structure solution: generated initial models for SUR1 and Kir6.2, built and refined Kir6.2 model, deposited final structure and density maps to database. **CY:** Cryo-EM data collection. Image processing and generation of final EM map. Structure solution: built and refined SUR1 model. Writing: original draft (methods), revision. Figure making (Fig.1, Table 1). **EAR:** Sample preparation: generation of virus, cell culture and protein expression. **JFF:** Cryo-EM data collection. **QX:** aided in structure refinement. **MRW:** Writing: aided in Kir6.2 structural interpretation, edited manuscript draft and revision. **JZC:** Experimental design. Writing: original draft (methods), revision. Figure making (Fig.2A, Table 1). **SLS:** Experimental design, conceived of project. Writing: original draft and revision; Figure making.

## **Abstract**

$K_{ATP}$  channels are metabolic sensors that couple cell energetics to membrane excitability. In pancreatic  $\beta$ -cells, channels formed by SUR1 and Kir6.2 regulate insulin secretion and are the targets of antidiabetic sulfonylureas. Here, we used cryo-EM to elucidate structural basis of channel assembly and gating. The structure, determined in the presence of ATP and the sulfonylurea glibenclamide, at  $\sim 6\text{\AA}$  resolution reveals a closed Kir6.2 tetrameric core with four peripheral SUR1s each anchored to a Kir6.2 by its N-terminal transmembrane domain (TMD0). Intricate interactions between TMD0, the loop following TMD0, and Kir6.2 near the proposed  $PIP_2$  binding site, and where ATP density is observed, suggest SUR1 may contribute to ATP and  $PIP_2$  binding to enhance Kir6.2 sensitivity to both. The SUR1-ABC core is found in an unusual inward-facing conformation whereby the two nucleotide binding domains are misaligned along a two-fold symmetry axis, revealing a possible mechanism by which glibenclamide inhibits channel activity.

## **Introduction**

Studies into the electric mechanisms of insulin release of the pancreatic  $\beta$ -cell in the early 1980s led to the discovery and identification of an ATP-sensitive potassium ( $K_{ATP}$ ) channel as the key molecular link between glucose metabolism and insulin secretion (Ashcroft & Rorsman, 1990; Cook & Bryan, 1998). Subsequent cloning and characterization revealed the  $\beta$ -cell  $K_{ATP}$  channel as a complex of two proteins: a potassium channel Kir6.2 of the inwardly rectifying  $K^+$  channel family, and a sulfonylurea receptor SUR1, a member of the ATP binding cassette (ABC) transporter protein family (Inagaki et al., 1995).

Physiological activity of  $K_{ATP}$  channels is determined primarily by the relative concentrations of ATP and ADP: ATP inhibits, whereas MgADP stimulates channel activity (Nichols, 2006). As  $K_{ATP}$  channels set the  $\beta$ -cell membrane potential, this regulation by nucleotides endows them the ability to sense metabolic changes and translate those into changes in membrane excitability, which ultimately initiates or stops insulin secretion (Ashcroft, 2005). Another key player for  $K_{ATP}$  function is membrane phosphatidylinositol-4,5-bisphosphate ( $PIP_2$ ); as in all other Kir family members,  $PIP_2$  is required for channel opening and sets the intrinsic open probability ( $P_o$ ) of the channel (Hibino et al., 2010; Nichols, 2006). Mutations disrupting channel assembly or the above gating properties result in insulin secretion disorders, with loss- or gain-of-function mutations causing congenital hyperinsulinism (HI) or permanent neonatal diabetes mellitus (PNDM), respectively (Ashcroft, 2005). Importantly,  $K_{ATP}$  channels are the targets of sulfonylureas, one of the most commonly prescribed treatments for type 2 diabetes, which stimulate insulin secretion by inhibiting channel activity (Gribble & Reimann, 2003). In particular, glibenclamide (GBC) binds the channel with nanomolar affinity and was instrumental for the purification and cloning of SUR1 (Aguilar-Bryan et al., 1995).

A member of the Kir channel family, Kir6.2 consists of two transmembrane helices and N- and C-terminal cytoplasmic domains (Hibino et al., 2010). By comparison, SUR1, a member of the ABC transporter family, is much larger in size. In addition to a characteristic ABC core structure comprising two transmembrane domains (TMD1 & 2) and two cytoplasmic nucleotide binding domains (NBD1 & 2), it has an N-terminal extension that contains a transmembrane domain (TMD0) followed by a long, cytoplasmic loop “L0” which connects to the ABC core (Aguilar-Bryan et al., 1995; Tuszny et al., 2006). Kir6.2 and SUR1 are uniquely dependent on

each other for expression and function (Inagaki et al., 1995). Interestingly, unlike most ABC transporters such as the cystic fibrosis transmembrane conductance regulator (CFTR) and the multidrug resistant protein P-glycoprotein, SUR1 itself has no known ion channel or transporter activity; instead, its function is to regulate Kir6.2 channels (Aguilar-Bryan et al., 1995; Inagaki et al., 1995; Wilkens, 2015). A central question is how the two proteins assemble and function as a complex to sense metabolic signals.

Biochemical and biophysical studies have indicated that the  $K_{ATP}$  channel is an octamer of four Kir6.2 and four SUR1 subunits. ATP and  $PIP_2$  bind Kir6.2 directly to close or open the channel, respectively (Baukrowitz et al., 1998; Shyng & Nichols, 1998; Tanabe et al., 1999; Tucker et al., 1997). Although Kir6.2 alone can be gated by ATP and  $PIP_2$ , its sensitivities to both ATP and  $PIP_2$  are increased by SUR1 by ~10-fold (Baukrowitz et al., 1998; Enkvetchakul et al., 2000; Shyng & Nichols, 1998; Tucker et al., 1997). How SUR1 sensitizes Kir6.2 to ATP inhibition and  $PIP_2$  stimulation remains unclear. In contrast to ATP inhibition of the channel which does not depend on  $Mg^{2+}$  and ATP hydrolysis, nucleotide stimulation of the channel is conferred by SUR1 and requires  $Mg^{2+}$  (Ashcroft & Gribble, 1998; Gribble, Ashfield, et al., 1997; Gribble, Tucker, Haug, et al., 1998; Nichols, 2006). Evidence suggests that MgATP and MgADP interact with the nucleotide binding domains (NBDs) of SUR1 and either through MgATP hydrolysis or direct MgADP binding at NBD2, promote NBDs dimerization and channel opening (de Wet et al., 2012; Nichols, 2006; Zingman et al., 2007). Moreover, GBC has been proposed to inhibit  $K_{ATP}$  channels by preventing Mg-nucleotide stimulation (de Wet & Proks, 2015), and may do so by stabilizing the ABC core of SUR1 in an inward-facing conformation (Ortiz et al., 2012) but direct evidence is lacking.

In order to understand how the channel functions as a complex to respond to physiological and pharmacological molecules and mechanisms by which channel mutations cause disease, detailed structural information is crucial. Here, we used cryo-EM to elucidate the structural basis of  $K_{ATP}$  channel assembly and gating.

## Results

### *Structure determination*

To obtain sufficient quantity of purified channel complexes we used rat insulinoma INS-1 cells, which naturally express  $K_{ATP}$  channels, for overexpression. Cells were transduced with recombinant adenoviruses encoding genes for a FLAG-tagged hamster SUR1 and a rat Kir6.2 (Pratt et al., 2009), which are 95 and 96% identical to the human sequences, respectively. These heterologously expressed channels have gating properties indistinguishable from endogenous  $K_{ATP}$  channels (Pratt et al., 2009). Channel integrity was found to be best preserved when membranes were solubilized in digitonin and channels purified in the presence of 1  $\mu$ M glibenclamide (GBC) and 1 mM ATP (see Materials & Methods) (Fig.1), which was the condition used for cryo-EM structure determination.

Single-particle analysis using RELION identified two three-dimensional (3D) classes of particles with distinct conformations in the cytoplasmic domain of Kir6.2 (see discussion below). The dominant class (~60%) produced a reconstruction which has an overall resolution of 6.7Å (FSC=0.143) with C4 symmetry imposed (Fig. 1-figure supplements 1 and 2; Table 1). With masking the FSC measurement at 0.143 reached 5.8Å and the Kir6.2 core 5.1Å. The other class

yielded a reconstruction with an overall unmasked resolution  $\sim 7.6\text{\AA}$ , and masked whole channel and Kir6.2 core  $\sim 7.2\text{\AA}$  and  $6.9\text{\AA}$ , respectively. The higher resolution map was used for model building and structural analysis. All transmembrane (TM) helices were clearly resolved in the density map (76 total; 17 from each SUR1, 2 from each Kir6.2; Fig.2), and contained significant side-chain density which allowed for registration of the models.

Kir6.2 is a member of the highly conserved Kir channel family in which several structures have been solved (Hibino et al., 2010). By contrast, SUR1 is one of the few ABC transporter proteins which have an N-terminal extension consisting of a transmembrane domain termed TMD0 followed by a long intracellular loop (the third intracellular loop, ICL3) termed L0, in addition to an ABC core structure comprising two transmembrane domains (TMD1 & 2) and two nucleotide binding domains (NBD1 & 2) (Tusnady et al., 2006). The Kir6.2 and SUR1 ABC core domain models were built initially from homologous Kir and ABC transporter structures (sequence and model comparisons with templates shown in Fig.2-supplements 1-4) and then refined to fit the density. Because there is no known structural template for the TMD0-L0 of SUR1, this region was modelled *de novo*.

#### *Overall architecture of the $K_{ATP}$ channel*

The structure shows that the  $K_{ATP}$  channel is an octamer built around a Kir6.2 tetramer with each subunit complexed to one SUR1 (Fig.2). The complex is  $\sim 200\text{\AA}$  in width in the longest dimension and  $\sim 125\text{\AA}$  in height, and is shaped like a propeller with the Kir6.2 pore and TMD0 forming a compact central core and the SUR1-ABC core structure forming the blades.

A long-standing question has been where TMD0 and L0 are in relation to Kir6.2 and the ABC core structure, as this region has been shown to be crucial for channel assembly and gating (Babenko & Bryan, 2003; Chan et al., 2003; Schwappach et al., 2000). An earlier model hypothesized TMD0 to be sandwiched between Kir6.2 and the TMDs of the ABC core (Bryan et al., 2004), but a later cryo-negative stain single-particle EM study of a channel formed by a SUR1-Kir6.2 fusion protein placed TMD0 next to Kir6.2 in between two adjacent SUR1-ABC core domains (Mikhailov et al., 2005). In our structure, TMD0-L0 sits in between the SUR1 and Kir6.2 subunits, and is the primary point of contact between the SUR1-ABC core and Kir6.2 (Fig.2).

#### *The Kir6.2 tetramer is in a closed conformation*

The Kir6.2 tetramer is the best resolved region in the complex (Fig.3A). Side-chain density of many residues, in particular those in the two TM helices are visible (Fig.3B). With knowledge of existing Kir channel structures, this allowed for confident model building (see Materials and Methods; sequence comparison with the template is shown in Fig.2-supplement 1).

A vertical slice through the middle of the channel highlights the K<sup>+</sup> conduction pathway (Fig.3C). The three constriction points correspond to the selectivity filter, inner helix gate, and G-loop gate in other known Kir structures (Hansen et al., 2011; Whorton & MacKinnon, 2011). In Kir6.2, the inner helix gate is formed by F168 in M2 just below the central cavity. In our model, there is only ~6Å between opposing atoms of the gate (~3Å when considering the van der Waals radii), which is too narrow to allow passage of a ~8Å diameter hydrated K<sup>+</sup> ion (Fig.3D). The G-loop gate formed at the apex of the cytoplasmic domains is shown in Fig.3E. A comparison of closed (Kir3.2 apstate) and open (Kir3.2-R201A + PIP<sub>2</sub>) G-loop structures in

relation to Kir6.2 suggests that this gate is also closed (Fig.3E). Together, these observations indicate a closed channel structure, which is expected since the sample contained saturating concentrations of inhibitory ATP and GBC.

Interestingly, 3D classification identified two classes with distinct conformations in the cytoplasmic domain (CTD) of Kir6.2. The two classes differ by a rigid-body rotation of the CTD of  $\sim 14^\circ$  (Fig.1-supplement 2F). A similar rotation has been observed in multiple Kir channel members and has been associated with channel gating (Clarke et al., 2010; Whorton & MacKinnon, 2013). However, the TMD and gates as well as the density corresponding to bound ATP (see below) in both classes are largely unaffected, suggesting rotational freedom for the CTD in the closed state. Whether this rotation represents a conformational transition that occurs during gating needs further investigation.

#### *Identification of the ATP binding pocket*

A hallmark of the  $K_{ATP}$  channel is its inhibition by intracellular ATP. Mutagenesis and biochemical studies suggest that ATP binds directly to Kir6.2 (Tanabe et al., 1999; Tucker et al., 1997), and that residues in both N- and C-terminal domains are involved (Antcliff et al., 2005; Nichols, 2006). However, while Kir6.2 is sensitive to ATP in the absence of SUR1 ( $IC_{50} \sim 100 \mu M$ ), SUR1 increases this sensitivity by  $\sim 10$ -fold ( $IC_{50} \sim 10 \mu M$ ) (Tucker et al., 1997). Where ATP binds and how SUR1 enhances the sensitivity to ATP inhibition remain key questions.

Since our preparation contained 1 mM ATP, we reasoned that ATP is likely bound to the channel. Indeed, we observed a prominent bulge in the EM density that is too large to be

accounted for by the main chain and the surrounding side-chains. The density is about the size of an ATP molecule and is immediately adjacent to K185, a residue that has been implicated in ATP binding (John et al., 2003; Tanabe et al., 1999; Tucker et al., 1997). Extensive mutagenesis of the K185 residue assessing the effects of various amino acid substitutions on channel sensitivity to inhibition by ATP, ADP, and AMP has provided strong evidence that this residue is important for binding to the  $\beta$ -phosphate of ATP (Jons et al., 2006). We used this information to guide the initial docking of ATP into the density and then refined with the surrounding protein in RSRef (Chapman et al., 2013).

An overview of the ATP binding site from the side (Fig.4A), and from the top (Fig.4B), with ATP colored in red, illustrates that the pocket is at the interface of adjacent Kir6.2 N and C domains. A close-up view (Fig.4C) shows that the docked ATP is surrounded by residues I182, L205, Y330, F333, and G334 from the same subunit, and R50 from the adjacent subunit. The adenine ring is pointing towards the N-terminus of subunit A, and could be supported by I182, L205, Y330 and F333 of subunit B. R50 in subunit A is in a position that would allow it to interact with the  $\gamma$ -phosphate but may also interact with the adenine ring, which would explain mutagenesis data indicating that the interaction of R50 and ATP is not entirely electrostatic (John et al., 2003). K185 is only  $\sim 3\text{\AA}$  from the  $\beta$  phosphate, while the  $\alpha$ -phosphate is close to the main-chain nitrogen of G334 (Fig.4C, D). Importantly, most residues surrounding the ATP density have been mutated and shown to affect ATP sensitivity (Antcliff et al., 2005), providing direct validation of our structure.

In our structure, we see that the density corresponding to ATP is located on the periphery of the Kir6.2 cytoplasmic domain, and traversed by the N-terminal segment of L0 of SUR1

immediately following TMD0 (Fig.4B), with the C $\alpha$  of K205 coming within only  $\sim 10\text{\AA}$  of the site (Fig.4D). Interestingly, we have previously shown that mutation of K205 of L0 to alanine or glutamate reduce ATP sensitivity by  $\sim 10$ -fold (Pratt et al., 2012). While there is no density in the map to allow placement of the K205 side chain, its C $\alpha$  position lies directly over the site and is poised to make electrostatic contribution to ATP binding. This finding offers a mechanism by which SUR1 could enhance the ATP-sensitivity of the Kir6.2 channel.

#### *Interactions between TMD0-L0 of SUR1 and Kir6.2*

As shown in Fig.2, TMD0-L0 is sandwiched between the SUR1-ABC core structure and Kir6.2. In the map, densities corresponding to TMD0 and L0 are clearly seen, particularly TMD0, with much of this domain reaching  $5\text{\AA}$  resolution. This is in contrast to a recent cryo-EM study of another ABC transporter containing a TMD0, TAP1/2, where TMD0 could not be resolved (Oldham et al., 2016), possibly because SUR1-TMD0 in our structure is stabilized by Kir6.2. Overall, TMD0 is a five helix bundle which contains an extracellular N-terminal segment of 25 residues with a brief helical stretch, and mostly short loops connecting helices 2-3, 3-4, and 4-5, but a longer ICL1 of  $\sim 14$  residues connecting TM1-2 (Fig. 5A). The N-terminus containing the FLAG-peptide was disordered up until residue C6 of SUR1 where a highly conserved disulfide bond is formed with C26 (Fukuda et al., 2011) at the entrance to TM1. This region contacts the Kir6.2 turret and pore loop (Fig. 5-supplement 1A), suggesting a role in assembly and functional coupling with the pore. A number of HI-causing mutations in the N-terminal extracellular loop of TMD0 including C6G, G7R, V21D, N24K, and C26S, which disrupt channel biogenesis efficiency or gating have been reported (Martin et al., 2016; Yan et al., 2007), further supporting the significance of this region in channel assembly and gating.

In the transmembrane region, TM1 of TMD0 and the M1 helix of Kir6.2 are the primary sites of interaction. These helices make close contact throughout their entire length (Fig.5A) and at residue P45 in TM1, a kink is introduced that places the trajectory of the two helices in alignment (Fig.5-supplement 1B). There are many potential hydrophobic interactions between opposing faces of these helices, which may facilitate association of the complex (Fig.5-supplement 1C). Indeed, multiple HI-causing mutations in TM1 of TMD0 (F27S, A30T, L31P, L40R) have been shown to impair channel assembly and surface expression (Martin et al., 2016), likely by disrupting interactions between the two helices.

On the cytoplasmic side, there are intimate interactions between the ICLs of TMD0, the start of L0, the Kir6.2 binding pocket (cytoplasmic ends of M1 and M2 helices) identified based on other PIP<sub>2</sub>-bound Kir structures (Hansen et al., 2011; Whorton & MacKinnon, 2011), and the Kir6.2 ATP binding pocket. As shown in Fig.5B and C, the hypothetically docked PIP<sub>2</sub> is surrounded by the cytoplasmic loop connecting TM3 and 4 (ICL2; E128-P133) of TMD0 and the N-terminal stretch of L0 (K192-K199) from one SUR1 subunit, and the cytoplasmic end of TM1 (K57) of TMD0 from the adjacent SUR1 subunit. Previous studies have shown that TMD0 and the N-terminal section of L0 increase the  $P_o$  of Kir6.2 to resemble intact channels (Babenko & Bryan, 2003; Chan et al., 2003). As  $P_o$  is determined by PIP<sub>2</sub> interactions, our structure suggests these regions may contribute directly to PIP<sub>2</sub> binding to account for the increase in PIP<sub>2</sub> sensitivity conferred by SUR1 (Enkvetchakul et al., 2000). Below PIP<sub>2</sub> and near the periphery of Kir6.2 lies ATP, separated from PIP<sub>2</sub> by L0 (Fig. 5B, C) and also ICL2 of TMD0 (Fig.5B, E). The ICL2 sits directly atop the Kir6.2 N-terminus, just before the interfacial helix (i.e. the “slide

helix”) at Q52 (Fig.5D), and simultaneously contacts ICL1 of TMD0 and the most C-terminal portion of TMD0 at TM5. Mutation of E128 (E128K, a HI mutation) and F132 (F132L, a PNDM mutation) in ICL2 as well as Q52 in Kir6.2 (Q52R, a PNDM mutation) is known to disrupt channel gating by ATP and PIP<sub>2</sub> (Pratt et al., 2009; Proks et al., 2004; Proks et al., 2006) (Fig.5C, D). Our finding that this region is close to both the ATP and PIP<sub>2</sub> sites illustrates that it is well positioned to contribute to gating regulation by both, explaining the effects of these disease mutations.

#### *L0 of SUR1 couples the TMD0/Kir6.2 central core to the ABC core of SUR1*

L0 (i.e. ICL3) is nestled between TMD0 and the ABC core of SUR1, and comprises ~90 amino acids. We have modeled L0 as a polyalanine chain with two helical segments that are strongly supported by the map, one an amphipathic helix from L224-A240 and the other from L260-D277, which connects to TMD1. In the model, the N- and C-terminal stretches of L0 make a “V,” with the intervening sequence (L213-L260) forming a hairpin structure at the apex (Fig.6A, B). This hairpin structure is simultaneously bridging multiple sites within TMD0 with the ABC core structure (TMs 15+16), and may also interact with the Kir6.2 N-terminus (A45-Q52), which would allow L0 to transduce signals from the ABC core to gate the channel. The strategic placement of L0 is consistent with its multiple functional roles reported, including regulation of channel  $P_o$ , sensitivity to ATP inhibition, and sensitivity to Mg-nucleotide stimulation (Babenko & Bryan, 2003; Chan et al., 2003; Masia, De Leon, et al., 2007).

Another role of L0 that has been reported is interaction with GBC (Winkler et al., 2012). GBC is a second generation sulfonylurea containing a sulfonylurea group and a benzamido

moiety that binds  $K_{ATP}$  channels with nanomolar affinity ( $K_D \sim 1$  nM) (Gribble & Reimann, 2003). L0 has been proposed to participate in binding to the benzamido group, with mutation Y230A in L0 reducing GBC binding. We find that the amphipathic helix of L0 containing Y230 sits next to TM16 containing S1238, a residue which when mutated disrupts binding of the sulfonyleurea group (Ashfield et al., 1999). The two residues are separated by  $\sim 20$  Å (C $\alpha$  to C $\alpha$ ), which explains how the two residues distant in the primary sequence can both contribute to binding. Although at the current resolution, we are unable to discern the density for GBC, it is likely to be bound given its high affinity. The model can now be used to guide future studies to clearly define the GBC binding site.

#### *The SUR1 ABC core in an anomalous inward-facing conformation*

The SUR1 core is built from two homologous halves, TMD1-NBD1 and TMD2-NBD2. Each of the 12 combined TM helices from both TMD1 and TMD2 are clearly resolved, as well as the short lateral “elbow” helices leading into the first helix of each TMD (TM6 and TM12) (Fig. 7A, B). Characteristic of other ABC exporters, there is a domain swap at the extracellular linker between helices 3 and 4 of each TMD (Jin et al., 2012; Kim et al., 2015), such that each “half” of the ABC core is composed of TMs 1-3, and 6 of one TMD, plus TMs 4 and 5 of the other (Fig. 7A).

Overall the SUR1-ABC core is in an inward-facing conformation, with the NBDs clearly separated (Fig. 7C). This is consistent with other ABC exporter structures solved without Mg-nucleotides. However, in contrast to other ABC exporters of known structure whereby transporter halves are related by either a true or a pseudo two-fold symmetry axis, depending on

whether the two halves are identical or not (Wilkens, 2015), we find a clear rotation and a translation of TMD1-NBD1 relative to TMD2-NBD2, such that TMD1-NBD1 is  $\sim 15^\circ$  off the symmetry axis and is translated by  $\sim 10$  Å horizontally (relative to the membrane) (Fig. 7C). In this configuration, the SUR1 NBDs likely could not dimerize without a twisting motion to align the dimerization interface.

Dimerization of NBDs in SUR1 has been proposed to follow MgATP hydrolysis or MgADP binding to stimulate channel activity (Nichols, 2006), and GBC inhibits channel activity by preventing Mg-nucleotide stimulation (de Wet & Proks, 2015; Gribble & Reimann, 2003). As discussed above, given its high affinity GBC is likely to be bound in our structure. Thus, an interesting hypothesis is that the twisted conformation is caused by GBC binding, which would suggest that GBC prevents MgADP from stimulating the channel by causing a misalignment of the NBDs dimerization interface. Alternatively, the conformation may be unique to SUR1 and that Mg-nucleotide binding/hydrolysis is required to restore symmetry for dimerization. In this case, GBC may block stimulation by clamping down L0 and preventing it from communicating with Kir6.2. A structure in the absence of GBC will be needed to test these hypotheses.

## **Discussion**

The structure reported here provides the first glimpse of the detailed domain organization of  $K_{ATP}$  channels and the intricate structural interactions between SUR1 and Kir6.2. These data offer mechanistic insight into how SUR1 and Kir6.2 function as a complex to regulate insulin secretion (Fig.8A). We propose that like other ABC transporters (Wilkens, 2015) the ABC core

of SUR1 switches between an inward-facing and outward-facing conformations as MgATP undergoes hydrolysis at NBD2 and induces NBD dimerization. The conformational switch at the ABC core causes movement of the L0 and TMD0, which alters channel interactions with ATP and PIP<sub>2</sub> by remodeling the interface formed by the cytoplasmic domain of Kir6.2, the bottom of the Kir6.2 transmembrane helices, the intracellular loops of TMD0 and the N-terminal segment of L0. In this way, the SUR1 “transport” cycle is coupled to Kir6.2 opening or closing rather than transport of substrates through SUR1 itself.

Our structure highlights the critical role of SUR1-TMD0 in the association of the two subunits. In addition to contacts made by TM1 of Kir6.2 and the first TM helix of TMD0 which are consistent with previous structure-function studies (Schwappach et al., 2000), there are also new interactions revealed by the structure in the extracellular domain of TMD0 and the turret/pore loop of Kir6.2 as well as the cytoplasmic domains of TMD0 and Kir6.2. Indeed, TMD0 appears to harbor more mutations that disrupt channel biogenesis and trafficking than other regions of SUR1 (Martin et al., 2013; Martin et al., 2016). It is worth noting that many mutations in TMD0 which impair channel biogenesis and trafficking can be rescued by pharmacological chaperones, specifically sulfonylureas such as GBC (Chen, Olson, et al., 2013; Martin et al., 2016; Yan et al., 2004; Yan et al., 2007). As our structure is obtained in the presence of GBC, an important question to address in the future is whether GBC alters structural interactions between TMD0 and Kir6.2 to correct biogenesis/trafficking defects caused by TMD0 mutations.

The interface between TMD0-L0 and Kir6.2 in the cytoplasmic domain near the proposed PIP<sub>2</sub> binding site and where ATP density is observed suggests TMD0-L0 may directly enforce PIP<sub>2</sub> or ATP binding to enhance Kir6.2 sensitivity to both, and also explains the effects of many disease mutations in this region. Although in our structure the Kir6.2 is bound to ATP with the pore in a closed conformation, a gating scheme whereby in the presence of PIP<sub>2</sub> remodeling of the interfaces near the ATP and PIP<sub>2</sub> sites leads to channel opening may be envisioned. Future studies comparing structures in the absence of ATP and with or without PIP<sub>2</sub> are needed to understand in detail the structural changes involved in gating.

The L0 region before the elbow helix leading to TMD1 in SUR1 was modeled de novo, with an amphipathic helix from L224-A240 and a helix from L260-D277 that are strongly supported by the density map. Part of L0 (from a.a. 214 on) is conserved in CFTR and the multidrug resistance-associated proteins MRPs (Zhang & Chen, 2016). Interestingly, in the recently reported CFTR structure this loop which the authors named the “lasso motif” also contains an amphipathic helix followed by another helix before the elbow helix (Zhang & Chen, 2016). Our structural model of L0 is in line with the CFTR model of the corresponding loop. In CFTR or MRP-1, this loop has been shown to be involved in trafficking regulation by syntaxin 1A (Naren et al., 1998; Peters et al., 2001) or association with the plasma membrane (Bakos et al., 2000), respectively. It would be interesting to determine whether L0 of SUR1 has similar roles.

A striking feature observed in our structure is the unexpected twisted inward-facing conformation of the SUR1-ABC core that is distinct from other ABC transporter apo-state structures (Wilkins, 2015). This observation suggests a possible mechanism in which GBC

inhibits channel activity by preventing dimerization of NBDs in the presence of Mg-nucleotides (Fig.8B). As GBC is known to inhibit the activity of other ABC transporter proteins including CFTR (Schultz et al., 1996) and the multidrug resistance protein MDR (Golstein et al., 1999), the mechanism we propose could have broader implications. Intriguingly, close examination of the recently published zebrafish CFTR structure where the inhibitory R-domain is present (Zhang & Chen, 2016) and the TAP transporter structure with an inhibitory viral peptide bound (Oldham et al., 2016) also indicates misalignment of the two NBDs albeit to lesser degrees, further suggesting that NBDs misalignment may be a common theme in ABC transporters bound to inhibitory ligands.

In summary, the novel insight gained from our structure lays the foundation for future structural and functional studies. In particular, structures bound with various stimulatory and inhibitory ligands will further advance understanding of the detailed mechanisms of channel gating. Some regions known to be important for channel assembly and gating such as the distal N- and C-termini of Kir6.2 as well as several linker loops in SUR1 are not well resolved in the current map (see Materials and methods for details). An equally important future goal is to stabilize these regions and obtain higher resolution structures to fully visualize the channel.

## **Materials and methods**

*Construction of recombinant adenoviruses.* Construction of the hamster SUR1 (94.5% protein sequence identity with human SUR1) with an N-terminal FLAG-tag (f-SUR1) and rat Kir6.2 (96.15% protein sequence identity with human Kir6.2) recombinant adenoviruses was as described previously (Lin et al., 2005; Pratt et al., 2009). A FLAG tag (DYKDDDDK) was

engineered at the N-terminus of SUR1 for affinity purification of the channel complex. In brief, the gene encoding the rat Kir6.2 was cloned into pShuttle, and recombined with the pAdEasy vector in the BJ5183 strain of *Escherichia Coli*. Positive recombinants were selected, and pAdEasy plasmids containing the correct insert were used to transfect HEK293 cells for virus production. The SUR1 recombinant adenovirus was constructed using a modified pShuttle plasmid (AdEasy kit, Stratagene) containing a tetracycline-inducible promoter. Recombinant viruses were amplified in HEK293 cells and purified according to the manufacturer's instructions.

*K<sub>ATP</sub> channel expression and purification.* INS-1 cells clone 832/13 (from Dr. Christopher Newgard) (Hohmeier et al., 2000) were plated in 15 cm plates and cultured for 24 h in RPMI 1640 with 11.1 mM D-glucose (Invitrogen) supplemented with 10% fetal bovine serum, 100 units/ml penicillin, 100 µg/ml streptomycin, 10 mM HEPES, 2 mM glutamine, 1 mM sodium pyruvate, and 50 µM β-mercaptoethanol. For channel expression, cells were co-infected with three recombinant adenoviruses, one encoding Kir6.2, one f-SUR1, and one encoding tetracycline-inhibited transactivator (tTA) for the tTA-regulated f-SUR1 expression (Pratt et al., 2009). Cells at ~70% confluent density were washed once with phosphate-buffered saline (PBS) and then incubated for 3 h at 37°C in OPTI-MEM without serum and a mixture of viruses with the multiplicity of infection (M.O.I.) of each virus determined empirically to optimize the maturation efficiency of the channel complex as judged by the abundance of the SUR1 and Kir6.2 bands as well as the ratio of the mature complex glycosylated versus the immature core-glycosylated SUR1 bands. Medium was then replaced with fresh growth medium plus 1 mM sodium butyrate and 1 µM glibenclamide (GBC) to enhance expression and maturation (Yan et

al., 2004), and the cells were further incubated at 37°C for 36-48 hours. Cells were harvested in PBS, pelleted, flash frozen in liquid nitrogen, and stored at -80°C until purification.

For channel purification, cells were resuspended in hypotonic buffer (15 mM KCl, 10 mM HEPES, 1.5 mM MgCl<sub>2</sub>) and allowed to swell for 20 min on ice. Cells were then lysed with a tight-fitting Dounce homogenizer, then centrifuged at 20,000xg for 60 min. Membranes were resuspended in buffer A (150 mM NaCl, 25 mM HEPES, 50 mM KCl, 1 mM ATP, 1 μM GBC, 4% Trehalose) with protease inhibitors (cocktail tablets from Roche) and then solubilized with 0.5% Digitonin for 90 min. Solubilized membranes were separated from insoluble materials by centrifugation (100,000xg for 30min at 4°C) and then incubated with anti-FLAG M2 affinity agarose gel for 4-5 hours. The protein-bound agarose gel was washed with 5 column volumes of buffer B (150 mM NaCl, 25 mM HEPES, 50 mM KCl, 1 mM ATP, 1 μM GBC, 0.05% Digitonin) and bound proteins eluted in the same buffer with FLAG peptide. Eluted proteins were concentrated using a centricon filter (100 kD cutoff) to a final concentration of ~0.7-1 mg/ml. Purified proteins were further fractionated by size exclusion chromatography using a Suprose 6 column and fractions analyzed by blue native gel electrophoresis and SDS-PAGE (Fig. 1A, B).

*Sample preparation and data acquisition for cryo-EM analysis.* Digitonin solubilized K<sub>ATP</sub> complexes (in the presence of 1 mM ATP and 1 μM GBC) were first examined by negative-staining EM (1% w/v uranyl acetate, on continuous thin-carbon coated grids) to confirm the integrity of the full complex (Fig. 1C). For cryo-EM imaging, due to low particle distribution with holey-carbon grids, we experimented with two types of grids: UltrAufoil gold grids and C-

flat grids coated in-house with 5 nm of gold on each side, and used both in the final data collection. The grids were first glow-discharged by EasyGlow® at 20 mA for 45 seconds, then 3  $\mu$ L of purified K<sub>ATP</sub> complex was loaded onto the grid, blotted (2-4 s blotting time, force -4, and 100% humidity) and cryo-plunged into liquid ethane cooled by liquid nitrogen using a Vitrobot Mark III (FEI).

Single-particle cryo-EM data was collected on a Titan Krios 300 kV cryo-electron microscope (FEI) in the Multi-Scale Microscopy Core at Oregon Health & Science University, assisted by the automated acquisition program SerialEM. Images were recorded on the Gatan K2 Summit direct electron detector in the counting mode at the nominal magnification 81,000x (calibrated image pixel-size 1.720 Å), with varying defocus between -1.2 and -3.5  $\mu$ m across the dataset (Fig.1D). To contain the beam radiation damage and reduce electron coincidence loss in the K2 counting-mode recording, the dose rate was kept around 2.0  $e^-/\text{Å}^2/\text{sec}$ , frame rate at 2 frames/sec and 40 frames in each movie, which gave the total dose of approximately 40  $e^-/\text{Å}^2$ . In total, 4,339 movies were recorded, from which ~35,000 particles were used in final reconstructions (Fig.1-supplements 1,2).

*Image processing.* The raw frame stacks were gain-normalized and then aligned and dose-compensated using Unblur (Grant & Grigorieff, 2015) (Table 1). CTF was estimated from the aligned frame sums using CTFFIND4 (Rohou & Grigorieff, 2015). To reduce the possibility of bias and capture every possible particle view, an initial set of 350,000 potential particles (referred to as “peaks” in Fig.1-supplement 1) were picked using DoGPicker (Voss et al., 2009) with a broad threshold range for subsequent 2D classification using RELION (Scheres, 2012).

2D classification was able to remove the large number of false positives and aggregates, and resulted in ~35,000 particles with 2D classes in which secondary structure was already apparent (Fig.1E). These class averages revealed that the side views also adopted a preferred orientation. Upon imposing C4 symmetry, the angular sampling space was filled in along three orthogonal axes (Fig.1-supplement 2A), which greatly improved the quality of the 3D reconstruction. The final rounds of refinement with C4 symmetry revealed two 3D classes (Fig.1-supplement 1). The dominant class, derived from 20,707 particles had an overall resolution of ~6.7Å, and application of a mask improved the resolution of the overall structure to 5.8Å and the central Kir6.2 domain to 5.1Å (Fig.1-supplement 2B). The second class, derived from 14,115 particles, had an overall unmasked resolution of ~7.6Å, and masking improved the resolution of the overall structure to 7.2Å and for the central Kir6.2 domain to 6.9Å (Fig.1-supplement 2C). All resolutions were reported using the 0.143 criterion with gold-standard FSC and phase-randomization correction for the use of masks (Chen, McMullan, et al., 2013). Resolution was further confirmed using local-resolution as measured using ResMap (Kucukelbir et al., 2014), and by observing criterion such as helical pitch starting to become visible, and density bumps for some of the larger side chains (see examples shown in Fig.3B). Maps were B-factor corrected during post-processing using the K2 MTF, and the fitting procedure described by Rosenthal and Henderson (Rosenthal & Henderson, 2003). The two 3D classes differ in the cytoplasmic domain of Kir6.2 where a rotation of ~14° relative to each other was observed (Fig.1-supplement 2F).

*Model building.* Local resolution measurements using ResMap and masked FSCs showed that some parts of the complex including Kir6.2 and TMDs of SUR1 had significantly better resolution, in the 5Å range, than the overall resolution of 6.3Å, while other parts such as the

NBDs of SUR1 had worse resolution, estimated to be in the 8Å range. Moreover, some parts of the channel complex, such as the TMD0 and L0 of SUR1 do not have existing homology models. Therefore, different strategies were used to model the channel complex, as detailed below.

For Kir6.2, a homology model was built from Kir3.2 (PDB ID: 3SYA) using MODELLER (Webb & Sali, 2016) and served as the initial model. The model was docked into the density in UCSF Chimera (Pettersen et al., 2004); the fit was improved by rigid body refinement of domains in RSRef (Chapman et al., 2013), followed by iterative rounds of real-space refinement in COOT (Emsley et al., 2010) and stereochemically restrained torsion angle refinement in CNS (Brunger et al., 1998), substituting in the RSRef real-space target function (Chapman et al., 2013), adding ( $\phi, \psi$ ) backbone torsion angle restraints, and imposing non-crystallographic symmetry (NCS) constraints. The final model contained residues 32-356 (Fig.2-supplement 1). The distal N- and C-termini of Kir6.2, although interesting regions implicated in channel assembly and gating (Devaraneni et al., 2015; Enkvetchakul et al., 2000; Zerangue et al., 1999), lacked strong density. Therefore, they were not included in the model. For the SUR1 core structure, the sequence was divided into three segments: TMD1, NBD1, and TMD2-NBD2. A TMD1 homology model was built using PCAT-1 (PDB ID: 4RY2) (Fig.2-supplement 2), NBD1 was modelled from the NDB1 of mouse P-glycoprotein (PDB ID: 4M1M) (Fig.2-supplement 3), and TMD2 and NBD2 were modelled together from chain B of TM287/288 (PDB ID: 4Q4HB) (Fig.2-supplement 4); all homology models were built with MODELLER. These models were docked into the density in Chimera.

SUR1 had some disordered regions (744-770, 928-1000, 1319-1343), particularly in the linkers between TMDs and NBDs, and in NBD1, that were not seen in our map. These regions were removed from the homology models before proceeding with refinement. The TM helices were then manually adjusted in COOT, as a substantial adjustment was needed to move them into density. The domains were then refined in the same steps as outlined for Kir6.2, except that before the final manual adjustments in COOT and final density gradient optimization, a batch of torsion angle simulated annealing optimization was inserted, again using RSRef/CNS and the same torsion angle restraints and NCS constraints. The final model for the ABC core structure contained residues 284-616 (TMD1), 675-739 and 762-930 (NBD1), 981-1044 and 1060-1321 (TMD2), and 1325-1577 (NBD2).

TMD0 and L0 domains of SUR1 (a.a. 1-295) are some of the most interesting and novel regions of the  $K_{ATP}$  complex for which there is no existing homology model. These domains were therefore modeled *de novo*. Even though embedded in a micelle, all of the transmembrane helices in TMD0 are clearly visible in the density map. The visibility of helical pitch and some side chains allowed confident modeling and refinement of the TM helices. With the predominantly alpha-helical nature of this domain, continuous loop density between most of the TM helices, and the presence of residues with bulky side chains, we were able to build the ~200 residues of TMD0 with a good degree of confidence. Of less certainty was the L0 region of SUR1 that sits between TMD0 and TMD1. While there was an easily identifiable region of the map corresponding to L0, the scarcity of secondary structures in this region made it difficult to build with the same degree of confidence. This was further complicated by the high likelihood that some of the observed density may be attributable to the ligand GBC, a high affinity

antagonist which has been shown to interact with this region (Bryan et al., 2004). Nonetheless, we made a best effort to model the residues in L0 primarily to verify that (1) a plausible model could be built into this density, and (2) that the observed density was sufficient to account for all the amino acids in this loop. The L0 model we built fulfilled both criteria, and as such, allowed for a better interpretation and understanding of the electron density map. We did not, however, attempt to draw any definitive conclusions about specific residues or GBC density from our tentative modeling of L0.

Note we used two different software suites, RSRef and PHENIX (Adams et al., 2010), to confirm the consistency of our individual models of Kir6.2 and the SUR1 ABC core structure upon refinement into our electron density. The full final models were refined with all the constraints available in PHENIX real-space refinement: torsion angles, bond lengths, Ramachandran, and secondary structure. This was done initially with side-chains in place to ensure that the refinement did not place residues in implausible configurations (Fig.3B shows examples of residues that were particularly well-resolved and served as anchor points for building and refining the model). Evaluation of these refined models confirmed that the model could be refined to fit the density quite well while maintaining good stereochemical statistics (Table 1). However, as many of the side chains did not have much, if any, supporting density, a final pass was made throughout the entire model to remove these side-chains prior to PDB deposition (PDB ID: 5TWV). The resulting model was very similar to the full-atom refinement, but had better statistics (Table 1) primarily due to the reduced possibility of clashes.

**Acknowledgements:** We thank Nicholas Caputo for assistance with microscope operation and data collection, Dr. Omar Davulcu and Dr. Michael Chapman for assistance on structure

refinement using RSRef. We are grateful to Dr. Eric Gouaux and Dr. Michael Chapman for helpful discussion and comments on the manuscript. We also thank the staff at the Multiscale Microscopy Core (MMC) of Oregon Health & Science University (OHSU), the OHSU-FEI living lab and Intel for technical support. This work was supported by the National Institutes of Health grants R01DK066485] (to S.-L. S.) and F31DK105800 (to G.M.M.).

---

**Table 1 | Statistics of cryo-EM data collection, 3D reconstruction and model building.**

---

**Data collection/processing**

Microscope	Krios
Voltage (kV)	300
Camera	Gatan K2
Camera mode	Counting
Defocus range ( $\mu\text{m}$ )	1.2 ~ 3.5
Exposure time (s)	20
Dose rate ( $\text{e}^-/\text{pixel}/\text{s}$ )	7
Magnified pixel size ( $\text{\AA}$ )	1.72
Total Dose ( $\text{e}^-/\text{\AA}^2$ )	40

**Reconstruction**

Software	RELION
Symmetry	C4
Particles refined	27371
Resolution (unmasked, $\text{\AA}$ )	6.7
Resolution (masked, $\text{\AA}$ )	5.8
Resolution (Kir6.2 masked, $\text{\AA}$ )	5.1
Map sharpening B-factor ( $\text{\AA}^2$ )	-250

**Model Statistics**

Map CC	0.95 (masked)
Resolution (FSC=0.5, $\text{\AA}$ )	5 $\text{\AA}$ (via phenix model-map FSC)
MolProbity score	2.26
C $\beta$ deviations	0

**Ramachandran**

Outliers	0.12%
Allowed	4.68%
Favored	95.20%

**RMS deviations**

Bond length	0.005
Bond angles	1.262

---

## Figure Legends

**Fig. 1. Purification and single-particle EM imaging of the SUR1/Kir6.2  $K_{ATP}$  channel.** (A) Size exclusion chromatography (SEC) profile of affinity purified  $K_{ATP}$  channels on a Suprose 6 column showing peak elution at ~11.5 ml (the red rectangle). (B) *Left*: Blue native gel showing the size of the purified complex at ~1 mDa (arrow) corresponding to four SUR1 and four Kir6.2. Input: samples eluted from anti-FLAG M2 agarose beads; void: sample from the SEC void fraction; 11.5 ml: sample from the SEC 11.5 ml elution fraction. *Right*: SDS-PAGE of the 11.5 ml fraction showing SUR1 (lower band: core-glycosylated; upper band: complex-glycosylated) and Kir6.2 as the main proteins. A vertical line separates MW markers from the sample lane in the same gel. (C) Negative-stain two-dimensional class averages showing topdown views (1, 2) and side views (3, 4) of the channel complex. (D) A representative cryoEM micrograph of  $K_{ATP}$  channel particles imaged on an UltrAufoil grid. (E) Representative two-dimensional class averages of  $K_{ATP}$  channels.

### Figure 1 - supplement 1. Cryo-EM data processing flow-chart.

**Fig. 1-supplement 2. Cryo-EM density map analysis.** (A) Euler angle distribution plot of all particles included in the calculation of the final map. (B and C) Fourier shell coefficient (FSC) curves of unmasked and masked whole complex, as well as masked Kir6.2 maps showing resolutions corresponding to FSC=0.143 for the two 3D classes. (D and E) 3D density map with colored local resolution viewed from the side (D) and the bottom (E). (F) Comparison of the cytoplasmic domain of Kir6.2 of the two 3D classes showing a counterclockwise rotation of ~14° of class 2 relative to class 1.

**Fig. 2. Three-dimensional reconstruction of the  $K_{ATP}$  channel.** (A) Cryo-EM density map of the  $K_{ATP}$  channel complex at an overall resolution of 5.8Å, viewed from the side. The four Kir6.2

subunits in the center are colored blue, SUR1 is in orange (TMD0), lavender (L0), green (TMD1/NBD1), and yellow (TMD2/NBD2). Gray bars indicate approximate positions of the lipid bilayer. (B) View of the complex from the cytoplasmic side. (C and D) Cross-sections of the density map. The planes where the sections 1 and 2 are made are shown in (A). (E) Model of SUR1 and Kir6.2 constructed from the EM density map viewed from the side. A Kir6.2 tetramer and only two SUR1 subunits are shown for clarity. (F) The model viewed from the extracellular side.

**Fig.2-supplement 1. Sequence and structure comparison between Kir6.2 and Kir3.2.** (A) Sequence alignment of rat Kir6.2 and mouse Kir3.2. Only the Kir3.2 sequence that was used to solve the structure in the PIP<sub>2</sub>-bound state is shown (PDB ID: 3SYA). Transmembrane helices in this and Extended Data Figs.5-7 are colored dark blue. Kir6.2 sequence with no corresponding secondary structures shown at the top was not modeled due to lack of density in the map. (B) Superposition of the Kir6.2 structure and the structure of Kir3.2 (PDB ID: 3SYA) viewed from different angles. Blue: Kir6.2; lavender: Kir3.2.

**Fig.2-supplement 2. Sequence alignment and structure comparison between SUR1 TMD1 and a bacterial peptidase-containing ABC transporter PCAT-1 (PDB ID: 4RY2).** The structure 4RY2 of PCAT-1 was used for homology modeling of SUR1 TMD1 (a.a. 284-616). (A) Alignment of the hamster SUR1 sequence from 1-624 and the sequence of PCAT-1 in the crystal structure 4RY2. (B) Superposition of the PCAT-1 structure 4RY2 and the final model of TMD1 of SUR1.

**Fig.2-supplement 3. Sequence alignment and structure comparison between SUR1 NBD1 and the mouse P-glycoprotein NBD1 (PDB ID: 4MLM).** The NBD1 structure of the mouse P-glycoprotein (mPgp; PDB ID: 4MLM) was used for homology modeling of SUR1 NBD1. (A)

Alignment of the hamster SUR1 sequence from 631-930 and the sequence of mPgp NBD1 in the crystal structure 4MLM. (B) Superposition of the mPgp-NBD1 and the final modeled NBD1 structure of SUR1.

**Fig.2-supplement 4. Sequence alignment and structure comparison between SUR1 TMD2-NBD2 and a bacterial ABC exporter TM287/288 (PDB ID: 4Q4H).** The structure 4Q4H of TM287/288 was used for homology modeling of SUR1 TMD2-NBD2. (A) Alignment of the hamster SUR1 sequence from 961-1982 and the sequence of TM287/288 in the crystal structure 4Q4H. (B) Superposition of the TM287/288 structure 4Q4H and the final modeled TMD2-NBD2 structure of SUR1.

**Fig. 3. Kir6.2 in a closed conformation.** (A) Cryo-EM density map of Kir6.2 at 5.1Å resolution. (B) Density of M1 and M2. Residues with clear side chain density are labeled. (C) A central slice through the density highlighting the ion permeation pathway. (D) View of the inner helix gate (F168) looking down the pore from the extracellular side. Kir3.2 apo (yellow, PDB ID: 3SYO) and Kir3.2-R201A+PIP<sub>2</sub> (red, 3SYQ) structures were aligned to the region surrounding the gate. (E) Comparison of G-loop conformations of Kir6.2 and Kir3.2 (3SYO and 3SYQ) by alignment of the cytoplasmic domain; same coloring as in (D). The distance shown in (D) and (E) is between the main chains; the constriction should be even narrower due to side chains that should be protruding into the pore, as is seen in homologous structures. Density depictions contoured to 2.5σ in (B, D, E).

**Fig. 4. The ATP binding pocket.** (A and B) Overview of ATP site from the side and from the top. (C and D) Difference map calculated from model prior to ATP docking, contoured to 3σ. Residues surrounding the ATP density are labeled. Side chains of residues with supporting

density are shown. The N-terminus from Kir6.2 subunit A is colored in cyan and R50 is labeled followed by (A). The adjacent subunit is colored in blue, and SUR1-L0 is colored lavender, with the K205 position labeled.

**Fig. 5. The interface between TMD0 and the N-terminal segment of L0 with Kir6.2.** (A) Overall structure of the interface region, with TMD0 in orange, Kir6.2 in blue, and L0 in lavender. ECL: extracellular loop; ICL: intracellular loop; IF helix: interfacial (slide) helix. (B and C) Detailed view of the region boxed in red in (A) shown in ribbon (B) and surface (C) representations. ATP is docked as in Fig.3 and PIP<sub>2</sub> was docked hypothetically using PIP<sub>2</sub> bound Kir3.2 and Kir2.2 structures for placement. (D) A side view of the ICL2 showing close interactions with the Kir6.2 IF helix. E128 and F132, mutation of which alters channel  $P_o$  and ATP sensitivity, are highlighted. (E) A top-down view of this region with both docked ATP (in the back) and PIP<sub>2</sub> in view.

**Fig.5-supplement 1. Interactions between TMD0 and Kir6.2.** (A) Interactions of SUR1 N-terminus with the pore loop and turret of Kir6.2. Note continuous density extending from the pore loop to the N-term/extracellular loop 2 (ECL2) and from the turret to the short helical segment of ECL1. Map is displayed at  $2.5\sigma$ . (B) The Kir6.2 M1-SUR1 TM1 interface showing the tight association of these two helices and interaction between ICL2 and the Kir6.2 N-terminal interfacial (IF) helix. (C) Possible hydrophobic interactions between M1 (blue, Kir6.2) and TM1 (orange, SUR1) helices.

**Fig. 6. The SUR1-L0 connecting TMD0/Kir6.2 with the SUR1-ABC core.** (A) View of the L0 region from the side along the plane of the membrane; Kir6.2 density has been removed for clarity. The hairpin structure is outlined. (B) Slice through the N- and C-terminal segments of

L0. (C) Model of L0 highlighting relation between Y230 and S1238 (marked red) in TM16, which are separated by  $\sim 20\text{\AA}$  ( $C\alpha$  to  $C\alpha$ ). Side chain of Y230 is shown based on supporting density. The gray dashed line marks the approximate boundary of the inner leaflet of the lipid bilayer.

**Fig. 7. SUR1 with a twisted ABC core conformation in saturating concentrations of GBC.**

(A) Model of SUR1 with the various domains colored as in Figure 1, with each TM helix labelled. On the left, TMD1/NBD1 (green) is towards the front and TMD2/NBD2 (tan) is towards the back. (B) Cross-section of the SUR1 model, showing relative orientation of each of the 17 TM helices and a helix in L0. (C) Comparison of inward-facing ABC transporter structures: From left, *C elegans* Pgp (PDB code 4F4C); mouse Pgp (4M1M); hamSUR1. For each model, TMD2/NBD2 is colored tan. Lines on the side of the SUR1 NBDs denote the relative orientation of the NBD dimerization interface, demonstrating the observed twisting relative to other inward-facing structures.

**Fig. 8.  $K_{ATP}$  channel gating model.** (A) Cartoon illustrating how changes in the ATP/ADP ratio upon feeding and fasting alter the equilibrium between the inward-facing and outward-facing states of the SUR1-ABC core and interactions of the channel with ATP and  $PIP_2$  to control channel activity. (B) Model of the hypothesized mechanism whereby GBC causes misalignment of the NBDs to prevent Mg-nucleotides activation of  $K_{ATP}$  channels. In both A and B, Kir6.2 transmembrane helices: green; Kir6.2 cytoplasmic domain: lime green; SUR1-TMD0/L0: magenta; SUR1-TMD1/2: blue; SUR1-NBDs: orange; GBC: yellow; ATP: red;  $PIP_2$ : cerulean. Note the different states shown are not meant to reflect the actual conformational transitions.

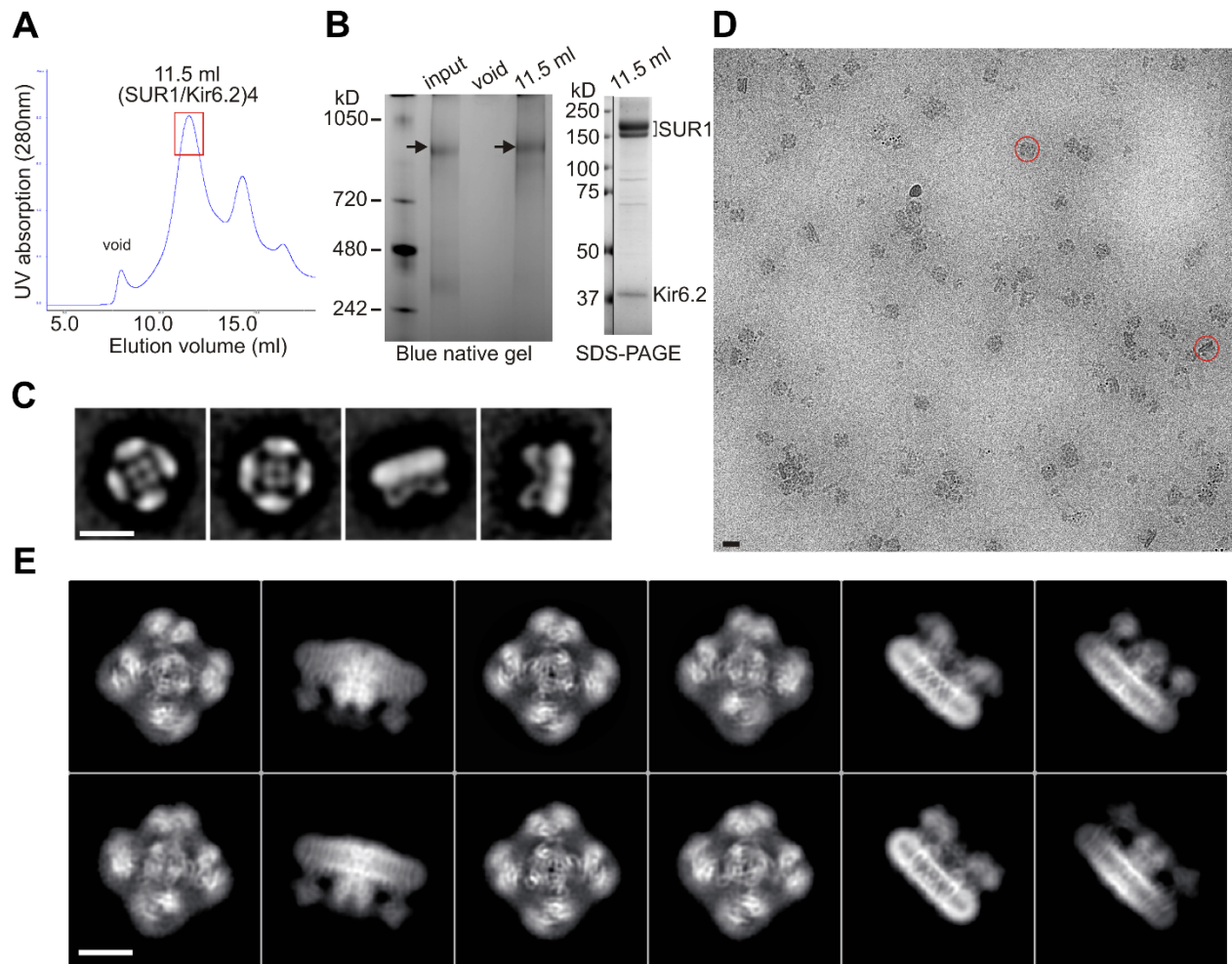


**Figure 1**

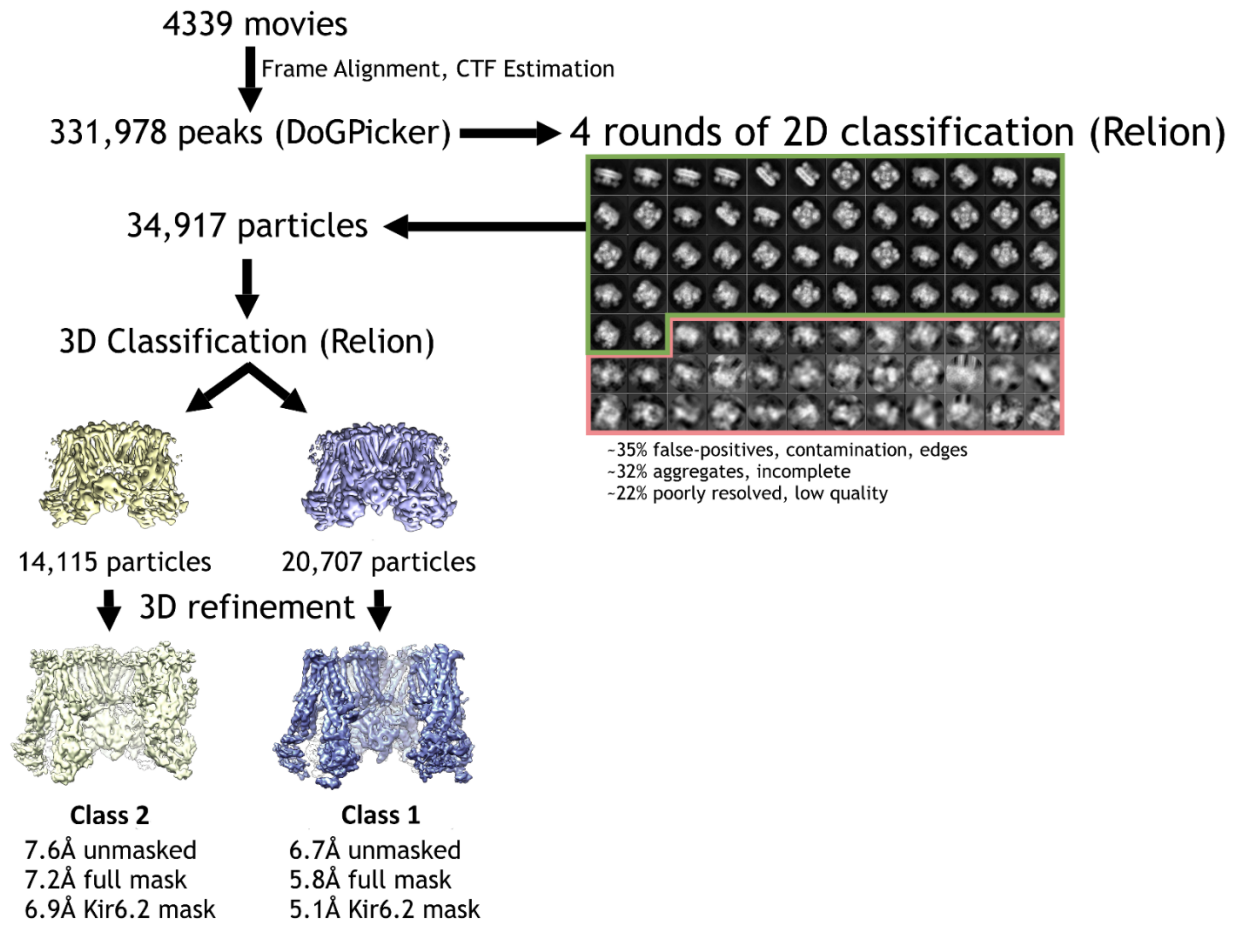


**Figure 1 - supplement 1**

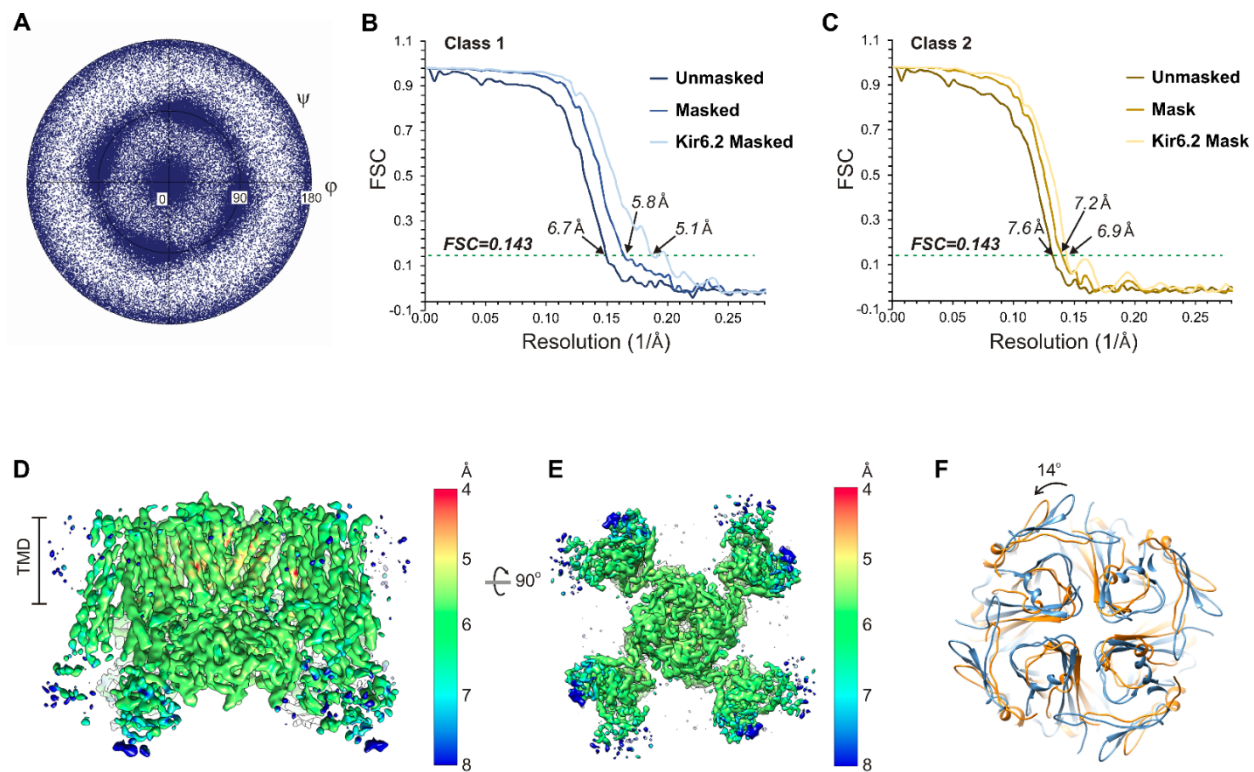
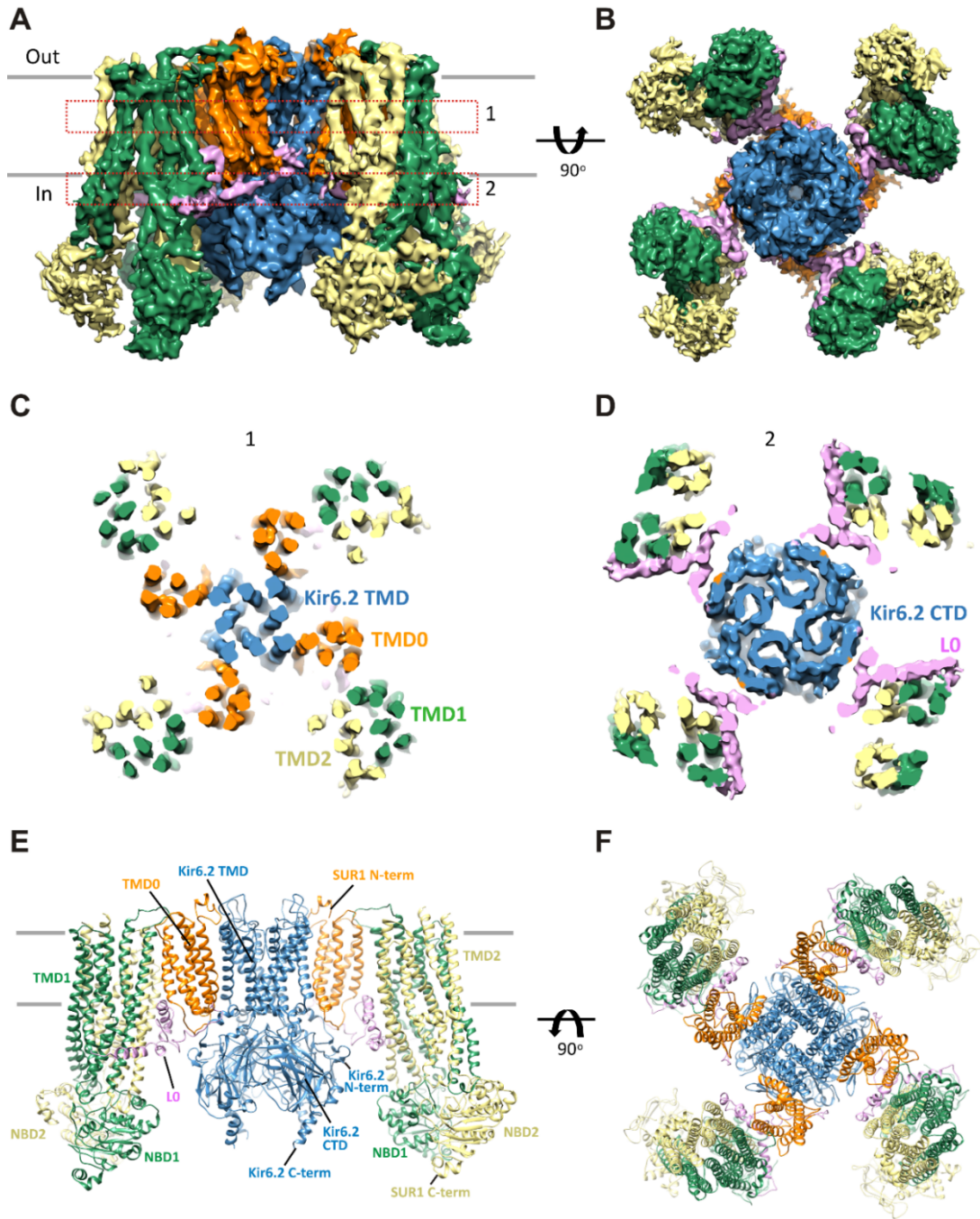


Figure 1 - supplement 2



**Figure 2**

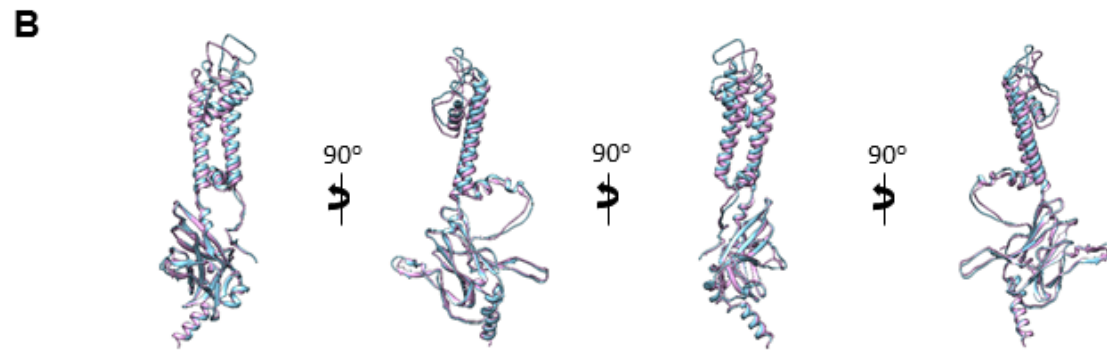
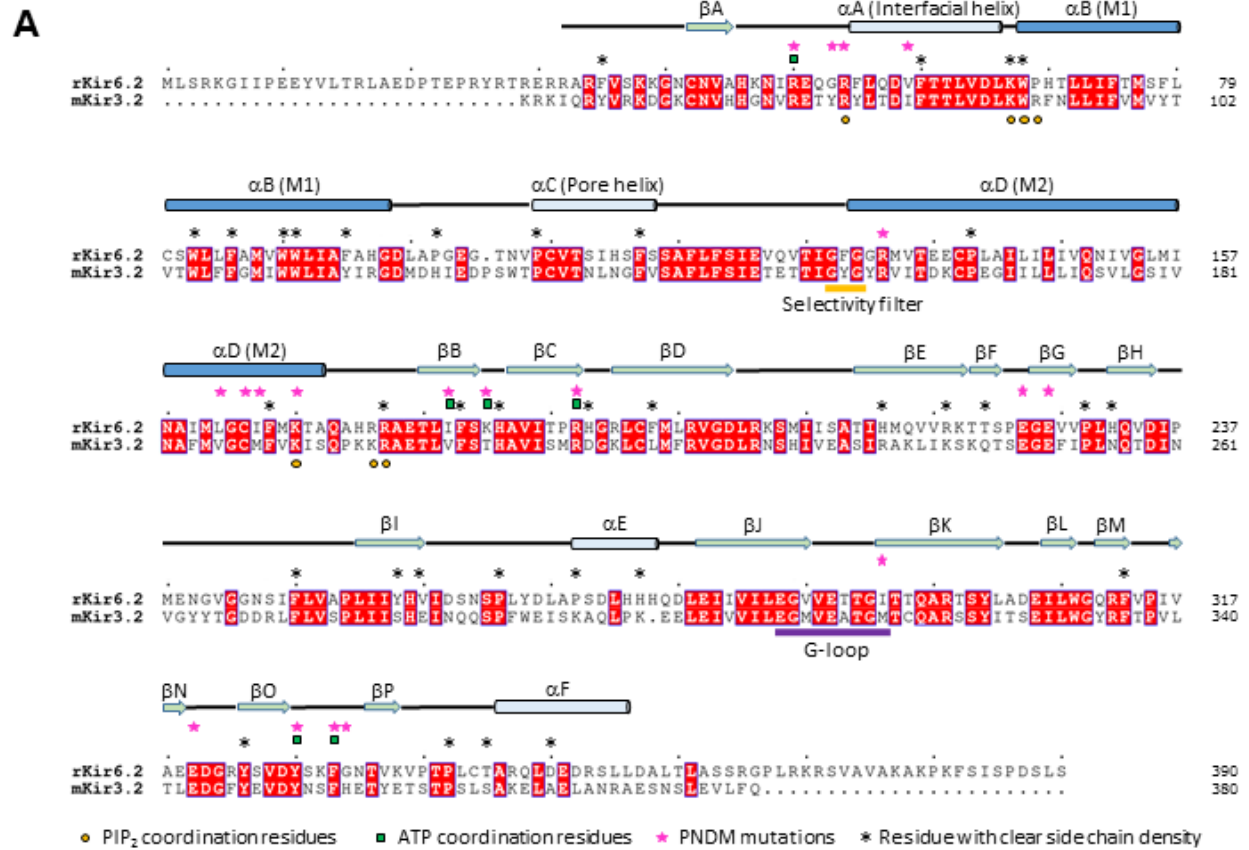


Figure 2 - supplement 1

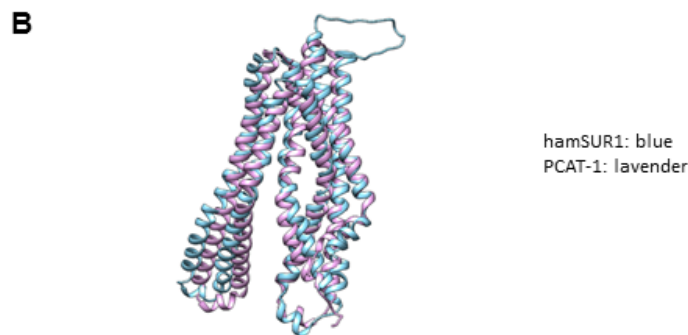
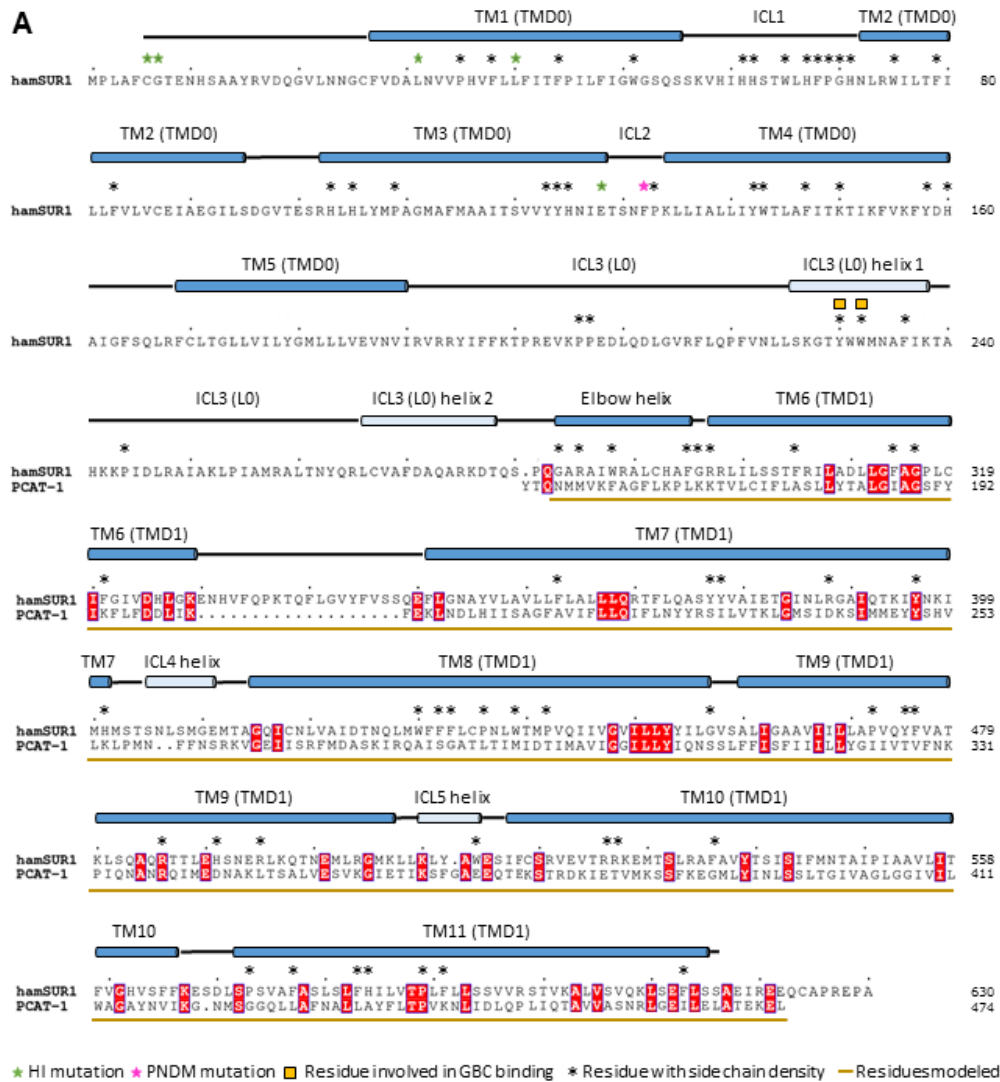


Figure 2 - supplement 2

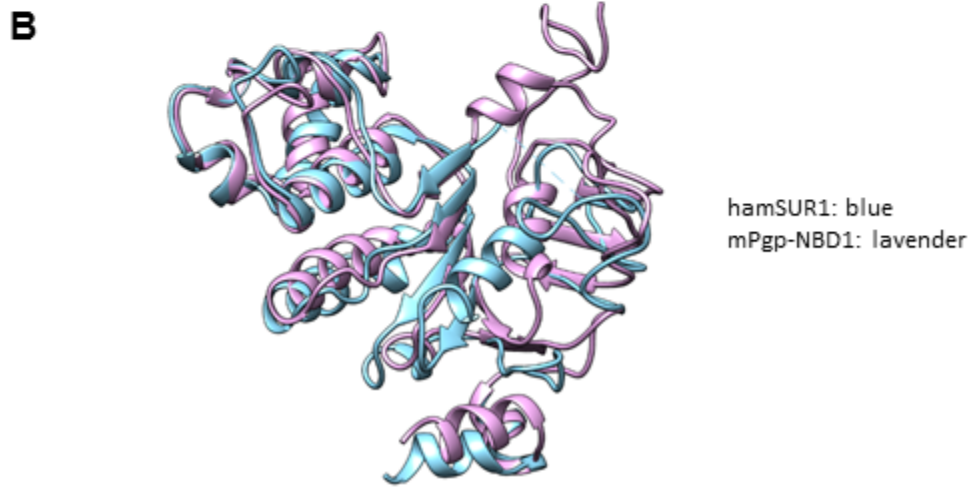
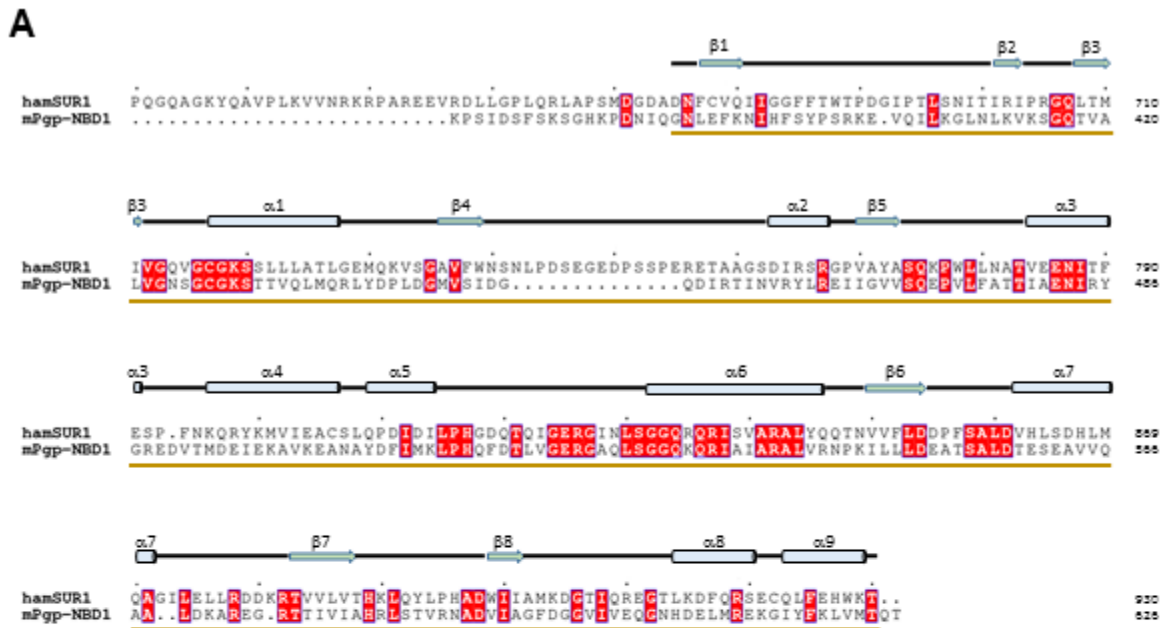
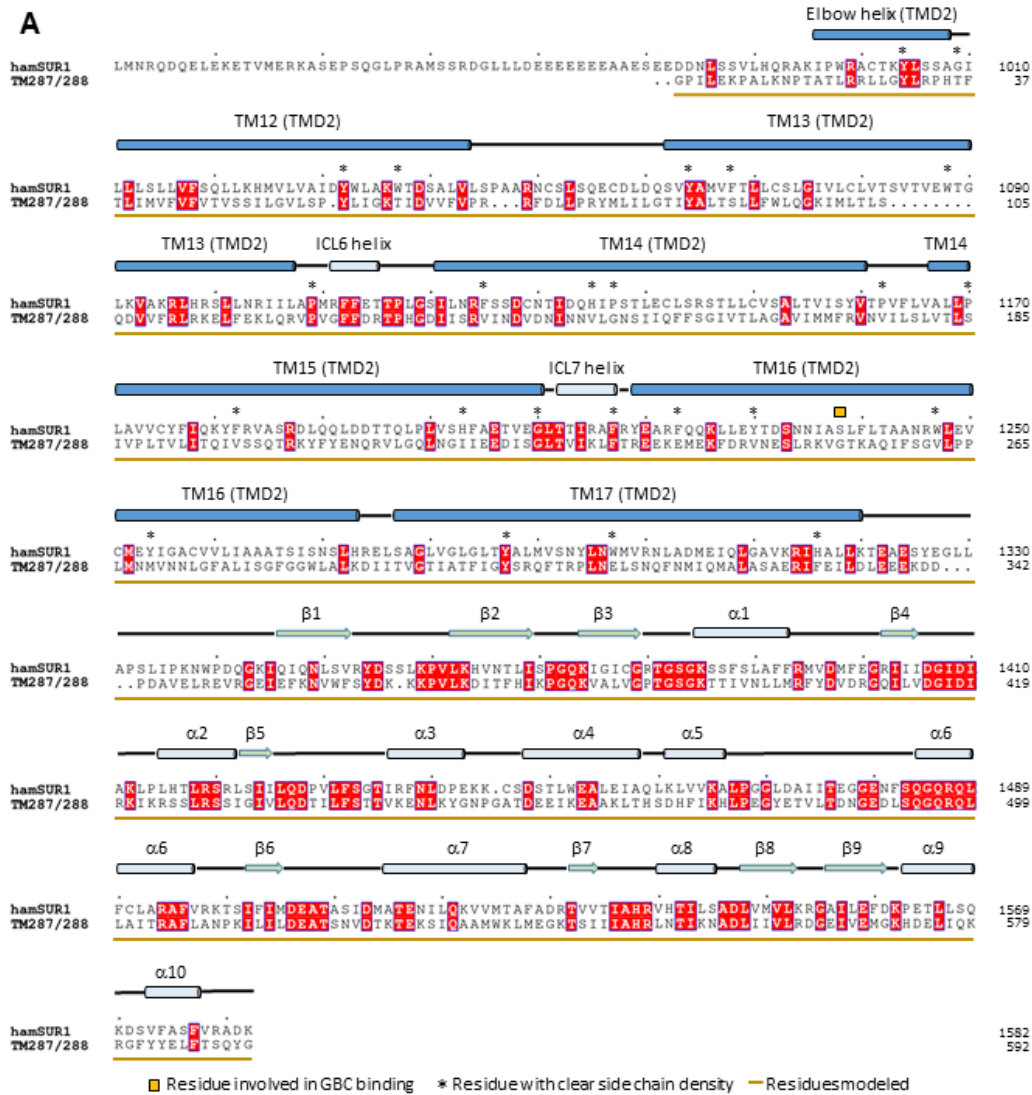
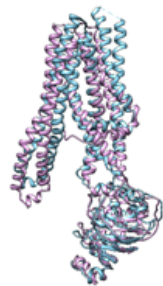


Figure 2 - supplement 3



**B**



hamSUR1: blue  
TM287/288: lavender

Figure 2 - supplement 4

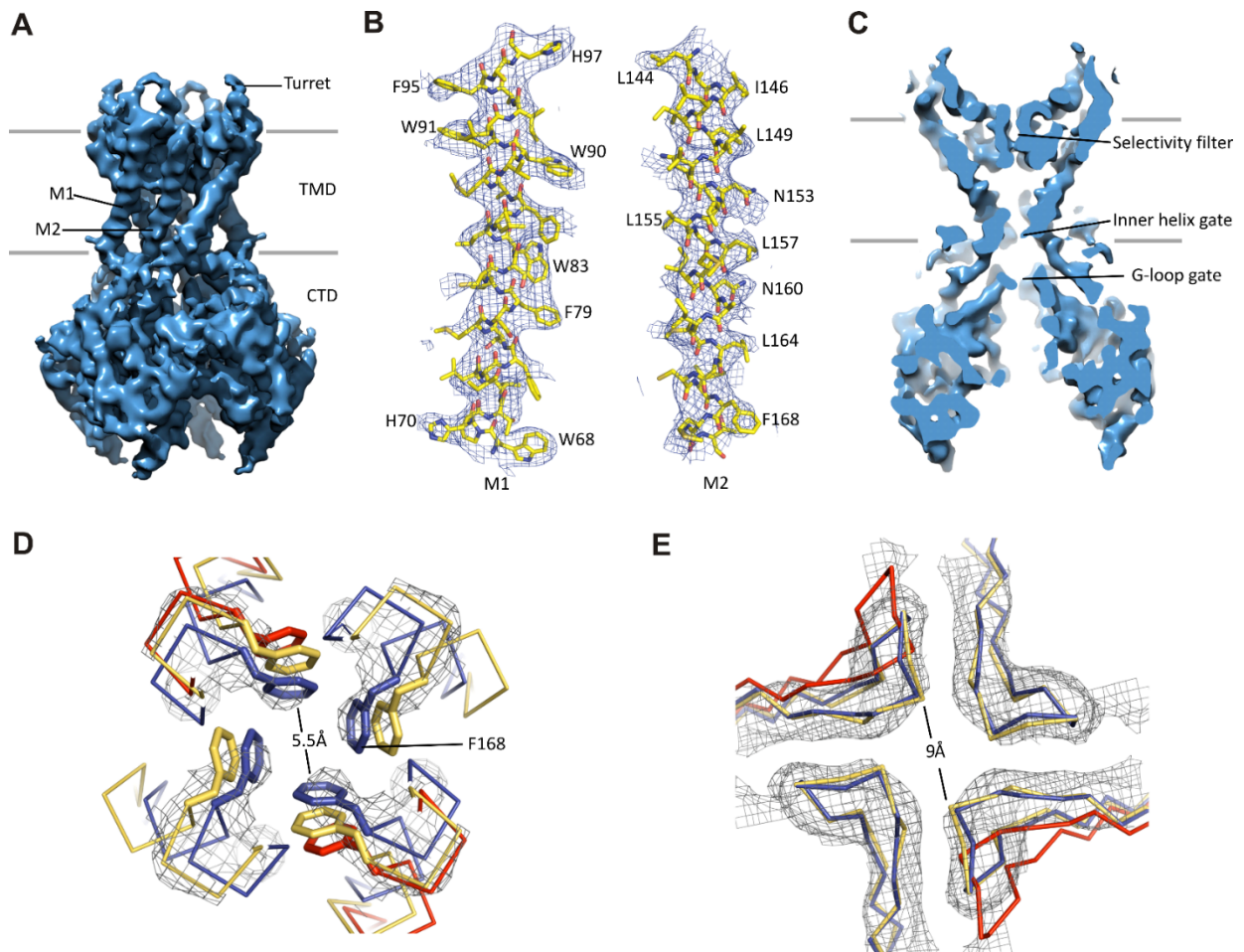


**Figure 3**

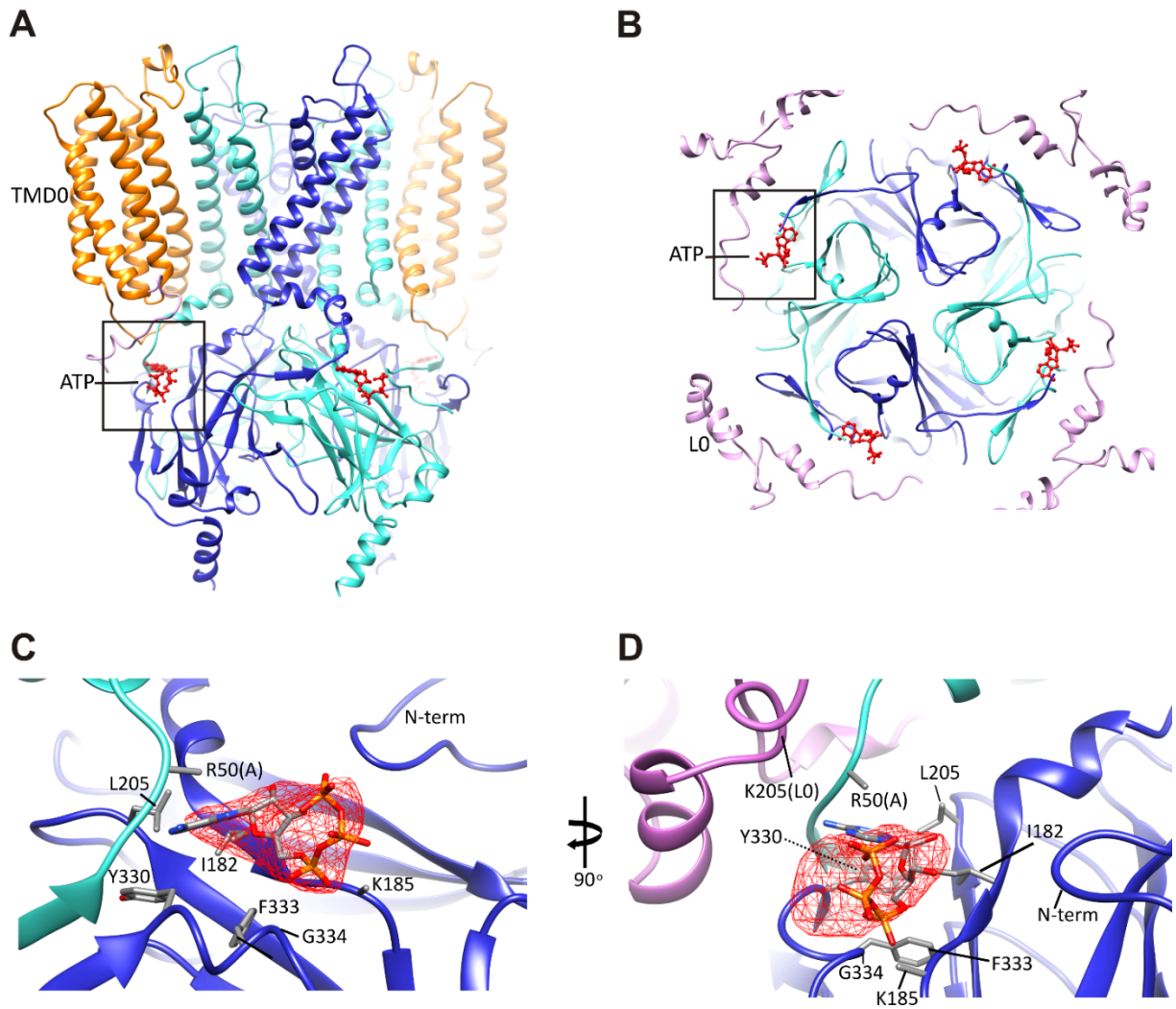


**Figure 4**

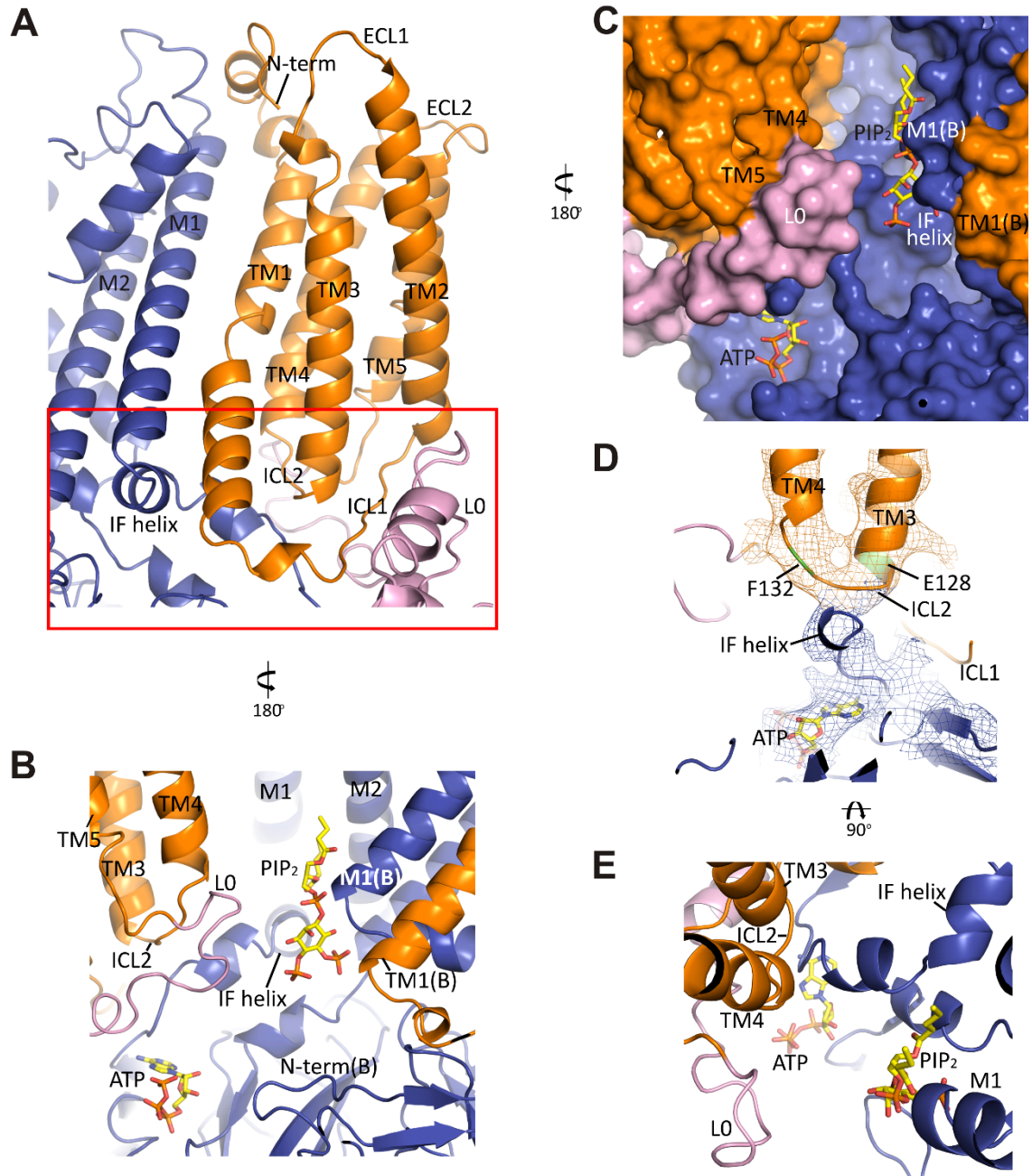


**Figure 5**

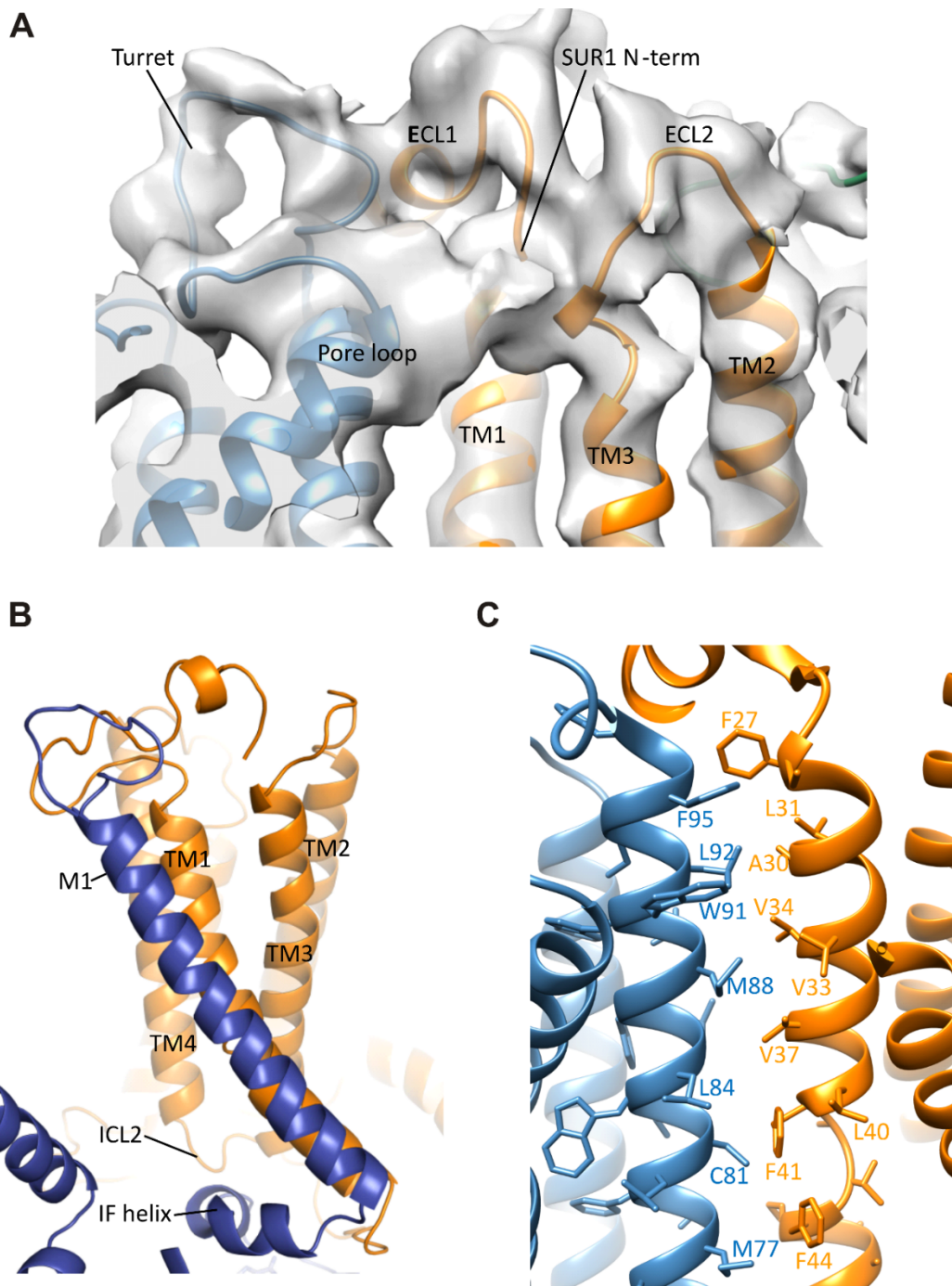


**Figure 5 - supplement 1**

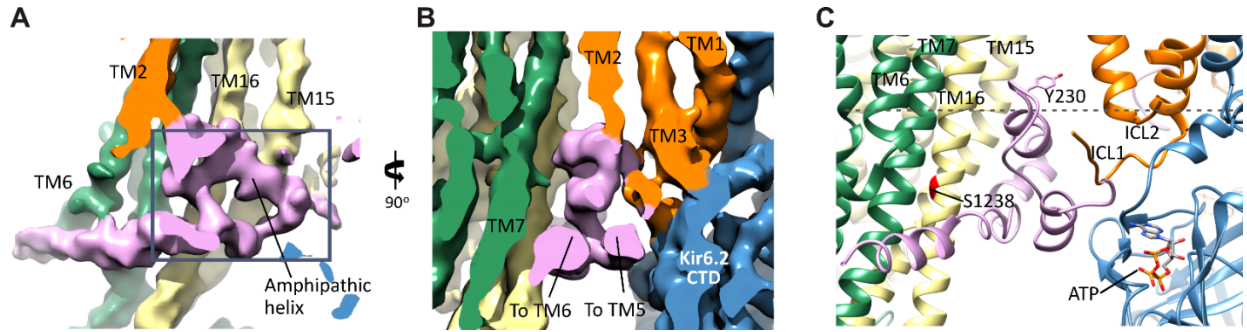


**Figure 6**

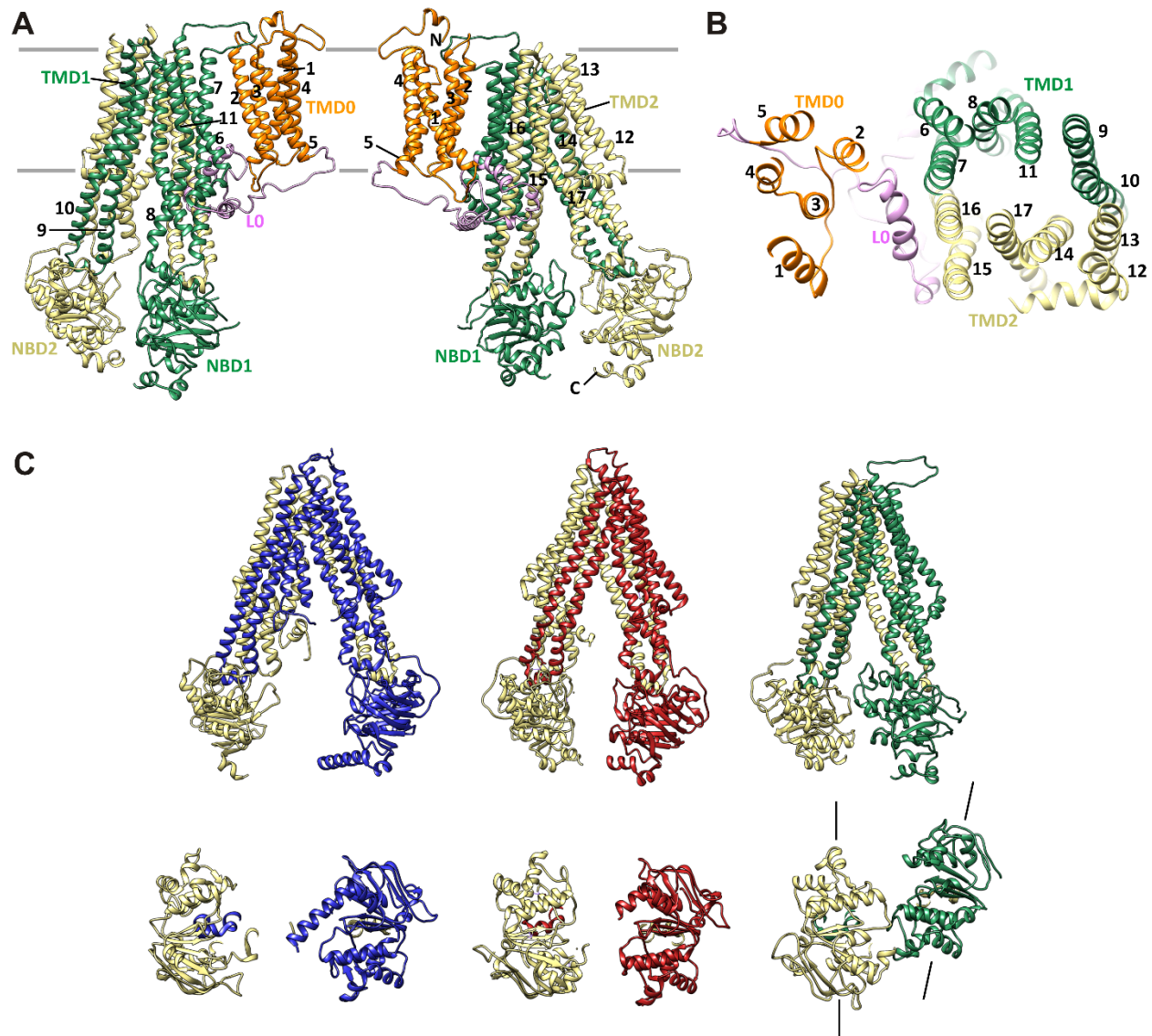


**Figure 7**

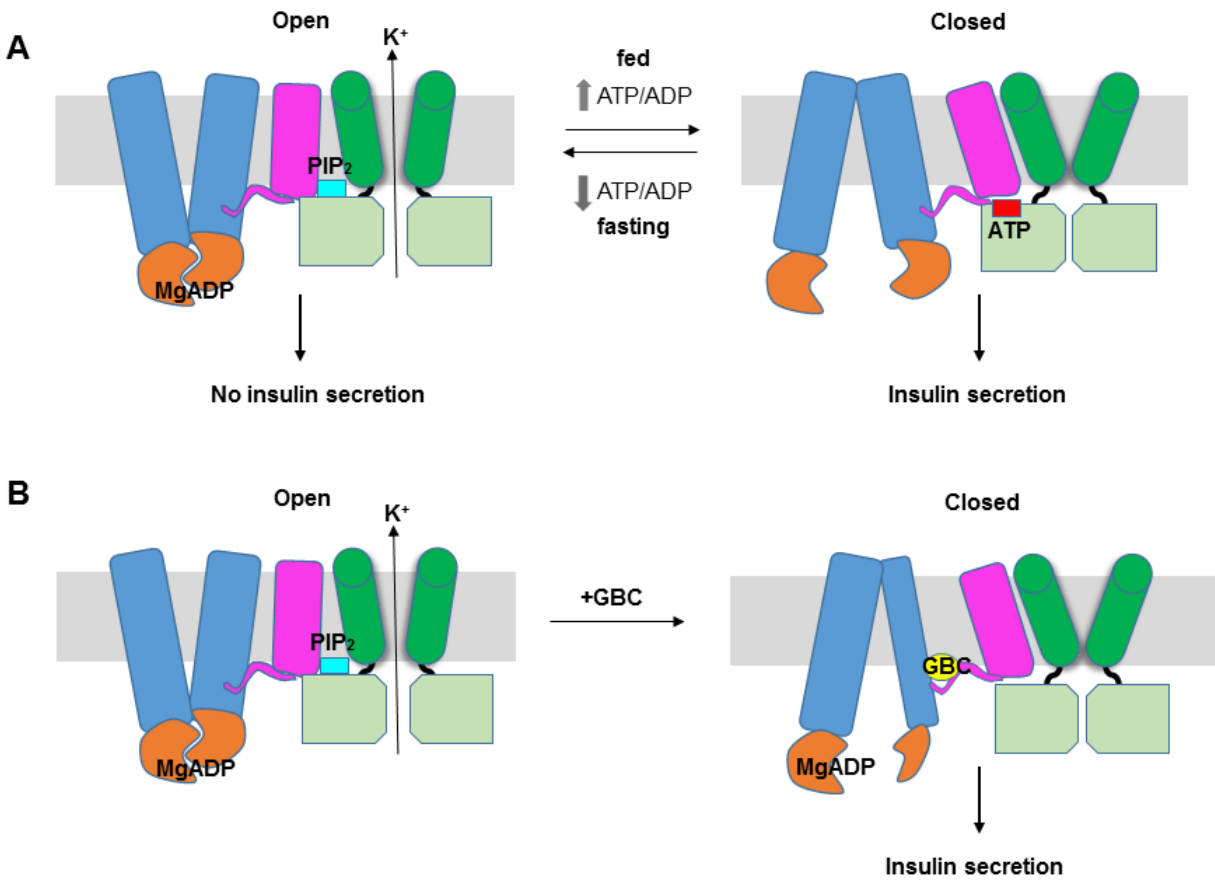


**Figure 8**

## References Cited

- Adams, P.D., P.V. Afonine, G. Bunkoczi, V.B. Chen, I.W. Davis, N. Echols, J.J. Headd, L.W. Hung, G.J. Kapral, R.W. Grosse-Kunstleve, A.J. McCoy, N.W. Moriarty, R. Oeffner, R.J. Read, D.C. Richardson, J.S. Richardson, T.C. Terwilliger, and P.H. Zwart. 2010. PHENIX: a comprehensive Python-based system for macromolecular structure solution. *Acta crystallographica. Section D, Biological crystallography*. 66:213-221.
- Aguilar-Bryan, L., C.G. Nichols, S.W. Wechsler, J.P.t. Clement, A.E. Boyd, 3rd, G. Gonzalez, H. Herrera-Sosa, K. Nguy, J. Bryan, and D.A. Nelson. 1995. Cloning of the beta cell high-affinity sulfonylurea receptor: a regulator of insulin secretion. *Science*. 268:423-426.
- Antcliff, J.F., S. Haider, P. Proks, M.S. Sansom, and F.M. Ashcroft. 2005. Functional analysis of a structural model of the ATP-binding site of the KATP channel Kir6.2 subunit. *The EMBO journal*. 24:229-239.
- Ashcroft, F.M. 2005. ATP-sensitive potassium channelopathies: focus on insulin secretion. *The Journal of clinical investigation*. 115:2047-2058.
- Ashcroft, F.M., and F.M. Gribble. 1998. Correlating structure and function in ATP-sensitive K<sup>+</sup> channels. *Trends in neurosciences*. 21:288-294.
- Ashcroft, F.M., and P. Rorsman. 1990. ATP-sensitive K<sup>+</sup> channels: a link between B-cell metabolism and insulin secretion. *Biochemical Society transactions*. 18:109-111.
- Ashfield, R., F.M. Gribble, S.J. Ashcroft, and F.M. Ashcroft. 1999. Identification of the high-affinity tolbutamide site on the SUR1 subunit of the K(ATP) channel. *Diabetes*. 48:1341-1347.
- Babenko, A.P., and J. Bryan. 2003. Sur domains that associate with and gate KATP pores define a novel gatekeeper. *The Journal of biological chemistry*. 278:41577-41580.
- Bakos, E., R. Evers, G. Calenda, G.E. Tusnady, G. Szakacs, A. Varadi, and B. Sarkadi. 2000. Characterization of the amino-terminal regions in the human multidrug resistance protein (MRP1). *Journal of cell science*. 113 Pt 24:4451-4461.
- Baukrowitz, T., U. Schulte, D. Oliver, S. Herlitze, T. Krauter, S.J. Tucker, J.P. Ruppersberg, and B. Fakler. 1998. PIP2 and PIP as determinants for ATP inhibition of KATP channels. *Science*. 282:1141-1144.
- Brunger, A.T., P.D. Adams, G.M. Clore, W.L. DeLano, P. Gros, R.W. Grosse-Kunstleve, J.S. Jiang, J. Kuszewski, M. Nilges, N.S. Pannu, R.J. Read, L.M. Rice, T. Simonson, and G.L. Warren. 1998. Crystallography & NMR system: A new software suite for macromolecular structure determination. *Acta crystallographica. Section D, Biological crystallography*. 54:905-921.
- Bryan, J., W.H. Vila-Carriles, G. Zhao, A.P. Babenko, and L. Aguilar-Bryan. 2004. Toward linking structure with function in ATP-sensitive K<sup>+</sup> channels. *Diabetes*. 53 Suppl 3:S104-112.
- Chan, K.W., H. Zhang, and D.E. Logothetis. 2003. N-terminal transmembrane domain of the SUR controls trafficking and gating of Kir6 channel subunits. *The EMBO journal*. 22:3833-3843.
- Chapman, M.S., A. Trzynka, and B.K. Chapman. 2013. Atomic modeling of cryo-electron microscopy reconstructions--joint refinement of model and imaging parameters. *Journal of structural biology*. 182:10-21.
- Chen, P.C., E.M. Olson, Q. Zhou, Y. Kryukova, H.M. Sampson, D.Y. Thomas, and S.L. Shyng. 2013a. Carbamazepine as a novel small molecule corrector of trafficking-impaired ATP-

- sensitive potassium channels identified in congenital hyperinsulinism. *The Journal of biological chemistry*. 288:20942-20954.
- Chen, S., G. McMullan, A.R. Faruqi, G.N. Murshudov, J.M. Short, S.H. Scheres, and R. Henderson. 2013b. High-resolution noise substitution to measure overfitting and validate resolution in 3D structure determination by single particle electron cryomicroscopy. *Ultramicroscopy*. 135:24-35.
- Clarke, O.B., A.T. Caputo, A.P. Hill, J.I. Vandenberg, B.J. Smith, and J.M. Gulbis. 2010. Domain reorientation and rotation of an intracellular assembly regulate conduction in Kir potassium channels. *Cell*. 141:1018-1029.
- Cook, D.L., and J. Bryan. 1998. ATP-sensitive K<sup>+</sup> channels come of age. *Trends in pharmacological sciences*. 19:477-478.
- de Wet, H., and P. Proks. 2015. Molecular action of sulphonylureas on KATP channels: a real partnership between drugs and nucleotides. *Biochemical Society transactions*. 43:901-907.
- de Wet, H., K. Shimomura, J. Aittoniemi, N. Ahmad, M. Lafond, M.S. Sansom, and F.M. Ashcroft. 2012. A universally conserved residue in the SUR1 subunit of the KATP channel is essential for translating nucleotide binding at SUR1 into channel opening. *The Journal of physiology*. 590:5025-5036.
- Devaraneni, P.K., G.M. Martin, E.M. Olson, Q. Zhou, and S.L. Shyng. 2015. Structurally distinct ligands rescue biogenesis defects of the KATP channel complex via a converging mechanism. *The Journal of biological chemistry*. 290:7980-7991.
- Emsley, P., B. Lohkamp, W.G. Scott, and K. Cowtan. 2010. Features and development of Coot. *Acta crystallographica. Section D, Biological crystallography*. 66:486-501.
- Enkvetchakul, D., G. Loussouarn, E. Makhina, S.L. Shyng, and C.G. Nichols. 2000. The kinetic and physical basis of K(ATP) channel gating: toward a unified molecular understanding. *Biophysical journal*. 78:2334-2348.
- Fukuda, Y., L. Aguilar-Bryan, M. Vaxillaire, A. Dechaume, Y. Wang, M. Dean, K. Moitra, J. Bryan, and J.D. Schuetz. 2011. Conserved intramolecular disulfide bond is critical to trafficking and fate of ATP-binding cassette (ABC) transporters ABCB6 and sulfonylurea receptor 1 (SUR1)/ABCC8. *The Journal of biological chemistry*. 286:8481-8492.
- Golstein, P.E., A. Boom, J. van Geffel, P. Jacobs, B. Masereel, and R. Beauwens. 1999. P-glycoprotein inhibition by glibenclamide and related compounds. *Pflugers Archiv : European journal of physiology*. 437:652-660.
- Grant, T., and N. Grigorieff. 2015. Measuring the optimal exposure for single particle cryo-EM using a 2.6 Å reconstruction of rotavirus VP6. *eLife*. 4:e06980.
- Gribble, F.M., R. Ashfield, C. Ammala, and F.M. Ashcroft. 1997. Properties of cloned ATP-sensitive K<sup>+</sup> currents expressed in *Xenopus* oocytes. *The Journal of physiology*. 498 ( Pt 1):87-98.
- Gribble, F.M., and F. Reimann. 2003. Sulphonylurea action revisited: the post-cloning era. *Diabetologia*. 46:875-891.
- Gribble, F.M., S.J. Tucker, T. Haug, and F.M. Ashcroft. 1998. MgATP activates the beta cell KATP channel by interaction with its SUR1 subunit. *Proceedings of the National Academy of Sciences of the United States of America*. 95:7185-7190.
- Hansen, S.B., X. Tao, and R. MacKinnon. 2011. Structural basis of PIP<sub>2</sub> activation of the classical inward rectifier K<sup>+</sup> channel Kir2.2. *Nature*. 477:495-498.

- Hibino, H., A. Inanobe, K. Furutani, S. Murakami, I. Findlay, and Y. Kurachi. 2010. Inwardly rectifying potassium channels: their structure, function, and physiological roles. *Physiological reviews*. 90:291-366.
- Hohmeier, H.E., H. Mulder, G. Chen, R. Henkel-Rieger, M. Prentki, and C.B. Newgard. 2000. Isolation of INS-1-derived cell lines with robust ATP-sensitive K<sup>+</sup> channel-dependent and -independent glucose-stimulated insulin secretion. *Diabetes*. 49:424-430.
- Inagaki, N., T. Gonoi, J.P.t. Clement, N. Namba, J. Inazawa, G. Gonzalez, L. Aguilar-Bryan, S. Seino, and J. Bryan. 1995. Reconstitution of IKATP: an inward rectifier subunit plus the sulfonylurea receptor. *Science*. 270:1166-1170.
- Jin, M.S., M.L. Oldham, Q. Zhang, and J. Chen. 2012. Crystal structure of the multidrug transporter P-glycoprotein from *Caenorhabditis elegans*. *Nature*. 490:566-569.
- John, S.A., J.N. Weiss, L.H. Xie, and B. Ribalet. 2003. Molecular mechanism for ATP-dependent closure of the K<sup>+</sup> channel Kir6.2. *The Journal of physiology*. 552:23-34.
- Jons, T., D. Wittschieber, A. Beyer, C. Meier, A. Brune, A. Thomzig, G. Ahnert-Hilger, and R.W. Veh. 2006. K<sup>+</sup>-ATP-channel-related protein complexes: potential transducers in the regulation of epithelial tight junction permeability. *Journal of cell science*. 119:3087-3097.
- Kim, J., S. Wu, T.M. Tomasiak, C. Mergel, M.B. Winter, S.B. Stiller, Y. Robles-Colmanares, R.M. Stroud, R. Tampe, C.S. Craik, and Y. Cheng. 2015. Subnanometre-resolution electron cryomicroscopy structure of a heterodimeric ABC exporter. *Nature*. 517:396-400.
- Kucukelbir, A., F.J. Sigworth, and H.D. Tagare. 2014. Quantifying the local resolution of cryo-EM density maps. *Nature methods*. 11:63-65.
- Lin, C.W., F. Yan, S. Shimamura, S. Barg, and S.L. Shyng. 2005. Membrane phosphoinositides control insulin secretion through their effects on ATP-sensitive K<sup>+</sup> channel activity. *Diabetes*. 54:2852-2858.
- Martin, G.M., P.C. Chen, P. Devaraneni, and S.L. Shyng. 2013. Pharmacological rescue of trafficking-impaired ATP-sensitive potassium channels. *Frontiers in physiology*. 4:386.
- Martin, G.M., E.A. Rex, P. Devaraneni, J.S. Denton, K.E. Boodhansingh, D.D. DeLeon, C.A. Stanley, and S.L. Shyng. 2016. Pharmacological Correction of Trafficking Defects in ATP-Sensitive Potassium Channels Caused by Sulfonylurea Receptor 1 Mutations. *The Journal of biological chemistry*.
- Masia, R., D.D. De Leon, C. MacMullen, H. McKnight, C.A. Stanley, and C.G. Nichols. 2007. A mutation in the TMD0-L0 region of sulfonylurea receptor-1 (L225P) causes permanent neonatal diabetes mellitus (PNDM). *Diabetes*. 56:1357-1362.
- Mikhailov, M.V., J.D. Campbell, H. de Wet, K. Shimomura, B. Zadek, R.F. Collins, M.S. Sansom, R.C. Ford, and F.M. Ashcroft. 2005. 3-D structural and functional characterization of the purified KATP channel complex Kir6.2-SUR1. *The EMBO journal*. 24:4166-4175.
- Naren, A.P., M.W. Quick, J.F. Collawn, D.J. Nelson, and K.L. Kirk. 1998. Syntaxin 1A inhibits CFTR chloride channels by means of domain-specific protein-protein interactions. *Proceedings of the National Academy of Sciences of the United States of America*. 95:10972-10977.
- Nichols, C.G. 2006. KATP channels as molecular sensors of cellular metabolism. *Nature*. 440:470-476.

- Oldham, M.L., R.K. Hite, A.M. Steffen, E. Damko, Z. Li, T. Walz, and J. Chen. 2016. A mechanism of viral immune evasion revealed by cryo-EM analysis of the TAP transporter. *Nature*. 529:537-540.
- Ortiz, D., P. Voyvodic, L. Gossack, U. Quast, and J. Bryan. 2012. Two neonatal diabetes mutations on transmembrane helix 15 of SUR1 increase affinity for ATP and ADP at nucleotide binding domain 2. *The Journal of biological chemistry*. 287:17985-17995.
- Peters, K.W., J. Qi, J.P. Johnson, S.C. Watkins, and R.A. Frizzell. 2001. Role of snare proteins in CFTR and ENaC trafficking. *Pflugers Archiv : European journal of physiology*. 443 Suppl 1:S65-69.
- Pettersen, E.F., T.D. Goddard, C.C. Huang, G.S. Couch, D.M. Greenblatt, E.C. Meng, and T.E. Ferrin. 2004. UCSF Chimera--a visualization system for exploratory research and analysis. *Journal of computational chemistry*. 25:1605-1612.
- Pratt, E.B., F.F. Yan, J.W. Gay, C.A. Stanley, and S.L. Shyng. 2009. Sulfonylurea receptor 1 mutations that cause opposite insulin secretion defects with chemical chaperone exposure. *The Journal of biological chemistry*. 284:7951-7959.
- Pratt, E.B., Q. Zhou, J.W. Gay, and S.L. Shyng. 2012. Engineered interaction between SUR1 and Kir6.2 that enhances ATP sensitivity in KATP channels. *The Journal of general physiology*. 140:175-187.
- Proks, P., J.F. Antcliff, J. Lippiat, A.L. Gloyn, A.T. Hattersley, and F.M. Ashcroft. 2004. Molecular basis of Kir6.2 mutations associated with neonatal diabetes or neonatal diabetes plus neurological features. *Proceedings of the National Academy of Sciences of the United States of America*. 101:17539-17544.
- Proks, P., A.L. Arnold, J. Bruining, C. Girard, S.E. Flanagan, B. Larkin, K. Colclough, A.T. Hattersley, F.M. Ashcroft, and S. Ellard. 2006. A heterozygous activating mutation in the sulphonylurea receptor SUR1 (ABCC8) causes neonatal diabetes. *Human molecular genetics*. 15:1793-1800.
- Rohou, A., and N. Grigorieff. 2015. CTFFIND4: Fast and accurate defocus estimation from electron micrographs. *Journal of structural biology*. 192:216-221.
- Rosenthal, P.B., and R. Henderson. 2003. Optimal determination of particle orientation, absolute hand, and contrast loss in single-particle electron cryomicroscopy. *Journal of molecular biology*. 333:721-745.
- Scheres, S.H. 2012. RELION: implementation of a Bayesian approach to cryo-EM structure determination. *Journal of structural biology*. 180:519-530.
- Schultz, B.D., A.D. DeRoos, C.J. Venglarik, A.K. Singh, R.A. Frizzell, and R.J. Bridges. 1996. Glibenclamide blockade of CFTR chloride channels. *The American journal of physiology*. 271:L192-200.
- Schwappach, B., N. Zerangue, Y.N. Jan, and L.Y. Jan. 2000. Molecular basis for K(ATP) assembly: transmembrane interactions mediate association of a K<sup>+</sup> channel with an ABC transporter. *Neuron*. 26:155-167.
- Shyng, S.L., and C.G. Nichols. 1998. Membrane phospholipid control of nucleotide sensitivity of KATP channels. *Science*. 282:1138-1141.
- Tanabe, K., S.J. Tucker, M. Matsuo, P. Proks, F.M. Ashcroft, S. Seino, T. Amachi, and K. Ueda. 1999. Direct photoaffinity labeling of the Kir6.2 subunit of the ATP-sensitive K<sup>+</sup> channel by 8-azido-ATP. *The Journal of biological chemistry*. 274:3931-3933.

- Tucker, S.J., F.M. Gribble, C. Zhao, S. Trapp, and F.M. Ashcroft. 1997. Truncation of Kir6.2 produces ATP-sensitive K<sup>+</sup> channels in the absence of the sulphonylurea receptor. *Nature*. 387:179-183.
- Tusnady, G.E., B. Sarkadi, I. Simon, and A. Varadi. 2006. Membrane topology of human ABC proteins. *FEBS letters*. 580:1017-1022.
- Voss, N.R., C.K. Yoshioka, M. Radermacher, C.S. Potter, and B. Carragher. 2009. DoG Picker and TiltPicker: software tools to facilitate particle selection in single particle electron microscopy. *Journal of structural biology*. 166:205-213.
- Webb, B., and A. Sali. 2016. Comparative Protein Structure Modeling Using MODELLER. *Current protocols in bioinformatics / editorial board, Andreas D. Baxevanis ... [et al.]*. 54:5 6 1-5 6 37.
- Whorton, M.R., and R. MacKinnon. 2011. Crystal structure of the mammalian GIRK2 K<sup>+</sup> channel and gating regulation by G proteins, PIP<sub>2</sub>, and sodium. *Cell*. 147:199-208.
- Whorton, M.R., and R. MacKinnon. 2013. X-ray structure of the mammalian GIRK2-beta gamma G-protein complex. *Nature*. 498:190-197.
- Wilkins, S. 2015. Structure and mechanism of ABC transporters. *F1000prime reports*. 7:14.
- Winkler, M., P. Kuhner, U. Russ, D. Ortiz, J. Bryan, and U. Quast. 2012. Role of the amino-terminal transmembrane domain of sulphonylurea receptor SUR2B for coupling to K(IR)6.2, ligand binding, and oligomerization. *Naunyn-Schmiedeberg's archives of pharmacology*. 385:287-298.
- Yan, F., C.W. Lin, E. Weisiger, E.A. Cartier, G. Taschenberger, and S.L. Shyng. 2004. Sulphonylureas correct trafficking defects of ATP-sensitive potassium channels caused by mutations in the sulphonylurea receptor. *The Journal of biological chemistry*. 279:11096-11105.
- Yan, F.F., Y.W. Lin, C. MacMullen, A. Ganguly, C.A. Stanley, and S.L. Shyng. 2007. Congenital hyperinsulinism associated ABCC8 mutations that cause defective trafficking of ATP-sensitive K<sup>+</sup> channels: identification and rescue. *Diabetes*. 56:2339-2348.
- Zerangue, N., B. Schwappach, Y.N. Jan, and L.Y. Jan. 1999. A new ER trafficking signal regulates the subunit stoichiometry of plasma membrane K(ATP) channels. *Neuron*. 22:537-548.
- Zhang, Z., and J. Chen. 2016. Atomic Structure of the Cystic Fibrosis Transmembrane Conductance Regulator. *Cell*. 167:1586-1597 e1589.
- Zingman, L.V., A.E. Alekseev, D.M. Hodgson-Zingman, and A. Terzic. 2007. ATP-sensitive potassium channels: metabolic sensing and cardioprotection. *Journal of applied physiology*. 103:1888-1893.

## Chapter 4

### Anti-diabetic drug binding site in a mammalian $K_{ATP}$ channel revealed by Cryo-EM

Gregory M. Martin<sup>1</sup>, Balamurugan Kandasamy<sup>1</sup>, Frank DiMaio<sup>2</sup>, Craig Yoshioka<sup>3\*</sup>, & Show-Ling Shyng<sup>1\*</sup>

<sup>1</sup>Department of Biochemistry and Molecular Biology, Oregon Health & Science University, Portland, OR 97239, USA; <sup>2</sup> Department of Biochemistry, University of Washington, Seattle WA 98195, USA; <sup>3</sup>Department of Biomedical Engineering, Oregon Health & Science University, 2730 SW Moody Ave, Portland, OR 97239, USA.

\*Correspondence to: Show-Ling Shyng ([shyngs@ohsu.edu](mailto:shyngs@ohsu.edu)), Department of Biochemistry and Molecular Biology, School of Medicine, Oregon Health & Science University, 3181 S.W. Sam Jackson Park Road, Portland, OR 97239, or Craig Yoshioka ([yoshiokc@ohsu.edu](mailto:yoshiokc@ohsu.edu)), Department of Biomedical Engineering, Oregon Health & Science University, 2730 SW Moody Ave, Portland, OR 97239, USA.

**Published in:** Martin GM, Kandasamy B, DiMaio F, Yoshioka C, Shyng SL. (2017). Anti-diabetic drug binding site in a mammalian  $K_{ATP}$  channel revealed by cryo-EM. *eLife*. October 24; 6.

#### Author Contributions

**GMM:** Experimental design, conceived of project. Writing: original draft and revision; Figure making. Sample preparation: cell culture and protein expression, protein purification, cryo-EM sample prep. Cryo-EM data collection. Cryo-EM image processing, generation of final cryo-EM map. Structure solution: rebuilt and re-refined SUR1 and Kir6.2 models. Deposited final structures and maps to database. **BK:** Made constructs for mutation of GBC binding site. Performed experiments for Figure 7. **FD:** Aided in re-building and re-refining structures with Rosetta. **CY:** Experimental design. Cryo-EM data collection. Image processing and generation of final EM map. Writing: original draft (methods), revision, Figure making (Fig. 1-figure supplements 1 and 2, Table 1). **SLS:** Experimental design, conceived of project. Writing: original draft and revision; Figure making.

## **Abstract**

Sulfonylureas are anti-diabetic medications that act by inhibiting pancreatic  $K_{ATP}$  channels composed of SUR1 and Kir6.2. The mechanism by which these drugs interact with and inhibit the channel has been extensively investigated, yet it remains unclear where the drug binding pocket resides. Here, we present a cryo-EM structure of a hamster SUR1/rat Kir6.2 channel bound to a high-affinity sulfonylurea drug glibenclamide and ATP at 3.63Å resolution, which reveals unprecedented details of the ATP and glibenclamide binding sites. Importantly, the structure shows for the first time that glibenclamide is lodged in the transmembrane bundle of the SUR1-ABC core connected to the first nucleotide binding domain near the inner leaflet of the lipid bilayer. Mutation of residues predicted to interact with glibenclamide in our model led to reduced sensitivity to glibenclamide. Our structure provides novel mechanistic insights of how sulfonylureas and ATP interact with the  $K_{ATP}$  channel complex to inhibit channel activity.

## **Introduction**

ATP-sensitive potassium ( $K_{ATP}$ ) channels are unique hetero-octameric complexes each composed of four inwardly rectifying Kir6 channel subunits and four sulfonylurea receptor (SUR) subunits belonging to the ATP binding cassette (ABC) transporter protein family (Aguilar-Bryan & Bryan, 1999; Nichols, 2006). In pancreatic  $\beta$ -cells,  $K_{ATP}$  channels formed by Kir6.2 and SUR1 are gated by intracellular ATP and ADP, with ATP inhibiting channel activity while  $Mg^{2+}$ -complexed ATP and ADP stimulating channel activity (Aguilar-Bryan & Bryan, 1999; Ashcroft, 2007). During glucose stimulation, the intracellular ATP to ADP ratio increases following glucose metabolism, which favors channel closure by ATP, resulting in membrane depolarization,  $Ca^{2+}$  influx, and exocytosis of insulin granules. In this way,  $K_{ATP}$  channels are

able to control insulin secretion according to blood glucose levels. Mutations that disrupt channel function are known to cause a spectrum of insulin secretion disorders (Ashcroft, 2005; Koster, Permutt, et al., 2005). Specifically, loss-of-function mutations result in congenital hyperinsulinism, whereas gain-of-function mutations lead to transient or permanent neonatal diabetes (Ashcroft, 2005). The pivotal role of  $K_{ATP}$  channels in insulin secretion regulation makes them an important drug target.

Discovered in the 1940s, sulfonylureas have been a mainstay of type 2 diabetes therapy for more than half a century (Sola et al., 2015). The medical importance of this class of drugs has led to its evolution into several generations of agents, including first-generation sulfonylureas such as tolbutamide and second-generation agents such as the high-affinity sulfonylurea glibenclamide (GBC) (Gribble & Reimann, 2003; Sola et al., 2015). All sulfonylureas stimulate insulin secretion to reduce plasma glucose levels by inhibiting the activity of  $\beta$ -cell  $K_{ATP}$  channels (Gribble & Reimann, 2003). More recently, they have also become the primary pharmacotherapy for neonatal diabetes patients carrying gain-of-function  $K_{ATP}$  channel mutations (Aguilar-Bryan & Bryan, 2008; Ashcroft, 2007; Sagen et al., 2004). Despite their clinical importance and decades of research, how sulfonylureas interact with and inhibit  $K_{ATP}$  channel activity remains poorly understood.

To begin to address the structural mechanisms by which ATP and sulfonylureas such as GBC inhibit  $K_{ATP}$  channels to stimulate insulin secretion, we recently carried out single particle cryo-EM and determined the structure of the  $\beta$ -cell  $K_{ATP}$  channel complex in the presence of ATP and GBC (Martin, Yoshioka, et al., 2017). While our initial structure at a resolution of 5.7Å revealed

the overall architecture of the channel and location of the ATP molecule, it was unable to clearly define the GBC binding site and the atomic details associated with ATP binding. A concurrent study by Li et al. (Li et al., 2017) reported another cryo-EM  $K_{ATP}$  channel structure at 5.6Å resolution, also in the presence of GBC but without ATP, in which the GBC binding site was proposed to lie near the cytoplasmic linker between the first and second transmembrane domains of SUR1; however, the assignment of the GBC density was tentative. To resolve the binding sites for ATP and GBC, we performed additional studies and improved the resolution of the  $K_{ATP}$  channel structure bound to GBC and ATP to ~3.6Å. The higher resolution structure not only clearly defines the GBC and ATP binding pockets but also provides novel insights into the mechanisms of channel inhibition by ATP and GBC.

## **Results**

### *Structure determination*

To obtain a structure of  $K_{ATP}$  channels bound to GBC and ATP, channels comprising a rat Kir6.2 and FLAG-tagged hamster SUR1 (96 and 95% sequence identity to human sequences, respectively) were expressed in rat insulinoma INS-1 832/13 cells (Hohmeier et al., 2000), affinity purified, and imaged in the presence of 1mM ATP (no  $Mg^{2+}$ ) and 1μM GBC, as described previously (Martin, Yoshioka, et al., 2017). To improve resolution, we adjusted sample and grid preparation parameters (for details see Materials and Methods) to optimize ice thickness and particle orientation distributions, which both increased the overall quality and quantity of single particles.

3D classification in Relion yielded one four-fold symmetric class, which reached an overall resolution of 4.07Å after refinement (Fig. 1-figure supplements 1; Table 1). Particles from this class were further classified and refined using Frealign (Grigorieff, 2016), which yielded a map with improved resolution of 3.63Å (Fig. 1-figure supplements 1; Table 1). The local resolution, as estimated by Bsoft, varied from 3.2Å in the Kir6.2 transmembrane domain (TMD) to ~5Å in the SUR1 nucleotide binding domains (NBDs) (Fig. 1-figure supplements 2). Overall, the map displays excellent connectivity to allow for model building (Fig.1). We have constructed a full atomic model for all of Kir6.2 minus disordered N- and C-termini, and for TMD0 of SUR1, as this part of the map was well resolved, with clear side-chain density for most residues. The ABC core of SUR1 displayed greater variability in resolution: the inner helices (relative to Kir6.2/TMD0) were also very well resolved (between 3.5 and 4Å resolution) to permit nearly complete atomic model building, while the most exposed helices (TMs 9, 10, 12, and 13) showed signs of flexibility, and were only built as polyalanine chains. This was also the case for the NBDs, for which we only refined our previously-deposited NBD models as rigid bodies (see Materials and Methods).

### *Structural overview*

The  $K_{ATP}$  channel is built around a tetrameric Kir6.2 core with each subunit in complex with one SUR1 (Fig.1B-E), as observed previously (Martin, Yoshioka, et al., 2017). Each Kir6.2 has the typical Kir channel architecture of an N-terminal cytoplasmic domain, a TMD consisting of two TMs termed M1 and M2 interspersed by a pore loop and selectivity filter, and a “tether” helix that links the TMD to the larger C-terminal cytoplasmic domain (CTD) (Fig.2A, Fig.2-figure

supplement 1). In our new structure, constrictions in the selectivity filter (T130), bundle crossing (F168), and the G-loop (G295, I296) are clearly seen (Fig.2B, C) to indicate a closed pore.

SUR1 is one of only a handful of ABC transporters which possesses an N-terminal transmembrane domain, TMD0, in addition to an ABC core structure comprising two TMDs of 6 helices each and two cytosolic NBDs (Tusnady et al., 2006; Wilkens, 2015) (Fig.2D). In the structure, TMD0 is a well-resolved 5-TM bundle (Fig.2D, Fig.2-figure supplement 2). A long intracellular loop L0 which tethers TMD0 to the ABC core is found to contain both cytosolic and amphipathic domains (Fig.2D, Fig.2-figure supplement 2). The C-terminal 2/3 of L0 is homologous to the “lasso motif” observed in CFTR (Liu et al., 2017; Zhang & Chen, 2016) and MRP1 (Johnson & Chen, 2017), and indeed, the structures are very similar (Fig.2E). SUR1 is found in an “inward-facing” conformation, with NBDs clearly separated and the vestibule formed by TMD1/TMD2 open towards the cytoplasm. As we noted previously, the two TMD-NBDs show a  $\sim 15^\circ$  rotation and  $\sim 10\text{\AA}$  horizontal translation relative to each other (Fig.2F) (Martin, Yoshioka, et al., 2017). This lack of symmetry is also seen in recently reported CFTR and MRP1 inward-facing structures (Johnson & Chen, 2017; Liu et al., 2017; Zhang & Chen, 2016). The separation between the two NBDs in our structure is similar to that seen in MRP1 bound to its substrate leukotriene C4 (Johnson & Chen, 2017)(see Fig.2F). Like SUR1 in which only NBD2 is capable of hydrolyzing ATP while NBD1 harbors a degenerate ATPase site, CFTR and MRP1 also have two asymmetric NBDs (Wilkens, 2015), suggesting the relative rotation and translation between the two TMD-NBD halves may be a common characteristic of ABC transporters with asymmetric NBDs.

### *Unique molecular interactions between SUR1 and Kir6.2*

Among all Kir channels, Kir6.1/Kir6.2 are the only members known to couple to an ABC transporter (Hibino et al., 2010); and among all ABC transporters, SUR1/SUR2 are the only ones known to couple to an ion channel (Wilkins, 2015). These proteins are also unique in that they are co-dependent for both expression and function (Inagaki et al., 1995; Zerangue et al., 1999). How SUR1 and Kir6.2 achieve this unique regulation has been a long standing question in the field.

In the structure, we find a series of hydrophobic and polar interactions mediated exclusively by TMD0 and L0 of SUR1 with Kir6.2 (Fig. 3). The extracellular N-terminus of SUR1 closely contacts the turret and pore loop of Kir6.2 (Fig.3A-D), while TM1 of TMD0 and the M1 helix of Kir6.2 form a series of hydrophobic interactions running the length of the helices (Fig.3E). On the cytoplasmic side, the intracellular loops ICL1, ICL2, and the N-terminal portion of L0 (Fig.3C, 3D), prior to the “lasso motif,” cluster around the Kir6.2 N-terminus which harbors the slide helix and key ATP-binding residues and also forms part of an intersubunit  $\beta$ -sheet (Fig.3B, 3F).

Of all the Kir channel family members which display a high degree of sequence conservation, only Kir6.1 or Kir6.2 co-assemble with SUR proteins, raising the interesting question of what molecular interactions confer this specificity. While many residue pairs in the interface are conserved in either the Kir or ABC transporter family, a couple residue pairs are unique to both Kir6.2 and SUR1. Among these, H70 within the M1 helix of Kir6.2 forms an edge-to-face  $\pi$ -stacking interaction with W51 of TM1 of TMD0 (Fig.3E), and Q57 of the Kir6.2

slide helix contacts F132 of ICL2 (Fig.3F). F132 is a well-studied permanent neonatal diabetes mutation which causes very high  $P_o$  but also reduces physical interaction between TMD0 and Kir6.2 (Proks et al., 2007), supporting its role as a critical part of the interface. To our knowledge, mutational studies of Kir6.2 Q57 and H70, and SUR1 W51 have not been reported; it would be interesting to test the role of these residues in channel assembly and function in the future.

#### *The ATP binding site*

Non-hydrolytic binding of intracellular ATP to the cytoplasmic domains of Kir6.2 induces rapid and reversible closure of the pore (Nichols, 2006). We have previously reported the location of the ATP-binding site at the interface of the cytoplasmic N- and C-terminal domains from two adjacent subunits (Martin, Yoshioka, et al., 2017), giving 4 equivalent sites for the Kir6.2 tetramer. In the current map, there is strong cryo-EM density for the ATP as well as surrounding residues (Fig.4., Fig.4-figure supplement 1), allowing for detailed analysis of the mode of ATP binding as well as the possible mechanism of inhibition.

In the structure, the ATP is directly below the inner membrane leaflet and is partially exposed to solvent (Fig.4). The bound ATP appears to adopt a conformation similar to that found in other non-canonical,  $Mg^{2+}$ -independent ATP-binding sites, such as the P2X receptor (Hattori & Gouaux, 2012), in which the phosphate groups are folded towards the adenine ring (Fig.4B, C). This places the  $\beta$ - and  $\gamma$ -phosphates to interact with basic residues contributed by the N- and C- termini of Kir6.2. The pocket itself is formed by the overlap of three distinct cytoplasmic structures: an N-terminal peptide (binding residues N48 and R50; subunit A)

immediately before the Kir channel “slide helix”; a C-terminal  $\beta$ -sheet (I182 and K185; subunit B) immediately following the TMD-CTD tether helix (see Fig.2A, Fig.2-figure supplement 1); and a short, solvent-exposed helical segment (Y330, F333, G334; subunit B) (Fig.4C). Note an unassigned protruding density close to the ATP density was observed (Fig.4-figure supplement 1A). This is reminiscent of a coordinating magnesium ion often observed in other high-resolution structures of proteins bound with ATP or GTP (Bauer et al., 2000; Oliva et al., 2004). Interestingly, early studies of  $K_{ATP}$  channel gating showed that, while  $Mg^{2+}$  is not necessary as a cofactor in ATP inhibition, MgATP can inhibit as effectively as free ATP (Lederer & Nichols, 1989). Although we did not include  $Mg^{2+}$  in our sample, a possibility that low concentrations of  $Mg^{2+}$  might be present in the buffer cannot be excluded.

The  $\alpha$ - phosphate of ATP is coordinated by the main-chain nitrogen of G334 and K185, while the  $\beta$ - and  $\gamma$ -phosphates are coordinated by side-chain nitrogens of K185 and R50, respectively (Fig.4C, Fig.4-figure supplement 1C). The ribose group is in close contact with the I182 and F333 side chains; the adenine ring stacks against the aliphatic portion of the R50 side chain as well as Y330, and is H-bonded to the main chain nitrogen of R50, and main chain oxygen of N48 and Y330 (Fig.4C, Fig.4-figure supplement 1D, 1E). The aforementioned residues have all been shown previously to reduce ATP inhibition when mutated to other amino acids (Antcliff et al., 2005; Cukras et al., 2002; Drain et al., 1998; Li et al., 2005; Proks et al., 1999; Tammaro et al., 2005; Tucker et al., 1998), consistent with a role of these residues in ATP gating. Notably, sequence comparison reveals that a key difference between Kir6.2 and other Kir channels is G334, which in other Kir channels is occupied by larger amino acids. Substitution of glycine at this position by a larger amino acids such as histidine seen in Kir2 or Kir3 channels

would create steric hindrance to prevent ATP binding. This may explain, at least in part, why Kir6.2 is the only Kir channel sensitive to ATP regulation.

*Structural interactions around the ATP binding site and their relationship to the PIP<sub>2</sub> binding site*

A number of residues within the vicinity of the ATP-binding site such as E179, R201, and R301 have previously been shown to reduce ATP sensitivity (Haider et al., 2005; Shyng et al., 2000) and could be involved in ATP binding. However, from the structure it is clear these residues contribute indirectly (Fig.5). E179 and R301 were both proposed to interact with the adenine ring (Haider et al., 2005). In our structure, neither residue forms direct interactions with ATP (Fig.5A, 5C). E179 appears to interact with R54 from the adjacent Kir6.2 and may be part of the network that stabilizes the interaction between R50 and ATP (Fig.5C). R301 is found to interact with Q299 in the same  $\beta$ -strand that is part of a  $\beta$ -sheet in the Kir6.2 CTD (Fig. 5A; see also Fig.2-figure supplement 1). Interestingly, R301 is one of the most highly mutated residues in congenital hyperinsulinism (Snider et al., 2013); mutation of R301, in addition to mildly reducing ATP sensitivity, results in rapid decay of channel activity that can be reversed by increasing PIP<sub>2</sub> concentrations in the membrane (Lin et al., 2008; Shyng et al., 2000). Based on our structure, it is likely that mutation of this residue disrupts structural integrity of the Kir6.2 CTD necessary for stable channel interaction with PIP<sub>2</sub> and ATP. By contrast, R201 is one of the most highly mutated residues in neonatal diabetes (Ashcroft, 2005). It has been proposed that R201 coordinates the  $\alpha$ -phosphate of ATP (Haider et al., 2005). However, in the structure R201 is found on the  $\beta$ -strand directly below that of I182 and K185, and is too distant to directly interact with ATP. Instead, R201 is sandwiched between the benzene rings of F333 and F315,

forming a dual cation- $\pi$  interaction that likely stabilizes the ATP-binding site (Fig. 5B). Mutation of R201 would therefore destabilize this interaction to indirectly reduce ATP inhibition.

Another interesting residue is Q52. The PNDM mutation Q52R causes extremely high  $P_o$  and very low ATP sensitivity (Koster, Remedi, et al., 2005; Lin et al., 2006; Proks et al., 2004). In the structure, Q52 interacts with R50 which coordinates the  $\gamma$ -phosphate of ATP, but is also interacting with R54, which orients the R54 side chain towards the ATP site and away from the PIP<sub>2</sub> site nearby (Fig.5C). In the PIP<sub>2</sub> bound Kir2.2 structure, the Kir6.2 R54 equivalent arginine residue interacts with the tether helix near PIP<sub>2</sub> binding residues (Hansen et al., 2011), suggesting that R54 may be important for Kir6.2 -PIP<sub>2</sub> interactions. Interestingly, mutation of R50 or R54 to an alanine has been reported to reduce sensitivity to both ATP and PIP<sub>2</sub> (Cukras et al., 2002). From our structure, it is easy to envision how mutation of any of these residues can disrupt the interaction network to affect gating by either ligand.

It is also important to note that in our structure, Q52 is in close proximity to E203 in the L0 of SUR1 immediately following TMD0. We have previously shown that engineered interactions between Kir6.2 residue 52 and SUR1 residue 203 via a Kir6.2-Q52E and SUR1-E203K ion pair increases channel sensitivity to ATP by nearly two orders of magnitude, and that crosslinking of the two residues via a Kir6.2-Q52C and SUR1-E203C mutant pair induces spontaneous channel closure in the absence of ATP (Pratt et al., 2012). In addition, our previous studies have shown that ATP binding involves residues from not only the N-terminus of Kir6.2 such as R50 but also residues in SUR1-L0 such as K205 (Martin, Yoshioka, et al., 2017; Pratt et al., 2012). Together

these studies lead us to propose that the inhibitory effect of ATP is partially due to stabilizing the interaction between this N-terminal region of Kir6.2 and L0 of SUR1 (see Discussion).

### *The GBC binding site*

Sulfonylureas stimulate insulin secretion by inhibiting pancreatic  $K_{ATP}$  channels (Aguilar-Bryan & Bryan, 1999). GBC, also known as glyburide, is a second generation sulfonylurea that contains both a sulfonylurea moiety and a benzamido moiety, and binds  $K_{ATP}$  channels with nM affinity (Gribble & Reimann, 2003). Despite intense investigation the GBC binding site has remained elusive. Early studies using chimeras of SUR1 and SUR2A, which are known to have lower sensitivity to GBC than SUR1, suggest the involvement of TMs 14-16; in particular mutating S1238 in SUR1 to Y (note in some papers, this is numbered as S1237) as seen in SUR2A compromised GBC binding and block (Ashfield et al., 1999; Winkler et al., 2007). Subsequent studies using  $^{125}\text{I}$ -azido-GBC photolabeling implicated involvement of L0 of SUR1; specifically, two mutations Y230A and W232A in L0 severely compromised photolabeling of SUR1 (Vila-Carriles et al., 2007). These studies led to a model in which S1238 and Y230/W232 constitute two ends of a bipartite binding pocket, each recognizing opposite ends of GBC (Bryan et al., 2004; Winkler et al., 2007); however, whether one or both contribute directly to GBC binding remained unknown.

In the current reconstruction we find well defined, non-protein density within the TMDs of SUR1, with a size and shape which closely matches that of a GBC molecule (Fig.6, Fig.6-figure supplement 1A). One end of the density is in direct contact with S1238 and resembles the cyclohexyl moiety long presumed to constitute the “A” site that is abolished by the S1238Y

mutation (Ashfield et al., 1999; Bryan et al., 2004). We used this to guide the initial docking of GBC, which could then be readily refined into the density together with SUR1.

The binding pocket is contoured to precisely accommodate GBC, and the combination of polar and hydrophobic residues help explain the sub-nM affinity of SUR1 for this sulfonylurea (Fig. 6C, Fig.6-figure supplement 1B, C). A primary anchor is composed of two arginine residues, R1246 and R1300, which coordinate each oxygen of the sulfonyl group. Each nitrogen of the urea moiety is coordinated by T1242 and N1245, and the adjacent benzene and cyclohexyl groups (adjacent to the sulfonyl and urea groups, respectively) are stabilized by a series of hydrophobic interactions contributed by TM helices from both TMD1 (TM6, 7, 8) and TMD2 (TM16). As a second-generation sulfonylurea, GBC contains another lipophilic group adjacent to an amide linker, which is lacking in first-generation compounds like tolbutamide (Gribble & Reimann, 2003). This group, a 1-chloro-4-methoxy-benzene, is encircled by a ring of hydrophilic and hydrophobic side chains. In particular, the Cl appears to hydrogen bond with the amino group of N437, while the methoxy is H-bonded to the hydroxyl group of Y377. Y377 also seems to contribute a  $\pi$ - $\pi$  stacking interaction with the benzene ring. In the structure, the previously proposed sulfonylurea binding residue S1238 juxtaposes the cyclohexyl group of GBC, with only  $\sim 3\text{\AA}$  separation between the C $\beta$  of S1238 and the 6-carbon ring of GBC (Fig.6C; Fig.6-figure supplement 1D). Mutation of this residue to a tyrosine may alter interaction with GBC to compromise high affinity binding of GBC.

In order to validate the proposed binding site, we mutated a subset of key GBC-binding residues listed above to alanine and tested their response to 100 nM and 1 $\mu$ M GBC with Rb<sup>+</sup>

efflux experiments, which measure channel activity and response to GBC in intact cells. All six mutations, R306A, Y377A, N437A, T1242A, R1246A, and R1300A trafficked normally and responded as WT to metabolic inhibition (Fig. 7A, 7B, 7D). Strikingly, all six mutants showed significantly reduced or complete absence of inhibition at 100 nM, and five mutants (R306A, Y377, N437A, T1242, and R1246A) showed significantly reduced sensitivity compared to WT even at 1  $\mu$ M GBC (Fig. 7C, D). The four most GBC-insensitive mutants, R306A, Y377A, N437A, and T1242A were further analyzed by inside-out patch-clamp recording. Although these mutants were still sensitive to GBC inhibition, the extent of inhibition at steady-state was less compared to WT channels at 10nM and 100nM (Fig. 7, figure supplement 1). Also worth noting, while inhibition of WT channels was nearly irreversible, inhibition of mutants was more reversible, consistent with the mutants having reduced affinity for GBC (Fig. 7-figure supplement 1). Together these results provide strong functional evidence for the GBC binding pocket defined in our structure.

#### *The role of SUR1-Y230 and W232 in GBC interaction*

In the previously proposed bipartite binding model for GBC (Bryan et al., 2004), the pocket was formed from two overlapping regions: at one end was S1238 of TMD2, and at the other was L0 involving residues Y230 and W232, part of the “lasso motif” observed in CFTR (Zhang & Chen, 2016) and MRP1 (Johnson & Chen, 2017). Mutation of Y230 to an alanine has also been shown to reduce the ability of GBC to inhibit channel activity (Devaraneni et al., 2015; Yan et al., 2006). In our current structure, Y230 is too distant to interact directly with GBC. However, the binding pocket is close to the L0-TMD interface, where the L0 amphipathic helix forms a series of mostly hydrophobic interactions with transmembrane helices from TMD1/2 that line the GBC

binding pocket. Here, we find that Y230 stacks closely against the aliphatic portion of the R1246 side chain, which in turn coordinates an oxygen of the sulfonyl group of GBC (Fig.6D; Fig.6-figure supplement 1E). W232 appears to form a strong interaction with M233, which interacts directly with two alanines, A1243 and A1244, on the opposite side of TM16 where two GBC interacting residues T1242 and N1245 are located (Fig.6D; Fig.6-figure supplement 1D). These observations indicate an important but clearly indirect role for Y230 and W232 in GBC binding.

#### *Comparison with previous $K_{ATP}$ channel structures*

To date, two  $K_{ATP}$  channel structures have been reported, one from our group (Martin, Yoshioka, et al., 2017) in the presence of GBC and ATP at 5.7Å resolution, and the other by Li et al. (Li et al., 2017) in the presence of GBC but absence of ATP at 5.6Å resolution. The structure presented here is also in the presence of ATP and GBC and is nearly identical to the structure we published previously but with much improved resolution, allowing for accurate modelling of nearly all side-chains, many of which were absent in our previous structure (Martin, Yoshioka, et al., 2017). To gain insight into the conformational difference between ATP-bound and ATP-free channels and how resolution of the map may affect structural interpretation, we compared our current structure with that of Li et al. in detail.

Overall, we find that the two structures are also very similar, both in terms of organization of the complex and conformations of Kir6.2 and SUR1 individually (Fig. 8). Since the structure from Li et al. lacks ATP whereas our structure is bound to ATP, it suggests that either ATP does not induce significant conformational change of the channel or that GBC, which is present in

both structures, stabilizes the channel in a conformation that resembles an ATP-bound state. The latter possibility is intriguing as it offers a potential mechanism by which GBC inhibits channel activity.

Despite overall similarity, there are some key differences between our current structure and that of Li et al. which warrant addressing, especially with regard to interpretation of the cryo-EM density and structural modeling of the GBC-binding site. In Li et al, they attributed GBC to unassigned density surrounding Y230 and W232, two residues previously proposed to be involved in sulfonylurea binding (Vila-Carriles et al., 2007). However, in their structure, they did not model residues 214-222 of SUR1-L0, which happen to lie close to their “GBC” density (Fig.8-figure supplement 1A, 1B). Docking our current structure into their map (Fig.8-figure supplement 1A, 1B, blue), we find that the density they observed matches well to those residues left out of their model, corresponding to approximately R216-F221. Moreover, the size and shape of the density surrounding those residues in our current reconstruction are reminiscent of their “GBC” density, albeit a higher-resolution version (Fig.8-figure supplement 1C, 1D). Interestingly, having identified the GBC binding site using our higher resolution structure, we re-inspected our previous 5.7Å map as well as the map by Li et al. and found unassigned density near the GBC binding site that corresponds to the size and shape of GBC in both (Fig.8-figure supplement 2).

Another difference between our structures and the structures reported by Li et al. concerns the location of PIP<sub>2</sub> (Li et al., 2017; Martin, Yoshioka, et al., 2017). In both studies, membranes containing channel proteins were solubilized in digitonin with no addition of exogenous PIP<sub>2</sub> in

subsequent purification steps. It is possible that some endogenous PIP<sub>2</sub> might have been co-purified with the channel in our studies. We have observed what appears to be a heterogeneous mixture of lipids and detergent near the predicted PIP<sub>2</sub> binding site in all of our reconstructions, but were unable to clearly distinguish the identity of this density, even at improved resolution. We therefore did not model PIP<sub>2</sub> in our earlier structure or the current structure. By contrast, Li et al. tentatively assigned extra density between two Kir6.2 subunits in one of their 3D classes as PIP<sub>2</sub> and proposed that it underlies the more dilated inner helices of two of the four Kir6.2 subunits in that class (Li et al., 2017). Unfortunately, the resolution of the 3D class in which PIP<sub>2</sub> was observed was 8.5Å and no cryo-EM density map was available, making it difficult to compare with our structures directly. Future studies will be needed to resolve this problem.

## **Discussion**

The structure presented in this study is the first to reveal in detail the ATP and GBC binding sites in the SUR1/Kir6.2 K<sub>ATP</sub> channel complex. The clear density for ATP and GBC as well as all residues involved in binding of both ligands in the current EM map allowed us to present a detailed atomic interpretation of ATP and GBC binding to the channel. Importantly, the binding pockets we identified are supported by strong functional data. In addition, the structure uncovers many molecular interactions that indirectly impact ATP and GBC gating, and those that underlie SUR1-Kir6.2 interactions. The structural information gained offers key insights into possible mechanisms of how the two ligands both inhibit K<sub>ATP</sub> channels to stimulate insulin secretion.

*The ATP binding site and mechanism of ATP inhibition*

The Kir6.2 interfacial ATP binding site model was first proposed by Antcliff et al. (Antcliff et al., 2005) based on ligand docking, homology modeling of Kir channel crystal structures, and structure-function mutagenesis data. Although some interactions in the original model between Kir6.2 residues and ATP are observed in our structure, many others require new interpretations. First, the ATP molecule adopts a conformation with the  $\gamma$ -phosphate bent towards the adenine ring (Fig.4), which is reminiscent of that observed in P2X receptors, an ATP activated ion channel (Hattori & Gouaux, 2012). Second, our structure suggests that E179, R201, and R301 rather than contributing directly to ATP binding are critical for interactions with other residues that support the ATP binding residues or general structural integrity of the Kir6.2 CTD for stable channel interaction with PIP<sub>2</sub> (Fig.5). Elucidation of the structural role of R201 and R301 helps us to understand the mechanisms by which mutation of these residues cause insulin secretion disease. Finally, although in our structure PIP<sub>2</sub> is not present or resolved, the residues previously proposed to be involved in PIP<sub>2</sub> binding or gating based on functional studies (Cukras et al., 2002; Shyng et al., 2000) and crystal structures of PIP<sub>2</sub> bound Kir2.2 and 3.2 channels (Hansen et al., 2011; Whorton & MacKinnon, 2011) can be clearly modeled, which reveals the intricate relationship between ATP binding residues and those involved in PIP<sub>2</sub> binding or gating (Fig.5C) and offers insight into how the channel senses ATP and PIP<sub>2</sub>.

We propose that ATP, by binding to a pocket created by the N-terminus and CTD from two adjacent Kir6.2 subunits with contributions from L0 of SUR1, acts to stabilize interactions between the Kir6.2 N-terminus and L0 to prevent movements necessary to open the channel (Fig. 9A). This model is consistent with our previous study showing that crosslinking of SUR1-L0 with the N-terminus of Kir6.2 near the ATP binding site locks the channel closed even without

ATP (Pratt et al., 2012). Previous studies have shown that ATP and PIP<sub>2</sub> functionally antagonize each other through allosteric regulation (Enkvetchakul et al., 2000) and that ATP can bind both closed and open channels (Enkvetchakul et al., 2001; Li et al., 2000). One interesting question is whether the interaction network we observed in the present ATP-bound structure undergoes remodeling in PIP<sub>2</sub>-bound open state. An open state structure of the K<sub>ATP</sub> channel bound to PIP<sub>2</sub> will be needed to understand the full extent of conformational change associated with ATP and PIP<sub>2</sub> gating.

#### *Mechanistic insights of GBC binding and inhibition*

The binding site of the high affinity sulfonylurea GBC has been studied by many groups. These studies have implicated the involvement of transmembrane helices in the SUR1-ABC core, L0, and the N-terminus of Kir6.2 (Ashfield et al., 1999; Bryan et al., 2004; Vila-Carriles et al., 2007). Yet, the precise binding pocket for this commonly used anti-diabetic drug has remained unresolved. In the structure presented here, we were able to clearly assign the GBC density in the TM bundle connected to NBD1, with residues from TM6, 7, 8, 11 in TMD1 and TM16 and 17 from TMD2 contributing to GBC interactions. Importantly, our model is supported by functional data using both <sup>86</sup>Rb<sup>+</sup> efflux assays and electrophysiological recordings. Moreover, our structure clarifies how Y230, which have previously been proposed to contribute to GBC binding based on indirect biochemical or functional assays (Vila-Carriles et al., 2007), can affect GBC binding or gating indirectly by supporting residues that are directly engaged in GBC binding.

The mechanism by which GBC inhibits channel activity is complex. In Fig. 9B, we present a hypothetical model to explain the current structural and functional data. In the presence of

MgATP/ADP, there is evidence that the NBDs of SUR1 undergo dimerization to switch the SUR1-ABC core structure from an inward-facing conformation to an outward-facing conformation to antagonize the inhibitory effect of ATP at the Kir6.2 site, and GBC binding to SUR1 stabilizes the SUR1-ABC core in an inward-facing conformation to prevent MgATP/ADP from opening the channel (Ortiz et al., 2012) (Fig.9B). In the absence of MgATP/ADP where the SUR1-ABC core is expected to be in an inward-facing conformation, channels are still able to open with high probability (Lin et al., 2003) and GBC also causes rapid inhibition of channel activity under such a condition (Fig.7-figure supplement 1A), suggesting GBC can inhibit channels in an MgATP/ADP independent manner. While the mechanism by which GBC inhibits channel activity in the absence of MgATP/ADP is not clear, we hypothesize that it may involve modulating interactions between the distal N-terminus of Kir6.2 and SUR1. The distal N-terminal 30 amino acids of Kir6.2 have been shown to be important for the binding or effect of GBC in a number of studies (Devaraneni et al., 2015; Koster, Sha, & Nichols, 1999; Kuhner et al., 2012; Reimann et al., 1999; Vila-Carriles et al., 2007). Moreover, it is known to be involved in regulating channel open probability by interacting with L0 of SUR1 (Babenko, Gonzalez, & Bryan, 1999; Shyng et al., 1997). In our map, there is a lack of strong density N-terminal to position 32 of Kir6.2, suggesting this region is flexible. However, it is worth noting that our previous study using engineered unnatural amino acid Azido-*p*-phenylalanine placed at the distal N-terminus of Kir6.2 (amino acid position 12 or 18) has demonstrated that GBC increased crosslinking of Kir6.2 to SUR1 (Devaraneni et al., 2015). Thus, we hypothesize that GBC binding to the TMD bundle next to the L0 amphipathic helix of SUR1 stabilizes the interactions between the N-terminus of Kir6.2 and SUR1 to prevent the movement of Kir6.2 N-terminus that is needed to open the gate (Fig.8B). Although GBC is a potent inhibitor of  $K_{ATP}$  channels, it does

not completely eliminate channel activity, unlike ATP. Channels exposed to saturating concentrations of GBC can be further inhibited by addition of ATP (see Fig.7-figure supplement 1A; Fig.8B). Whether GBC and ATP binding events are completely independent remains an open question. Comparison of channel structures without either inhibitors or with only a single inhibitor will be needed to address the issue.

The residues which play a specific and critical role in GBC binding are also very likely important for binding of other sulfonylureas. While we only tested GBC, we predict that R1246 and R1300, which coordinate the sulfonyl group, and T1242 and N1245, which coordinate the urea group, will also be critical for binding of other sulfonylureas such as tolbutamide (Gribble & Reimann, 2003). In addition to sulfonylureas, glinides such as rapaglinide and nateglinide which lack the sulfonylurea moiety (Gribble & Reimann, 2003), and a structurally unrelated compound carbamazepine (Chen, Olson, et al., 2013; Devaraneni et al., 2015) are also known to inhibit  $K_{ATP}$  channels. Elucidating the role of the various GBC binding residues in channel interactions with the different channel inhibitors will be important for understanding channel inhibition mechanisms and for rational design of new drugs with desired properties.

#### *Conservation of GBC binding residues in other SUR proteins and ABCC transporters*

Multiple sequence alignment of 15 SUR1 orthologs from diverse genera shows relatively high sequence identity throughout the sequence relative to human; from 95% (hamster) to 75% (seahorse). Interestingly, the segments of the helices from TMD1 and TMD2 which comprise the GBC binding site show exceptionally high conservation, with every one of the 12 residues which most closely line the GBC pocket absolutely conserved in 15 out of the 15 sequences. The

high degree of conservation suggests the importance of the interface formed by these transmembrane helices. It would be important to determine in the future whether this interface is involved in the conformational switch of the SUR1-ABC core and its communication with Kir6.2.

Interestingly, SUR2 (*ABCC9*), the closest homolog of SUR1 (67% sequence identity), while also shows high conservation of the GBC binding residues (10/12), differs in two positions that correspond to S1238 and T1242 (Y and S respectively in SUR2). SUR2 assembles with Kir6.1 or Kir6.2 to form  $K_{ATP}$  channel subtypes found in the heart, skeletal muscle, and vascular smooth muscle. These channels are known to have lower sensitivity to GBC inhibition than channels formed by SUR1 and Kir6.2 (Inagaki et al., 1996). Variations at these two key GBC binding residues likely explains their different pharmacological sensitivity to GBC (Ashfield et al., 1999; Inagaki et al., 1996).

In addition to targeting  $K_{ATP}$  channels, GBC has been shown to inhibit other ABC transporters within the C subfamily (ABCC), including MRP1 and CFTR, albeit at lower affinity ( $\sim 30\mu\text{M}$  for both CFTR and MRP1) (Payen et al., 2001; Schultz et al., 1996). Of all the residues within the GBC binding pocket, only two appear to be highly conserved across different members of the ABCC subfamily: R1246 and R1300. In fact, R1246 is strictly conserved within 11 of 12 ABCC homologs (Gln in ABCC10), and R1300 in 10 of 12 (Asn in CFTR and Ser in ABCC10). In the cryo-EM structure of MRP1 bound to substrate LTC-4 (Johnson & Chen, 2017), R1196 (equivalent to R1246 in SUR1) forms a salt bridge with a carboxylic acid group of LTC-4 and is also in the same rotameric conformation as R1246 in SUR1. Further, F221

(equivalent to Y230 in SUR1) also seems to form the equivalent hydrophobic stacking interaction with R1196 as Y230 does with R1246 in SUR1; this phenomenon is also observed in the human CFTR structure (F17 and R1097) (Liu et al., 2017). Such structural conservation likely explains the GBC sensitivity in other ABCC homologues, and suggests a critical role for this pair of residues in the function and/or structure of ABCC proteins.

In summary, we presented a  $K_{ATP}$  channel structure with improved resolution that allowed us to definitively identify the ATP and GBC binding sites. The novel insight gained from this structure significantly advances our understanding of how these two ligands interact with the channel to exert an inhibitory effect. As inhibition of  $K_{ATP}$  channels by sulfonylureas remains an important therapeutic intervention to control type 2 diabetes and neonatal diabetes, and there is a need for drugs that specifically target a  $K_{ATP}$  channel subtype, our study offers a starting point for future structure-guided drug development to mitigate diseases caused by  $K_{ATP}$  channel dysfunction.

## Materials and methods

### Key Resources Table

Reagent type (species) or resource	Designation	Source or reference	Identifiers
<b>Recombinant DNA/adenovirus</b>			
FLAG-tagged SUR1 (Cricetus cricetus) in AdEasy	ham f-SUR1	PMID: 28092267	N/A
Kir6.2 (Rattus norvegicus) in	rat Kir6.2	PMID: 28092267	N/A
tTA adenovirus		PMID: 28092267	N/A
FLAG-tagged SUR1 (Cricetus cricetus) in pECE	f-SUR1	PMID: 11226335	N/A

Kir6.2 ( <i>Rattus norvegicus</i> ) in pCDNA3	PMID: 14707124	N/A
<b>Cell lines</b>		
INS-1 clone 832/13 ( <i>Rattus norvegicus</i> )	PMID: 10868964	RRID:CVCL_7226
COS-M6 ( <i>Chlorocebus aethiops</i> ) COSm6	PMID: 11226335	RRID:CVCL_8561
<b>Software/Algorithms</b>		
Serial EM	PMID: 16182563	<a href="http://bio3d.colorado.edu/SerialEM">http://bio3d.colorado.edu/SerialEM</a>
MOTIONCOR2	PMID: 28250466	<a href="http://msg.ucsf.edu/em/software/motioncor2">http://msg.ucsf.edu/em/software/motioncor2</a>
CTFFIND4	PMID: 26278980	<a href="http://grigoriefflab.janelia.org/ctffind4">http://grigoriefflab.janelia.org/ctffind4</a>
DoGPicker	PMID: 19374019	<a href="https://sbgrid.org/software/titles/dogpicker">https://sbgrid.org/software/titles/dogpicker</a>
Relion-2	PMID: 27845625	<a href="https://www2.mrc-lmb.cam.ac.uk/relion">https://www2.mrc-lmb.cam.ac.uk/relion</a>
Frealign	PMID: 27572728	<a href="http://grigoriefflab.janelia.org/frealign">http://grigoriefflab.janelia.org/frealign</a>
Bsoft	PMID: 11472087	<a href="https://lsbr.niams.nih.gov/bsoft/">https://lsbr.niams.nih.gov/bsoft/</a>
COOT	PMID: 20383002	<a href="http://www2.mrc-lmb.cam.ac.uk/personal/pemsley/coot">http://www2.mrc-lmb.cam.ac.uk/personal/pemsley/coot</a>
RosettaCM	PMID: 24035711	<a href="https://www.rosettacommons.org">https://www.rosettacommons.org</a>
UCSF Chimera	PMID: 15046863	<a href="http://www.cgl.ucsf.edu/chimera">http://www.cgl.ucsf.edu/chimera</a>
Pymol	PyMOL	<a href="https://pymol.org/2">https://pymol.org/2</a>
MolProbity	PMID: 20057044	<a href="http://molprobity.biochem.duke.edu">http://molprobity.biochem.duke.edu</a>
T-Coffee	PMID: 10964570	<a href="http://www.tcoffee.org/Projects/tcoffee/">http://www.tcoffee.org/Projects/tcoffee/</a>
<b>Chemicals/Commercial Kits/Antibodies</b>		
Digitonin	Calbiochem	CAS 11024-24-1
ATP	Sigma-Aldrich	A7699
Glibenclamide	Sigma-Aldrich	G0639
QuikChange mutagenesis kit	Agilent	200515
<b>Key Resources Table continued</b>		
FuGENE®6	Promega	E2691
Anti-FLAG M2 affinity gel	Sigma-Aldrich	A2220
FLAG peptide	Sigma-Aldrich	F3290
Anti-SUR1 ( <i>Oryctolagus cuniculus</i> )	PMID: 17575084	N/A
Super Signal West Femto	Pierce	PI34095
<b>Other</b>		
R1.2/1.3 300 mesh UltrAuFoil grids	Quantifoil	Q27507

*Cell lines used for protein expression.* INS-1 cells clone 832/13 and COSm6 cells were used for protein expression (see below). The identify of these cell lines has been authenticated (see Key Resources Table above). These cell lines are not on the list of commonly misidentified cell lines maintained by the International Cell Line Authentication Committee. The mycoplasma contamination testing was performed routinely in the lab and shown to be negative for the work described here.

*Protein expression and purification.*  $K_{ATP}$  channels were expressed and purified as described previously (Martin, Yoshioka, et al., 2017). Briefly, the genes encoding pancreatic  $K_{ATP}$  channel subunits, which comprise a hamster SUR1 and a rat Kir6.2 (94.5% and 96.2% sequence identity to human, respectively), were packaged into recombinant adenoviruses (Lin et al., 2005; Pratt et al., 2009); Both are WT sequences, except for a FLAG tag (DYKDDDDK) that had been engineered into the N-terminus of SUR1 for affinity purification. INS-1 cells clone 832/13 (Hohmeier et al., 2000), a rat insulinoma cell line, were infected with the adenoviral constructs in 15 cm tissue culture plates. Protein was expressed in the presence of 1mM Na butyrate and 5  $\mu$ M GBC to aid expression of the channel complex. 40-48 hours post-infection, cells were harvested by scraping and cell pellets were frozen in liquid nitrogen and stored at  $-80^{\circ}\text{C}$  until purification.

For purification, cells were resuspended in hypotonic buffer (15mM KCl, 10mM HEPES, 0.25 mM DTT, pH 7.5) and lysed by Dounce homogenization. The total membrane fraction was prepared, and membranes were resuspended in buffer A (0.2M NaCl, 0.1M KCl, 0.05M HEPES, 0.25mM DTT, 4% sucrose, 1mM ATP, 1 $\mu$ M GBC, pH 7.5) and solubilized with 0.5% Digitonin.

The soluble fraction was incubated with anti-FLAG M2 affinity agarose for 4 hours and eluted with buffer A (without sugar) containing 0.25 mg/mL FLAG peptide. Purified channels were concentrated to ~1-1.5 mg/mL and used immediately for cryo grid preparation.

*Sample preparation and data acquisition for cryo-EM analysis.* In our previous data sets, most micrographs were of ice that was either too thin, which tended to exclude channel complex from the hole and induce highly preferred orientation, or of ice that was too thick, which gave good particle distribution and good angular coverage, but had lower contrast. Thus the current data set was the result of efforts to optimize ice thickness in order to retain high contrast and particle distribution. This was achieved through varying blotting time and also through extensive screening of the grid in order to find optimal regions. Two grids were imaged from the same purification and were prepared as follows: 3  $\mu$ L of purified K<sub>ATP</sub> channel complex was loaded onto UltrAufoil gold grids which had been glow-discharged for 60 seconds at 15 mA with a Pelco EasyGlow ®. The sample was blotted for 2s (blot force -4; 100% humidity) and cryo-plunged into liquid ethane cooled by liquid nitrogen using a Vitrobot Mark III (FEI).

Single-particle cryo-EM data was collected on a Titan Krios 300 kV cryo-electron microscope (FEI) in the Multi-Scale Microscopy Core at Oregon Health & Science University, assisted by the automated acquisition program SerialEM. Images were recorded on the Gatan K2 Summit direct electron detector in super-resolution mode, post-GIF (20eV window), at the nominal magnification 81,000x (calibrated image pixel-size of 1.720Å; super-resolution pixel size 0.86Å); defocus was varied between -1.4 and -3.0  $\mu$ m across the dataset (Table 1). The dose rate was kept around 2.7 e<sup>-</sup>/Å<sup>2</sup>/sec, with a frame rate of 4 frames/sec, and 60 frames in each

movie, which gave a total dose of approximately  $40 \text{ e}^-/\text{\AA}^2$ . In total, 2180 movies were recorded.

*Image processing.* The raw frame stacks were gain-normalized and then aligned and dose-compensated using Motioncor2 (Zheng et al., 2017) with patch-based alignment (5x5). CTF parameters were estimated from the aligned frame sums using CTFFIND4 (Rohou & Grigorieff, 2015). Particles were picked automatically using DoGPicker (Voss et al., 2009) with a broad threshold range in order to reduce bias. Subsequently, each image was analyzed manually in order to recover any particles missed by automatic picking and remove obviously bad micrographs from the data set. This resulted in  $\sim 250,000$  raw particles as input for subsequent 2D classification using Relion-2 (Kimanius et al., 2016). After four rounds of 2D classification,  $\sim 160,000$  particles remained in the data set, in which only classes displaying fully assembled complexes and high signal/noise were selected. These 160K particles were re-extracted at  $1.72 \text{ \AA}/\text{pixel}$  and were used as input for 3D classification in Relion-2. Note only images collected in the current study were used for the 3D reconstruction described below.

Extensive 3D classification was performed in order to sample the heterogeneity within the data. Symmetry was not imposed at this step in order to select only the best four-fold symmetric classes. Up to 4 consecutive rounds of classification were performed, specifying 4 or 5 classes per round. Individual classes and combinations of classes were refined independently and lead to very similar structures. The two best classes from round 2 were combined ( $\sim 63,000$  particles), and then particles were re-extracted from super-resolution micrographs with a box size of 600 pixels. A soft mask encompassing the entire complex was used during refinement in Relion, with C4 symmetry imposed, which resulted in a  $4.07 \text{ \AA}$  reconstruction using the gold-standard

FSC cutoff (Fig.1-figure supplement 1D). These particle assignments were then imported into FREALIGN (Grigorieff, 2016) with the unbinned particle data and further classified and refined. To prevent overfitting, the resolution limit for every alignment iteration never exceeded the 0.9 value of the FREALIGN calculated FSC. The final round of refinement was done with an alignment limit of 4.8Å, and the 0.143 value of the FSC was 3.63Å (Fig.1-figure supplement 1D, 2C). The masking in FREALIGN used the low-pass filtering (40Å) and weighting (0.3) options to best minimize the effect of the micelle on alignment. A 'Score to Weight Constant' of 3.0 was used. Local resolution was calculated on unfiltered half maps with the Bsoft package, which showed the resolution was highest in the Kir.6.2/TMD0 core, as well as the SUR1 helices surrounding the GBC-binding pocket (between 3.3-3.7), and lowest in the NBDs and some of the external helices of TMD1/TMD2 of SUR1 (Fig.1-figure supplement 2B).

*Model building.* In our previous reconstruction, many side-chains were left out of the final model as there was not sufficient density to support their placement (Martin, Yoshioka, et al., 2017). In the current reconstruction, there is good density for nearly every side chain of Kir6.2, TMD0, and the inner helices of the ABC core structure of SUR1. Thus using our previous structure as the starting template, we rebuilt nearly all of the structure with RosettaCM (Song et al., 2013), using the density as an additional constraint. This region included Kir6.2, TMD0/L0, and TMD1 and TMD2. The lowest energy models were very similar to one another, thus the lowest energy model was selected for each region. The resulting model was then minimized once in CNS (Brunger et al., 1998), substituting in the RSRef real-space target function (Chapman et al., 2013), adding ( $\phi, \psi$ ) backbone torsion angle restraints, and imposing non-crystallographic symmetry (NCS) constraints. In the density map, NBD1 and NBD2 showed

signs of disorder, so our previously deposited NBD models were left as polyalanine chains and only refined as rigid bodies with RSRef. The distal N- and C-termini of Kir6.2, as well as the linker between NBD1 and TMD2 in SUR1 were not observed in the density map, and thus were left out the model. The final model contains residues 32-352 for Kir6.2, and residues 6-615 (TMD0/L0 + TMD1), 678-744 and 770-928 (NBD1), 1000-1044 and 1061-1319 (TMD2), and 1343-1577 (NBD2) for SUR1. All structure figures were produced with UCSF Chimera (Pettersen et al., 2004) and PyMol (<http://www.pymol.org>). Pore radius calculations were performed with HOLE (Smart et al., 1996).

### *Sequence alignments*

Multiple sequence alignment was performed with the T-Coffee server (Notredame et al., 2000). Output was saved in Clustal Aln format, and then imported and visualized in UCSF Chimera.

*Functional studies of GBC binding mutants.* Point mutations were introduced into hamster SUR1 cDNA in pECE using the QuikChange site-directed mutagenesis kit (Stratagene). Mutations were confirmed by DNA sequencing. Mutant SUR1 cDNAs and rat Kir6.2 in pcDNA1 were co-transfected into COSm6 cells using FuGENE®6, as described previously (Devaraneni et al., 2015) and used for Western blotting,  $^{86}\text{Rb}^+$  efflux assays, and electrophysiology as described below.

For Western blotting, cells were lysed in 20 mM HEPES, pH 7.0/5 mM EDTA/150 mM NaCl/1% Nonidet P-40 with CompleteTR protease inhibitors (Roche) 48-72 hours post-transfection. Proteins in cell lysates were separated by SDS/PAGE (8%), transferred to

nitrocellulose membrane, probed with rabbit anti-SUR1 antibodies against a C-terminal peptide of SUR1 (KDSVFASFVRADK), followed by HRP-conjugated anti-rabbit secondary antibodies (Amersham Pharmacia), and visualized by chemiluminescence (Super Signal West Femto; Pierce) with FluorChem E (ProteinSimple).

For  $^{86}\text{Rb}^+$  efflux assays, cells were plated and transfected in 12-well plates. Twenty-four to thirty-six hours post-transfection, cells were incubated overnight in medium containing  $^{86}\text{RbCl}$  (0.1  $\mu\text{Ci/ml}$ ). The next day, cells were washed in Krebs-Ringer solution twice and incubated with metabolic inhibitors (2.5 $\mu\text{g/ml}$  oligomycin and 1mM 2-deoxy-D-glucose) in Krebs-Ringer solution for 30 min in the presence of  $^{86}\text{Rb}^+$ . Following two quick washes in Krebs-Ringer solutions containing metabolic inhibitors and 0.1% DMSO (vehicle control), 100nM GBC, or 1 $\mu\text{M}$  GBC, 0.5 ml of the same solution was added to each well. At the end of 2.5 minutes, efflux solution was collected for scintillation counting and new solution was added. The steps were repeated for 5, 7.5, 15, 25, and 40 min cumulative time points. After the 40 min time point efflux solution was collected, cells were lysed in Krebs-Ringer containing 1% SDS.  $^{86}\text{Rb}^+$  in the solution and the cell lysate was counted. The percentage efflux was calculated as the radioactivity in the efflux solution divided by the total activity from the solution and cell lysate, as described previously (Chen, Olson, et al., 2013; Yan et al., 2007). Note we used higher concentrations of GBC for these experiments than the electrophysiology experiments described below as in the latter the channels were exposed directly in isolated membrane patches to GBC, thus requiring lower concentrations. Experiments were repeated three-four times and for each experiment, untransfected cells were included as a negative control.

For electrophysiology experiments, cells co-transfected with SUR1 and Kir6.2 along with the cDNA for the green fluorescent protein GFP (to facilitate identification of transfected cells) were plated onto glass coverslips twenty-four hours after transfection and recordings made in the following two days. All experiments were performed at room temperature as previously described (Devaraneni et al., 2015). Micropipettes were pulled from non-heparinized Kimble glass (Fisher Scientific) on a horizontal puller (Sutter Instrument, Co., Novato, CA, USA). Electrode resistance was typically 1-2 M $\Omega$  when filled with K-INT solution containing 140 mM KCl, 10 mM K-HEPES, 1 mM K-EGTA, pH 7.3. ATP was added as the potassium salt. Inside-out patches of cells bathed in K-INT were voltage-clamped with an Axopatch 1D amplifier (Axon Inc., Foster City, CA). ATP (as the potassium salt) or GBC at 10nM or 100nM were added to K-INT as specified in the figure legend. All currents were measured at a membrane potential of -50 mV (pipette voltage = +50 mV). Data were analyzed using pCLAMP10 software (Axon Instrument). Off-line analysis was performed using Microsoft Excel programs. Data were presented as mean $\pm$ standard error of the mean (s.e.m).

### **Data Resources**

The accession numbers for the structure presented in this paper are PDB: 6BAA and EMD: EMD-7073.

### **Acknowledgements**

The INS-1 cell clone 832/13 was kindly provided by Dr. Christopher Newgard. We thank Emily Rex and Zhongying Yang for technical assistance, and Dr. Matt Whorton, Dr. Dale Fortin, and Veronica Cochrane for critical readings of the manuscript. We also thank the staff at the

Multiscale Microscopy Core (MMC) of Oregon Health & Science University (OHSU), the OHSU-FEI living lab and Intel for technical support. This work was supported by the National Institutes of Health grants R01DK066485 (to S.-L. S.) and F31DK105800 (to G.M.M.).

**Table 1 | Statistics of cryo-EM data collection, 3D reconstruction and model building.**

<b>Data collection/processing</b>	
Microscope	Krios
Voltage (kV)	300
Camera	Gatan K2 Summit
Camera mode	Super-resolution
Defocus range ( $\mu\text{m}$ )	-1.4 ~ -3.0
Movies	2180
Frames/movie	60
Exposure time (s)	15
Dose rate ( $\text{e}^-/\text{pixel}/\text{s}$ )	8
Magnified pixel size ( $\text{\AA}$ )	1.72 (Super-resolution pixel size 0.86)
Total Dose ( $\text{e}^-/\text{\AA}^2$ )	~40
<b>Reconstruction</b>	
Software	Relion & Frealign
Symmetry	C4
Particles refined	59,417
Resolution (Relion masked)	4.07 $\text{\AA}$
Resolution (Frealign masked)	3.63 $\text{\AA}$
<b>Model Statistics</b>	
Map CC	0.758 (masked)
Clash score	9.10
Molprobity score	1.9
C $\beta$ deviations	0
<b>Ramachandran</b>	
Outliers	0.12%
Allowed	6.31%
Favored	93.57%
<b>RMS deviations</b>	
Bond length	0.01
Bond angles	1.11

## Figure Legends

**Fig. 1. Overall structure of the  $K_{ATP}$  channel bound to ATP and GBC.** (A) Linear sequence diagram for the Kir6.2 and SUR1 polypeptides, with primary domains colored to match the panels below. Numbers indicate residue number at the beginning and end of each domain. (B) Cryo-EM density map of the  $K_{ATP}$  channel complex at 3.63Å resolution, viewed from the side. Gray bars indicate approximate position of the bilayer. (C) View of map from extracellular side. (D). Structural model of the complex, with ligands ATP (green) and GBC (red) in boxes. (E) View of the model from the extracellular side.

**Fig. 1-figure supplement 1. Data collection and image processing workflow.** (A) Representative micrograph at 81,000x (1.72 Å/pixel; 0.86 Å/pixel super-resolution) after alignment with Motioncor2. A few  $K_{ATP}$  channel complexes of various orientation have been outlined. (B) Power spectrum calculated with Ctffind4, with information extending out to 3.6Å. (C) Select 2D classes from the final round of classification. (D) Overview of the data processing workflow. Particle picking was performed automatically with DoGPicker as well as with manual inspection. All other image processing steps were performed in Relion-2 and Frealign.

**Fig. 1-figure supplement 2. Cryo-EM density map analysis.** (A) Euler angle distribution plot of all particles included in the calculation of the final map. (B) The EM density map with colored local resolution estimation using Bsoft. (C) Fourier shell coefficient (FSC) curves between two half-datasets calculated by Frealign. The refinement limit of 4.8Å used in Frealign is indicated by the vertical dotted line. (D) FSC curves between the refined structure and the map calculated from the full dataset (FSC sum, orange), the half-map used in refinement (FSC work, grey), and the other half-map (FSC free, gold).

**Fig. 2. Structural highlights of Kir6.2 and SUR1.** (A) Two subunits of the Kir6.2 tetramer, one colored in blue and one in white, highlighting the conserved Kir channel structural features. Note the ATP-binding site is at the interface of the cytoplasmic N- and C-terminal domains of adjacent subunits. (B) Close-up of the Kir6.2 pore, showing solvent-accessible volume as a mesh. The two primary gates are 1) the helix bundle-crossing (HBC), formed by the confluence of the M2 helices at F168; 2) the G-loop, formed at the apex of the CTD by G295 and I296. (C) Plot of pore radius as a function of length along pore axis. (D) Structure of SUR1 in inward-facing conformation, indicating overall domain organization. Note clear separation of NBDs. Transmembrane helices 1-17 are numbered. (E) Structural conservation of L0 with the lasso domain observed in MRP1. Full structures of SUR1 (blue) and leukotriene C4-bound MRP1 (orange) minus TMD0 were used for structural alignment. (F) Separation ( $C\alpha$  to  $C\alpha$ , indicated by the dashed line) between Walker A and signature motif in NBD1 (left) and NBD2 (right) (G716::S1483 and S831::G1382 in SUR1, G681::S1430 and S769::G1329 in MRP1).

**Fig. 2-figure supplement 1. Cryo-EM density map of key structural features in Kir6.2.** For the  $\beta$ -sheets only backbone is shown.

**Fig. 2-figure supplement 2. Cryo-EM density map of transmembrane helices and the lasso (L0) motif of SUR1.** Only backbone is shown.

**Fig. 3. The interface between SUR1 and Kir6.2.** (A) Surface representation of the complex. SUR1-binding surface on Kir6.2 colored in magenta, and Kir6.2-binding surface on SUR1 is in cyan. TMD0/L0 is colored in light gray, and Kir6.2 and the ABC core of SUR1 are in dark gray. (B) Cartoon model of Kir6.2, with interface residues colored in magenta. The intersubunit  $\beta$ -sheet formed by  $\beta$  strands A, N, and O shown in Fig.2-figure supplement 2. (C and D) Surface

and cartoon models of SUR1, with interface residues in cyan. (E) Interface between M1 (Kir6.2; magenta) and TM1 (SUR1; cyan), highlighting key interactions. (F) Intersection of ICL2 (cyan) and N-terminus/slide helix (magenta), showing interaction between Q57 (Kir6.2) and F132 (SUR1). The dashed lines indicate selected van der Waals or electrostatic (H-bonding or charge-charge) interactions between two residues to aid visualization.

**Fig. 4. The ATP binding pocket.** (A) Surface representation of a Kir6.2 tetramer in complex with one SUR1, colored by Coulombic surface potential. ATP pocket is boxed in yellow. (B) Close-up of ATP binding pocket boxed in (A). Note close proximity of L0 to the pocket on Kir6.2. (C) Interactions within ATP-binding pocket, with residues directly interacting with ATP colored in magenta. The Kir6.2 subunit containing R50 is colored green, with the adjacent subunit colored blue. The dashed lines indicate possible van der Waals or electrostatic interactions to aid visualization.

**Fig.4.-figure supplement 1. (A and B)** Cryo-EM density for ATP, contoured to  $3.5\sigma$ . (C, D, E) Cryo-EM density for residues surrounding ATP.

**Fig. 5. Important molecular interactions surrounding the ATP binding site.** (A) Electrostatic interaction between R301 and Q299, viewed from the interior of Kir6.2 and looking out toward the cytoplasm. These residues are found on an internal  $\beta$ -sheet  $12\text{\AA}$  from ATP ( $C\alpha$  of R301 to ribose of ATP) (B) Dual interaction between R201 and F315, likely via cation- $\pi$ , and hydrophobic stacking between aliphatic portion of R201 side chain and F333, again viewed from the Kir6.2 interior. These residues are found directly below ATP ( $\sim 9\text{\AA}$  from  $C\alpha$  of R201 to ribose of ATP). (C) Relationship between R50, Q52, R54, and E179 of Kir6.2 near the ATP and  $\text{PIP}_2$  binding sites. The dashed lines indicate possible van der Waals or electrostatic interactions to aid visualization.

**Fig. 6. The GBC binding site in SUR1.** (A) Ribbon diagram of SUR1 showing location of GBC, which is primarily coordinated by the inner helices of TMD1 (purple) and TMD2 (cyan). (B) Slice view of model in (A) viewed from the extracellular side. Note juxtaposition of L0 to helices in ABC core directly interacting with GBC. (C) Close-up of GBC binding pocket, showing all residues which immediately line the pocket and seem to form direct contact with GBC; a subset of these residues were mutated to test their role in GBC binding (Fig. 7). (D) Magnified view in (B), highlighting indirect roles of Y230 and W232 (L0) in GBC binding. These both likely stabilize interactions between residues on helix 16 of TMD2 and GBC, at the same time anchoring this helix of L0 to the ABC core structure.

**Fig.6-figure supplement 1. GBC binding site.** (A) Cryo-EM density of GBC, contoured to  $3\sigma$ . (B, C, D, E) Cryo-EM density of residues near GBC, contoured to  $3.5\sigma$ . (F) Close-up surface representation view of the GBC binding pocket. The basic portion comprises N1245, R1246, and R1300, while the acid end is formed by S1238 and D1193.

**Fig. 7. Functional testing of GBC binding residues.** (A) Residues in SUR1 selected to be mutated to alanine. (B) Western blot of WT and mutant SUR1 co-expressed with Kir6.2 in COS cells. Two SUR1 bands corresponding to the core-glycosylated immature protein (lower band) and the complex-glycosylated mature protein (upper band) are detected. The vertical line in the middle of the blot separates two parts of the same blot. (C) Representative efflux profiles of WT channels and T1242A mutant channels in cells pretreated with metabolic inhibitors for 30 min in the presence of 0.1% DMSO (cont), 100nM GBC, or 1 $\mu$ M GBC. Untransfected cells (unt) served as a control. Efflux was normalized to the maximal value observed at 40 min for direct comparison. (D) Quantification of percent efflux of all mutants compared to WT. Each bar

represents the mean±s.e.m. of 3-4 biological repeats. \*  $p < 0.05$  by one-way ANOVA with Newman-Keuls *post hoc* test.

**Fig. 7-figure supplement 1. Functional testing of GBC binding residues by electrophysiology.** (A) Examples of inside-out patch clamp recordings of WT and various mutant channels. Recordings were made at +50mV in symmetric K<sup>+</sup> solutions and inward currents shown as upward deflections. (B) Quantification of residual currents (expressed as percent of initial currents observed in K-INT solution) after exposure to 10nM or 100nM GBC, with values taken when the currents reached a steady level. The value for “recovery after washout” was taken at ~100 seconds after the patch was returned to K-INT solution following a brief exposure to 1mM ATP (to check baseline). Each bar represents mean±s.e.m. of 3-6 patches, which represent the number of biological repeats. \*  $p < 0.05$  by one-way ANOVA with Newman-Keuls *post hoc* test.

**Fig. 8. Comparison of the current structure with the GBC-bound, ATP-free structure from Li et al. (PDB ID: 5WUA).** (A) Overlay of the Kir6.2 structure viewed on the side. (B) Overlay of the Kir6.2 membrane helices viewed from the top. (C) Overlay of the Kir6.2 cytoplasmic domain. (D) Side view of the overlay of the SUR1 structure. (E) Overlay of the SUR1 transmembrane helices 1-17 viewed from the top. In all panels, the higher resolution structure from the current study is colored in blue, and the 5WUA structure from Li et al. is colored in tan.

**Fig. 8-figure supplement 1. Reinterpretation of the GBC cryo-EM density proposed in Li et al.** (A, B) Cryo-EM density of 5WUA near SUR1-L0 where GBC binding site was proposed (approximately the boxed region shown in A). Note only W231 and W232 of SUR1-L0 were modeled in the density shown. (C, D) Cryo-EM density from the current study and the corresponding structural model in the same region shown in (A) and (B).

**Fig. 8-figure supplement 2. (A)** Cryo-EM density of 5TWV near the GBC binding site identified in the present study. **(B)** Cryo-EM density of 5WUA near the GBC binding site identified in the current study. In both (A) and (B), unassigned density with shape and size that can accommodate GBC is observed.

**Fig. 9. ATP and GBC gating models. (A)** Hypothetical model illustrating that ATP binds to a pocket formed by the N-terminus and CTD of Kir6.2 (from two adjacent subunits), with contribution from L0 of SUR1. This stabilizes the channel in a closed state that is energetically unfavorable for transitioning into an open state. **(B)** Hypothetical model of GBC gating. In the absence of nucleotides, GBC binds to the TM bundle juxtaposing L0, which stabilizes the distal N-terminus of Kir6.2 to greatly reduce channel open probability and promote channel closure. Addition of ATP further closes the channel by preventing residual free N-terminus from moving channels into an open state (see panel A). In the presence of MgATP/ADP, the SUR1-ABC core can transition from an inward-facing conformation to an outward conformation upon dimerization of the NBDs to antagonize ATP inhibition on Kir6.2 and promote channel opening; GBC binding stabilizes the SUR1-ABC core in the inward-facing conformation and shifts the equilibrium towards channel closure. The dashed lines between states illustrate the near irreversible binding of GBC. In both A and B, Kir6.2 transmembrane helices: dark blue; Kir6.2 cytoplasmic domain: pale blue; Kir6.2 slide helix and N-terminus from adjacent subunit: light blue cylinder and thick light blue line, respectively; SUR1-TMD0/L0: magenta; SUR1-TMD1: light purple; SUR1-NBD1: dark purple; SUR1-TMD2: cerulean; SUR1-NBD2: deep cerulean; GBC: yellow; ATP: red. Note the different states shown are not meant to reflect the actual kinetic transitions, but the hypothesized stable states.

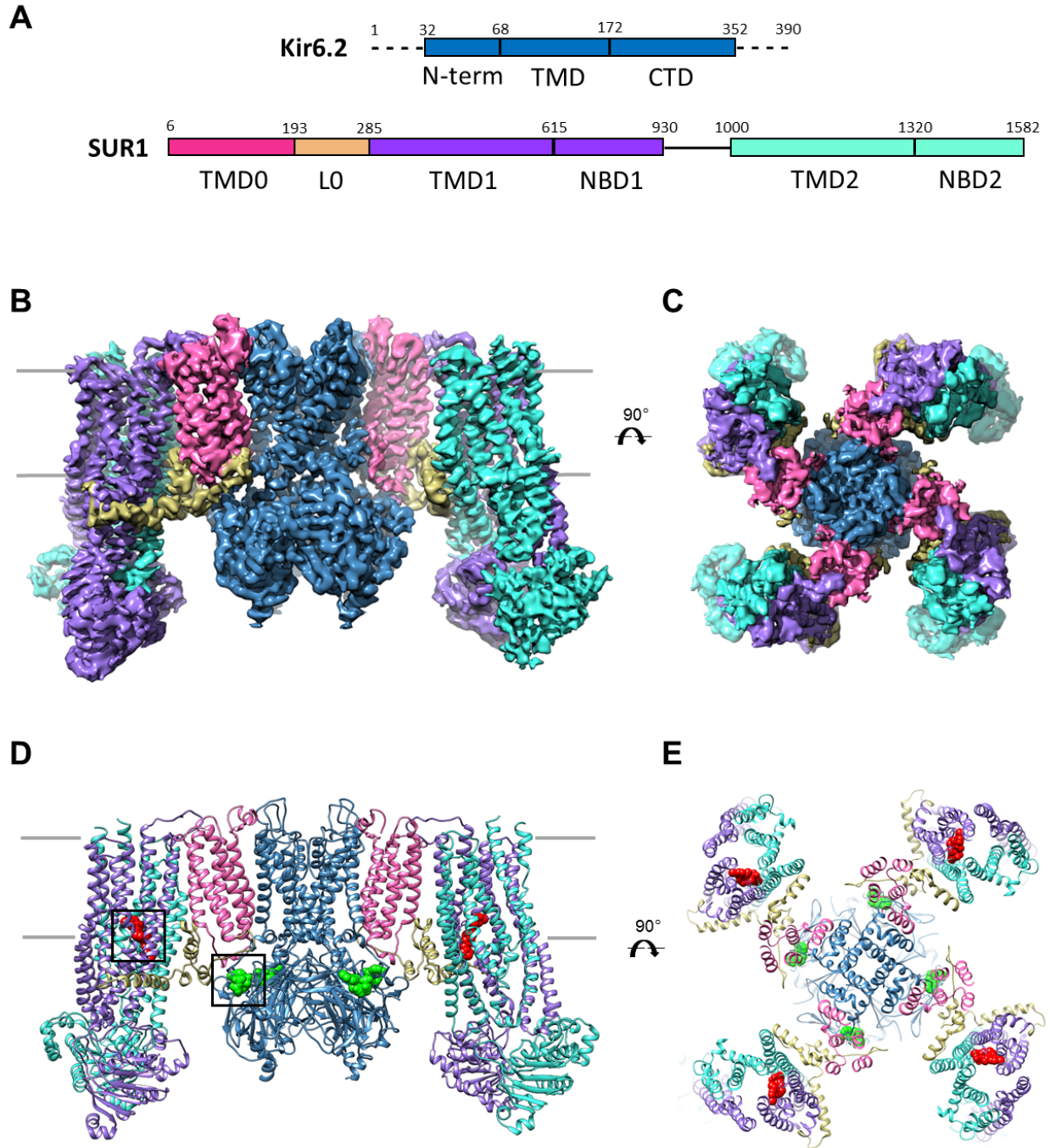


**Figure 1**

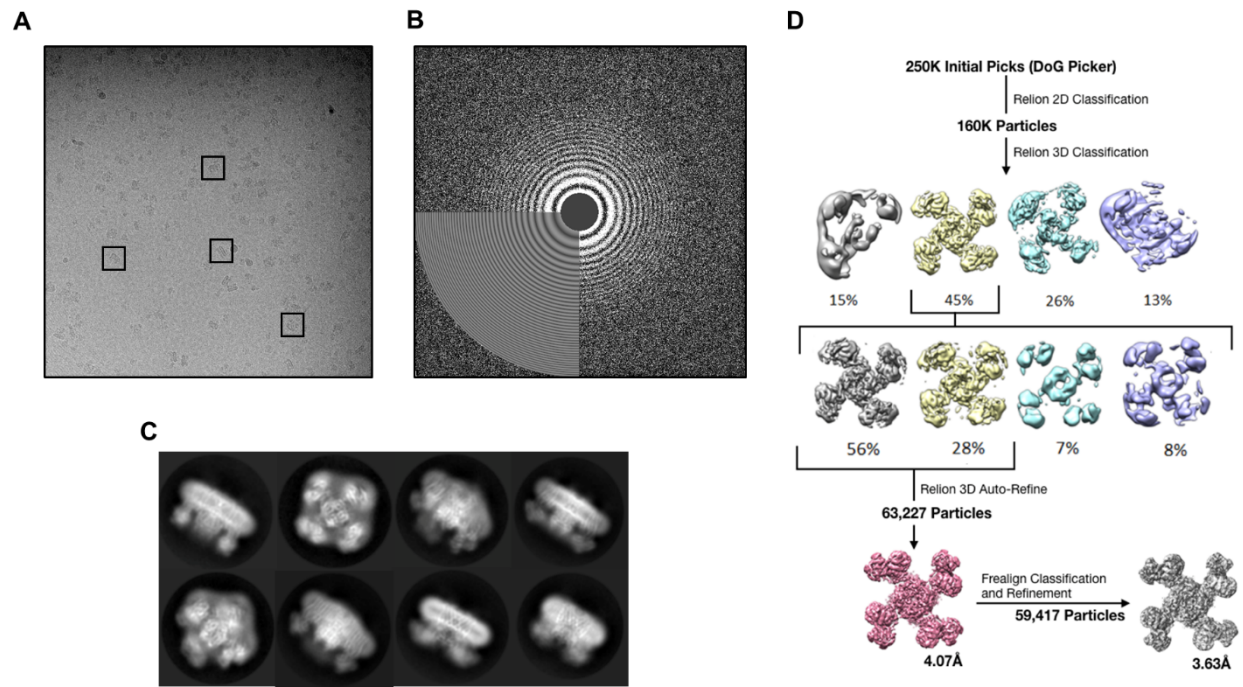
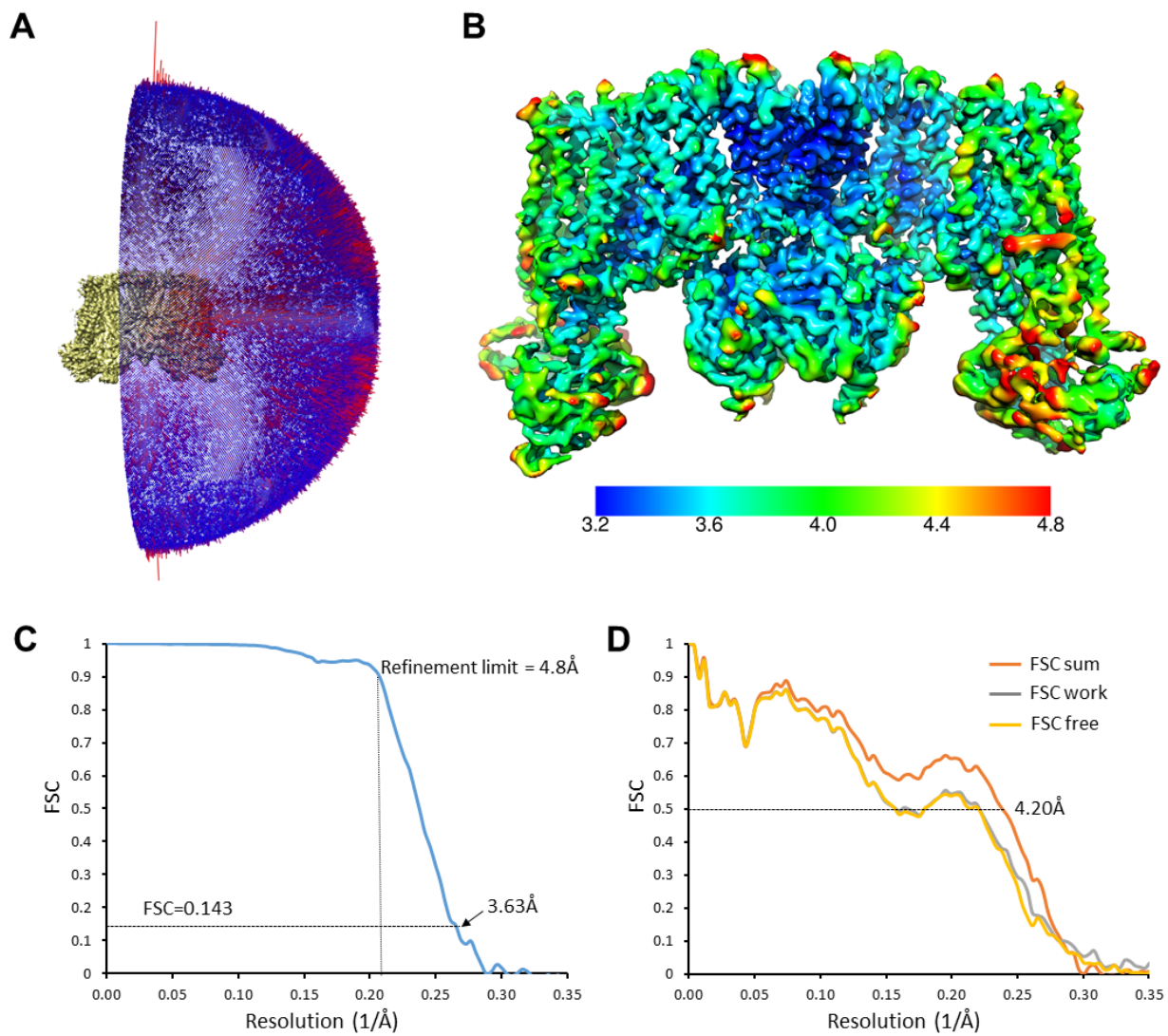


Figure 1 - supplement 1



**Figure 1 - supplement 2**

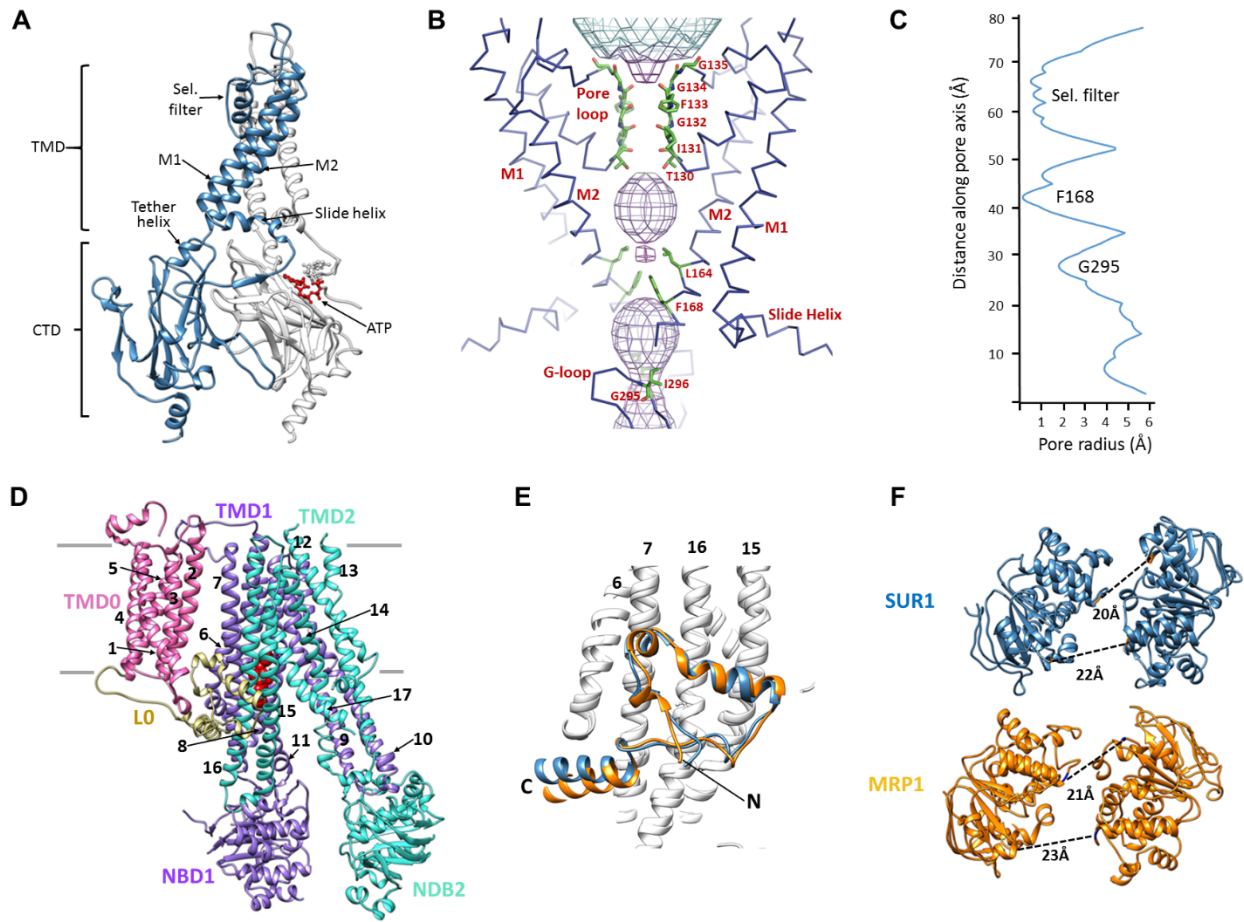
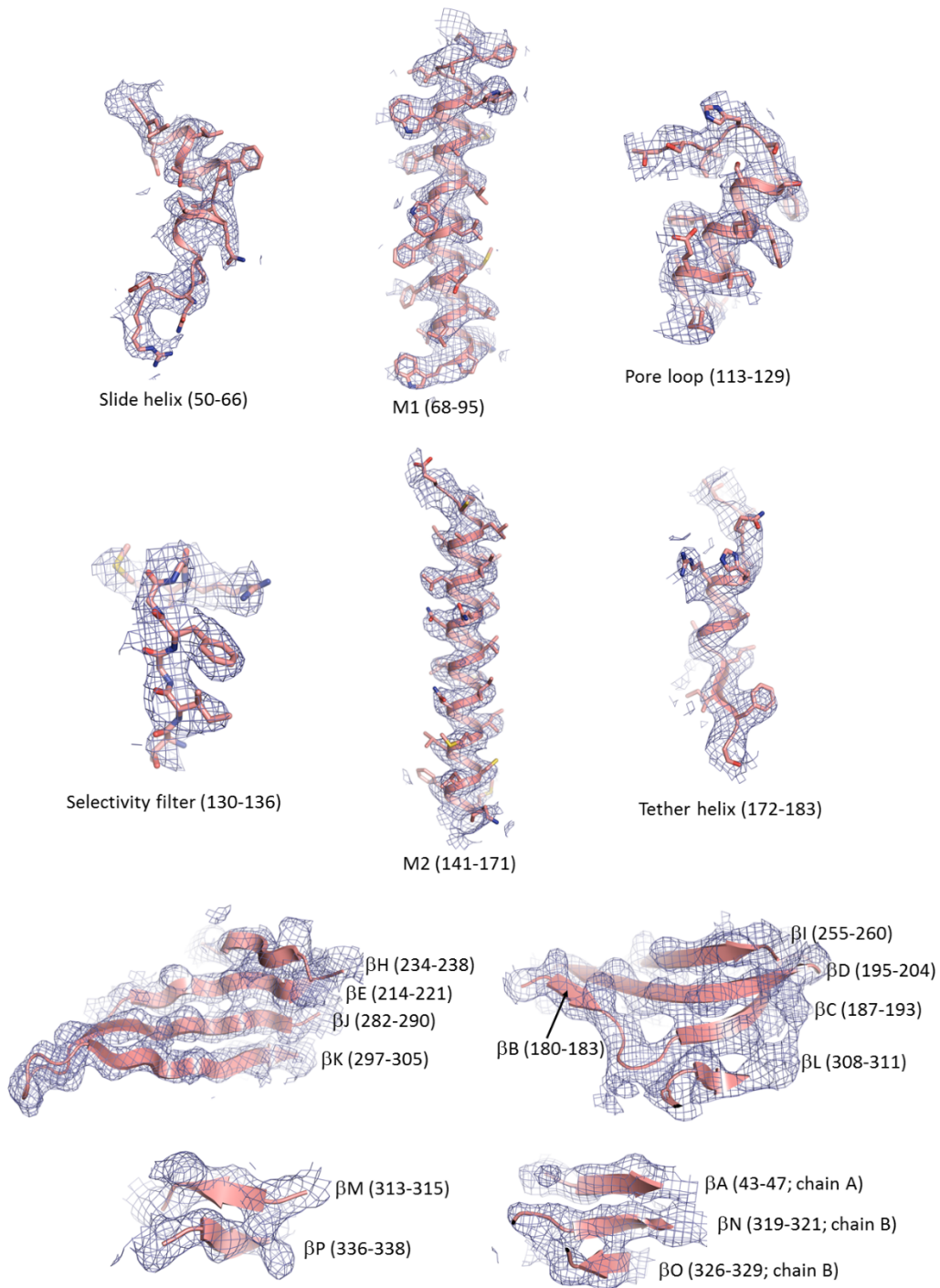
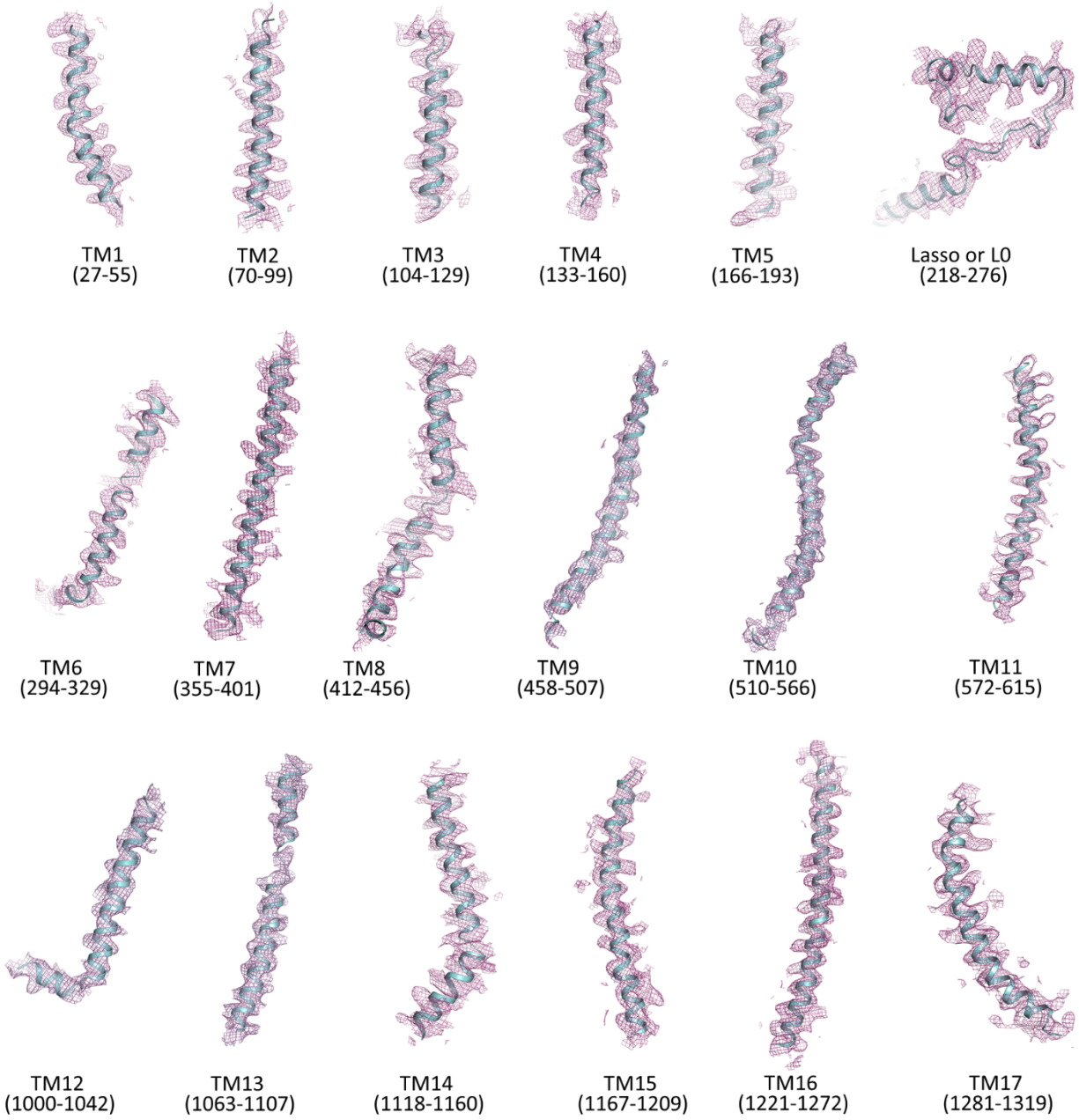


Figure 2



**Figure 2 - supplement 1**



**Figure 2 - supplement 2**

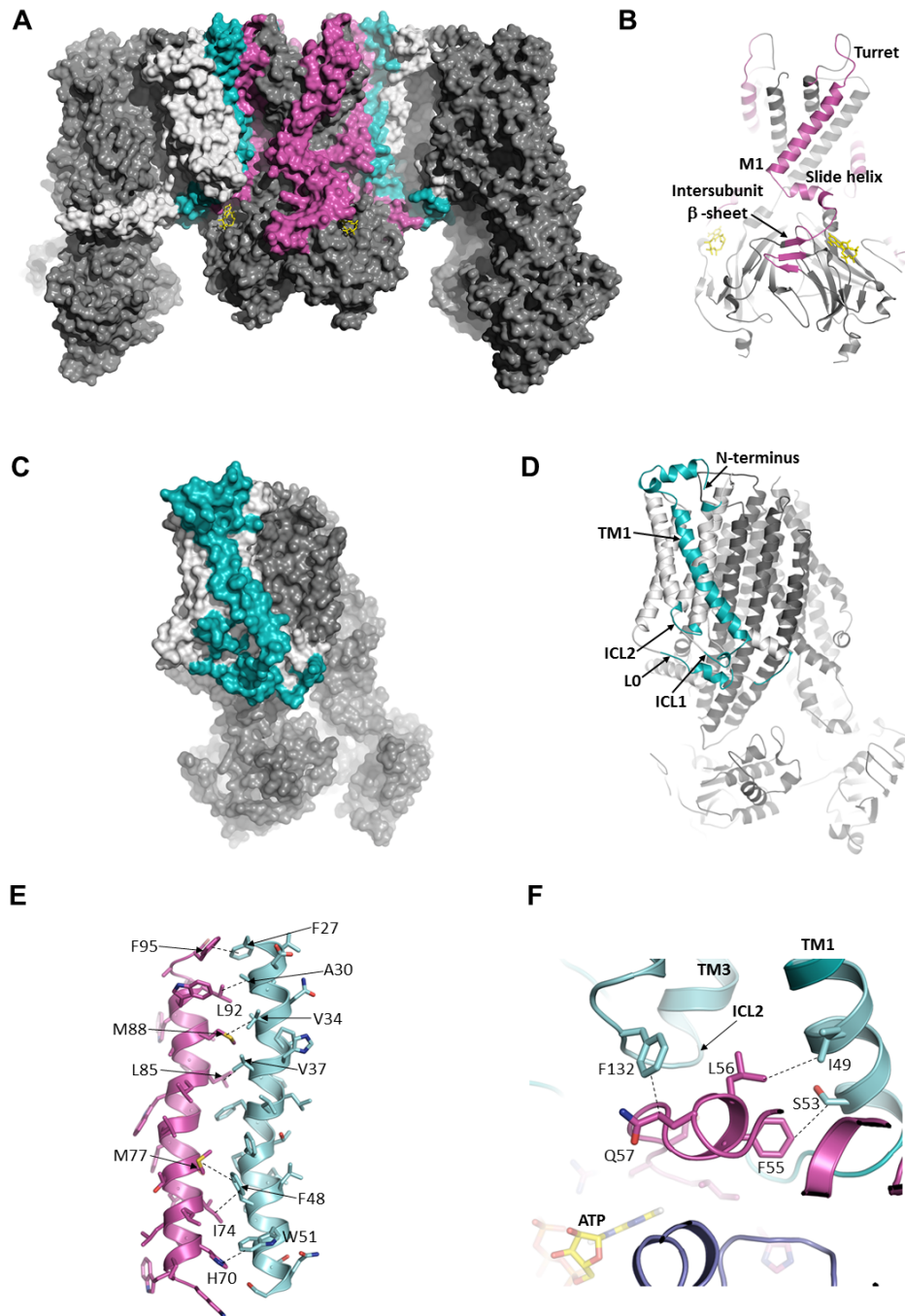


**Figure 3**

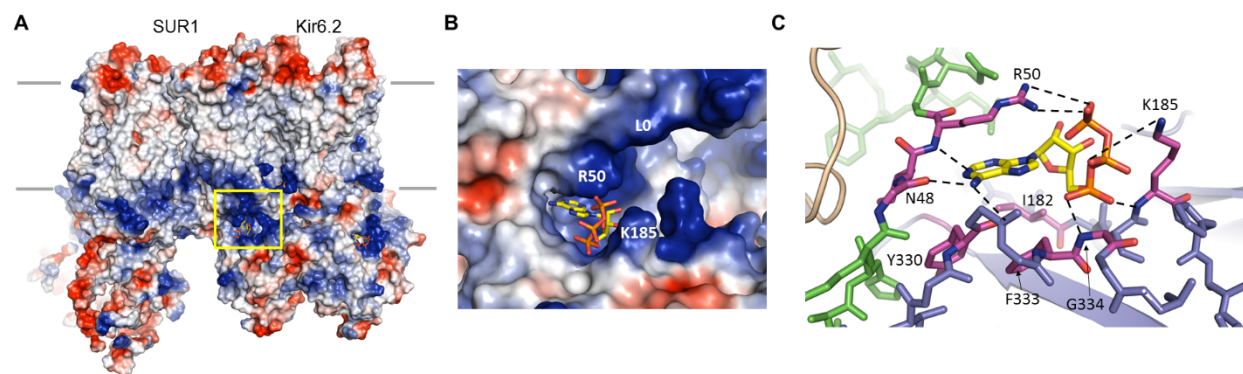


**Figure 4**

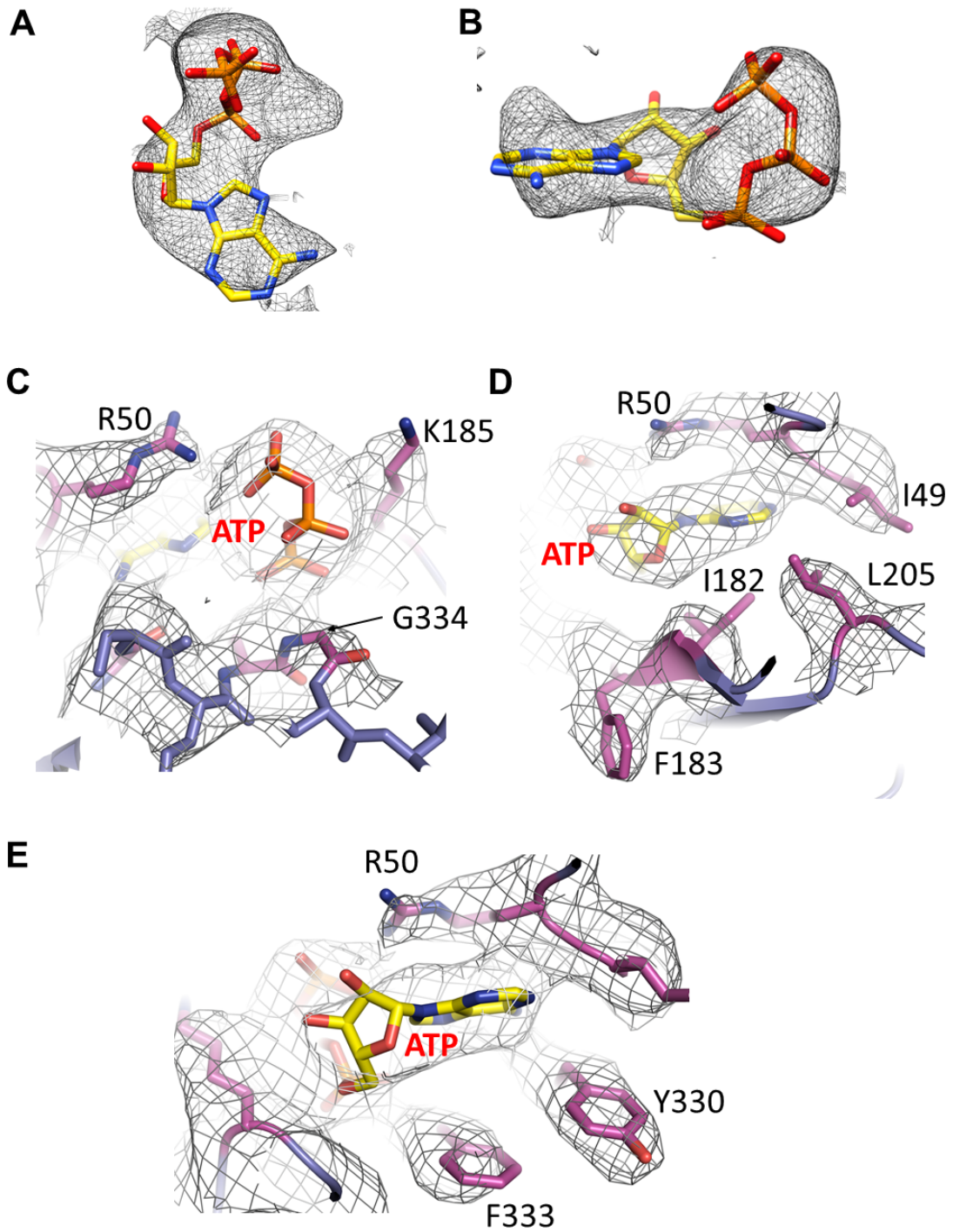
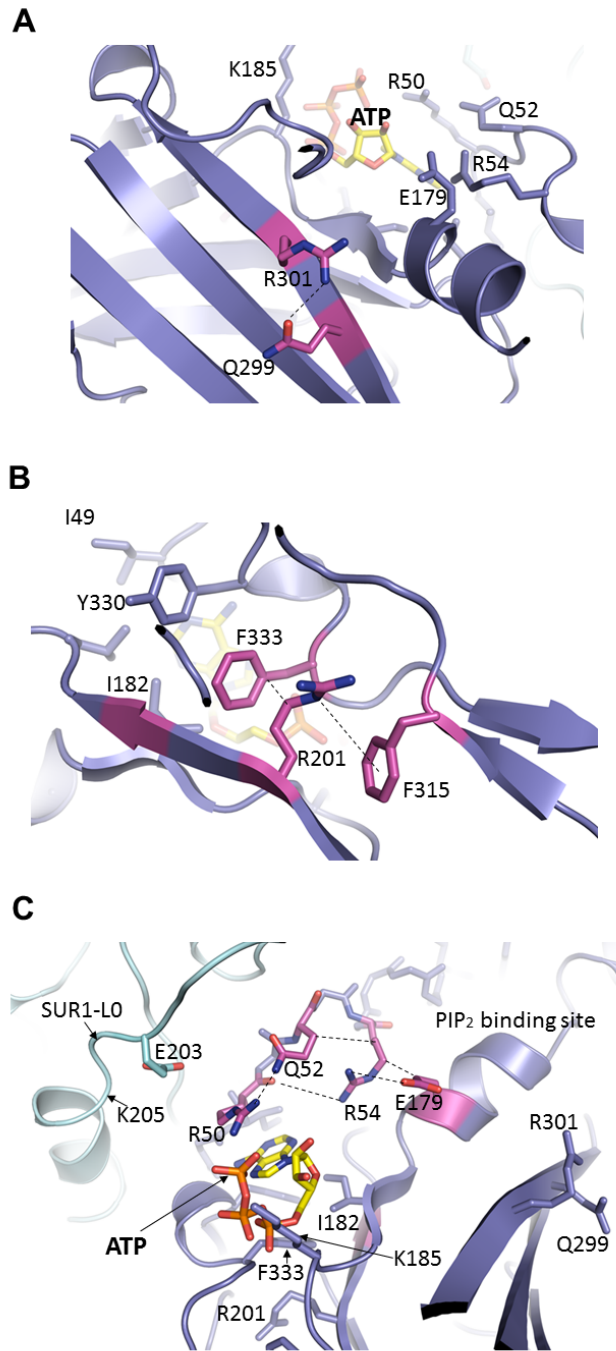
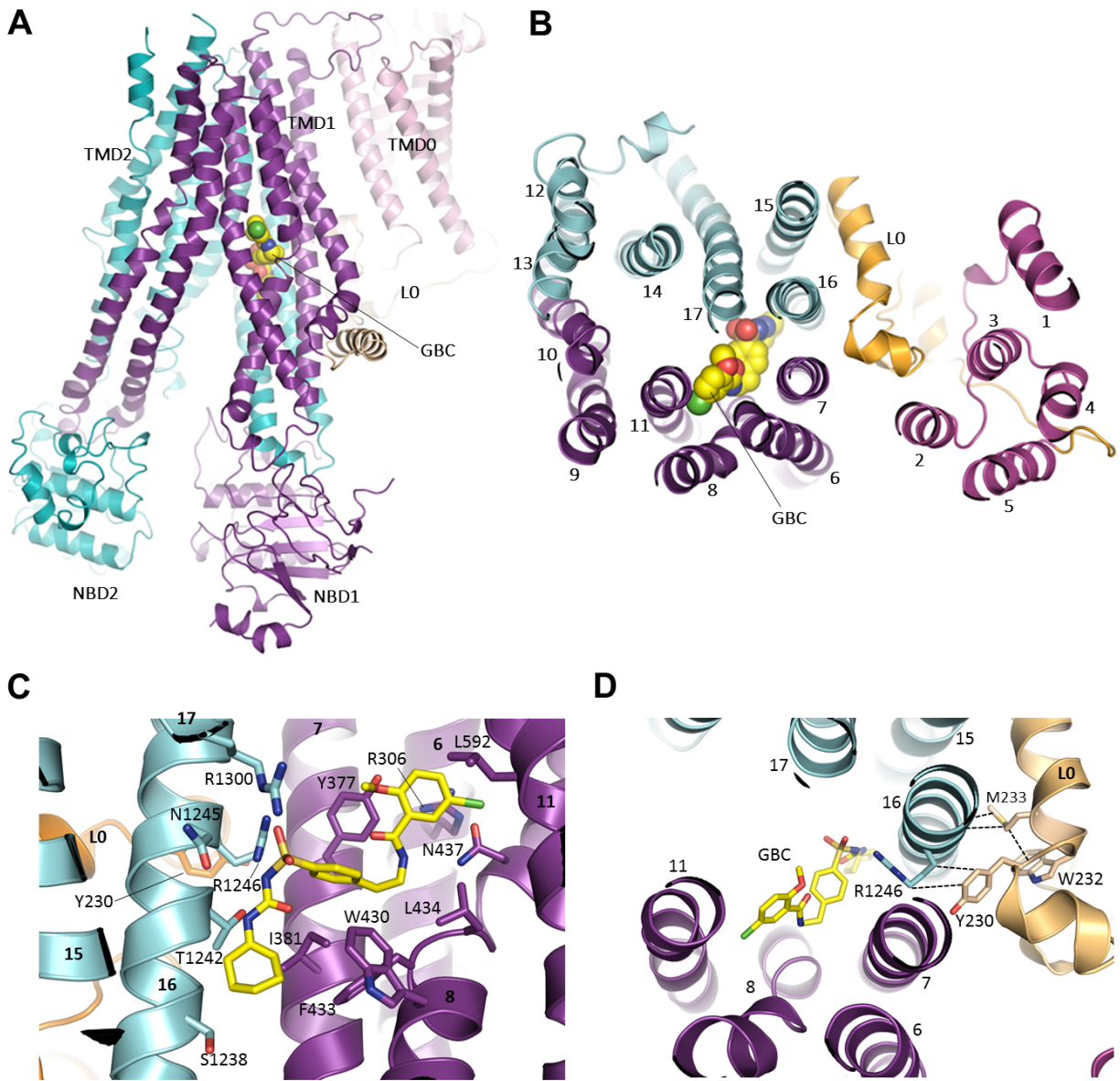


Figure 4 - supplement 1



**Figure 5**



**Figure 6**

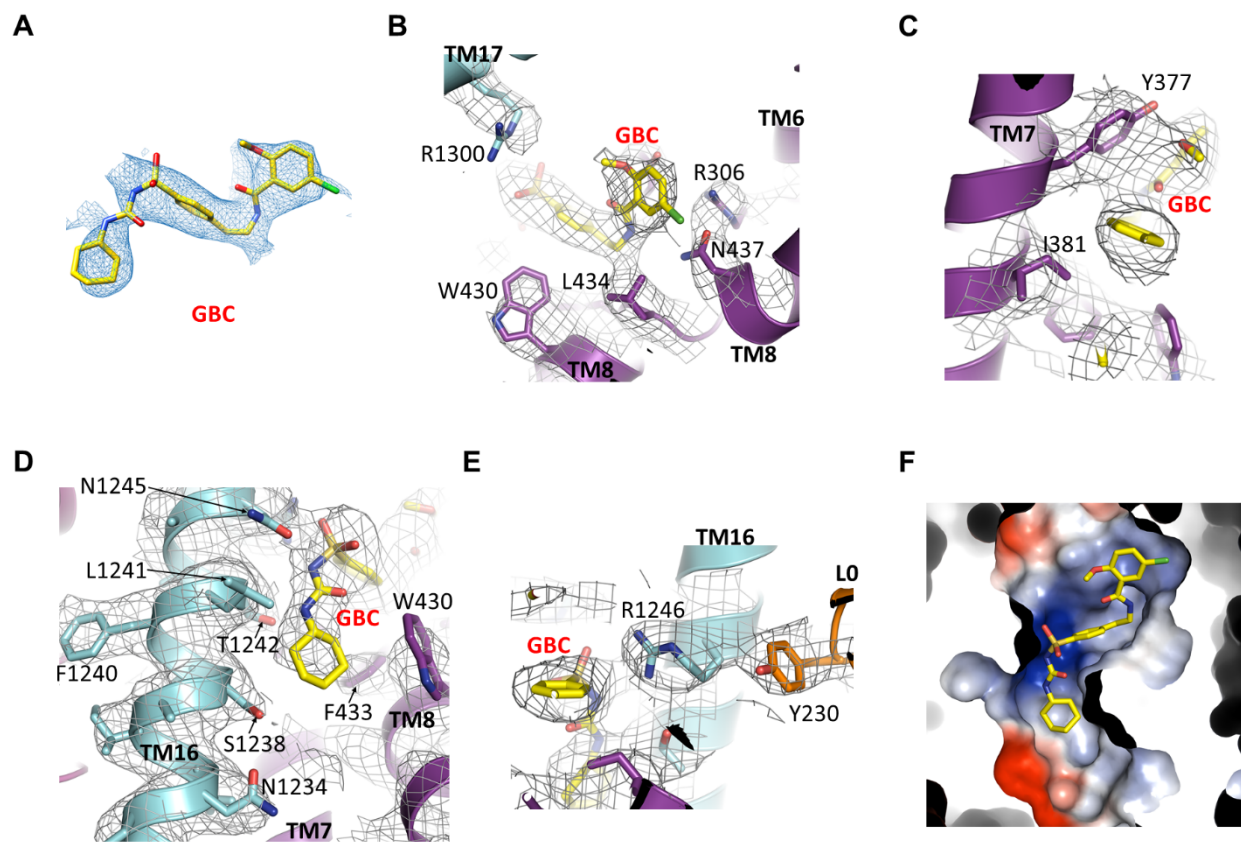


**Figure 6 - supplement 1**

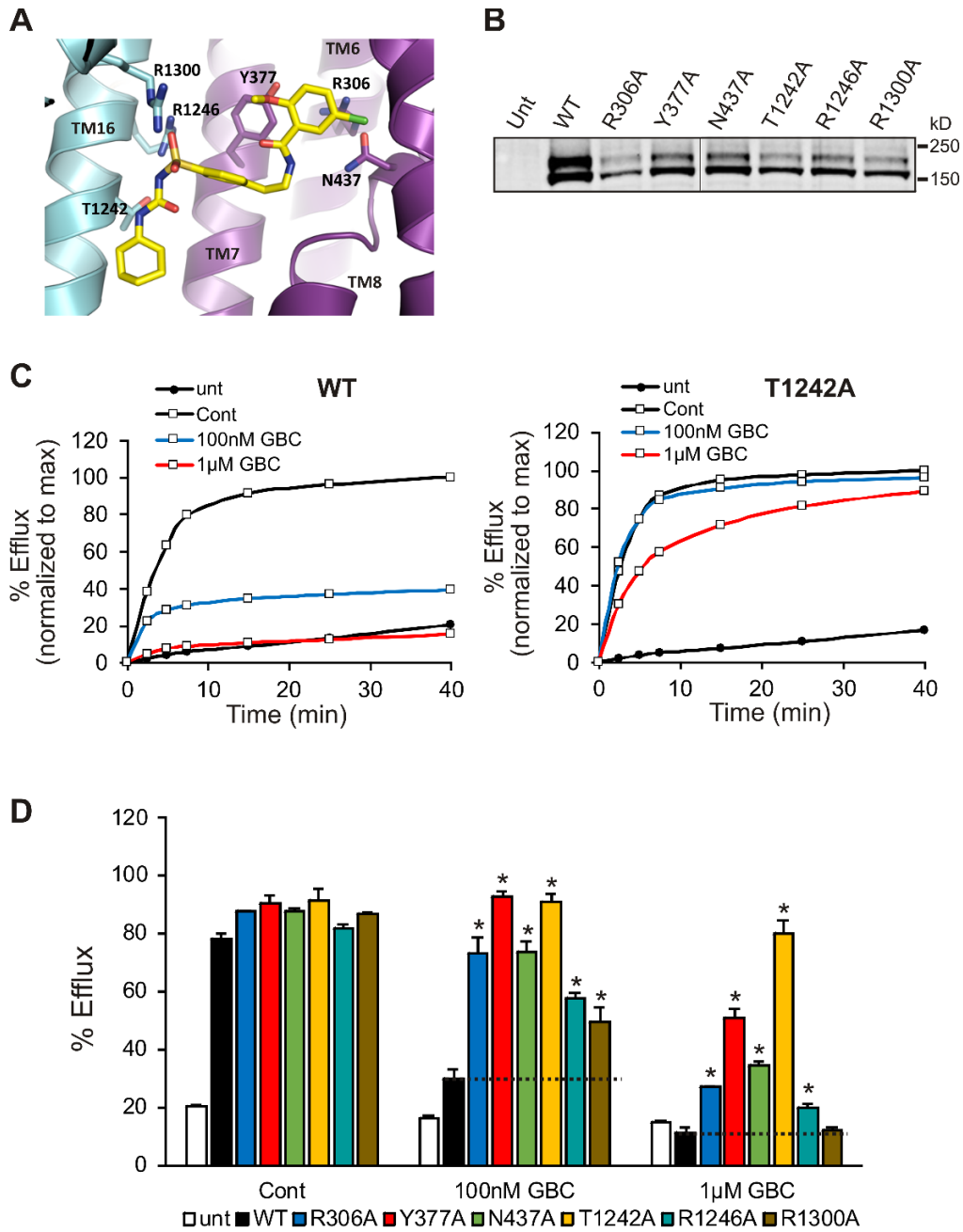


**Figure 7**

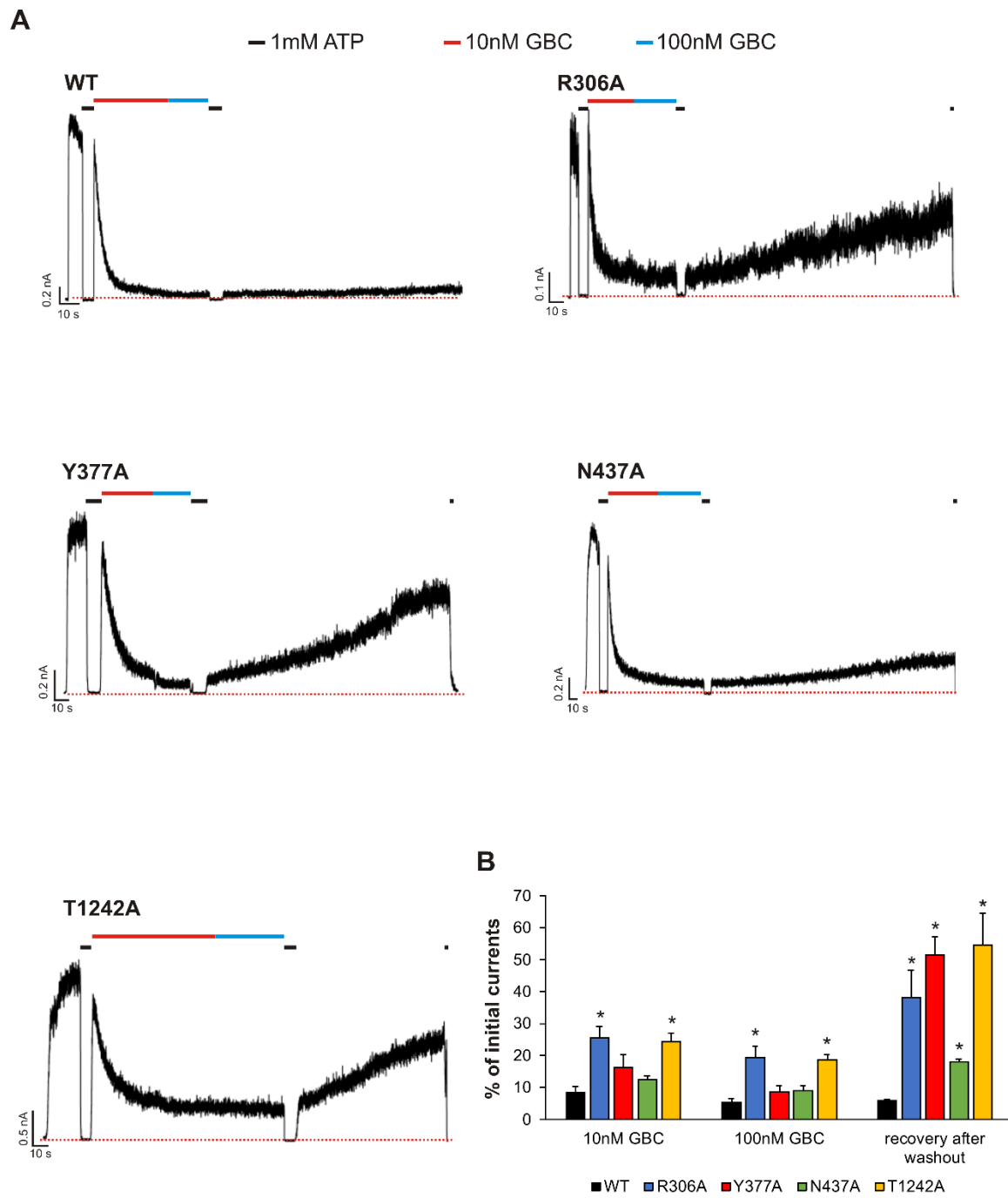


**Figure 7 - supplement 1**

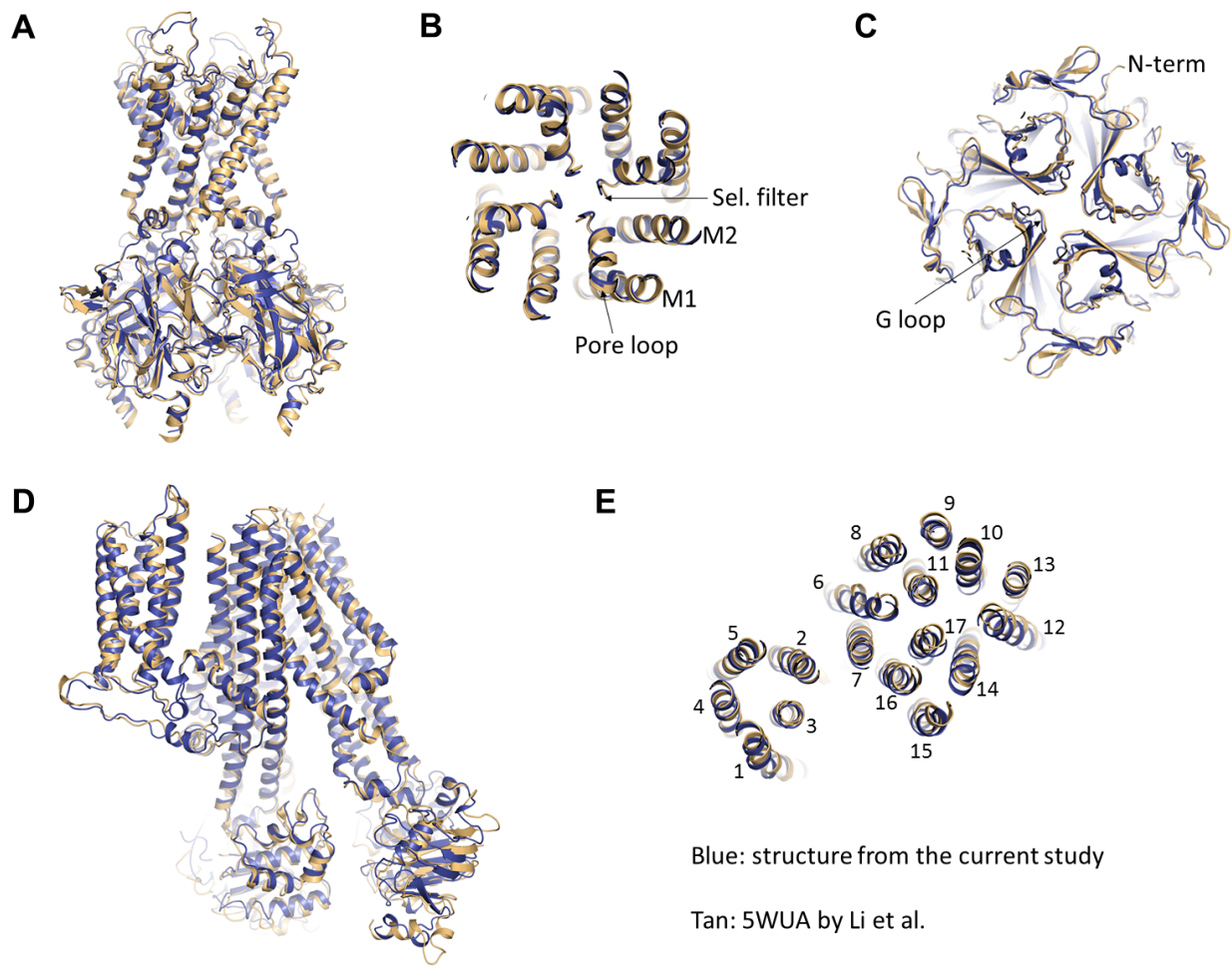


**Figure 8**

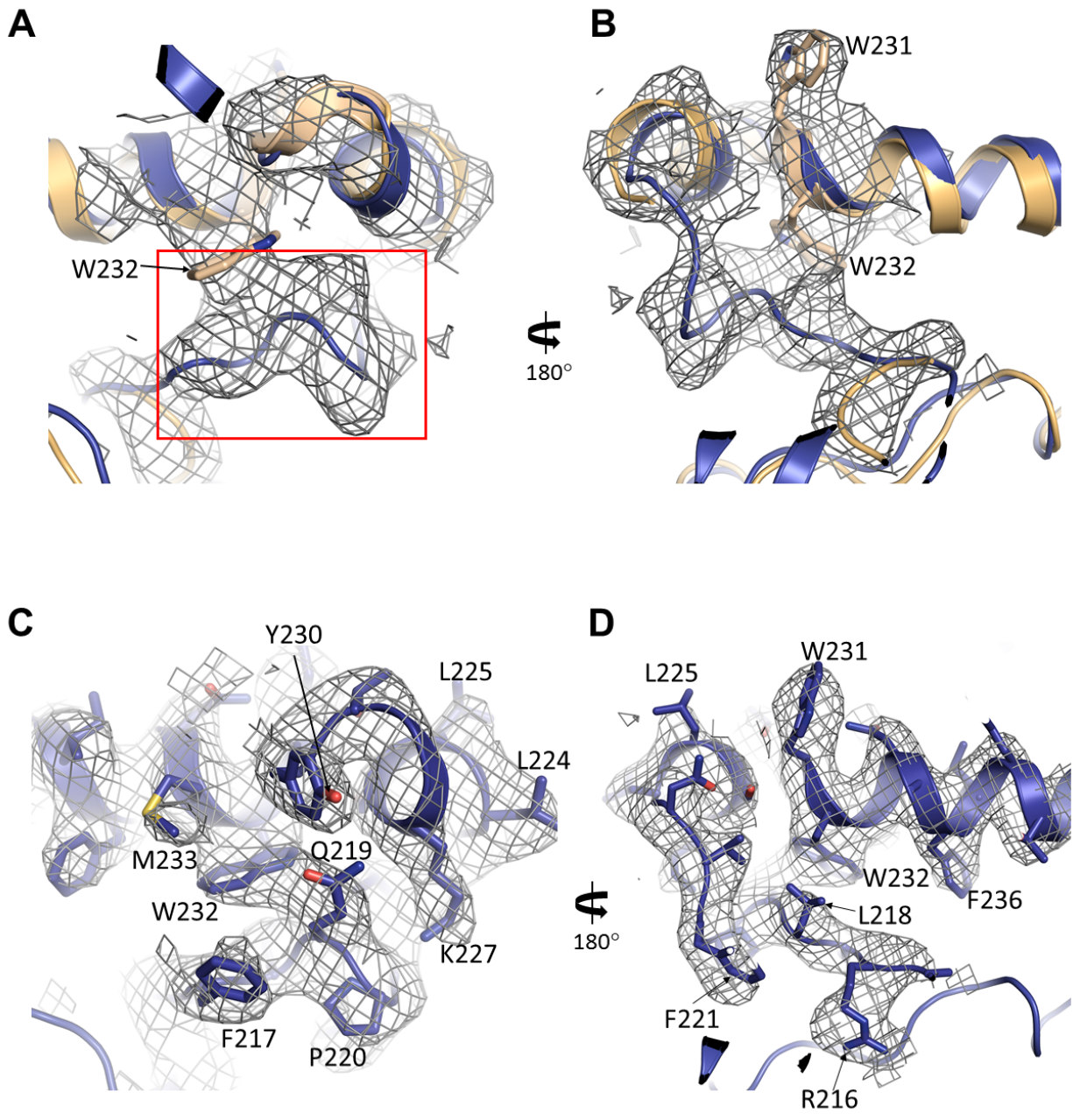
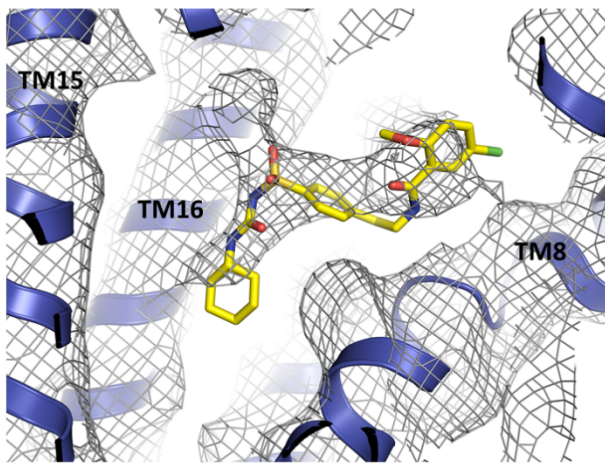


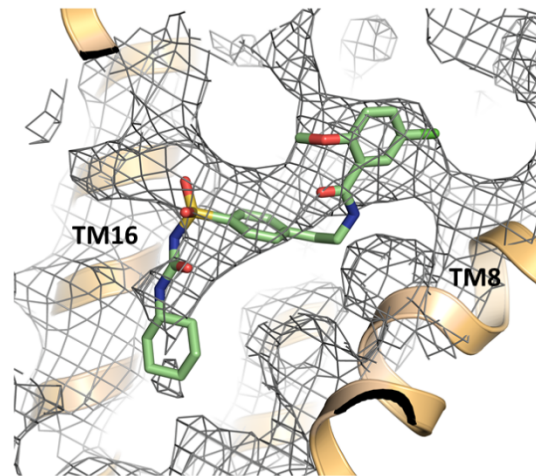
**Figure 8 - supplement 1**

**A**



5TWV (Martin et al.)

**B**



5WUA (Li et al.)

**Figure 8 - supplement 2**

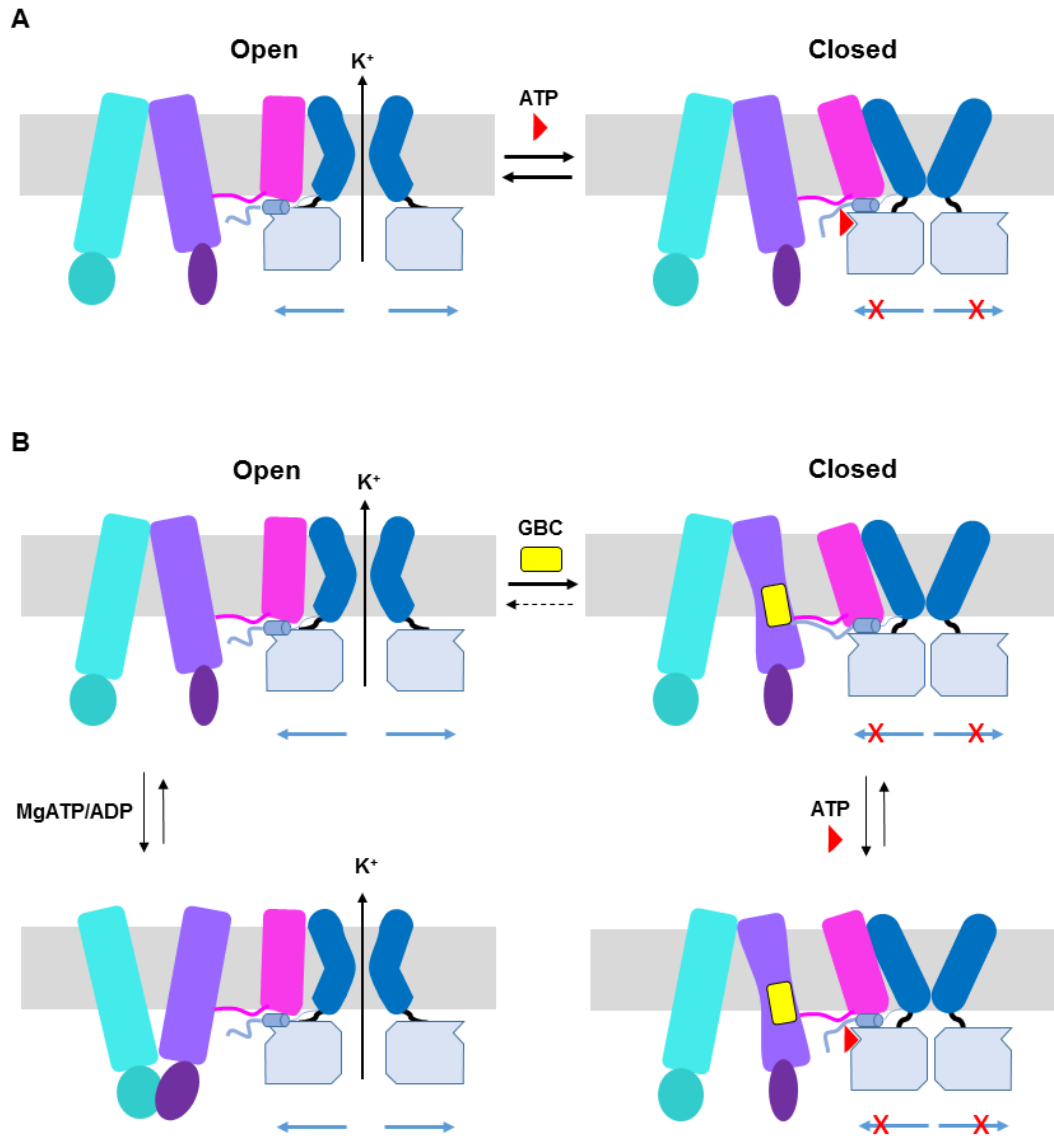


**Figure 9**

## References Cited

- Aguilar-Bryan, L., and J. Bryan. 1999. Molecular biology of adenosine triphosphate-sensitive potassium channels. *Endocrine reviews*. 20:101-135.
- Aguilar-Bryan, L., and J. Bryan. 2008. Neonatal diabetes mellitus. *Endocrine reviews*. 29:265-291.
- Antcliff, J.F., S. Haider, P. Proks, M.S. Sansom, and F.M. Ashcroft. 2005. Functional analysis of a structural model of the ATP-binding site of the KATP channel Kir6.2 subunit. *The EMBO journal*. 24:229-239.
- Ashcroft, F.M. 2005. ATP-sensitive potassium channelopathies: focus on insulin secretion. *The Journal of clinical investigation*. 115:2047-2058.
- Ashcroft, F.M. 2007. The Walter B. Cannon Physiology in Perspective Lecture, 2007. ATP-sensitive K<sup>+</sup> channels and disease: from molecule to malady. *American journal of physiology. Endocrinology and metabolism*. 293:E880-889.
- Ashfield, R., F.M. Gribble, S.J. Ashcroft, and F.M. Ashcroft. 1999. Identification of the high-affinity tolbutamide site on the SUR1 subunit of the K(ATP) channel. *Diabetes*. 48:1341-1347.
- Babenko, A.P., G. Gonzalez, and J. Bryan. 1999. The N-terminus of KIR6.2 limits spontaneous bursting and modulates the ATP-inhibition of KATP channels. *Biochemical and biophysical research communications*. 255:231-238.
- Bauer, C.B., H.M. Holden, J.B. Thoden, R. Smith, and I. Rayment. 2000. X-ray structures of the apo and MgATP-bound states of Dictyostelium discoideum myosin motor domain. *The Journal of biological chemistry*. 275:38494-38499.
- Brunger, A.T., P.D. Adams, G.M. Clore, W.L. DeLano, P. Gros, R.W. Grosse-Kunstleve, J.S. Jiang, J. Kuszewski, M. Nilges, N.S. Pannu, R.J. Read, L.M. Rice, T. Simonson, and G.L. Warren. 1998. Crystallography & NMR system: A new software suite for macromolecular structure determination. *Acta crystallographica. Section D, Biological crystallography*. 54:905-921.
- Bryan, J., W.H. Vila-Carriles, G. Zhao, A.P. Babenko, and L. Aguilar-Bryan. 2004. Toward linking structure with function in ATP-sensitive K<sup>+</sup> channels. *Diabetes*. 53 Suppl 3:S104-112.
- Chapman, M.S., A. Trzynka, and B.K. Chapman. 2013. Atomic modeling of cryo-electron microscopy reconstructions--joint refinement of model and imaging parameters. *Journal of structural biology*. 182:10-21.
- Chen, P.C., E.M. Olson, Q. Zhou, Y. Kryukova, H.M. Sampson, D.Y. Thomas, and S.L. Shyng. 2013a. Carbamazepine as a novel small molecule corrector of trafficking-impaired ATP-sensitive potassium channels identified in congenital hyperinsulinism. *J. Biol. Chem*. 288:20942-20954.
- Chen, P.C., E.M. Olson, Q. Zhou, Y. Kryukova, H.M. Sampson, D.Y. Thomas, and S.L. Shyng. 2013b. Carbamazepine as a novel small molecule corrector of trafficking-impaired ATP-sensitive potassium channels identified in congenital hyperinsulinism. *The Journal of biological chemistry*. 288:20942-20954.
- Cukras, C.A., I. Jeliaskova, and C.G. Nichols. 2002. The role of NH<sub>2</sub>-terminal positive charges in the activity of inward rectifier KATP channels. *The Journal of general physiology*. 120:437-446.

- Devaraneni, P.K., G.M. Martin, E.M. Olson, Q. Zhou, and S.L. Shyng. 2015. Structurally distinct ligands rescue biogenesis defects of the KATP channel complex via a converging mechanism. *The Journal of biological chemistry*. 290:7980-7991.
- Drain, P., L. Li, and J. Wang. 1998. KATP channel inhibition by ATP requires distinct functional domains of the cytoplasmic C terminus of the pore-forming subunit. *Proceedings of the National Academy of Sciences of the United States of America*. 95:13953-13958.
- Enkvetchakul, D., G. Loussouarn, E. Makhina, and C.G. Nichols. 2001. ATP interaction with the open state of the K(ATP) channel. *Biophysical journal*. 80:719-728.
- Enkvetchakul, D., G. Loussouarn, E. Makhina, S.L. Shyng, and C.G. Nichols. 2000. The kinetic and physical basis of K(ATP) channel gating: toward a unified molecular understanding. *Biophysical journal*. 78:2334-2348.
- Gribble, F.M., and F. Reimann. 2003. Sulphonylurea action revisited: the post-cloning era. *Diabetologia*. 46:875-891.
- Grigorieff, N. 2016. FREALIGN: An Exploratory Tool for Single-Particle Cryo-EM. *Methods in enzymology*. 579:191-226.
- Haider, S., J.F. Antcliff, P. Proks, M.S. Sansom, and F.M. Ashcroft. 2005. Focus on Kir6.2: a key component of the ATP-sensitive potassium channel. *Journal of molecular and cellular cardiology*. 38:927-936.
- Hansen, S.B., X. Tao, and R. MacKinnon. 2011. Structural basis of PIP2 activation of the classical inward rectifier K<sup>+</sup> channel Kir2.2. *Nature*. 477:495-498.
- Hattori, M., and E. Gouaux. 2012. Molecular mechanism of ATP binding and ion channel activation in P2X receptors. *Nature*. 485:207-212.
- Hibino, H., A. Inanobe, K. Furutani, S. Murakami, I. Findlay, and Y. Kurachi. 2010. Inwardly rectifying potassium channels: their structure, function, and physiological roles. *Physiological reviews*. 90:291-366.
- Hohmeier, H.E., H. Mulder, G. Chen, R. Henkel-Rieger, M. Prentki, and C.B. Newgard. 2000. Isolation of INS-1-derived cell lines with robust ATP-sensitive K<sup>+</sup> channel-dependent and -independent glucose-stimulated insulin secretion. *Diabetes*. 49:424-430.
- Inagaki, N., T. Gonoi, J.P. Clement, C.Z. Wang, L. Aguilar-Bryan, J. Bryan, and S. Seino. 1996. A family of sulfonylurea receptors determines the pharmacological properties of ATP-sensitive K<sup>+</sup> channels. *Neuron*. 16:1011-1017.
- Inagaki, N., T. Gonoi, J.P.t. Clement, N. Namba, J. Inazawa, G. Gonzalez, L. Aguilar-Bryan, S. Seino, and J. Bryan. 1995. Reconstitution of IKATP: an inward rectifier subunit plus the sulfonylurea receptor. *Science*. 270:1166-1170.
- Johnson, Z.L., and J. Chen. 2017. Structural Basis of Substrate Recognition by the Multidrug Resistance Protein MRP1. *Cell*. 168:1075-1085 e1079.
- Kimanius, D., B.O. Forsberg, S.H. Scheres, and E. Lindahl. 2016. Accelerated cryo-EM structure determination with parallelisation using GPUs in RELION-2. *eLife*. 5.
- Koster, J.C., M.A. Permutt, and C.G. Nichols. 2005a. Diabetes and insulin secretion: the ATP-sensitive K<sup>+</sup> channel (K ATP) connection. *Diabetes*. 54:3065-3072.
- Koster, J.C., M.S. Remedi, C. Dao, and C.G. Nichols. 2005b. ATP and sulfonylurea sensitivity of mutant ATP-sensitive K<sup>+</sup> channels in neonatal diabetes: implications for pharmacogenomic therapy. *Diabetes*. 54:2645-2654.

- Koster, J.C., Q. Sha, and C.G. Nichols. 1999. Sulfonylurea and K(+)-channel opener sensitivity of K(ATP) channels. Functional coupling of Kir6.2 and SUR1 subunits. *The Journal of general physiology*. 114:203-213.
- Kuhner, P., R. Prager, D. Stephan, U. Russ, M. Winkler, D. Ortiz, J. Bryan, and U. Quast. 2012. Importance of the Kir6.2 N-terminus for the interaction of glibenclamide and repaglinide with the pancreatic K(ATP) channel. *Naunyn-Schmiedeberg's archives of pharmacology*. 385:299-311.
- Lederer, W.J., and C.G. Nichols. 1989. Nucleotide modulation of the activity of rat heart ATP-sensitive K<sup>+</sup> channels in isolated membrane patches. *The Journal of physiology*. 419:193-211.
- Li, L., X. Geng, M. Yonkunas, A. Su, E. Densmore, P. Tang, and P. Drain. 2005. Ligand-dependent linkage of the ATP site to inhibition gate closure in the KATP channel. *The Journal of general physiology*. 126:285-299.
- Li, L., J. Wang, and P. Drain. 2000. The I182 region of k(ir)6.2 is closely associated with ligand binding in K(ATP) channel inhibition by ATP. *Biophysical journal*. 79:841-852.
- Li, N., J.X. Wu, D. Ding, J. Cheng, N. Gao, and L. Chen. 2017. Structure of a Pancreatic ATP-Sensitive Potassium Channel. *Cell*. 168:101-110 e110.
- Lin, C.W., Y.W. Lin, F.F. Yan, J. Casey, M. Kochhar, E.B. Pratt, and S.L. Shyng. 2006. Kir6.2 mutations associated with neonatal diabetes reduce expression of ATP-sensitive K<sup>+</sup> channels: implications in disease mechanism and sulfonylurea therapy. *Diabetes*. 55:1738-1746.
- Lin, C.W., F. Yan, S. Shimamura, S. Barg, and S.L. Shyng. 2005. Membrane phosphoinositides control insulin secretion through their effects on ATP-sensitive K<sup>+</sup> channel activity. *Diabetes*. 54:2852-2858.
- Lin, Y.W., J.D. Bushman, F.F. Yan, S. Haidar, C. MacMullen, A. Ganguly, C.A. Stanley, and S.L. Shyng. 2008. Destabilization of ATP-sensitive potassium channel activity by novel KCNJ11 mutations identified in congenital hyperinsulinism. *The Journal of biological chemistry*. 283:9146-9156.
- Lin, Y.W., T. Jia, A.M. Weinsoft, and S.L. Shyng. 2003. Stabilization of the activity of ATP-sensitive potassium channels by ion pairs formed between adjacent Kir6.2 subunits. *The Journal of general physiology*. 122:225-237.
- Liu, F., Z. Zhang, L. Csanady, D.C. Gadsby, and J. Chen. 2017. Molecular Structure of the Human CFTR Ion Channel. *Cell*. 169:85-95 e88.
- Martin, G.M., C. Yoshioka, E.A. Rex, J.F. Fay, Q. Xie, M.R. Whorton, J.Z. Chen, and S.L. Shyng. 2017. Cryo-EM structure of the ATP-sensitive potassium channel illuminates mechanisms of assembly and gating. *eLife*. 6.
- Nichols, C.G. 2006. KATP channels as molecular sensors of cellular metabolism. *Nature*. 440:470-476.
- Notredame, C., D.G. Higgins, and J. Heringa. 2000. T-Coffee: A novel method for fast and accurate multiple sequence alignment. *Journal of molecular biology*. 302:205-217.
- Oliva, M.A., S.C. Cordell, and J. Lowe. 2004. Structural insights into FtsZ protofilament formation. *Nature structural & molecular biology*. 11:1243-1250.
- Ortiz, D., P. Voyvodic, L. Gossack, U. Quast, and J. Bryan. 2012. Two neonatal diabetes mutations on transmembrane helix 15 of SUR1 increase affinity for ATP and ADP at nucleotide binding domain 2. *The Journal of biological chemistry*. 287:17985-17995.

- Payen, L., L. Delugin, A. Courtois, Y. Trinquart, A. Guillouzo, and O. Fardel. 2001. The sulphonylurea glibenclamide inhibits multidrug resistance protein (MRP1) activity in human lung cancer cells. *British journal of pharmacology*. 132:778-784.
- Pettersen, E.F., T.D. Goddard, C.C. Huang, G.S. Couch, D.M. Greenblatt, E.C. Meng, and T.E. Ferrin. 2004. UCSF Chimera--a visualization system for exploratory research and analysis. *Journal of computational chemistry*. 25:1605-1612.
- Pratt, E.B., F.F. Yan, J.W. Gay, C.A. Stanley, and S.L. Shyng. 2009. Sulfonylurea receptor 1 mutations that cause opposite insulin secretion defects with chemical chaperone exposure. *The Journal of biological chemistry*. 284:7951-7959.
- Pratt, E.B., Q. Zhou, J.W. Gay, and S.L. Shyng. 2012. Engineered interaction between SUR1 and Kir6.2 that enhances ATP sensitivity in KATP channels. *The Journal of general physiology*. 140:175-187.
- Proks, P., J.F. Antcliff, J. Lippiat, A.L. Gloyn, A.T. Hattersley, and F.M. Ashcroft. 2004. Molecular basis of Kir6.2 mutations associated with neonatal diabetes or neonatal diabetes plus neurological features. *Proceedings of the National Academy of Sciences of the United States of America*. 101:17539-17544.
- Proks, P., F.M. Gribble, R. Adhikari, S.J. Tucker, and F.M. Ashcroft. 1999. Involvement of the N-terminus of Kir6.2 in the inhibition of the KATP channel by ATP. *The Journal of physiology*. 514 ( Pt 1):19-25.
- Proks, P., K. Shimomura, T.J. Craig, C.A. Girard, and F.M. Ashcroft. 2007. Mechanism of action of a sulphonylurea receptor SUR1 mutation (F132L) that causes DEND syndrome. *Human molecular genetics*. 16:2011-2019.
- Reimann, F., S.J. Tucker, P. Proks, and F.M. Ashcroft. 1999. Involvement of the n-terminus of Kir6.2 in coupling to the sulphonylurea receptor. *The Journal of physiology*. 518 ( Pt 2):325-336.
- Rohou, A., and N. Grigorieff. 2015. CTFFIND4: Fast and accurate defocus estimation from electron micrographs. *Journal of structural biology*. 192:216-221.
- Sagen, J.V., H. Raeder, E. Hathout, N. Shehadeh, K. Gudmundsson, H. Baevre, D. Abuelo, C. Phornphutkul, J. Molnes, G.I. Bell, A.L. Gloyn, A.T. Hattersley, A. Molven, O. Sovik, and P.R. Njolstad. 2004. Permanent neonatal diabetes due to mutations in KCNJ11 encoding Kir6.2: patient characteristics and initial response to sulfonylurea therapy. *Diabetes*. 53:2713-2718.
- Schultz, B.D., A.D. DeRoos, C.J. Venglarik, A.K. Singh, R.A. Frizzell, and R.J. Bridges. 1996. Glibenclamide blockade of CFTR chloride channels. *The American journal of physiology*. 271:L192-200.
- Shyng, S., T. Ferrigni, and C.G. Nichols. 1997. Control of rectification and gating of cloned KATP channels by the Kir6.2 subunit. *The Journal of general physiology*. 110:141-153.
- Shyng, S.L., C.A. Cukras, J. Harwood, and C.G. Nichols. 2000. Structural determinants of PIP(2) regulation of inward rectifier K(ATP) channels. *The Journal of general physiology*. 116:599-608.
- Smart, O.S., J.G. Neduvellil, X. Wang, B.A. Wallace, and M.S. Sansom. 1996. HOLE: a program for the analysis of the pore dimensions of ion channel structural models. *Journal of molecular graphics*. 14:354-360, 376.
- Snider, K.E., S. Becker, L. Boyajian, S.L. Shyng, C. MacMullen, N. Hughes, K. Ganapathy, T. Bhatti, C.A. Stanley, and A. Ganguly. 2013. Genotype and phenotype correlations in 417

- children with congenital hyperinsulinism. *The Journal of clinical endocrinology and metabolism*. 98:E355-363.
- Sola, D., L. Rossi, G.P. Schianca, P. Maffioli, M. Bigliocca, R. Mella, F. Corliano, G.P. Fra, E. Bartoli, and G. Derosa. 2015. Sulfonylureas and their use in clinical practice. *Archives of medical science : AMS*. 11:840-848.
- Song, Y., F. DiMaio, R.Y. Wang, D. Kim, C. Miles, T. Brunette, J. Thompson, and D. Baker. 2013. High-resolution comparative modeling with RosettaCM. *Structure*. 21:1735-1742.
- Tammaro, P., C. Girard, J. Molnes, P.R. Njolstad, and F.M. Ashcroft. 2005. Kir6.2 mutations causing neonatal diabetes provide new insights into Kir6.2-SUR1 interactions. *The EMBO journal*. 24:2318-2330.
- Tucker, S.J., F.M. Gribble, P. Proks, S. Trapp, T.J. Ryder, T. Haug, F. Reimann, and F.M. Ashcroft. 1998. Molecular determinants of KATP channel inhibition by ATP. *The EMBO journal*. 17:3290-3296.
- Tusnady, G.E., B. Sarkadi, I. Simon, and A. Varadi. 2006. Membrane topology of human ABC proteins. *FEBS letters*. 580:1017-1022.
- Vila-Carriles, W.H., G. Zhao, and J. Bryan. 2007. Defining a binding pocket for sulfonylureas in ATP-sensitive potassium channels. *FASEB journal : official publication of the Federation of American Societies for Experimental Biology*. 21:18-25.
- Voss, N.R., C.K. Yoshioka, M. Rademacher, C.S. Potter, and B. Carragher. 2009. DoG Picker and TiltPicker: software tools to facilitate particle selection in single particle electron microscopy. *Journal of structural biology*. 166:205-213.
- Whorton, M.R., and R. MacKinnon. 2011. Crystal structure of the mammalian GIRK2 K<sup>+</sup> channel and gating regulation by G proteins, PIP<sub>2</sub>, and sodium. *Cell*. 147:199-208.
- Wilkens, S. 2015. Structure and mechanism of ABC transporters. *F1000prime reports*. 7:14.
- Winkler, M., D. Stephan, S. Bieger, P. Kuhner, F. Wolff, and U. Quast. 2007. Testing the bipartite model of the sulfonylurea receptor binding site: binding of A-, B-, and A + B-site ligands. *The Journal of pharmacology and experimental therapeutics*. 322:701-708.
- Yan, F.F., J. Casey, and S.L. Shyng. 2006. Sulfonylureas correct trafficking defects of disease-causing ATP-sensitive potassium channels by binding to the channel complex. *The Journal of biological chemistry*. 281:33403-33413.
- Yan, F.F., Y.W. Lin, C. MacMullen, A. Ganguly, C.A. Stanley, and S.L. Shyng. 2007. Congenital hyperinsulinism associated ABCC8 mutations that cause defective trafficking of ATP-sensitive K<sup>+</sup> channels: identification and rescue. *Diabetes*. 56:2339-2348.
- Zerangue, N., B. Schwappach, Y.N. Jan, and L.Y. Jan. 1999. A new ER trafficking signal regulates the subunit stoichiometry of plasma membrane K(ATP) channels. *Neuron*. 22:537-548.
- Zhang, Z., and J. Chen. 2016. Atomic Structure of the Cystic Fibrosis Transmembrane Conductance Regulator. *Cell*. 167:1586-1597 e1589.
- Zheng, S.Q., E. Palovcak, J.P. Armache, K.A. Verba, Y. Cheng, and D.A. Agard. 2017. MotionCor2: anisotropic correction of beam-induced motion for improved cryo-electron microscopy. *Nature methods*. 14:331-332.

## Chapter 5

### A structural mechanism for pharmacological chaperone rescue of trafficking-impaired $K_{ATP}$ channels

Gregory M. Martin, Laura Innes, Balamurugan Kandasamy, Craig Yoshioka, Zhongying Yang, & Show-Ling Shyng

#### Author Contributions

**GMM:** Experimental design, conceived of project. Writing: original draft. Figure making. Sample preparation: protein purification, cryo-EM sample preparation for ATP only and ATP+Repaglinide structures. Cryo-EM data collection for ATP only and ATP+Repaglinide structures. Cryo-EM image processing, generation of final maps, and structure refinement for all structures. **LI:** Sample preparation (protein purification and cryo-EM sample prep) and data collection for CBZ structure. **BK:** Performed experiments for Figure 7. Made constructs and performed experiments for Figure 8. **ZYY:** Sample preparation: generation of virus, cell culture and protein expression for each structure. **CY:** Experimental design. Cryo-EM data collection for each structure. Image processing for CBZ structure. **SLS:** Experimental design, conceived of project. Figure making.

*THIS IS A MANUSCRIPT IN PREPARATION*

## Abstract

Pharmacological chaperones (PCs) are specific, small molecule correctors of protein misfolding with the potential to treat proteostasis disorders, in which improper protein expression or targeting contributes to disease. Cystic fibrosis resulting from the  $\Delta F508$  mutation in the cystic fibrosis transmembrane conductance regulator (CFTR) is perhaps the most well-studied instance, in which the deletion of F508 causes a folding defect in CFTR which results in degradation and loss of plasma membrane expression. We have identified a diverse set of PCs which overcome analogous folding/trafficking defects in the pancreatic  $K_{ATP}$  channel, a critical regulator of glucose-stimulated insulin secretion. We sought to understand the structural basis for the PC mechanism of three structurally unrelated allosteric inhibitors of the  $K_{ATP}$  channel, carbamazepine (CBZ), glibenclamide (GBC), and repaglinide (RPG) by cryo-EM. We find that each inhibitor binds to the same pocket in the regulatory subunit SUR1 which likely involves the distal Kir6.2 N-terminus, a  $\sim 30$  amino acid peptide and critical regulator of  $K_{ATP}$  channel function and assembly. PC binding has a minimal effect on SUR1 structure, but strengthens a cytoplasmic interface between SUR1 and Kir6.2 by inducing a rigid body motion in the Kir6.2 cytoplasmic domain. Mutation of key residues within the binding pocket diminishes or eliminates inhibition by each drug, and also abolishes their ability to rescue CHI-causing trafficking mutations in SUR1. We propose a model by which CBZ, GBC, and RPG, despite their chemical uniqueness, rescue  $K_{ATP}$  channel trafficking mutations *in trans* by binding to the same pocket on SUR1 involving the Kir6.2 N-terminus to strengthen interactions between SUR1 and Kir6.2 during assembly in the ER, which overcomes partial misfolding as a result of mutations distant from the site of drug action.

## Introduction

Congenital hyperinsulinism (CHI) is a rare yet potentially life-threatening disease characterized by unregulated insulin secretion despite severe hypoglycemia (Stanley, 2016), and the most common cause is loss-of-function mutations within the pancreatic ATP-sensitive K<sup>+</sup> channel (K<sub>ATP</sub>) (Aguilar-Bryan et al., 2001; Ashcroft, 2007). These channels are large, heterooctameric complexes comprising two proteins in 1:1 stoichiometry: a regulatory subunit sulfonylurea receptor 1 (SUR1) subunit and a pore-forming inward-rectifier K<sup>+</sup> channel Kir6.2 (Clement et al., 1997; Inagaki et al., 1997; Shyng & Nichols, 1997). By responding directly to levels of ADP and ATP, which activate and inhibit channel activity, respectively (Nichols, 2006; Rorsman & Trube, 1985), K<sub>ATP</sub> channels couple intracellular glucose metabolism to the membrane potential and in the pancreas are critical mediators of glucose-stimulated insulin secretion. CHI-causing mutations within the K<sub>ATP</sub> channel are found throughout the SUR1 and Kir6.2 protein sequences and result in loss of channel activity by either a gating defect causing very low open probability (P<sub>O</sub>) and/or by a trafficking defect, in which assembly of the channel complex is disrupted leading to loss of channel expression at the plasma membrane (Martin et al., 2013). Individuals with CHI gating mutations can, in some cases, be successfully treated with the K<sub>ATP</sub> channel opener diazoxide, whereas CHI resulting from K<sub>ATP</sub> channel trafficking defects are more severe and often require partial or near complete pancreatectomy to avoid permanent brain damage which can result from sustained hypoglycemia. Thus there is a need for an alternative treatment for these patients.

The majority of CHI trafficking mutations are found with the SUR1 subunit, which is a member of the exporter class of the ABC transporter superfamily. These proteins all share a common fold of two transmembrane domains TMD1 and TMD2 interspersed by two cytosolic

nucleotide binding domains NBD1 and NBD2. In addition, SUR1, along with only a few other family members, contains an additional N-terminal transmembrane region called TMD0. In the  $K_{ATP}$  channel, TMD0 mediates physical and functional interactions between SUR1 and Kir6.2 and has a profound effect on Kir6.2 gating (Babenko & Bryan, 2003; Chan et al., 2003; Pratt et al., 2011). Interestingly, for CHI trafficking mutations within TMD0, it was discovered that the plasma membrane expression could be restored by incubating cells with sulfonylureas or glinides (Martin et al., 2013; Yan et al., 2004; Yan et al., 2006; Yan et al., 2007), allosteric  $K_{ATP}$  channel inhibitors which bind with high affinity to SUR1. These drugs act by enhancing assembly in the ER and are thus termed pharmacological chaperones (PCs). A novel  $K_{ATP}$  channel inhibitor and PC carbamazepine (CBZ) was recently identified (Chen, Olson, et al., 2013; Martin et al., 2016) which corrects  $K_{ATP}$  channel trafficking defects with similar efficacy as the most effective sulfonylurea glibenclamide (GBC), but in contrast to GBC inhibits channel activity reversibly allowing for restoration of  $K_{ATP}$  channel activity at the cell surface. CBZ is therefore a potential lead compound in identifying small-molecule therapies for this form of CHI.

Despite their diversity of chemical structure (Figure 1A), sulfonylureas, glinides, and CBZ all appear to rescue TMD0 trafficking mutations via a similar mechanism which we hypothesize to involve direct binding of these drugs to the same binding pocket on SUR1, and that by doing so stabilize interactions between SUR1 and the Kir6.2 distal N-terminus (Devaraneni et al., 2015; Martin et al., 2016). In the current study we sought to directly address (1) whether and how these diverse compounds all interact with the same site on SUR1, (2) the role of the Kir6.2 distal N-terminus in drug binding and thus in the mechanism of PC rescue of  $K_{ATP}$  channel trafficking defects, and (3) the mechanism of allosteric inhibition of Kir6.2 activity by drug interaction with SUR1. We previously solved cryo-EM structures of the  $K_{ATP}$  channel

complex simultaneously bound to ATP (at Kir6.2) and GBC (at SUR1) which elucidated the nature of these binding pockets and suggested mechanisms for how they each inhibit channel activity (Martin, Kandasamy, et al., 2017; Martin, Yoshioka, et al., 2017). Here we solve structures of the complex bound to CBZ or the highest affinity glinide repaglinide (RPG), both in the presence of ATP, or ATP only (SUR1 apo). We find that each inhibitor indeed binds to the same pocket in SUR1, and identify cryo-EM density that likely corresponds to the distal N-terminus of Kir6.2 which forms a direct interaction with the ligand. The binding site model was validated by efflux experiments, which demonstrate a critical role for most of the residues lining the sulfonylurea/CBZ/glinide binding pocket in drug sensitivity. Finally, we show that interaction with the binding pocket underlies the ability of these drugs to function as pharmacological chaperones for CHI trafficking mutations within TMD0. These studies provide direct structural evidence for a conserved rescue mechanism of  $K_{ATP}$  channel pharmacological chaperones and also suggest how an ABC transporter architecture may be adapted to regulate ion channel activity.

## **Results**

### *Structure determination*

For structure solution, we utilized the same construct as our previous studies which comprises a WT hamster SUR1 and WT rat Kir6.2 (95% and 96% identical to human, respectively), expressed in the rat insulinoma cell line INS-1 and purified with affinity chromatography via a FLAG tag at the N-terminus of SUR1. For the ATP dataset, channels were purified and data were collected in the presence of 2mM ATP (without  $Mg^{2+}$ ). The same procedure was used for the CBZ and RPG datasets, but in the presence of 10 $\mu$ M CBZ and 30 $\mu$ M RPG, respectively (final DMSO concentration of 0.1%).

3D classification in RELION or cisTEM yielded essentially one C4 symmetric class for each dataset; all other classes had either missing SUR1 subunits or large deviations from C4 symmetry and were not refined further. The final C4 refinement was performed in cisTEM, and the reported resolutions using the 0.143 FSC cutoff were 4.2, 3.6, and 5.6Å for ATP only, RPG+ATP, and CBZ+ATP, respectively. As before, the TM region is the most well-defined, and disorder increases at the very periphery of the complex (outer SUR1 helices). This is likely due to minor deviations from ideal C4 symmetry, which may originate from flexibility in the intracellular loop L0 which links TMD0 to the ABC core structure (TMD1/NBD1/TMD2/NBD2) of SUR1. Our previous ATP+GBC structure (PDB 6BAA) was used as the starting model for each reconstruction, and the structures were refined to match the experimental data. The NBDs again displayed the highest level of disorder, with NBD2 showing much more severe disorder than NBD1, therefore this region was modelled only through rigid body docking into the density.

### **Structure of the $K_{ATP}$ channel complex bound to ATP and allosteric inhibitors**

Not surprisingly, the structures of channel complex bound to ATP and CBZ/RPG are nearly identical to our previous ATP+GBC structure (Figure 1B, 1C), with both gates of Kir6.2 (the helix bundle crossing and G-loop gates) tightly closed. This suggests that by binding to SUR1, each compound (CBZ, GBC, RPG) inhibits channel activity via a similar mechanism, which involves at least in part stabilization of SUR1 in the “inward-facing” conformation in which NBDs are separated, which will prevent MgATP/MgADP mediated stimulation of channel activity. This notion is supported by recent  $K_{ATP}$  channel structures which suggest that the rearrangement of TMD1/TMD2 of SUR1 induced by NBD dimerization is prevented by the

presence of GBC in the binding pocket, which directly interacts with the TM helices undergoing significant motion during this step (Lee et al., 2017; Wu et al., 2018).

### **CBZ and RPG bind to the sulfonyleurea binding pocket**

We had previously shown that both GBC and CBZ inhibition of  $K_{ATP}$  channel activity could be nearly eliminated by the same two mutations in SUR1: S1238Y and Y230A (Devaraneni et al., 2015), while RPG inhibition is known to be disrupted only by Y230A but not S1238Y (Yan et al., JBC, 2006). This provided compelling, yet indirect evidence that these two compounds both bind to the same site on SUR1. However, it was difficult to imagine how such structurally unrelated compounds could achieve this. Thus we set out to examine this directly by solving structures in the presence or absence CBZ and RPG, which will simultaneously provide insight into the mechanism for the chaperone effect of these drugs and how SUR1 can bind with high affinity to such diverse compounds.

Accordingly, we observe strong cryo-EM density in both CBZ and RPG maps within the same site identified previously for GBC (Figure 2C, E). Further, this density is absent in the ATP only structure (Figure 2B), supporting its assignment as ligand. Interestingly, in the case of CBZ, the extent of the ligand density exceeds that which can be accounted for by only one CBZ molecule (Figure 2A). CBZ is known to adopt a U-shaped conformation in solution and in a crystal, and in the density map we observe two U-shaped contours. Further, CBZ is known to exhibit at least four polymorphic crystalline forms, all of which adopt a head-to-tail dimer mediated by complementary H-bonding between the carbonyl and amino groups (Cruz Cabeza et al., 2007). Thus it may be possible this occurs within the SUR1 binding pocket as well, such that a CBZ dimer confers CBZ the ability to simultaneously interact with residues on opposite ends of the binding pocket (i.e. S1238 and Y377) as if it were an extended ligand like GBC.

However, this could be the result of two CBZ molecules binding in a mutually exclusive fashion to either end of the pocket, and what is observed in the reconstruction is an average of the ensemble. One might suspect two separable affinities for CBZ if this were the case, but as of yet this has not been observed (Devaraneni et al., 2015). A higher resolution reconstruction coupled with data on the stoichiometry of the association between  $K_{ATP}$  and CBZ are needed to clarify this intriguing result.

The density for RPG, on the other hand, is compact and palm-shaped, and suggests that the molecule adopts a considerably folded shape upon binding to SUR1 (Figure 2E). Interestingly, RPG possesses a carboxylate group adjacent to a benzene ring, analogous to the sulfonyl group in GBC, which is also adjacent to a benzene (Figure 1A). Refinement of an RPG molecule into the density orients this carboxylate towards N1245, R1246, and R1300 (Figure 3C) which coordinate the sulfonyl group in the GBC-bound structure. Interestingly, unlike GBC and CBZ, S1238 is distant from the RPG density, consistent with previous binding and functional data showing that S1238Y does not impact RPG's ability to modulate channel function. The opposing helix is lined with hydrophobic residues (W430, F433, L434), which seem to support binding through a combination of van der Waals interactions and shape complementarity (Figure 3). This suggests that the particular combination of basic/polar and hydrophobic groups within the sulfonylurea binding pocket contribute to the ability of SUR1 to bind to a diversity of compounds with high affinity.

### **The impact of inhibitor binding to SUR1 on $K_{ATP}$ channel structure**

With structures of the  $K_{ATP}$  channel complex with and without SUR1 allosteric inhibitors (both in the presence of ATP) in hand, we can now examine their specific impact on channel structure. Figure 4A and 4C show an alignment between the ABC core structure of ATP+GBC

and ATP only structures. Surprisingly, CBZ/GBC/RPG have very little effect on the overall structure of SUR1, at least for this particular conformation in which NBDs are separated. There are, however, subtle rearrangements within the sulfonyleurea binding pocket between GBC-bound and RPG-bound structures which may explain the ability of SUR1 to sense these ligands (Figure 3C). The most obvious change is in W1297, which in the case of RPG, flips down to engage the ligand. As a result, the guanidinium group of R1300 must also flip down, which appears to strengthen its interaction with N1245. W430 also shifts slightly up and towards the inner cavity of SUR1 (coming out of the page in Figure 3C).

There may be minor rearrangements in the pocket between ATP only and ATP + inhibitor, but the resolution of the ATP only map in this region prevents definitive conclusions. However, it seems likely that in the case of R1246 and Y377, two residues which are both important for high GBC sensitivity, in the absence of ligand these form a cation- $\pi$  interaction which is broken as each residue engages different parts of the ligand upon drug binding. This is actually the case for MRP1, a close homolog of SUR1, in which R1196 and F385 (the equivalent residues to R1246 and Y377 in SUR1) form a cation- $\pi$  interaction in the apo state, and that upon LTC-4 binding these residues rearrange to participate in substrate binding (Johnson & Chen, 2017).

Figure 4B shows the effect of GBC binding to an ATP-bound state on the structure of Kir6.2. The structures were aligned relative to the pore loop and selectivity filter, which are relatively immobile parts of the structure. Interestingly, GBC/CBZ/RPG induce a rigid-body motion of the CTD relative to the TMD producing a 10° clockwise rotation (viewing down the pore from extracellular side) and a ~3Å vertical translation of the CTD toward inner leaflet of the bilayer. The direction of CTD rotation is opposite to what has been observed upon activation and

presumed opening of Kir3.2 (Whorton & MacKinnon, 2011, 2013) and also what is expected for Kir2.2 during opening based on simulations (Li et al., 2015). Thus a clockwise rotation in the CTD likely stabilizes the closed state of the pore. Further, the translation of the CTD towards the TMD likely acts to strengthen interactions between the N- and C-terminal domains and prevent CTD motion. This is supported by the fact that in the ATP+GBC reconstruction, the Kir6.2 CTD overall displays a high degree of order on par with the TMD, whereas the CTD in the ATP only reconstruction is more heterogeneous and is likely populating multiple substates that cannot be separated by classification.

The cytoplasmic portion of the Kir6.2 N-terminus also moves together with the cytoplasmic C-terminus and is indeed part of the rigid group comprising the CTD, thus an interesting consequence of this movement is that the  $\beta$ A strand on the Kir6.2 N-terminus more closely engages the first intracellular loop (ICL1) of TMD0 (Figure 5). In the ATP+GBC structure, this is in fact one of the most intimate points of contact between SUR1 and Kir6.2. We have shown previously that PCs like GBC and CBZ strengthen interactions between the Kir6.2 N-terminus and SUR1 which underlies their ability to rescue trafficking mutations (Devaraneni et al., 2015), therefore this may be one route by which these drugs achieve this.

### **The location of the distal N-terminus of Kir6.2**

Kir channels possess highly variable and presumably unstructured distal N-termini. In general, the role of this region in Kir channel function is unclear. In Kir6 channels however, the distal N-terminus is a critical component and has major roles in both interaction with SUR and in gating regulation. In particular, we have shown that the first 30 amino acids of Kir6.2 are critical for assembly with SUR1, and that this region forms direct interactions with SUR1 that are enhanced by sulfonylureas and CBZ (Devaraneni et al., 2015). The Kir6.2 distal N-terminus also

appears to contribute directly to the GBC binding pocket (Vila-Carriles et al., 2007), and is necessary for high affinity interaction with RPG (Hansen et al., 2005). Thus we suspected that this region may be present in our drug-bound reconstructions, and would likely be found near the sulfonylurea site.

We do in fact observe significant cryo-EM density immediately adjacent to CBZ, GBC, and RPG which appears as a roughly linear peptide inserting between the two TMDs of SUR1 from the intracellular side (Figure 6A). This density is also seen in the ATP only reconstruction, though it is not as strong or well-defined as in the drug-bound reconstructions (i.e. the density disappears at lower sigma values for the ATP only map after matching the intensity values between the reconstructions by shifting and rescaling with appropriate factors). Interestingly, in another recent ATP+GBC structure reported by another group (Wu et al., 2018), which utilized a SUR1-Kir6.2 fusion protein in which the SUR1 C-terminus is covalently linked to the Kir6.2 N-terminus, they did not observe this density. Thus presumably the covalent fusion either physically constrains the Kir6.2 N-terminus such that it prevents normal association with SUR1, or the added length due to the linker is too long for the SUR1 to accommodate in the inner cavity.

This has important implications for a  $K_{ATP}$  channel gating mechanism. The overall stability of the Kir6.2 N-terminus will likely be increased by direct interaction with SUR1, and this will consequently reduce mobility of the N-terminus and CTD that is needed to open the gates. This would in part explain how SUR1 can increase the ATP sensitivity of Kir6.2, as ATP interacts preferentially with the closed state (ATP sensitivity and  $P_O$  display an inverse relationship, but functionally ATP can interact with both open and closed states (Enkvetchakul et al., 2001). Further, as sulfonylureas bind to SUR1, they stabilize binding of the N-terminus to

SUR1 and reduce mobility of the CTD even further. Upon NBD dimerization, the inner vestibule of SUR1 will collapse and the N-terminus will unbind, allowing the CTD to (more) freely rotate, which could explain how MgADP binding to SUR1 reduces ATP sensitivity and increases  $P_O$  of Kir6.2.

However, the assignment of this density as the distal Kir6.2 N-terminus remains at this point speculation, albeit speculation supported by numerous orthogonal functional experiments from our group and from many others (Babenko & Bryan, 2002; Babenko, Gonzalez, & Bryan, 1999; Devaraneni et al., 2015; Koster, Sha, Shyng, et al., 1999; Martin et al., 2016). The resolution of the putative N-terminus prevents assignment of the sequence, and while we have shown that both Y12 and A18 of Kir6.2 directly interact with SUR1, the residues on SUR1 with which they interact are at present unknown. Future experiments that can either stabilize interaction of the N-terminus to allow direct assignment of the sequence or provide residue-residue contact information, like in the form of engineered disulfide bonds, are needed to validate this conclusion.

### **Functional validation of binding site model**

To test the role of specific residues on channel inhibition by CBZ and RPG and to identify a particular “signature” for each ligand within the pocket, we mutated (to Ala) various residues identified as important for drug interaction and compared with our previous data for GBC (Figure 7). We utilized  $^{86}\text{Rb}^+$  efflux experiments, in which  $\text{Rb}^+$  acts as a radioactive analog to  $\text{K}^+$  to allow for quantitative measurement of  $\text{K}^+$  channel activity in cells, and monitored the ability of GBC, CBZ, or RPG to inhibit efflux for each mutation when co-expressed with WT Kir6.2. We find that for each ligand, Y377 is critical for drug sensitivity, as would be expected based on the density, which for this residue overlaps directly with the density for each ligand.

We also see that T1242 plays a critical role, particularly in CBZ inhibition. Based on the model, one CBZ molecule would likely be unable to simultaneously interact with T1242 and Y377, which lends support to the hypothesis that CBZ binds to SUR1 as a dimer. However, in this case and in the case of each residue test, these effects could also be mediated allosterically, i.e. the mutation changes the structure of SUR1 to reduce drug sensitivity indirectly. Nonetheless, these experiments provide strong functional support to the CBZ and RPG binding site models. In the future, it will be worth testing drug binding more directly (e.g. intrinsic tryptophan fluorescence, microscale thermophoresis, etc.) to assess changes in affinity as a result of particular mutations in drug binding. Coupled with structural data, this would go a long way toward the goal of understanding how the sulfonylurea binding pocket achieves high affinity for a breadth of compounds.

### **Pharmacological chaperone function relies on an intact sulfonylurea binding site**

The definition of a pharmacological chaperone is that they bind specifically to a site on a receptor during biogenesis to overcome a folding defect, whereas chemical chaperones like glycerol act nonspecifically to enhance the intracellular folding environment. Thus with a model of the SUR1 allosteric inhibitor site in hand, we wished to test more directly the hypothesis that CBZ and sulfonylureas (like GBC) overcome CHI trafficking mutations by binding directly to SUR1. F27S-SUR1 is a well-characterized CHI trafficking mutation which responds strongly to both CBZ and GBC and has nearly undetectable surface expression in the absence of drug (Chen, Olson, et al., 2013). In an F27S background, we mutated multiple sites within the sulfonylurea binding pocket and examined the impact on the chaperone function of CBZ and GBC. We have shown previously that these mutations by themselves do not significantly alter  $K_{ATP}$  channel surface expression (Martin, Kandasamy, et al., 2017).

A simple method for examining trafficking of  $K_{ATP}$  channels is to examine the glycosylation profile of SUR1 on a western blot, as SUR1 contains two distinct bands which correspond to the immature form in the ER and the mature glycosylated form which has trafficked through the Golgi and presumably reached the plasma membrane. Due to ER retention/retrieval motifs in both SUR1 and Kir6.2, only fully assembled, octameric channel complexes can exit the ER (Zerangue et al., 1999), thus examining the ratio of the upper to lower bands of SUR1 gives a measure of the assembly of SUR1 with Kir6.2. In Figure 8, we see a complete absence of upper band for F27S in control (DMSO) and strong recovery when mutant is expressed in the presence of CBZ or GBC, with a processing efficiency which nearly resembles WT. However, for each of the binding site mutations tested within the F27S background, the chaperone ability of CBZ and GBC was nearly completely abolished. Therefore, these experiments allow us to conclude that CBZ, GBC, and presumably RPG, all rescue TMD0 trafficking mutations by directly binding to the same binding pocket in SUR1.

## **Discussion**

In this study we sought to more directly address the mechanism of pharmacological chaperone-mediated rescue of CHI trafficking mutations, and simultaneously probe the structural basis for recognition of diverse inhibitors by SUR1. We present three new cryo-EM structures bound to CBZ, RPG, and in the absence of ligand at SUR1 (ATP only) and compare to our previous GBC-bound structure. We find that overall the inhibitor bound structures are nearly identical, and that inhibitor binding to SUR1 has very little impact on the overall structure of SUR1 relative to SUR1 ligand-free. This may not be that surprising, as sulfonylureas are thought to stabilize the “inward-facing” conformation of SUR1 (Ortiz et al., 2012) and consequently reduce MgADP stimulation (Proks et al., 2014). This is actually what we observe

in our data, where inhibitor-bound SUR1 was simply rigidified relative to ligand free which improved the resolution of this region, particularly around the sulfonylurea binding site. However, we cannot rule out that ATP binding to Kir6.2 also stabilizes SUR1 in an inward-facing conformation, and this contributes to structural similarity between inhibitor-bound SUR1 vs. apo SUR1. A true apo structure of the channel complex (i.e. both SUR1 and Kir6.2 ligand-free) would help to clarify this.

Within the context of an ATP-bound Kir6.2 structure, we observe a rigid-body rotation and translation of the Kir6.2 CTD upon GBC/CBZ/RPG binding to SUR1. This is interesting in light of the fact that we also observe significant density within the inner vestibule of SUR1 which appears to be strengthened in drug-bound states. Based on a wealth of experimental data, this density is likely the distal N-terminus of Kir6.2, particularly given the fact that this region has long been thought to contribute directly to sulfonylurea and repaglinide binding. Thus GBC/CBZ/RPG may induce this rotation by binding to a pocket comprising SUR1 and the distal N-terminus, which in turn applies a force on the CTD to prevent further rotation (likely in the opposite direction) which is needed for the gates to open (see the following *Conclusions and Perspectives* chapter for further discussion).

This also has implications for the mechanism by which these drugs overcome CHI trafficking mutations in TMD0. We had previously provided indirect evidence that CBZ and GBC bind to the same site on SUR1 (Devaraneni et al., 2015) probably located somewhere within TMD2 based on the well-characterized S1238Y mutation (Ashfield et al., 1999), which abolishes high affinity sulfonylurea inhibition. Here we provide definitive evidence these two drugs, along with the other potent PC repaglinide, each bind to the same site within the inner TM bundle comprising residues from both TMD1 and TMD2, which does in fact contain S1238 and

also very likely the distal N-terminus of Kir6.2. We also show that mutation of a subset of these residues abolishes the ability of the CBZ and GBC to rescue TMD0 trafficking mutations, thus providing conclusive evidence of these drugs' status as PCs. This also helps clarify how drug binding to the sulfonylurea site can act in trans to overcome defects caused by mutations within TMD0, which is known to not interact directly with sulfonylureas. Because TMD0 is a completely separate domain with very little direct interaction with TMD1/TMD2 of SUR1 ((Martin, Kandasamy, et al., 2017; Martin et al., 2016), it seems unlikely that PCs overcome or prevent misfolding of TMD0 trafficking mutations at the site of the mutation. Rather, by directly binding to and stabilizing the distal N-terminus of Kir6.2, they help stabilize an otherwise transient interaction which is nonetheless crucial for assembly and trafficking of the channel complex out of the ER.

However, at present we cannot definitively assign the observed density to the N-terminus, thus this mechanism still remains speculative. Yet this is a very important point, because if this mechanism holds it suggests that rescue of these CHI trafficking mutations may simply rely on stabilizing the interaction of the N-terminus of Kir6.2 within the inner vestibule of SUR1 during assembly in the ER, and there may be other more effective ways to achieve this than inhibitor binding to the sulfonylurea site, which ultimately limits activity of rescued channels at the cell surface. Future experiments, likely a combination of biochemistry and structural biology, are needed to clarify this point, as the mechanism by which these drugs exert chaperone effects on  $K_{ATP}$  channels has direct implications for CHI patients with this class of mutation in TMD0.

## Figure Legends

**Figure 1.** The  $K_{ATP}$  channel in the presence of the diverse allosteric inhibitors. (A) Chemical structures of the drugs used in this study (carbamazepine and repaglinide) and our previous study (glibenclamide). (B) Comparison of overall structures of the  $K_{ATP}$  channel bound to CBZ and GBC, both in the presence of inhibitory ATP. Structures were aligned relative to the transmembrane domain of Kir6.2. CBZ+ATP is colored in tan, while GBC+ATP is in blue. In magenta are the locations of CBZ, within the TMs of SUR1 near the inner leaflet of the bilayer, and ATP, on the surface of the cytoplasmic domain which faces TMD0/L0. (C) Comparison of overall structures of the  $K_{ATP}$  channel bound to RPG and GBC, both in the presence of inhibitory ATP. Structures were aligned as in (B). GBC+ATP structure is colored blue, and RPG+ATP in cyan. The location of RPG and ATP are again shown by magenta spheres. Note overall similarity of structures bound each inhibitor.

**Figure 2.** The allosteric inhibitor binding site on SUR1. (A) Structure of inhibitor-bound SUR1, showing only L0 and the ABC core structure. Red box outlines the binding pocket shown in more detail in 2B-2E. Gray bars indicate approximate positions of the bilayer. (B-E) Structure of inhibitor binding site with experimental cryo-EM density map overlaid, all displayed after amplitude correction and low-pass filtering at the appropriate resolution. (B) ATP only. (C) CBZ + ATP. (D) GBC + ATP (PDB 6BAA; EMBD 7073). (E) RPG + ATP.

**Figure 3.** Details of GBC and RPG interaction in the sulfonylurea binding pocket.

Glibenclamide (GBC) and repaglinide (RPG) occupy slightly different subvolumes of the same binding pocket on SUR1, but appear to rely on a cluster of basic/polar residues N1245, R1246,

and R1300. (A) Structure of GBC+ATP (6BAA). (B) Structure of RPG+ATP. (C) Side-chain rearrangements between GBC+ATP (green) and RPG+ATP (purple). Arrows note direction of change from GBC to RPG structures. For W430, the direction of motion is mostly in the Z axis (coming out of the page).

**Figure 4.** The effect of inhibitory ligand binding to SUR1 on the structure of SUR1 and Kir6.2. (A) Comparison of SUR1 structure in the presence of ATP only (this paper, colored in orange) and ATP+GBC (6BAA, colored in blue). TMD0 and L0 are removed for clarity, but these also exhibit no observable change at the resolution of these reconstructions. (B) Structural difference in Kir6.2 in ATP and ATP+GBC states. The same conformation is seen in RPG and CBZ states. Only 2 of 4 subunits are shown for clarity. Note a  $\sim 3\text{\AA}$  vertical translation towards the membrane and a  $10^\circ$  clockwise rotation, as viewed down the pore from the extracellular side. (C) Cross-section of TMD1 and TMD2 of SUR1 in ATP, ATP+GBC/CBZ/RPG states, showing relative locations of each ligand.

**Figure 5.** Inhibitor binding to SUR1 strengthens a cytoplasmic interface between SUR1 and Kir6.2. Vertical translation of the Kir6.2 CTD in the GBC/CBZ/RPG + ATP structures (navy blue) relative to ATP only (orange) brings an N-terminal beta strand  $\beta A$  in close association with ICL1 of TMD0. This may contribute to the ability of these SUR1 ligands to stabilize the association between SUR1 and Kir6.2.

**Figure 6.** Location of the putative Kir6.2 N-terminus. (A) Cryo-EM density map of CBZ-bound SUR1 after amplitude correction and low-pass filtering to  $6\text{\AA}$ . L0 is colored in green, TMD1/NBD1 in dark blue and TMD2/NBD2 in light blue. In yellow is CBZ, and in magenta is the putative N-terminus of Kir6.2. Note direct contact between the magenta and yellow, suggesting the Kir6.2 N-terminus is directly involved in drug binding. (B) Cryo-EM density

map of ligand-free SUR1 (ATP only). L0 is in green, TMD1/NBD1 in orange, TMD2/NBD2 in light blue, and putative Kir6.2 N-terminus in magenta.

**Figure 7.** Functional validation of SUR1 binding site model by  $^{86}\text{Rb}^+$  efflux. COS cells were co-transfected with WT Kir6.2 and WT or mutant SUR1, with residues deemed important for drug binding each mutated to Ala. Cells were pre-treated with metabolic inhibitors (1mM deoxyglucose, 2.5 $\mu\text{g}/\text{ml}$  oligomycin) for 30 minutes (which activate  $\text{K}_{\text{ATP}}$  channels) in the presence of 0.1% DMSO (control), 100nM glibenclamide, 1 $\mu\text{M}$  repaglinide, or 50 $\mu\text{M}$  CBZ. Channel activity is reported as the amount of  $^{86}\text{Rb}^+$  in the efflux solution divided by the total amount of  $^{86}\text{Rb}^+$  in the well (efflux solution plus cell lysate).

**Figure 8.** Binding site mutations impair the ability of GBC and CBZ to rescue trafficking mutations within TMD0. COS cells were co-transfected with WT Kir6.2 and WT SUR1 (control), or WT Kir6.2 and F27S-SUR1 with or without GBC/CBZ binding site mutations. During expression, cells were treated with 0.1% DMSO (control), 5 $\mu\text{M}$  GBC, or 10 $\mu\text{M}$  CBZ. Cell were lysed 40 to 48 hours post-transfection and western blots were run for SUR1 and tubulin (loading control). The lower band of SUR1 corresponds to either SUR1 as a monomer or part of partially or fully assembled complexes with Kir6.2, while the upper band corresponds to SUR1 post-medial Golgi or at the plasma membrane as part of fully-assembled  $\text{K}_{\text{ATP}}$  channels.

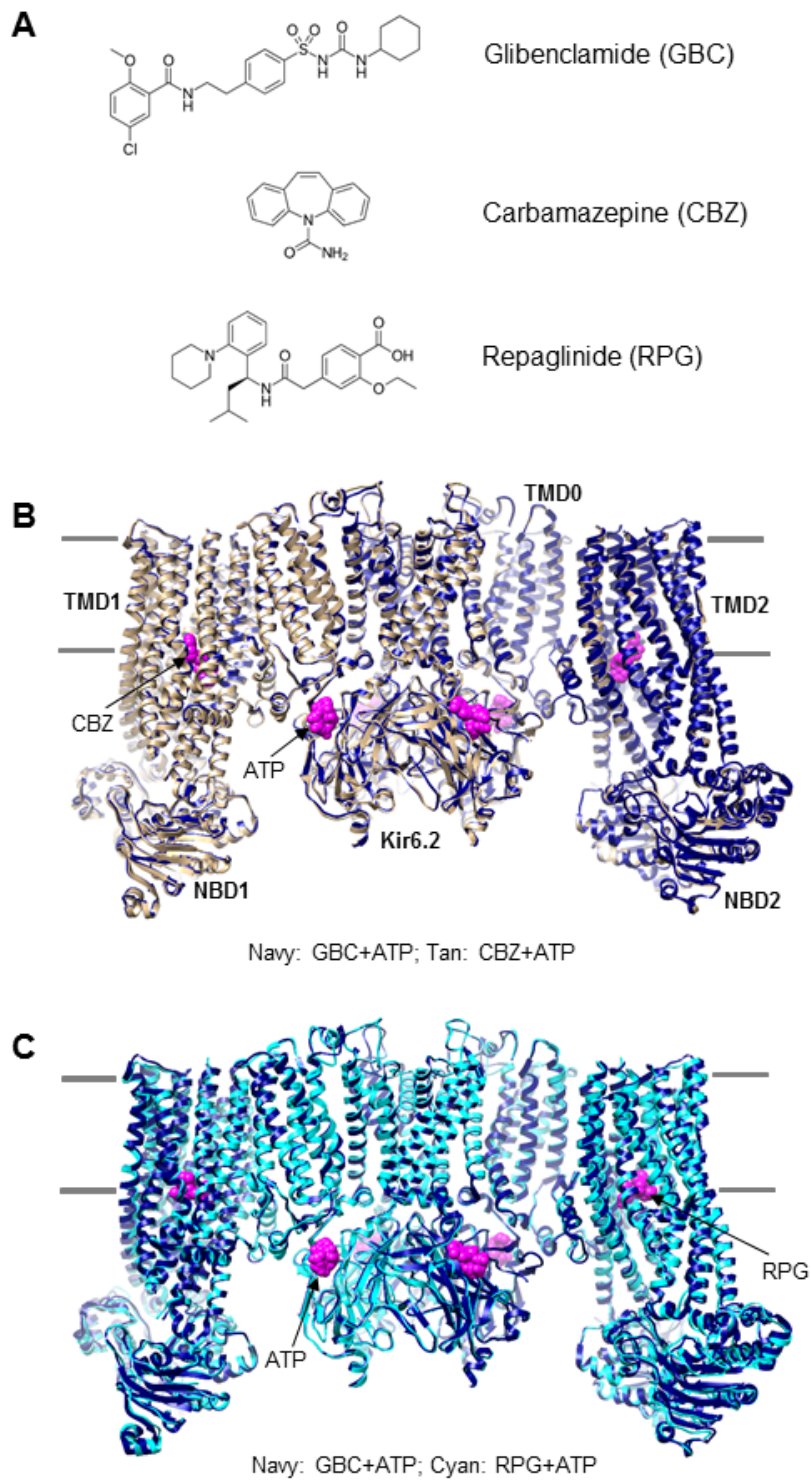


**Figure 1**

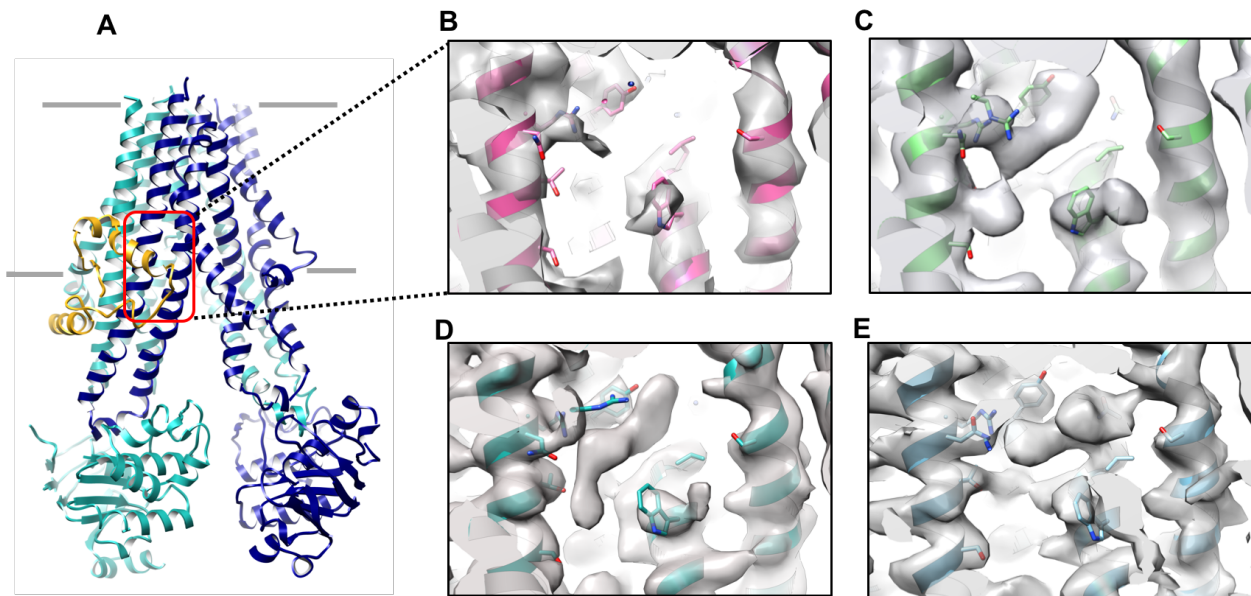


**Figure 2**

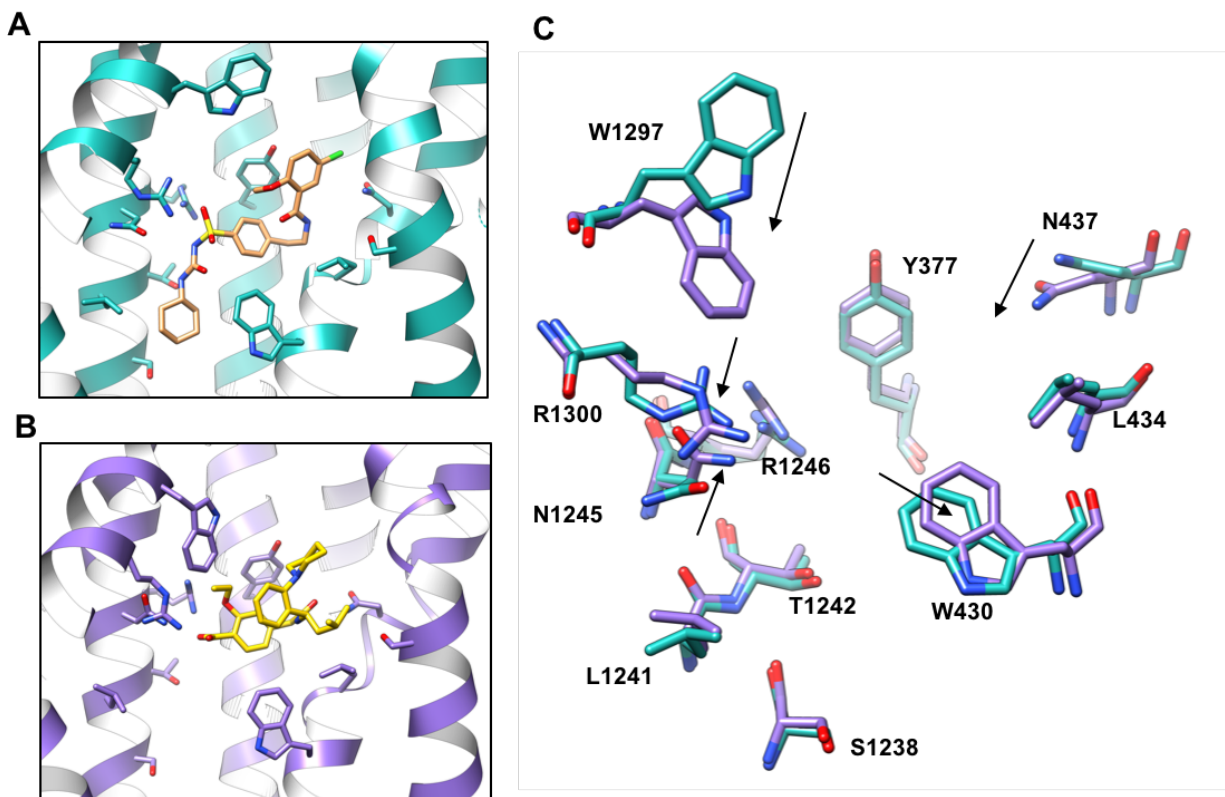


**Figure 3**

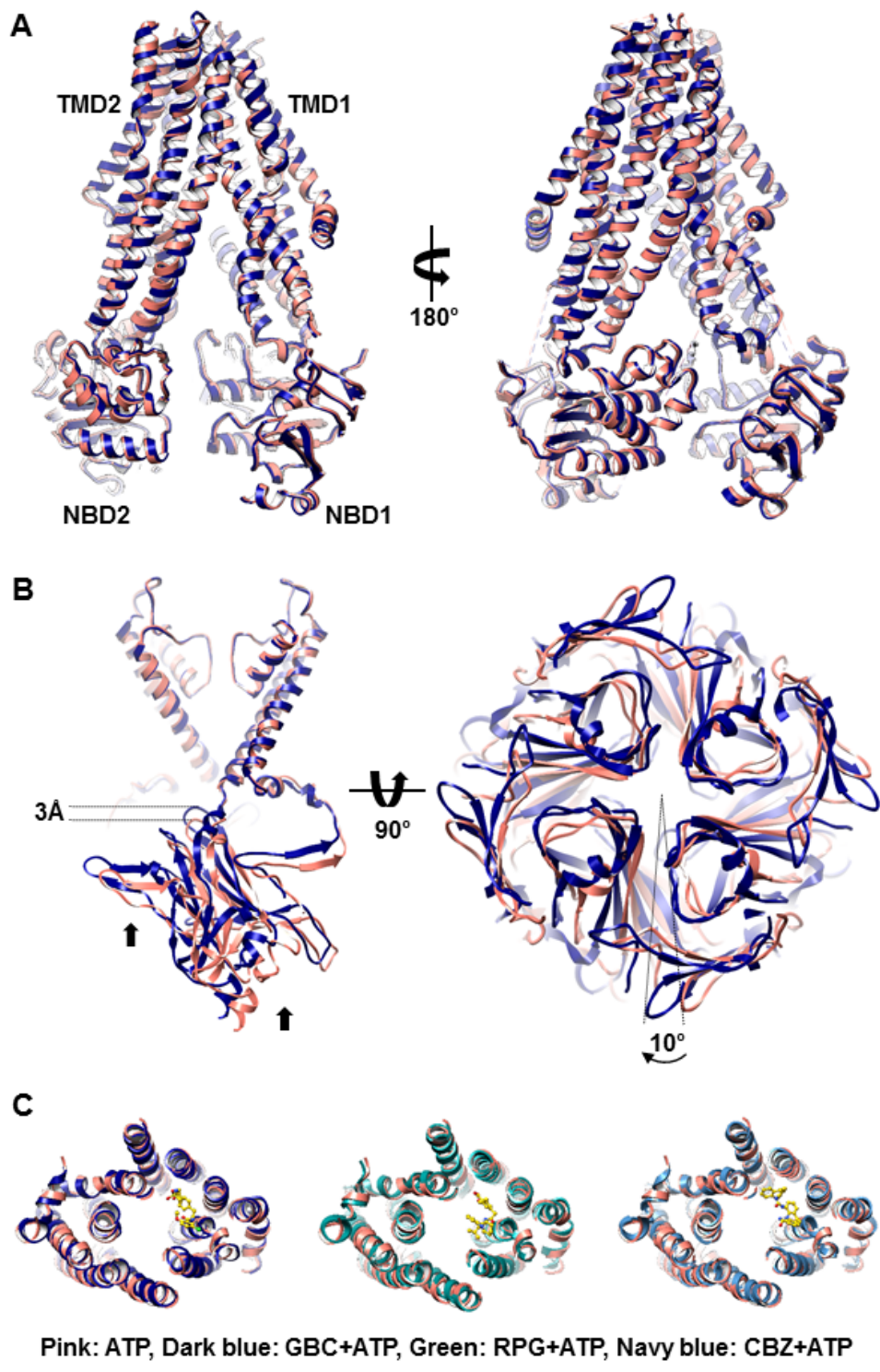


**Figure 4**

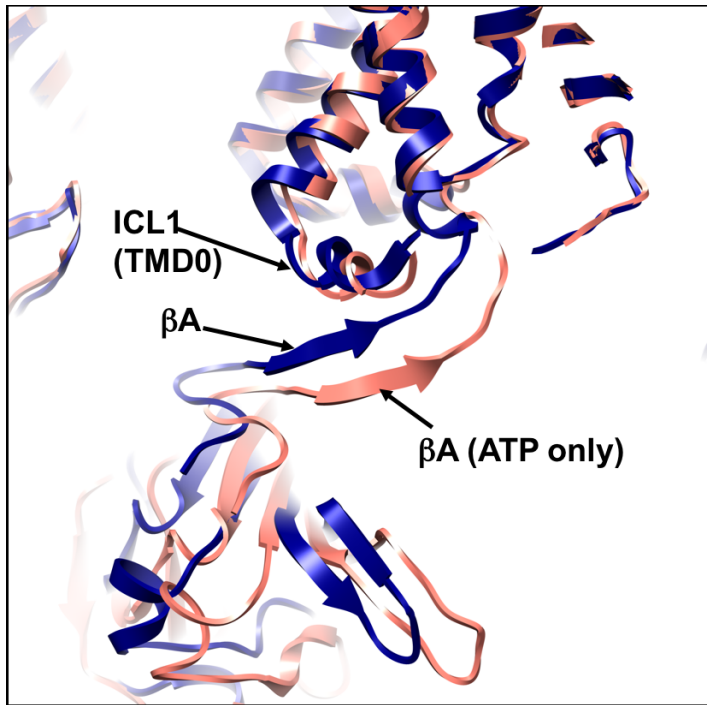


**Figure 5**

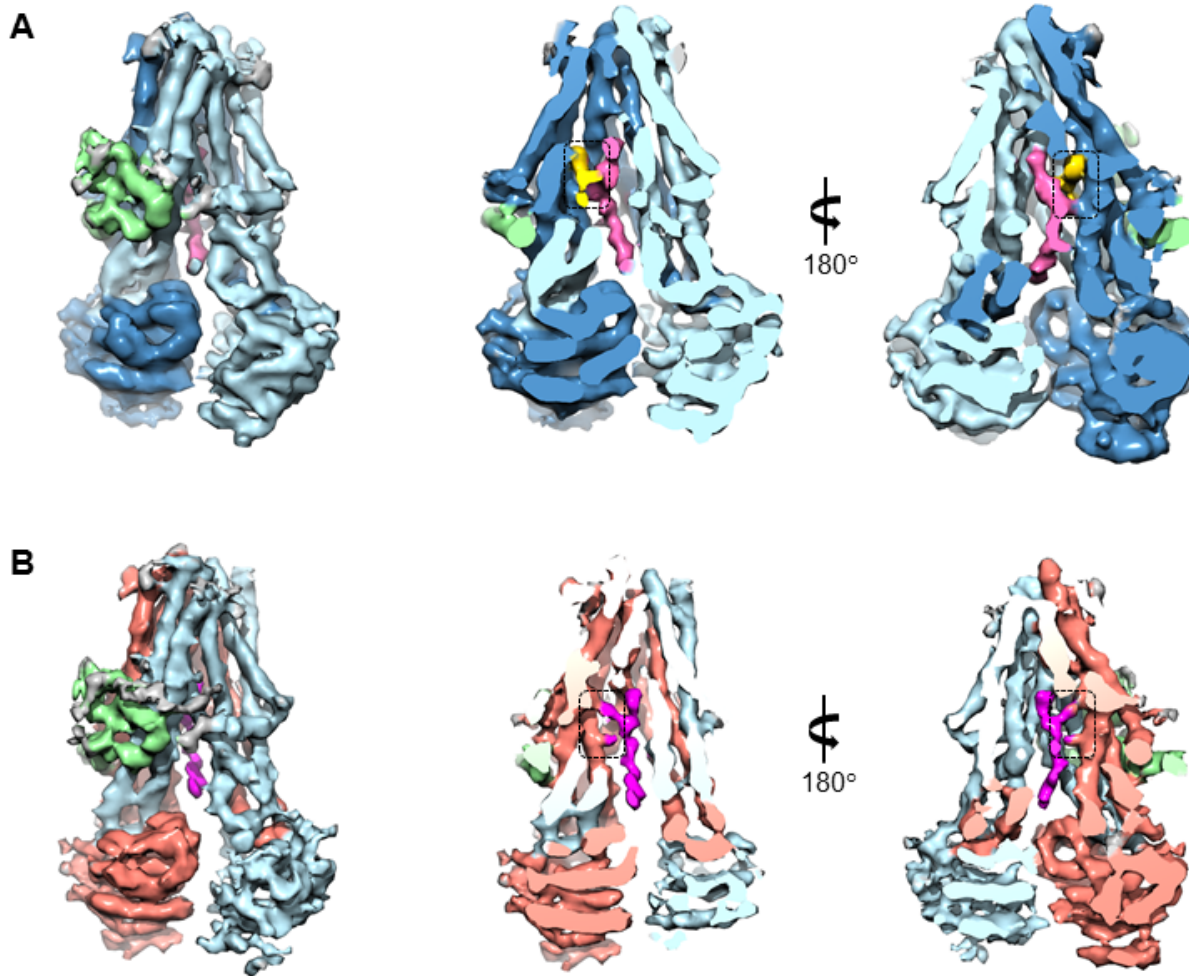


**Figure 6**

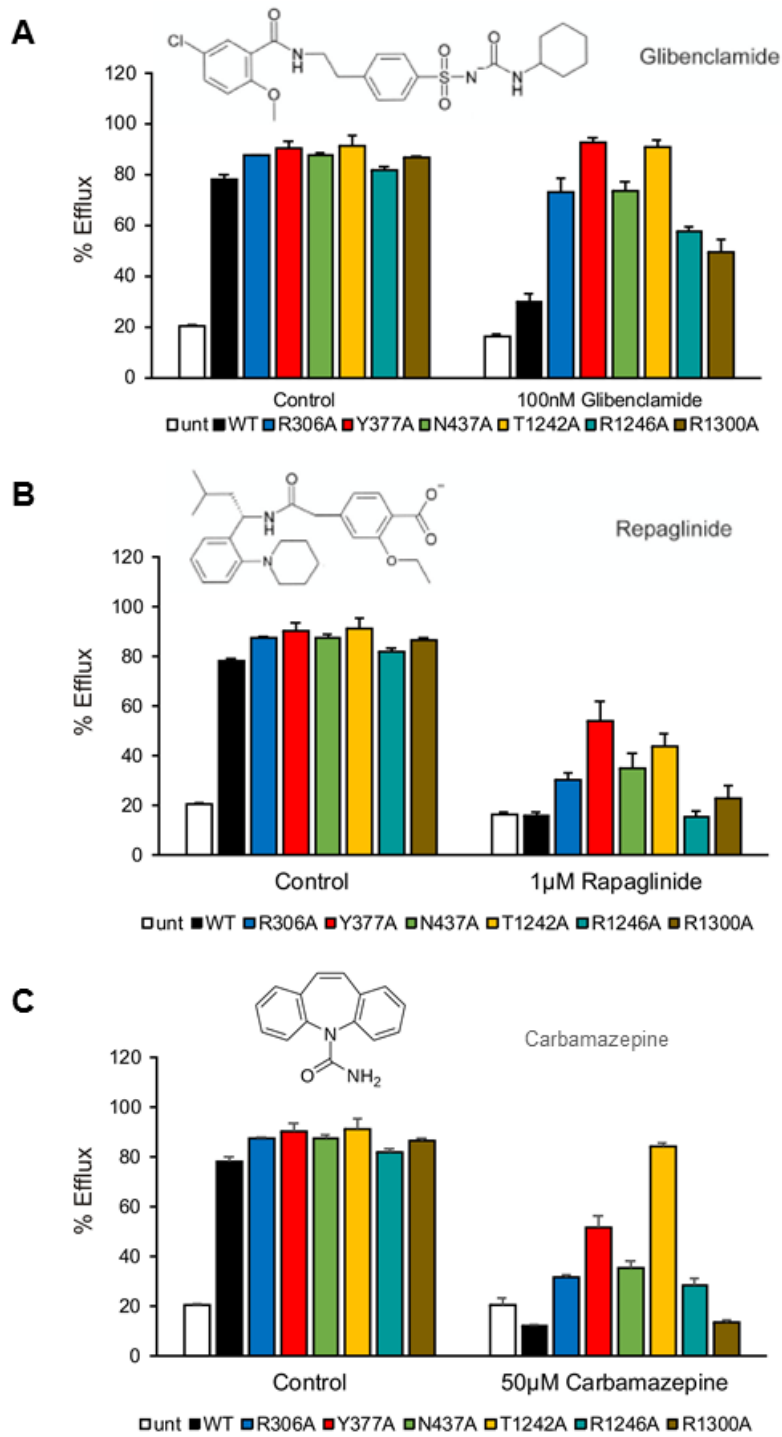


**Figure 7**

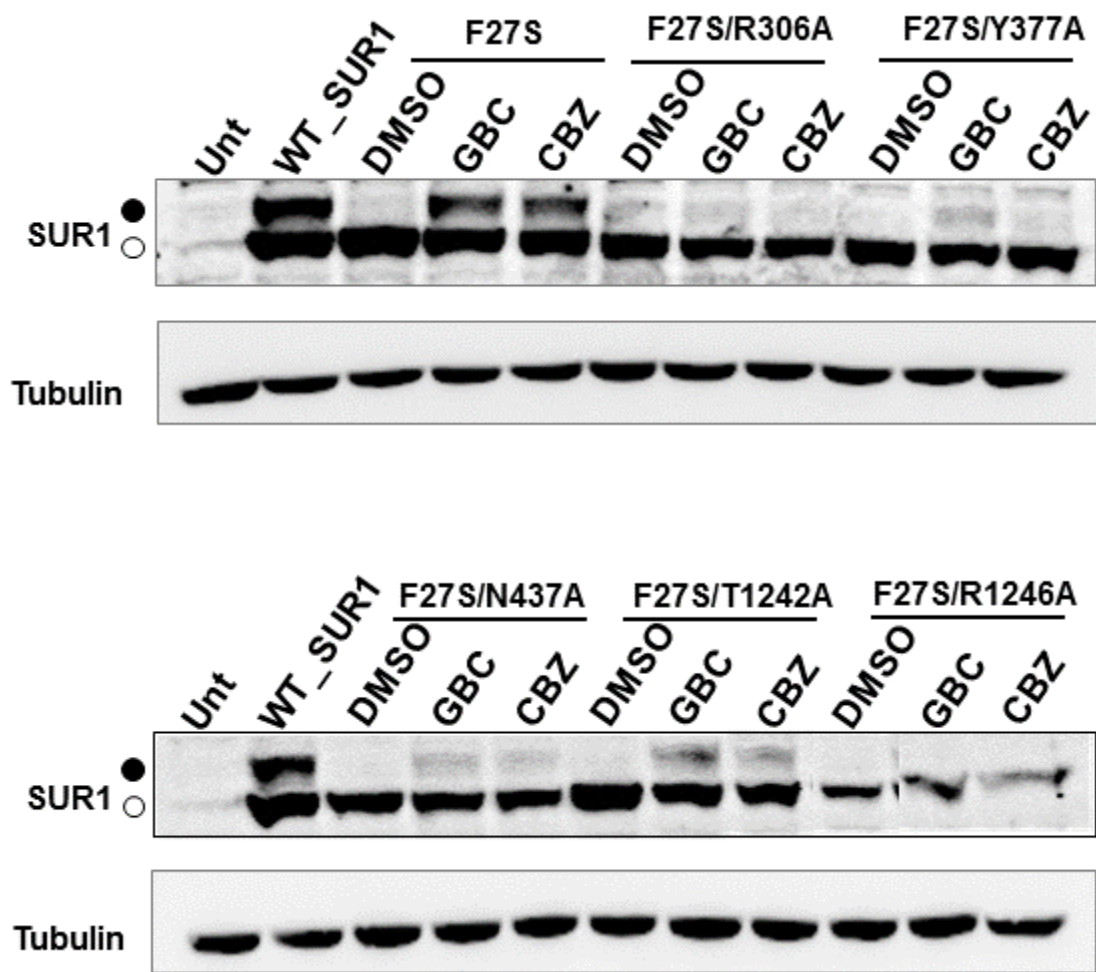


**Figure 8**

## References Cited

- Aguilar-Bryan, L., Bryan, J., & Nakazaki, M. (2001). Of mice and men: K(ATP) channels and insulin secretion. *Recent Prog Horm Res*, *56*, 47-68.
- Ashcroft, F. M. (2007). The Walter B. Cannon Physiology in Perspective Lecture, 2007. ATP-sensitive K<sup>+</sup> channels and disease: from molecule to malady. *Am J Physiol Endocrinol Metab*, *293*(4), E880-889. doi:10.1152/ajpendo.00348.2007
- Ashfield, R., Gribble, F. M., Ashcroft, S. J., & Ashcroft, F. M. (1999). Identification of the high-affinity tolbutamide site on the SUR1 subunit of the K(ATP) channel. *Diabetes*, *48*(6), 1341-1347.
- Babenko, A. P., & Bryan, J. (2002). SUR-dependent modulation of KATP channels by an N-terminal KIR6.2 peptide. Defining intersubunit gating interactions. *J Biol Chem*, *277*(46), 43997-44004. doi:10.1074/jbc.M208085200
- Babenko, A. P., & Bryan, J. (2003). Sur domains that associate with and gate KATP pores define a novel gatekeeper. *J Biol Chem*, *278*(43), 41577-41580. doi:10.1074/jbc.C300363200
- Babenko, A. P., Gonzalez, G., & Bryan, J. (1999). The N-terminus of KIR6.2 limits spontaneous bursting and modulates the ATP-inhibition of KATP channels. *Biochem Biophys Res Commun*, *255*(2), 231-238. doi:10.1006/bbrc.1999.0172
- Chan, K. W., Zhang, H., & Logothetis, D. E. (2003). N-terminal transmembrane domain of the SUR controls trafficking and gating of Kir6 channel subunits. *EMBO J*, *22*(15), 3833-3843. doi:10.1093/emboj/cdg376
- Chen, P. C., Olson, E. M., Zhou, Q., Kryukova, Y., Sampson, H. M., Thomas, D. Y., & Shyng, S. L. (2013). Carbamazepine as a novel small molecule corrector of trafficking-impaired ATP-sensitive potassium channels identified in congenital hyperinsulinism. *J Biol Chem*, *288*(29), 20942-20954. doi:10.1074/jbc.M113.470948
- Clement, J. P. t., Kunjilwar, K., Gonzalez, G., Schwanstecher, M., Panten, U., Aguilar-Bryan, L., & Bryan, J. (1997). Association and stoichiometry of K(ATP) channel subunits. *Neuron*, *18*(5), 827-838.
- Cruz Cabeza, A. J., Day, G. M., Motherwell, W. D. S., & Jones, W. (2007). Importance of Molecular Shape for the Overall Stability of Hydrogen Bond Motifs in the Crystal Structures of Various Carbamazepine-Type Drug Molecules. *Crystal Growth and Design*, *7*(1), 100-107.
- Devaraneni, P. K., Martin, G. M., Olson, E. M., Zhou, Q., & Shyng, S. L. (2015). Structurally distinct ligands rescue biogenesis defects of the KATP channel complex via a converging mechanism. *J Biol Chem*, *290*(12), 7980-7991. doi:10.1074/jbc.M114.634576
- Enkvetchakul, D., Loussouarn, G., Makhina, E., & Nichols, C. G. (2001). ATP interaction with the open state of the K(ATP) channel. *Biophys J*, *80*(2), 719-728. doi:10.1016/S0006-3495(01)76051-1
- Hansen, A. M., Hansen, J. B., Carr, R. D., Ashcroft, F. M., & Wahl, P. (2005). Kir6.2-dependent high-affinity repaglinide binding to beta-cell K(ATP) channels. *Br J Pharmacol*, *144*(4), 551-557. doi:10.1038/sj.bjp.0706082
- Hansen, S. B., Tao, X., & MacKinnon, R. (2011). Structural basis of PIP<sub>2</sub> activation of the classical inward rectifier K<sup>+</sup> channel Kir2.2. *Nature*, *477*(7365), 495-498. doi:10.1038/nature10370
- Inagaki, N., Gono, T., & Seino, S. (1997). Subunit stoichiometry of the pancreatic beta-cell ATP-sensitive K<sup>+</sup> channel. *FEBS Lett*, *409*(2), 232-236.

- Johnson, Z. L., & Chen, J. (2017). Structural Basis of Substrate Recognition by the Multidrug Resistance Protein MRP1. *Cell*, *168*(6), 1075-1085 e1079. doi:10.1016/j.cell.2017.01.041
- Koster, J. C., Sha, Q., Shyng, S., & Nichols, C. G. (1999). ATP inhibition of KATP channels: control of nucleotide sensitivity by the N-terminal domain of the Kir6.2 subunit. *J Physiol*, *515* ( Pt 1), 19-30.
- Lee, K. P. K., Chen, J., & MacKinnon, R. (2017). Molecular structure of human KATP in complex with ATP and ADP. *Elife*, *6*. doi:10.7554/eLife.32481
- Li, J., Lu, S., Liu, Y., Pang, C., Chen, Y., Zhang, S., . . . An, H. (2015). Identification of the Conformational transition pathway in PIP2 Opening Kir Channels. *Sci Rep*, *5*, 11289. doi:10.1038/srep11289
- Martin, G. M., Chen, P. C., Devaraneni, P., & Shyng, S. L. (2013). Pharmacological rescue of trafficking-impaired ATP-sensitive potassium channels. *Front Physiol*, *4*, 386. doi:10.3389/fphys.2013.00386
- Martin, G. M., Kandasamy, B., DiMaio, F., Yoshioka, C., & Shyng, S. L. (2017). Anti-diabetic drug binding site in a mammalian KATP channel revealed by Cryo-EM. *Elife*, *6*. doi:10.7554/eLife.31054
- Martin, G. M., Rex, E. A., Devaraneni, P., Denton, J. S., Boodhansingh, K. E., DeLeon, D. D., . . . Shyng, S. L. (2016). Pharmacological Correction of Trafficking Defects in ATP-Sensitive Potassium Channels Caused by Sulfonylurea Receptor 1 Mutations. *J Biol Chem*. doi:10.1074/jbc.M116.749366
- Martin, G. M., Yoshioka, C., Rex, E. A., Fay, J. F., Xie, Q., Whorton, M. R., . . . Shyng, S. L. (2017). Cryo-EM structure of the ATP-sensitive potassium channel illuminates mechanisms of assembly and gating. *Elife*, *6*. doi:10.7554/eLife.24149
- Nichols, C. G. (2006). KATP channels as molecular sensors of cellular metabolism. *Nature*, *440*(7083), 470-476. doi:10.1038/nature04711
- Ortiz, D., Voyvodic, P., Gossack, L., Quast, U., & Bryan, J. (2012). Two neonatal diabetes mutations on transmembrane helix 15 of SUR1 increase affinity for ATP and ADP at nucleotide binding domain 2. *J Biol Chem*, *287*(22), 17985-17995. doi:10.1074/jbc.M112.349019
- Pratt, E. B., Tewson, P., Bruederle, C. E., Skach, W. R., & Shyng, S. L. (2011). N-terminal transmembrane domain of SUR1 controls gating of Kir6.2 by modulating channel sensitivity to PIP2. *J Gen Physiol*, *137*(3), 299-314. doi:10.1085/jgp.201010557
- Proks, P., de Wet, H., & Ashcroft, F. M. (2014). Sulfonylureas suppress the stimulatory action of Mg-nucleotides on Kir6.2/SUR1 but not Kir6.2/SUR2A KATP channels: a mechanistic study. *J Gen Physiol*, *144*(5), 469-486. doi:10.1085/jgp.201411222
- Rorsman, P., & Trube, G. (1985). Glucose dependent K<sup>+</sup>-channels in pancreatic beta-cells are regulated by intracellular ATP. *Pflugers Arch*, *405*(4), 305-309.
- Shyng, S., & Nichols, C. G. (1997). Octameric stoichiometry of the KATP channel complex. *J Gen Physiol*, *110*(6), 655-664.
- Stanley, C. A. (2016). Perspective on the Genetics and Diagnosis of Congenital Hyperinsulinism Disorders. *J Clin Endocrinol Metab*, *101*(3), 815-826. doi:10.1210/jc.2015-3651
- Vila-Carriles, W. H., Zhao, G., & Bryan, J. (2007). Defining a binding pocket for sulfonylureas in ATP-sensitive potassium channels. *FASEB J*, *21*(1), 18-25. doi:10.1096/fj.06-6730hyp
- Whorton, M. R., & MacKinnon, R. (2011). Crystal structure of the mammalian GIRK2 K<sup>+</sup> channel and gating regulation by G proteins, PIP2, and sodium. *Cell*, *147*(1), 199-208. doi:10.1016/j.cell.2011.07.046

- Whorton, M. R., & MacKinnon, R. (2013). X-ray structure of the mammalian GIRK2-beta-gamma G-protein complex. *Nature*, 498(7453), 190-197. doi:10.1038/nature12241
- Wu, J. X., Ding, D., Wang, M., Kang, Y., Zeng, X., & Chen, L. (2018). Ligand binding and conformational changes of SUR1 subunit in pancreatic ATP-sensitive potassium channels. *Protein Cell*. doi:10.1007/s13238-018-0530-y
- Yan, F., Lin, C. W., Weisiger, E., Cartier, E. A., Taschenberger, G., & Shyng, S. L. (2004). Sulfonylureas correct trafficking defects of ATP-sensitive potassium channels caused by mutations in the sulfonylurea receptor. *J Biol Chem*, 279(12), 11096-11105. doi:10.1074/jbc.M312810200
- Yan, F. F., Casey, J., & Shyng, S. L. (2006). Sulfonylureas correct trafficking defects of disease-causing ATP-sensitive potassium channels by binding to the channel complex. *J Biol Chem*, 281(44), 33403-33413. doi:10.1074/jbc.M605195200
- Yan, F. F., Lin, Y. W., MacMullen, C., Ganguly, A., Stanley, C. A., & Shyng, S. L. (2007). Congenital hyperinsulinism associated ABCC8 mutations that cause defective trafficking of ATP-sensitive K<sup>+</sup> channels: identification and rescue. *Diabetes*, 56(9), 2339-2348. doi:10.2337/db07-0150
- Zerangue, N., Schwappach, B., Jan, Y. N., & Jan, L. Y. (1999). A new ER trafficking signal regulates the subunit stoichiometry of plasma membrane K(ATP) channels. *Neuron*, 22(3), 537-548.

## Chapter 6: Conclusions and Perspectives

Ever since it was discovered that the  $K_{ATP}$  channel was an obligate complex of a  $K^+$  channel (Kir6.2) and an ABC transporter (SUR1), the field has wondered what such a protein would look like. How has nature married two proteins from completely different and unrelated protein families? What sort of structures did it come up with in order to translate the intracellular energy state into electricity?

When I entered the field in 2013, the only structural information we had on the  $K_{ATP}$  channel complex came from a  $\sim 20\text{\AA}$  resolution cryo-EM map, which suggested the overall dimensions of the complex but was otherwise uninformative (Mikhailov et al., 2005). My timing turned out to be fortuitous, as a convergence of advances in camera technology and image processing software created a “revolution” in which near-impossible structural projects like the  $K_{ATP}$  channel could now potentially be solved to near-atomic resolution by cryo-EM.

Until I was aware of this seismic shift in structural biology, I had been doing what many good  $K_{ATP}$  channel biochemists and physiologists normally do: screening mutants, testing expression, recording activity, and trying to interpret the data within a generalizable model. But in terms of the CHI trafficking mutations within TMD0 of SUR1, which I had been studying, traditional approaches wouldn't allow us to fully answer questions like (1) why only mutations in TMD0 could be rescued by pharmacological chaperones like CBZ and GBC; (2) why Kir6.2 was necessary for the rescue effect; (3) why  $K_{ATP}$  channel PCs are all inhibitors; and (4) how inhibitor binding to a site outside of TMD0 can overcome defects specifically in this domain. Thus the work laid out in this dissertation is an attempt to answer these questions more directly with cryo-EM. These studies have greatly advanced our understanding of the mechanism of

K<sub>ATP</sub> channel regulation by diverse inhibitors and finally make possible rational drug design campaigns for this critical regulator of glucose homeostasis.

### **What can these structures tell us about K<sub>ATP</sub> channel gating?**

The hallmarks of K<sub>ATP</sub> channel ligand-dependent gating are (1) PIP2 is necessary for channel opening; (2) Kir6.2 has low intrinsic PIP2 sensitivity which is increased roughly 10-fold by SUR1; (3) ATP<sup>4-</sup> closes K<sub>ATP</sub> channels by interaction with Kir6.2; (4) SUR1 also increases the ATP sensitivity of Kir6.2 roughly 10-fold; (5) MgADP-induced dimerization of the SUR1 NBDs antagonizes ATP inhibition to increase channel P<sub>O</sub>. Multiple other groups have elucidated the structural change in SUR1 resulting from MgATP/ADP-dimerization of the NBDs (Lee et al., 2017; Wu et al., 2018), but every structure solved so far is closed and without PIP2, thus we are left to speculate on the antagonistic effects of ATP and PIP2. Nevertheless, based on what is known regarding Kir channel gating and the vast amount of K<sub>ATP</sub> channel experimental data, these structures allow for the genesis of some interesting hypotheses and a reasonable gating model.

#### *ATP sensitivity*

ATP and PIP2 display an inverse relationship, such that increased levels of one decrease sensitivity to the other (Fan & Makielski, 1999), thus we would expect that ATP either directly remodels the PIP2 binding site to decrease PIP2 affinity or that PIP2 disfavors interaction with the closed state. In Kir6.2, the PIP2 binding pocket is thought to comprise residues from the slide helix of one subunit (R54), and the base of the M1 helix (K67, W68) and the TMD-CTD linker (C-linker) (R176) of the adjacent subunit (Haider et al., 2007; Schulze et al., 2003). In my ATP+GBC structure, ATP binds to a pocket formed at the cytoplasmic interface of adjacent N- and C-terminal domains, just below the level of the slide helix and C-linker. Interestingly, the

putative PIP2-coordinating residue is oriented toward the ATP site and away from where PIP2 would bind. In this state, R54 appears to participate in an interaction network comprising R50, Q52, R54, and E179 which likely acts to stabilize interaction of R50 with the  $\gamma$ -phosphate of ATP. Based on this, I predict R54 is a “toggle,” the orientation of which is dependent on whether ATP or PIP2 is bound; thus ATP reduces PIP2 sensitivity directly via changes in R54.

As mentioned above, SUR1 also hypersensitizes Kir6.2 to ATP inhibition. In the ATP+GBC structure, we observe an N-terminal stretch of L0 in SUR1 (P201-L213), which immediately follows TMD0, within proximity of the ATP binding site and the Kir6.2 CTD, and at lower density map thresholds forms a link with R50 of Kir6.2. Our lab has shown that this segment has a profound effect on ATP sensitivity. Notably, E203 in L0 and Q52 in Kir6.2 form an interaction pair which can be physically cross-linked when both are mutated to Cys (E203C/Q52C) (Pratt et al., 2012). In this condition, the channel is locked in the closed state even in the absence of ATP, and the effect is immediately reversed upon addition of DTT. Based on numerous studies, it is expected that the Kir6.2 CTD must undergo a mostly rigid-body rotation as part of channel activation (see “Kir6.2 structure” in Chapter 1 for detailed discussion). Therefore ATP rigidifies the CTD and prevents channel activation by binding at the interface of adjacent subunits in the CTD that also involves the C-linker, which is thought to necessarily rearrange as the CTD rotates (Bavro et al., 2012; Li et al., 2015). Due to the close physical association, this N-terminal segment of L0 interacts with the CTD to either stabilize the CTD in an “ATP-competent” conformation, which would promote ATP binding, or with the true ATP-bound conformation to reduce ATP unbinding. In either case the result would be an apparent increase in ATP sensitivity of Kir6.2. This is actually observed experimentally, as another

variant of the E203/Q52 pair, E203K/Q52E, increases ATP sensitivity 100-fold (Pratt et al., 2012).

The crucial role of this cytoplasmic interface is further underscored by an unusually high density of neonatal diabetes (NDM) mutations found in this segment of L0 (P207-L213). This same stretch of amino acids was predicted to form a submembrane amphipathic helix called the "sliding helix" by analogy to the "slide helix" in Kir6.2 due to its important role in  $K_{ATP}$  channel gating (Babenko, 2005). Because of their status as NDM mutations, these all lead to increased channel opening, presumably through reduced ATP sensitivity and/or increased MgADP sensitivity. Interestingly, in each of my structures I observe a short helix corresponding to these residues which indeed shows a polar cytoplasmic face and hydrophobic membrane face. Therefore, I hypothesize that this segment of L0 stabilizes the Kir6.2 CTD in an ATP-bound conformation and moves laterally in the plane of the bilayer as a result of MgADP-induced dimerization of the NBDs; this rearrangement either modifies or weakens the L0-CTD interface, destabilizing ATP interaction and granting the CTD the mobility needed for channel activation.

All  $K_{ATP}$  structures solved thus far have either ATP or ADP bound to the ATP site on Kir6.2, and there is no observable rearrangement at this interface due to NBD dimerization. However, this hypothesis can be directly tested by solving a true MgADP-activated, PIP2-bound  $K_{ATP}$  channel structure. As MgADP antagonism of ATP inhibition is the only way  $K_{ATP}$  channels open in cells, due to intracellular ATP levels being >100-fold higher than the IC50 for ATP inhibition, visualization of this event is crucial to understanding  $K_{ATP}$  channel biology.

#### *The role of the Kir6.2 N-terminus*

In chapter 5, I speculate on the identify of unaccounted-for density within the inner vestibule of SUR1 which interacts directly with the sulfonylurea/CBZ/RPG binding site. We and

others (Wu et al., 2018) believe this to be the distal N-terminus of Kir6.2. In the absence of direct experimental validation, we rely on a significant amount of structure-function data which lead to this conclusion. Firstly, the distal N-terminus is clearly involved in interaction with sulfonylureas and glinides, as the N-terminal 20 amino acids are necessary for co-labelling of Kir6.2 with a photo-crosslinkable derivative of GBC (Vila-Carriles et al., 2007), and deletion of the N-terminal 14 residues reduces repaglinide affinity by ~100-fold (Hansen et al., 2005). Our lab has shown that two residues in the N-terminus, Y12 and A18, directly interact with SUR1 and that this interaction is strengthened by GBC and CBZ (Devaraneni et al., 2015).

Functionally, removal of the distal N-terminus ( $\Delta N32$ ) dramatically increases  $P_o$  (Babenko, Gonzalez, & Bryan, 1999) and reduces ATP sensitivity to roughly that of Kir6.2 channels expressed in the absence of SUR1 (Koster, Sha, Shyng, et al., 1999). Interestingly, addition of exogenous synthetic N-terminal peptide (Ntp) corresponding to the first 32 amino acids of Kir6.2 dose-dependently produced nearly the same effects on  $P_o$  (increase) and ATP sensitivity (decrease) as the  $\Delta N32$  truncation (Babenko & Bryan, 2002). Further, the effect was dependent on SUR1, as Ntp had no effect on Kir6.2 alone. This suggests that synthetic peptide can compete off native peptide for a binding site somewhere on SUR1, and that this interaction underlies the gating effects exerted by the N-terminus.

These data, together with our own CBZ/GBC/RPG-bound cryo-EM maps, in which SUR1 is in an "inward-facing" conformation, support a model in which the alternating access mechanism of the ABC transporter module of SUR1 determines its association with the Kir6.2 N-terminus. As in our structures, the N-terminus interacts with the SUR1 TMDs when they are open to the intracellular side. This interaction puts tension on the Kir6.2 CTD to stabilize the

closed state by preventing rotation of the CTD during the activation step of ligand-dependent gating (Figure 1A).

Thus allosteric inhibitors, like CBZ and GBC, which can inhibit channel activity in the absence of nucleotides (though not completely), achieve this by strengthening this interaction directly by simultaneously coordinating TMD1, TMD2, and the Kir6.2 N-terminus. This agrees well with data showing that the  $\Delta$ N32-Kir6.2 truncation abolishes the nucleotide independent inhibition of spontaneous  $K_{ATP}$  channel activity by sulfonylureas (Reimann et al., 1999). Upon MgADP/MgATP induced dimerization of the SUR1 NBDs, the vestibule closes which excludes the N-terminus (Figure 1B). This frees the CTD, which in general will increase  $P_O$  and by consequence reduce ATP sensitivity. This would explain how the  $\Delta$ N32 truncation produces both of the above functional effects, and how exogenous synthetic Ntp can also achieve the same result.

However, this still remains speculation absent direct evidence that this density in our maps is the N-terminus. Perhaps the most direct method is to solve a structure of SUR1 without Kir6.2, and even possibly with and without addition of the synthetic N-terminal peptide. If the density that once disappeared now reappears in SUR1+Ntp, then one has more or less definitive proof that the density is the N-terminus; then the task becomes to define the molecular nature of this compelling new interface.

### **What can the structure tell us about $K_{ATP}$ channel trafficking mutations?**

The driving force behind this dissertation has been to better understand the molecular basis for CHI trafficking mutations in TMD0, and how SUR1 allosteric inhibitors overcome only mutations in this domain. The structural work in chapters 2-4 has gone a long way toward this end. Importantly, we see that TMD0 is a compact and distinct domain which almost exclusively

mediates interactions between the ABC-core structure of SUR1 and Kir6.2. Thus at a coarse-grain level, we can understand how mutations could disrupt assembly of the complex. In terms of specific CHI mutations, the molecular defect appears fairly obvious. In the case of F27S, a well-characterized CHI mutation, we see that F27 is stacked closely against F95 in the M1 helix of Kir6.2, thus the mutation disrupts a key hydrophobic interface. In the case of R74W, we find that R74 forms a cation- $\pi$  interaction with Y124 of an adjacent helix; thus this may well be crucial for structural integrity of TMD0 itself.

More difficult to understand is how CBZ and GBC overcome the effect of these mutations. In comparing the ATP only structure with ATP+GBC, at the limit of the resolution of the ATP only map, the structures are identical. This is not surprising, as the sulfonylurea binding site is in TMD1/TMD2 of SUR1, which has almost no direct contact to TMD0. Thus it seems reasonable to conclude that CBZ and GBC are not actively correcting a folding defect in TMD0. As a consequence, they must act by stabilizing a misfolded conformation, thus the mutations are tolerated rather than truly corrected.

If our assignment of the inner vestibule density in SUR1 is correct and it is the N-terminus, this has profound implications for this discussion. As we had shown previously, the chaperone mechanism of sulfonylureas is dependent on Kir6.2 (Yan et al., 2006); thus in light of the structural data herein, CBZ and GBC must act by stabilizing an interface, and this interface comprises helices TMD1/TMD2 in SUR1 and the Kir6.2 N-terminus.

A critical point is whether stabilization of this interface is sufficient to rescue TMD0 trafficking mutations. If in the future we obtain residue-residue contact information regarding this interface, then we could test this directly, perhaps by engineering disulfide bonds to lock the interaction. Moreover, if this interface turns out to be both necessary and sufficient for the

trafficking rescue effect, then we could potentially try and design alternative ways to stabilize it outside of channel inhibitors. This would be a huge step towards realizing a therapy for patients with this class of mutation.

### **What have we learned from other $K_{ATP}$ channel structures?**

Cryo-EM structures of the channel complex published from two other groups during 2017 and early 2018 have broadened our understanding of  $K_{ATP}$  channel function. Here I will summarize what can (and cannot) be gleaned from these studies.

The first published structures of the channel complex were from our group (Martin, Yoshioka, et al., 2017) and a group in Beijing (Li et al., 2017), both using rodent SUR1 and Kir6.2 constructs. Our structure was solved in the presence of ATP and GBC, and theirs in the presence of GBC only. Interestingly, the GBC and GBC+ATP structures are nearly identical, at least at the main chain level. This is interesting, as it suggests that either 1) GBC stabilizes an ATP-bound conformation of Kir6.2, or 2) GBC and ATP-bound states are distinct, but the GBC-bound conformation is thermodynamically favored.

Despite the moderate resolution of our reconstruction (5-6Å), we were able to confidently identify the ATP binding site on Kir6.2, which was nearly exactly where the field had predicted based on decades of experiments. We left GBC unmodelled at this point, however, as much less was known regarding the GBC binding site and SUR1 was in general lower resolution than Kir6.2. This was in spite of unmodelled cryo-EM density close to S1238 in TM16, a predicted GBC-binding residue. The Beijing group identified what they considered non-protein density near W232, another suspected GBC-interacting residue, and suggested a "tentative" model for GBC binding. Examination of their deposited experimental density map stressed the "tentativeness" of this model, as what they considered ligand could have easily been portions of

L0 they left unmodelled. This uncertainty provided the impetus to solve another, higher resolution GBC-bound structure as in Chapter 4 (Martin, Yoshioka, et al., 2017), in which we were able to clearly identify GBC, which was near S1238 as suspected, and also show that the density the Beijing group had identified as GBC was indeed unmodelled L0.

Shortly after publication of our high resolution structure, a group at Rockefeller University published two  $K_{ATP}$  channel structures, which corresponded to the two dominant classes obtained from a dataset collected in the presence of MgATP and PIP2 (Lee et al., 2017). Presumably this was an attempt to capture the Mg-nucleotide and PIP2-bound activated/open state of the channel, as the structures so far had been bound to inhibitors with closed HBC and G-loop gates. Despite the presence of PIP2, both structures have inhibitory ATP bound to Kir6.2 and are closed at both gates. This suggests that under these conditions (8mM MgATP and 0.15mM PIP2), the ATP-bound state is favored and that this state is inaccessible to or has very low affinity for PIP2.

The fact that they did not observe any PIP2-bound activated/open classes is surprising, as one observes strong channel activation in the presence of saturating MgATP as long as there is sufficient PIP2 (Baukrowitz et al., 1998; Shyng & Nichols, 1998). Thus either the PIP2-bound state is less stable over the time course of their sample preparation (they allowed 3 hours of equilibration with ligands), or solubilized  $K_{ATP}$  channels behave differently than their counterparts within a native membrane environment.

One of the two classes, representing 18% of the total particles, is termed the "propeller" state and closely resembles the ATP/GBC bound structures, but with SUR1 in what might be called an "outward-occluded" state, in which the NBDs are dimerized and bound to Mg-ATP/ADP but with very little change in the outer half of TMD1/TMD2 (above the inner leaflet

of the bilayer), such that the TMD is still inaccessible to solvent from the extracellular side. This is in contrast to the outward-facing conformation, the state which most ABC transporters are assumed to attain following NBD dimerization, in which a rearrangement and bending of TMD1/TMD2 helices allow escape of substrate. In the SUR1 outward-occluded (propeller) state, the cytoplasmic and inner leaflet halves of multiple helices from TMD1 and TMD2 undergo significant rearrangement which results in a collapse of the GBC binding pocket. This immediately suggests a mechanism for the inhibition of channel activity by sulfonylureas: GBC, by binding to a site comprising helices from TMD1 and TMD2, acts as a physical block to prevent rearrangement of these helices that is necessary for NBD dimerization and thus Mg-nucleotide stimulation. However, this does not explain sulfonylureas' nucleotide-independent mechanism of inhibition.

Importantly, in the NBD dimerized "propeller" state, Kir6.2 and TMD0 remain nearly identical to the ATP/GBC-bound structure. There is also very little, if any, change in L0. However, this is difficult to say unequivocally, as the region of L0 corresponding to residues 196-213 (which forms an interaction with the Kir6.2 CTD and plays critical roles in gating) is poorly resolved in all structures and cannot be accurately modelled, thus we cannot rule out some subtle but significant difference in this stretch induced by NBD dimerization. Also, because the resolution of this class is lower, the authors could not conclude whether MgATP or MgADP is bound to NBD2 of SUR1 (NBD1 is catalytically inactive), i.e. it is unknown whether this is a pre- or post-hydrolytic state.

The other class, representing 60% of the particles in their dataset, differs markedly from any other  $K_{ATP}$  channel structure to date and is termed the "quatrefoil" state. Kir6.2 is still closed and ATP-bound, but, relative to their "propeller" state or our ATP/GBC structure, the CTD has

undergone a 10-15° counterclockwise rotation (viewed from extracellular side) and the TMD-CTD linker (C-linker) has become disordered, which agrees with the hypothesis that rigid-body CTD rotation is manifested in winding or unwinding of a helix in the C-linker.

In the quatrefoil state, the most striking difference is in SUR1, in which the ABC core structure has undergone a 90° CCW rotation about the C4 axis of Kir6.2 (viewed from intracellular side). TMD0 has remained unchanged, and as a result of the rotation of the rest of SUR1, forms a new interface with TMD1/TMD2. Also, NBD2 now faces the interior of the complex and forms a new interface with the Kir6.2 CTD. Maybe most surprising, almost all of L0 is disordered in this state, meaning ~80 amino acids have unfolded as a result of this transition.

The authors claim that MgATP is bound at NBD1 (degenerate site) and MgADP is bound at NBD2 (consensus site); as the sample contained only MgATP this would represent a true post-hydrolytic state. Thus it is tempting to speculate that MgATP hydrolysis provides the power stroke necessary for transition to the "quatrefoil" conformation, which could represent a Mg-nucleotide activated, "pre-open" state with reduced ATP sensitivity at Kir6.2.

There are a few caveats, however, which warrant cautious interpretation of these data. The most important of these is the construct used. Unlike our structures, solved with WT SUR1 and Kir6.2, this study utilized a SUR1-Kir6.2 fusion construct (KATP<sub>EM</sub>), in which the C-terminus of SUR1 is fused to the N-terminus of Kir6.2 through a 3X Ser-Ala (i.e. 6 amino acid) linker. The short length of this linker could alter K<sub>ATP</sub> channel gating properties, particularly given the fact that the Kir6.2 N-terminus very likely needs to associate with the SUR1 inner vestibule during normal K<sub>ATP</sub> channel function. This association is likely not possible in their fusion construct, due to the location of the C-terminus of SUR1 (68Å C $\alpha$ -C $\alpha$  separation between

F1577 and W430 in ATP+GBC structure; W430 is adjacent to upper portion of putative N-terminus density). In support of this, a more recent ATP+GBC reconstruction from the Beijing group, also using a SUR1-Kir6.2 fusion construct, lacked density for the N-terminus within the inner vestibule of SUR1 (Wu et al., 2018), in contrast to our WT ATP+GBC reconstruction. Further, the short linker may also introduce strain which could alter the equilibrium between conformations or induce a new conformation altogether. Because the quatrefoil state brings the C-terminus of SUR1  $\sim 12\text{\AA}$  closer to the N-terminus of Kir6.2 relative to the propeller state, this conformation could simply result from a relief of some of this strain.

The authors also point to the creation of a new interface between NBD2 of SUR1 and the Kir6.2 CTD in the quatrefoil state. This is potentially very interesting as the site on NBD2 is immediately adjacent the MgATP binding site, and thus suggests direct modulation of the Kir6.2 CTD by Mg-nucleotide binding to the NBDs. We therefore mutated to Ala each of the Kir6.2 residues involved in the putative interface (S273, H276, H277, H278) and tested Mg-nucleotide stimulation by  $\text{Rb}^+$ -efflux and patch clamping (Shyng and Kandasamy, unpublished). However, none of the mutations had any observable effect, which leads us to conclude that either 1) this interface has no consequence on Mg-nucleotide stimulation of the channel and is simply a by-product of the new conformation, or 2) the interface is non-physiological and the quatrefoil state is an artifact of the experimental conditions. More experiments such as these are thus needed to confirm the relevance or importance of this structure.

The most recent set of  $K_{\text{ATP}}$  channel structures from the Beijing group (Wu et al., 2018) were again presumably an attempt to obtain a Mg-nucleotide bound, PIP2-bound activated state. While the authors did not achieve this, they nevertheless have provided important validation of structures observed so far, particularly with respect to the Mg-nucleotide bound, NBD-dimerized

state. As mentioned, the authors utilize a SUR1-Kir6.2 fusion construct, this time with a much longer linker (39 amino acids), possibly to avoid potential artifacts of the genetic fusion. They report three structures: 1) a GBC+ATP $\gamma$ S structure, which not surprisingly is nearly identical to our ATP+GBC structure (Chapter 4); 2) an ATP $\gamma$ S-only, which is nearly identical to our ATP-only structure (Chapter 5); 3) a MgADP-bound structure, which is nearly identical to the MgATP-bound propeller conformation observed by the Rockefeller group (Lee et al., 2017).

The MgADP-bound structure is the most informative, because it shows that MgADP alone can induce NBD dimerization, as expected based on the ability of MgADP to stimulate in the absence of ATP, and that the MgADP-bound state of Kir6.2 is very similar if not identical to the MgATP bound state (i.e. the propeller conformation from (Lee et al., 2017)). Maybe most interestingly, the authors do not observe a quatrefoil conformation. Because the two MgATP-bound and MgADP-bound, NBD-dimerized "propeller" states are nearly identical, it seems unlikely that the difference in nucleotide is the reason for the absence of a quatrefoil state in the MgADP data. The more likely cause is either the different linker length of the genetic fusion (6 vs 39 amino acids) or the different detergents used for cryo-EM (Lee et al. used amphipol PMAL-C12; Wu et al. used digitonin). Interestingly, Lee et al. point to a hydrophobic mismatch between TM helices of TMD1/TMD2 and TMD0/Kir6.2 which exists in the propeller conformation and is rectified in the quatrefoil state by a 3Å vertical translation of the ABC core structure of SUR1 concomitant with the 90° CCW rotation about the C4 axis. In other words, in the quatrefoil state the TM helices of TMD1/TMD2 and TMD0/Kir6.2 are brought into register such that the extracellular end of the helices all lie on the same plane. In a bilayer, a result of this "hydrophobic mismatch" may be membrane curvature as the lipids adapt to minimize exposure to solvent. It is conceivable that this curvature is energetically unfavorable in a PMAL-

C12 micelle, an amphipol which presents an environment chemically quite distinct from both a membrane bilayer and traditional detergent micelles.

Taken together, these structures, including my own, have shed light on the mechanism of inhibition by sulfonylureas and ATP, how Mg-nucleotides impact the structure of SUR1, and suggest how they may desensitize Kir6.2 to ATP inhibition. These are all fundamental aspects of  $K_{ATP}$  channel function, and have thus greatly advanced our understanding of the underlying biology. However, at this point the rate of cryo-EM structure solution has perhaps outpaced the field's ability to directly test the hypotheses which are generated in the process. Some notable (and testable) examples include: 1) GBC binding blocks MgADP stimulation by preventing rearrangement of TMs 6, 7, 8, and 16 induced by NBD dimerization and 2) as a consequence GBC cannot bind to the NBD dimerized, outward-occluded state of SUR1; 3) SUR1 cannot achieve a true outward-facing conformation, which at least partly explains its lack of transport function; 4) ATP hydrolysis at NBD2 drives a rearrangement, in concert with L0, from a "propeller" to a "quatrefoil" conformation during channel activation; and 5) the Kir6.2 N-terminus binds to the inner vestibule of SUR1 and regulates the dynamics between inward-facing and outward-occluded states and in the process impacts the  $P_O$  of Kir6.2 via its direct link to the CTD.

All of these structures, however, are closed and without PIP2, despite the presence of saturating PIP2 in the MgADP/MgATP samples from the Rockefeller and Beijing groups. Thus the structural basis for PIP2 activation of the channel, how SUR1 hypersensitizes Kir6.2 to PIP2, and how MgADP overcomes ATP inhibition, remain open questions. Therefore, the most valuable structures to obtain in terms of understanding  $K_{ATP}$  channel gating and activation are of the complex bound to PIP2 and PIP2+MgADP. A PIP2 alone structure is useful as PIP2 in the

absence of nucleotide affords near maximal  $P_{O_2}$ , while addition of MgADP will presumably act to stabilize PIP2 interaction through a rearrangement in the L0-Kir6.2 CTD interface; having both structures would allow isolation of the effect of MgADP. The challenge which has been encountered so far is maximizing MgADP stimulation at SUR1 while limiting MgADP inhibition at Kir6.2. However, careful titration of MgADP in the presence of saturating PIP2 should allow one to identify a maximally activated population of channels. One could even do this in the presence of a constant MgATP concentration to try and recapitulate what may occur in the  $\beta$ -cell as Mg-nucleotide concentrations fluctuate during changes in blood sugar. While experimentally laborious, automated cryo-EM data collection strategies and advanced image classification schemes make this kind of study a possibility.

### **Concluding Remarks**

If seeing is believing, then this project has no doubt had a significant impact on the  $K_{ATP}$  channel field, as it's difficult to know how something works if you do not know what it looks like. But maybe the value of a discovery lies in what it cannot tell you, and in the case of the work presented here, that is a significant amount. For example, why do sulfonylureas and CBZ only correct trafficking mutations in TMD0 and not elsewhere in SUR1? The answer is not immediately obvious from any structure solved so far. In fact, based on the structure a logical conclusion might be the opposite, that these TMD0 trafficking mutations would be the only ones which *cannot* be rescued by PCs because they lie distant from the sulfonylurea binding site and are *the* critical link between SUR1 and Kir6.2. There is the possibility that trafficking mutations within the ABC core structure of SUR1 disrupt CBZ/GBC binding, but this seems unlikely for those in the NBDs. Maybe these mutations cause a more severe folding defect which cannot be overcome or tolerated, or maybe the chaperone mechanism by which CBZ and sulfonylureas act

simply does not apply to mutations outside of TMD0. There is probably an underlying fundamental aspect of  $K_{ATP}$  channel biology in this, and it may not be solved by looking at purified channels in isolation.

Nevertheless, this dissertation provides the field with a highly detailed framework for (re)interpreting past results and for designing new experiments. In terms of  $K_{ATP}$  channel gating, a PIP2-bound structure is absolutely essential to understand the role of SUR1 in channel activation and also why ATP actually inhibits the channel. The work has also provided high-resolution data on the sulfonylurea binding site in SUR1, and opens the door to rationally designing compounds which target, for instance, the  $\beta$ -cell  $K_{ATP}$  channel and not the cardiac channel. Finally, the possibility that the N-terminus of Kir6.2 binds to the inner vestibule of SUR1, as if it were substrate, hints at a very interesting evolutionary relationship between these two proteins, and likely ensures the fascination of future  $K_{ATP}$  channel scientists for years to come.

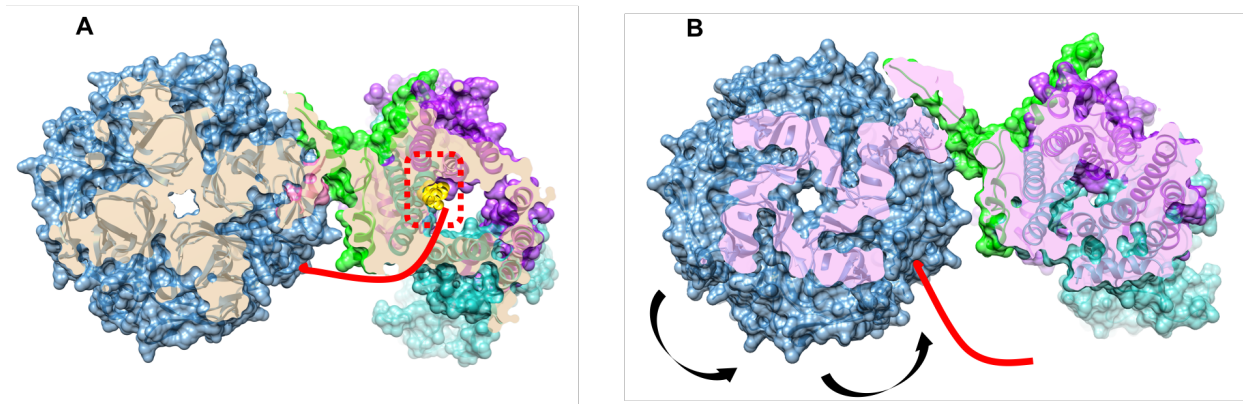


**Figure 1.** A model for gating regulation by the Kir6.2 N-terminus (red curve). (A) In an inward-facing state, the SUR1 inner vestibule is accessible to the Kir6.2 N-terminus. Binding is favored when ATP is bound to Kir6.2 CTD, and the interaction is strengthened through direct interactions of the N-terminus with sulfonylureas, glinides, or CBZ. (B) If inhibitors are not bound to the sulfonylurea binding pocket in SUR1, the N-terminus can dissociate as Mg-nucleotides cause NBD dimerization. The liberated N-terminus now frees the CTD to undergo transitions necessary for gating.

## References Cited

- Babenko, A. P. (2005). K(ATP) channels "vingt ans apres": ATG to PDB to Mechanism. *J Mol Cell Cardiol*, 39(1), 79-98. doi:10.1016/j.yjmcc.2004.12.004
- Babenko, A. P., & Bryan, J. (2002). SUR-dependent modulation of KATP channels by an N-terminal KIR6.2 peptide. Defining intersubunit gating interactions. *J Biol Chem*, 277(46), 43997-44004. doi:10.1074/jbc.M208085200
- Babenko, A. P., Gonzalez, G., & Bryan, J. (1999). The N-terminus of KIR6.2 limits spontaneous bursting and modulates the ATP-inhibition of KATP channels. *Biochem Biophys Res Commun*, 255(2), 231-238. doi:10.1006/bbrc.1999.0172
- Baukrowitz, T., Schulte, U., Oliver, D., Herlitze, S., Krauter, T., Tucker, S. J., . . . Fakler, B. (1998). PIP2 and PIP as determinants for ATP inhibition of KATP channels. *Science*, 282(5391), 1141-1144.
- Bavro, V. N., De Zorzi, R., Schmidt, M. R., Muniz, J. R., Zubcevic, L., Sansom, M. S., . . . Tucker, S. J. (2012). Structure of a KirBac potassium channel with an open bundle crossing indicates a mechanism of channel gating. *Nat Struct Mol Biol*, 19(2), 158-163. doi:10.1038/nsmb.2208
- Devaraneni, P. K., Martin, G. M., Olson, E. M., Zhou, Q., & Shyng, S. L. (2015). Structurally distinct ligands rescue biogenesis defects of the KATP channel complex via a converging mechanism. *J Biol Chem*, 290(12), 7980-7991. doi:10.1074/jbc.M114.634576
- Fan, Z., & Makielski, J. C. (1999). Phosphoinositides decrease ATP sensitivity of the cardiac ATP-sensitive K(+) channel. A molecular probe for the mechanism of ATP-sensitive inhibition. *J Gen Physiol*, 114(2), 251-269.
- Haider, S., Tarasov, A. I., Craig, T. J., Sansom, M. S. P., & Ashcroft, F. M. (2007). Identification of the PIP2-binding site on Kir6.2 by molecular modelling and functional analysis. *EMBO J*, 26(16), 3749-3759.
- Hansen, A. M., Hansen, J. B., Carr, R. D., Ashcroft, F. M., & Wahl, P. (2005). Kir6.2-dependent high-affinity repaglinide binding to beta-cell K(ATP) channels. *Br J Pharmacol*, 144(4), 551-557. doi:10.1038/sj.bjp.0706082
- Koster, J. C., Sha, Q., Shyng, S., & Nichols, C. G. (1999). ATP inhibition of KATP channels: control of nucleotide sensitivity by the N-terminal domain of the Kir6.2 subunit. *J Physiol*, 515 (Pt 1), 19-30.
- Lee, K. P. K., Chen, J., & MacKinnon, R. (2017). Molecular structure of human KATP in complex with ATP and ADP. *Elife*, 6. doi:10.7554/eLife.32481
- Li, J., Lu, S., Liu, Y., Pang, C., Chen, Y., Zhang, S., . . . An, H. (2015). Identification of the Conformational transition pathway in PIP2 Opening Kir Channels. *Sci Rep*, 5, 11289. doi:10.1038/srep11289
- Li, N., Wu, J. X., Ding, D., Cheng, J., Gao, N., & Chen, L. (2017). Structure of a Pancreatic ATP-Sensitive Potassium Channel. *Cell*, 168(1-2), 101-110 e110. doi:10.1016/j.cell.2016.12.028
- Martin, G. M., Yoshioka, C., Rex, E. A., Fay, J. F., Xie, Q., Whorton, M. R., . . . Shyng, S. L. (2017). Cryo-EM structure of the ATP-sensitive potassium channel illuminates mechanisms of assembly and gating. *Elife*, 6. doi:10.7554/eLife.24149
- Mikhailov, M. V., Campbell, J. D., de Wet, H., Shimomura, K., Zadek, B., Collins, R. F., . . . Ashcroft, F. M. (2005). 3-D structural and functional characterization of the purified

- KATP channel complex Kir6.2-SUR1. *EMBO J*, 24(23), 4166-4175.  
doi:10.1038/sj.emboj.7600877
- Pratt, E. B., Zhou, Q., Gay, J. W., & Shyng, S. L. (2012). Engineered interaction between SUR1 and Kir6.2 that enhances ATP sensitivity in KATP channels. *J Gen Physiol*, 140(2), 175-187. doi:10.1085/jgp.201210803
- Reimann, F., Tucker, S. J., Proks, P., & Ashcroft, F. M. (1999). Involvement of the n-terminus of Kir6.2 in coupling to the sulphonylurea receptor. *J Physiol*, 518 ( Pt 2), 325-336.
- Schulze, D., Krauter, T., Fritzenschaft, H., Soom, M., & Baukrowitz, T. (2003). Phosphatidylinositol 4,5-bisphosphate (PIP2) modulation of ATP and pH sensitivity in Kir channels. A tale of an active and a silent PIP2 site in the N terminus. *J Biol Chem*, 278(12), 10500-10505.
- Shyng, S. L., & Nichols, C. G. (1998). Membrane phospholipid control of nucleotide sensitivity of KATP channels. *Science*, 282(5391), 1138-1141.
- Vila-Carriles, W. H., Zhao, G., & Bryan, J. (2007). Defining a binding pocket for sulfonylureas in ATP-sensitive potassium channels. *FASEB J*, 21(1), 18-25. doi:10.1096/fj.06-6730hyp
- Wu, J. X., Ding, D., Wang, M., Kang, Y., Zeng, X., & Chen, L. (2018). Ligand binding and conformational changes of SUR1 subunit in pancreatic ATP-sensitive potassium channels. *Protein Cell*. doi:10.1007/s13238-018-0530-y
- Yan, F. F., Casey, J., & Shyng, S. L. (2006). Sulfonylureas correct trafficking defects of disease-causing ATP-sensitive potassium channels by binding to the channel complex. *J Biol Chem*, 281(44), 33403-33413. doi:10.1074/jbc.M605195200